

Durham E-Theses

Experimental probes to tell the kind of electroweak realisation apart

WEST, MIA,ROBIN,BYRON

How to cite:

WEST, MIA,ROBIN,BYRON (2024) *Experimental probes to tell the kind of electroweak realisation apart*, Durham theses, Durham University. Available at Durham E-Theses Online:
<http://etheses.dur.ac.uk/15565/>

Use policy

The full-text may be used and/or reproduced, and given to third parties in any format or medium, without prior permission or charge, for personal research or study, educational, or not-for-profit purposes provided that:

- a full bibliographic reference is made to the original source
- a [link](#) is made to the metadata record in Durham E-Theses
- the full-text is not changed in any way

The full-text must not be sold in any format or medium without the formal permission of the copyright holders.

Please consult the [full Durham E-Theses policy](#) for further details.

Experimental probes to tell the kind of electroweak realisation apart

Mia R. B. West

A Thesis presented for the degree of
Doctor of Philosophy



Institute for Particle Physics Phenomenology
Department of Physics
Durham University
United Kingdom
April 2024

Abstract

The discovery of the Higgs boson was the latest piece of the puzzle to be added to the electroweak sector of the Standard Model (SM), which, via the Higgs mechanism, provides fermions with masses and ensures unitarity in the SM. This is further backed up experimentally, with results thus far in agreement with the SM. However, the SM is incomplete and some attempts to fill in the blanks with new physics interfere with the mechanism of electroweak symmetry breaking, yet are still compatible with experiment. Definitively determining the true nature of electroweak symmetry breaking is key to understanding the electroweak sector, but is nonetheless an ambitious goal as a result of the high energy scales involved. We can, however, begin to uncover the next puzzle pieces at the lower energy scales of current colliders. Effective Field Theories (EFTs) are the rediscovered tool in a particle physicist's belt which will allow us to do this. They are a model-independent framework that can be used to classify the low-energy effects of heavy, new physics on experimental results which deviate from the Standard Model prediction.

The Standard Model Effective Field Theory (SMEFT), where the Higgs doublet transforms linearly under electroweak symmetry, is the most studied approach. However, the SMEFT is not as general an EFT as the Higgs EFT (HEFT), where electroweak symmetry transforms non-linearly. The question we attempt to address in this thesis is, is it SMEFT or HEFT\SMEFT? Or, equivalently, if electroweak symmetry is linearly or non-linearly realised. So far, nature has not been forthcoming. As such, we are interested in experimental probes which may answer this question.

We begin by considering collider phenomenology: how scattering amplitudes may differ between the two theories. In particular, we find partial evidence for a 'minimum distance' between the SM value for such amplitudes and HEFT\SMEFT theories, such that SMEFT becomes the sole theory whose amplitudes approach the SM. It is possible that, if non-decoupling new physics is lurking in the electroweak sector, we may be able to confirm a non-linear realisation by future collider programs.

Yet our question is a non-local one, with the decisive physics lying a distance

$\sim v$ away in field-space, with particle colliders only probing near the vacuum. We turn instead to non-perturbative physics. Firstly, to sphaleron solutions in HEFT\SMEFT, which we find are less phenomenologically significant. Secondly, to first order phase transitions, where detectable gravitational wave remnants, domain wall formation, and vacuum decay in the far distant future could take place, and single out HEFT\SMEFT theories. We find that results from cosmology are complimentary to those from particle colliders and the combination of both such measurements could help to pin down whether it is HEFT\SMEFT or SMEFT.

Declaration

The work in this thesis is based on research carried out at the Institute for Particle Physics Phenomenology, Durham University, United Kingdom. No part of this thesis has been submitted elsewhere for any other degree or qualification. This thesis is based partially on joint work, which is specified below.

1. Chapter 2 is based on [1]: R. Alonso and M. West, *Roads to the Standard Model*, Phys. Rev. D **105** (2022) 096028, [2109.13290].
2. Chapters 3 and 4 are based on [2]: R. Alonso, J. C. Criado, R. Houtz and M. West, *Walls, bubbles and doom – the cosmology of HEFT*, [2312.00881] (accepted for publication).

Other research projects published during my studies but not included in this thesis are:

1. [3]: R. Alonso, D. Dimakou, and M. West, *Fractional-charge hadrons and leptons to tell the Standard Model group apart*, [2404.03438]
2. [4]: J. Bennett, A. Callison, T. O’Leary, M. West, N. Chancellor, and V. Kendon, *Using copies can improve precision in continuous-time quantum computing*, Quantum Sci. Technol. **8** (2023) 035031, [2206.02545]
3. [5]: R. Alonso and M. West, *On the effective action for scalars in a general manifold to any loop order*, Phys. Lett. B **841** (2023) 137937, [2207.02050]

Copyright © 2024 by Mia R. B. West.

“The copyright of this thesis rests with the author. No quotations from it should be published without the author’s prior written consent and information derived from it should be acknowledged”.

Acknowledgements

Firstly, I would like to thank my advisor Rodrigo Alonso for his unwavering help and support throughout this PhD. I'm honestly not sure a better advisor exists.

Secondly, I would like to thank the PhD students of the IPPP (particularly the occupants of OC215 and Tommy). You've all been excellent and I wish you all the best of luck in the future.

Thirdly, all of the regular attendees for the IPPP EDI group. I'm so glad so many of you turn up every week with enthusiasm to take down the patriarchy. I would particularly like to thank my fellow organisers Yannick Ulrich and Thomas Stone who are both unparalleled email-writers and amazing people.

Fourthly, my siblings Sasha, who's been through so much these past 4 years but is just absolutely awesome, and Ludo, who's endless kindness is really not in keeping with traditional siblinghood. Do better.

My housemates Helen, Rollo, James, and our cat Tibbs who've always been there for me, making sure I have enough chocolate. I genuinely couldn't have done this without all of you (nor would I have wanted to!). It's been an absolute pleasure.

Finally, a huge thank you to Samson Chan, Despoina Dimakou, Helen Lawson, and James Maxwell for their comments on the manuscript.

Contents

Abstract	ii
Declaration	iv
Acknowledgements	vi
List of Figures	x
List of Tables	xix
Preface	2
1 Introduction	3
1.1 The Standard Model	3
1.1.1 Spontaneous Symmetry Breaking	9
1.2 Effective Field Theory	13
1.2.1 The Decoupling Theorem	15
1.2.2 HEFT	17
1.2.3 Power Counting in HEFT	19
1.2.4 A Note on Renormalisability and EFTs	21
1.3 Geometry of Scalar Particles	21
1.3.1 Summary of Differential Geometry	22

1.3.2	Geometry and HEFT	25
1.3.3	Re-gauging the Symmetry	27
1.3.4	SMEFT as a Special Case of HEFT	30
1.4	Longitudinal Vector Boson Scattering Amplitudes	33
1.5	Effective Field Theory and the S-Matrix	35
1.5.1	Perturbative Unitarity	36
1.5.2	LSZ Formula and Field-Redefinitions	40
1.5.3	Integrating Out a Particle	45
1.5.4	Example of Integrating Out a Particle	47
2	Roads to the Standard Model	51
2.1	Geometry and Amplitudes	53
2.1.1	Riemann Normal Coordinates	55
2.1.2	Experimental and Theory Constraints on Curvature	58
2.2	Correlation of curvature in SMEFT	61
2.3	Models as Probes into HEFT	63
2.3.1	Only h acquires a vev, SMEFT case	64
2.3.2	Both Φ and h break the symmetry, HEFT\SMEFT non-linearly realised theory space	65
2.4	Manifolds	69
2.4.1	Non-linearly Realised Theories with a Singularity	70
2.4.2	Smooth Non-linearly Realised Theories	71
2.5	Obstacles in the Road to the SM	72
2.6	Summary	76
3	Sphalerons in Non-Linearly Realised Theories	77
3.1	Sphalerons in the Standard Model	79
3.2	Modification of Sphaleron Solutions	84
3.3	Summary	89
4	The Cosmology of HEFT	91
4.1	The Thermal Effective Potential	96

4.2	Classical Action	103
4.3	The Thermal Effective Potential in Non-Linear Realised Theory Space	109
4.3.1	Calculation of the one-loop finite-temperature potential	111
4.3.2	Limitations of the calculation	116
4.3.3	Symmetry (non)restoration and roads to the SM	121
4.4	Domain Walls	127
4.5	Past and Future First Order Phase Transitions	133
4.5.1	First order electroweak phase transition	138
4.5.2	Doom: future vacuum decay	142
4.6	Gravitational Waves	148
4.7	Complementarity with LHC	155
4.8	Summary	162
5	Summary	165
A	UV model for non-linearly realised type A theory	167

List of Figures

1.1	Visual depiction of the space of HEFT theories. There is some evidence for the boundary between non-linearly realised electroweak theories and SMEFT theories belonging to the former, see e.g. Ref. [6].	32
1.2	Schematic representation of the Equivalence Theorem [7–10]. The external longitudinal gauge boson e.g. W_L^\pm can be approximated to be its corresponding Goldstone boson φ^\pm in the high-energy scattering limit, i.e. if the characteristic energy E of the process is much greater than the gauge boson mass.	33
1.3	Images	34
2.1	Diagrams for the $\mathcal{O}(s)$ contribution to the $WWhhh$ amplitude in the basis of eq. (2.14).	56
2.2	Theoretically (grey) and experimentally (up to blue) excluded (up to 95% confidence level) regions of the curvatures R_h, R_φ which are related to electroweak amplitudes as in eqs (2.30,2.29): and sensitivity limits of future colliders (HL-LHC, up to green; FCC, up to orange), also up to 95% confidence level. See text for detail. The plot scales linearly within the dashed box and logarithmically outside.	60

2.3	A selection of diagrams for the $WWhh$ and $WWWW$ amplitudes with the action in eq. (2.36)	62
2.4	Range of curvature for SMEFT and non-linearly realised theories, on the same background as Fig. 2.2. Two non-linearly realised theories are plotted: the yellow region shows curvature for the symmetric representation with $\langle\Phi\rangle \neq 0$, and the dark-grey region shows a hyperbolic manifold (see sec. 2.4). The black line shows SMEFT curvature: the purple and red dots represent the singlet and the symmetric representation with $\langle\Phi\rangle = 0$ examples from sec. 2.3 respectively. The outer-most to inner-most dots are evaluated with coupling $g_* = 1$ and heavy singlet mass: 500 GeV, 1 TeV, 1.5 TeV, 2 TeV and 4 TeV.	68
2.5	Examples of manifolds which belong in SMEFT (a), or in non-linearly realised theory space (b,c,d) with the gauge symmetry action being rotation around the z axis. SMEFT manifolds in (a) correspond to: Composite models (yellow), the SM (green), and negative curvature models (blue). Manifolds representing non-linearly realised theories (b,d) are smooth, while (c) presents a singularity and both (c,d) are in a class which resembles the SM around the vacuum. For (d), part of the manifolds have been cut out for better visualization.	71
3.1	Demonstration of trivial fig. 3.1a and non-trivial fig. 3.1b maps.	78
3.2	Fig. 3.2a: sphaleron energy as a function of n for different values of F_* . Fig. 3.2b: square root of the difference between the limit value of the energy as $n \rightarrow \infty$ (taken from $n = 10$) and the SM energy as a function of F_* , together with a linear fit.	87

4.1	In Fig. 4.1a, from top to bottom and left to right, 2D representations of the 4D scalar manifold for the SM case (top left) and type A theories with the metric of Eqs. (4.34, 4.39) and $\sin^2 \chi = 0.01, 0.1,$ and 0.2. The Goldstone bosons correspond to the angle around the z axis, while the Higgs h parametrises the surface in the orthogonal direction to them. Fig. 4.1b shows $M_W(h)/M_W(0)$ for the SM and the type A theories in Fig. 4.1a with the same colour coding.	93
4.2	The possible extrema histories in SMEFT, minima in blue and maxima in green.	94
4.3	Extrema histories we encounter in non-linearly realised theories with one extrema at high temperature and three at low temperature. . . .	95
4.4	Possible extrema histories for a single minimum at high and low temperature	96
4.5	Initial and $T = 0$ extrema we find as realisations in non-linearly realised theories without high-temperature symmetry restoration. . .	96
4.6	Schematic diagram of the tree level Higgs potential $V(h)$ in blue and in red the Higgs-dependent W mass, $v^2 m_W^2(h)$, in arbitrary units to set our conventions. Along the horizontal axis runs the Higgs field h . Fig. 4.6a shows the SM and SMEFT case, with $h \in [-v_+, \infty)$, and Fig. 4.6b shows the non-linearly realised theory case where $h \in (-\infty, \infty)$. The quantities v_{\pm}, v_* and δ are defined in Eqs. (4.49), (4.39) and (4.53) respectively.	106
4.7	The effect of the 4 free parameters of our effective Lagrangian on the tree-level potential $V(h)$ and the $F(h)$ function. Top: variation of the potential $V(h)$ with ϵ (left) and γ_4 (right). Bottom: variation of the $F(h)$ function with χ (left) and δ (right).	108

4.8	Field-dependent cut-off as estimated from perturbative unitarity to be $4\sqrt{\pi} R_I(h) ^{-1/2}$ for sectional curvatures $R_\varphi(h)$ (solid) and $R_h(h)$ (dashed) as defined in Eqs. (4.46) and (4.47). The parameter $\chi = \sqrt{0.1}$ and the following $\gamma_a = v/v_\star$ values are chosen as those that lead to domain walls, $\gamma_a = 1$ (see Sec. 4.4); the doom scenario, $\gamma_a = 1.1$ (see Sec. 4.5.2 and Fig. 4.25 in Sec. 4.7); and $\gamma_a = 1.2$ a conservative value for the observable bubble region shown in Fig. 4.24. For comparison, the nucleation temperature in phase transitions studied here is around 100 GeV.	111
4.9	Schematic representation of thermal histories for the extrema of the effective potential satisfying (left) and violating (right) the strong IR constraint.	119
4.10	One-loop effective potential plotted for $\chi = \sqrt{0.1}$, obeying the high-temperature symmetry restoration bound in Eq. (4.109). The benchmarks chosen here are $\gamma_4 = 1$, $\epsilon = 0.02$, $\delta = -0.1$. Fig. 4.10a and Fig. 4.10b show the potential evolution with temperature for $T = 246$ GeV and $T = 190$ GeV, respectively. Notice, in particular, the large χ smooths the potential around $\phi/v = 0$ in contrast to Fig. 4.11.	122
4.11	One-loop effective potential plotted for $\chi = 0.05$, which unlike Fig. 4.10, does not satisfy the high-temperature symmetry restoration bound in Eq. (4.109). The benchmarks chosen here are $\gamma_4 = 1$, $\epsilon = 0.02$, and $\delta = -0.1$. Fig. 4.11a and Fig. 4.11b show the potential evolution with temperature for $T = 246$ GeV and $T = 190$ GeV respectively. For this choice of χ , the potential is sharply peaked around $\phi/v = 0$ in contrast to Fig. 4.10.	123
4.12	Contribution V_{peak} of the $V'F'/F$ term to the effective potential. . . .	126

4.13	<p>Fig. 4.13a shows the (ϵ, γ_4) plane with excluded regions in darker green (from the upper bound on walls energy density, Eq. (4.132)), light gray horizontal (perturbativity, Eq. (4.90)), dark gray (wall annihilation before BBN, (4.131)). The region in dark purple is discarded if one is to have walls that survive long past the original phase transition (Eq. (4.126)). Also shown is the gravitational wave spectrum value at peak frequency $\Omega_{\text{GW}}(f_{\text{peak}})$ in the yellow gradient, see Eq. (4.155) and Sec. 4.6. Dashed lines for the peak frequencies run from $f_{\text{peak}} = 10^{-6}$ Hz on the far right to 10^{-10} Hz on the far left in intervals of 10, and in blue the region SKA [11] would be sensitive to (this region, however, is excluded by LHC bounds, see Sec. 4.7). Fig. 4.13b shows the (ϵ, δ) excluded by wall annihilation before BBN in dark grey vertical Eq. (4.131), and the regions discarded for long lived walls following from Eq. (4.127) (purple) and Eq. (4.128) (grey horizontal).</p>	132
4.14	<p>Schematic representation of the different cosmological phenomena arising in the (ϵ, δ) plane. The small diagrams at the top and the bottom borders represent the tree-level potential in black, and the finite-temperature corrections in grey.</p>	137
4.15	<p>Comparison of the four methods to compute the tunnelling bounce action, as described in detail in the text of Sec. 4.5.1. The displayed lines are evaluated for the parameters $\chi = \sqrt{0.1}, \epsilon = 0.04, \delta = -0.08$, with the results from <code>CosmoTransitions</code> in orange, <code>Anybubble</code> in blue, the quartic potential approximation in red, and the thin wall approximation in green.</p>	139

- 4.16 A slice of parameter space in ϵ, δ for which the region in colour following history Q_- meets the condition of Eq. (4.142) for some $T = T_N$, the nucleation temperature. For this plot, $\chi = \sqrt{0.1}$ and $\gamma_4 = 1.6$. The blank area in the upper region follows history Q_0 , as the thermal corrections favour the h_0 vacuum, leading to a SMEFT-like cosmological history. In the lower blank region while still following history Q_- , the condition for nucleation, Eq. (4.142), is not met for electroweak scale temperatures and as such we do not predict a first order phase transition in the early universe here. This and Fig. 4.17 occupy roughly quadrant IV of Fig. 4.14. 140
- 4.17 Extension of Fig. 4.16 to larger epsilon values and different histories, with $\gamma_4 = 1.6, \chi = \sqrt{0.1}$ as in the previous plot. The plot is discontinuous at $\epsilon = 1 - \sqrt{8/9}$ as a result of Eq. (4.53). For $\epsilon < 1 - \sqrt{8/9}$, the region in colour follows history Q_- and the blank, upper region above this follows history Q_0 as in Fig. 4.16. However, when $\epsilon > 1 - \sqrt{8/9}$, the $T = 0$ potential has a single minimum only and history R is followed for the region in colour. The blank region above only has a single minimum throughout its evolution. We note that the upper boundary from history R to a SMEFT-like history is slightly ambiguous as the potential becomes very flat and difficult to treat numerically. 143

- 4.18 Bounds on the (ϵ, δ) parameter space for the doom scenario at $\gamma_4 = 0.95$ and $\chi^2 = 0.1$. The upper-left grey region is excluded by the boundedness-from-below (dark) and perturbativity (light) criteria. The hatched region below the solid red line is excluded by the strong IR constraint, Eq. (4.88), while the dashed red line shows the weak version, Eq. (4.86). There is some noise associated with our method of numerically tracking the temperature evolution of the minima, and this noise is visible in the strong IR constraint curve. The blue region corresponds to the history displayed in Fig. 4.5, in which two minima exist in the high-temperature potential. The blue line separates the regions where the sign of the magnitude defined in Eq. (4.108) is positive or negative and is an estimate for the regions for histories $Q_{-,0}$ respectively 145
- 4.19 Top: excluded values of the lifetime of the universe as a function of γ_4 . Bottom: example points with the minimal lifetime allowed by boundedness from below in the second quadrant of the (ϵ, δ) plane, used to generate the blue line in the top plot. In these three plots, the shaded region is ruled out from various constraints: boundedness from below (darker, solid), perturbativity (lighter, solid), and LHC constraints (dashed). See Sec. 4.7 and Fig. 4.25 for more details on all the bounds shown in these plots. 147
- 4.20 The thermal parameters $T_N, \alpha, \beta/H_*, v_w$ for a slice of ϵ, δ parameter space with $\gamma_4 = 1.6$ and $\chi = \sqrt{0.1}$. The thermal parameters are defined respectively in Eqs. (4.142), (4.156), and (4.157) with the wall velocity estimated using prescription outlined in [12]. Note for a small region of parameter space, runaway bubbles with $v_w \rightarrow 1$ are predicted. However, the region is numerically noisy as a result of finite sampling. Fig. 4.16 is included again on the top left plot. . . . 151

- 4.21 The gravitational wave signal for $\gamma_4 = 1.6$, $\chi^2 = 0.1$. The GW signal curve is the maximal envelope of the power spectra obtained from varying ϵ and δ . To give a sense of the ϵ - and δ -dependence, the parameter space is broken up into subsets, and a resulting maximal envelope power spectrum is drawn for each subset. In Fig. 4.21a, the ϵ -dependence is emphasised by breaking the parameter space up into subsets of ϵ ranges as specified in the legend, while varying over all δ for each curve. In Fig. 4.21b, the δ -dependence is correspondingly emphasised, this time varying over all ϵ for each curve. The GW sensitivity curves are drawn for SKA [11], LISA [13], the Big Bang Observer (BBO) [14], and the Einstein telescope (ET) [15]. 153
- 4.22 The curvature plane $v^2 R_\varphi(0)$ and $v^2 R_h(0)$ as defined in Eq. (4.171). In colour is the region for high-temperature symmetry restoration (see Sec. 4.3.3), i.e. $\pi/2 > \chi > 0.3$. We vary γ_a^2 independently to account for varying $\epsilon, \delta, \gamma_4$. We note for interest but do not show on the plot for clarity that increasing γ_a^2 decreases the curvatures radially originating from $(v^2 R_h(0), v^2 R_\varphi(0)) = (0.0, 1.0)$. The area outside the blue dashed box is excluded by LHC bounds from Eq. (4.172). The FCC would be expected to be sensitive, assuming SM-like couplings, up to the small, inner box [16,17]. 156
- 4.23 (a) The $(\epsilon - \gamma_4)$ plane delineating the wall formation region in parameter space as in Fig. 4.13 with the addition of LHC bounds, Eq. (4.172), in the vertical gray shaded region. (b) Curve for the value of the spectrum at the peak frequency for the allowed region of parameter space taking into account LHC bounds and the sensitivity of SKA [11]. . . 158

- 4.24 Summary of first order phase transition parameter space for $\gamma_4 = 1.6$, $\chi^2 = 0.1$. The region in blue shows the combinations of (ϵ, δ) that we found to admit bubble nucleation while tunnelling from the false vacuum to the true vacuum today. The region in red (dark red) is excluded by the strong (weak) IR constraints. The pink (dark pink) regions are excluded by the boundedness from below (perturbativity) constraint. The light green (green) dashed lines show the LHC constraints on the curvature to the 1σ (2σ) level. The gray region is unphysical, yielding the wrong vacuum today. The regions of first order phase transitions that give a GW signal detectable at LISA (BBO) are shown in orange (cyan). Only a small sliver of parameter space gives signals observable only at BBO, more visible in Fig. 4.24b. 160
- 4.25 Top: Summary of the parameter space that leads to future vacuum decay (the doom scenario). Combination of Fig. 4.18 with LHC bounds in light green (1σ) and darker green (2σ). Bottom: Series of plots with the combination of LHC exclusion regions (delineated with dashed lines) and perturbativity to illustrate that values of $\gamma_4 < 0.85$ are ruled out by a combination of LHC and perturbativity bounds, and therefore discarded in our analysis. 161

List of Tables

- 1.1 Table showing the gauge transformations of SM matter fields (quarks, q , leptons, l , and the Higgs boson, H) under the SM gauge group. Note there are three generations of quarks and leptons in the SM. For the non-abelian groups, the number shown is the dimension of the representation the field transforms in. In particular, the **2,3** are the fundamental representations of $SU(2)_L, SU(3)_c$ respectively. For the abelian group $U(1)_Y$ we give the charge of the field under this group. The subscripts R and L distinguish left- and right-handed fermion fields. The left-handed quarks can be split into up-type (u, c, t) and down-type (d, s, b) types as $q_L = (u_L, d_L)$. One for each generation. The leptons pair (e, μ, τ) with their corresponding neutrino ($\nu_{e,\mu,\tau}$) as $l_L = (\nu, e)$. We have also grouped the right-handed fermions into a ‘doublet’ form $q_R = (u_R, d_R)$ and $l_R = (0, e_R)$. However, we emphasise that *the right-handed particles transform as singlets under $SU(2)_L$ and grouping them as above is simply for notational convenience* and not to do with their transformation under $SU(2)_L$. The $\sigma_3 = \text{Diag}(1, -1)$ is the third Pauli matrix. The hypercharge of, for example, the right-handed down quark is from extracting the lower component from $(\sigma_3 q_R)$, $1/6 + (-1)/2 = -1/3$ 8

3.1	Values of the sphaleron energy in units of $g/4\pi v$ (and corresponding radii ζ_a and ζ_h) at $F_\star = 0.2$ and varying n , as computed with methods A) and B)	87
4.1	True vacua at high and low temperatures for small ϵ and δ	135

Preface

The question of which electroweak symmetry realisation, linear or non-linear, is central to any model of new physics in the electroweak sector. Indeed, there are many reasons to expect new physics in this sector (e.g. the Hierarchy problem). With the LHC now in its precision era, however, we have additional means to hunt for such Beyond the Standard Model (BSM) physics in addition to looking for particle resonances. Very heavy BSM physics may begin to reveal itself at LHC energies by modifying particle couplings measurable by the LHC in the precision runs.

Unfortunately, many models of new, heavy physics (e.g. Loryons [18]) can yield similar coupling modifications, and as such we have a many-to-one problem on our hands. This is where Effective Field Theory (EFT) comes in: it is a model-independent and unbiased framework to classify the low-energy signatures of BSM physics, allowing particle physicists to explore the space of new models systematically.

Standard Model EFT (SMEFT) is the most common framework where electroweak symmetry is realised linearly. However, Higgs EFT (HEFT) is the more general EFT which allows for both linear and non-linear realisations.

It is the aim of this thesis to explore whether low energy experiment could definitively tell if electroweak symmetry is realised linearly or non-linearly in nature.

To do this, geometry is crucial. The reasons why and a review of the necessary

theory can be found in chapter 1. Following this, in chapter 2 we study scattering processes to see if differences in amplitudes could shed light on the dichotomy. It is clear, following this paper, that our question is a non-local one, i.e. that local scattering processes can only tell us so much. To this end, chapter 3 studies the non-local effect on sphalerons. This turns out to have limited phenomenology; as such, chapter 4 looks at observable effects in non-local, non-perturbative dynamics through cosmology, in particular, through gravitational wave phenomenology. Finally, we conclude our findings in chapter 5.

Finally, an apology to the reader: some key notation varies across different chapters. Although I have tried to keep consistent notation wherever possible, it may vary at times. Please refer to the introduction of the relevant chapter for its notation.

CHAPTER 1

Introduction

1.1 The Standard Model

The Standard Model is a quantum field theory based on the gauge symmetry group¹ $SU(3)_c \times SU(2)_L \times U(1)_Y$.² Particles exist as representations under the symmetry group, transforming under the group action. The representations we will be considering for the case of the particle content of the Standard Model are the fundamental and adjoint representations.

$SU(N)$ and $U(1)$ are Lie groups. A Lie group is a group in which the group operations of multiplication (μ) and inversion (i) are smooth

$$\mu : G \times G \rightarrow G, \mu(g_1, g_2) \mapsto g_1 g_2 \quad \text{Multiplication} \quad (1.1)$$

$$i : G \rightarrow G, i(g) \mapsto g^{-1} \quad \text{Inversion} \quad (1.2)$$

¹‘Gauge’ means the symmetry is a local one, i.e. where the symmetry is spacetime dependent.

²As an aside, this group is actually one of four possible choices consistent with the current particle spectrum, which have the same physics locally but differ globally. The groups differ by a quotient of the discrete group Z_p , $p = 1, 2, 3, 6$ [19], the phenomenological consequences of which have recently been under consideration. For example, different cases restrict the possible charges of particles allowed in their spectrum and a discovery of a fractionally charged particle might only be consistent with some of these groups [3, 20].

where $g_1, g_2, g \in G$. As a further aside, the requirement eq. (1.2) is being revisited and there has been a recent wealth of literature considering non-invertible generalised symmetries. See e.g. [21]. The dimension of the Lie group is given by the number, N , of such variables. A member of the group $g \in G$ can be obtained as follows:

$$g = e^{-i\theta^a T^a} = 1 - i\theta^a T^a + \mathcal{O}(\theta^2) \quad a = 1, 2, \dots, n \quad (1.3)$$

where the T^a are the infinitesimal group generators:

$$T^a = i \left. \frac{\partial g}{\partial \theta^a} \right|_{\vec{\theta}=0} \quad (1.4)$$

which obey the Lie algebra of the group

$$[T^a, T^b] = i f^{abc} T^c, \quad (1.5)$$

where $[\cdot, \cdot]$ is a Lie bracket. The real numbers f^{abc} are the structure constants of the group and are fully anti-symmetric.

Three Lie groups which we will encounter in this thesis are $SU(N)$, $O(N)$ and $U(1)$ and as such we will define them here.

The group $SU(N)$ is the group of $N \times N$ unitary matrices with determinant one,

$$U \in SU(N) \text{ where } U^\dagger U = U U^\dagger = \mathbb{I}_{N \times N} \text{ and } \det U = 1. \quad (1.6)$$

The dimension of the group is $N^2 - 1$. The group generators are also Hermitian.

The group $O(N)$ is the group of orthogonal $N \times N$ matrices,

$$O \in O(N) \text{ where } O^T O = O O^T = \mathbb{I}_{N \times N}. \quad (1.7)$$

The dimension of the group is $N(N - 1)/2$.

The group $U(1)$ is that whose action is to give the particle a complex phase, i.e.

$$U \in U(1) \text{ where } U = e^{iQ\theta}, \quad 0 \leq \theta < 2\pi, \quad (1.8)$$

where Q , an integer, is the charge of that particle.

Fundamental particles exist as the smallest non-trivial representation under the group. A representation of a group G of dimension p assigns to each group element g a $(p \times p)$ -matrix. In this thesis, we are interested in two representations of these groups:

- **Fundamental** The fundamental representation is the smallest non-trivial representation of the group. For instance, for $SU(N)$ the representation is obtained from the definition in eq. (1.6); it is in the linear space in which $N \times N$ matrices and as such has dimension N . The transformation matrix U in the fundamental representation can be obtained from the generators T_F in the fundamental representation via

$$U = \exp\{i\theta^a T_F^a\}, \quad (1.9)$$

where for a gauge theory the parameters θ^a are spacetime dependent. The generators in the fundamental representation are normalised with the convention that $\text{Tr}(T_F^a T_F^b) = \delta^{ab}/2$.

- **Adjoint** The generators for the adjoint representation $(T_{\text{adj}}^a)^{bc}$ are defined in terms of the structure constants as

$$(T_{\text{adj}}^a)^{bc} = -if^{abc}, \quad (1.10)$$

and has dimension $N^2 - 1$ (i.e. the same as that of the group G).

For example, for the group $SU(2)$ the generators of the group in the fundamental representation are $T_F^a = \sigma^a/2$, $a = 1, 2, 3$ the three Pauli matrices. The structure constants are $f^{abc} = \epsilon^{abc}$, i.e. the purely anti-symmetric symbol.

It must be that the physical results of our theory are invariant under gauge transformations. For example, electromagnetic gauge invariance demands charge conservation; this is verified to high-precision experimentally (see e.g. [22]). Therefore, our predictions should be manifestly gauge invariant. This we can achieve by ensuring the path integral we write down is gauge invariant. The path integral is the

key object in Quantum Field Theory from which we can obtain physical predictions. It is essentially the sum over all possible states of the system, and from this object we can derive its dynamical properties. For a set of fields ϕ_1, \dots, ϕ_n whose action functional is $S[\phi_1, \dots, \phi_n]$, the path integral is

$$Z = \int \mathcal{D}\phi_1 \dots \mathcal{D}\phi_n e^{iS[\phi_1, \dots, \phi_n]}. \quad (1.11)$$

We can equally write the action functional in terms of an integral over space-time of the Lagrangian density function:

$$S[\phi_1, \dots, \phi_n] = \int d^4x \mathcal{L}(\phi_1, \dots, \phi_n) \quad (1.12)$$

which we will abbreviate to ‘Lagrangian’ in this thesis, although technically the Lagrangian is what is obtained from integrating over 3-space. Into this function, we write all possible renormalisable, gauge, and Lorentz invariant terms for the particles in our chosen theory.

For example, taking a theory with a single complex scalar particle ϕ , we can write down the Lagrangian where ϕ transforms in the fundamental representation of $SU(N)$ (i.e. $U \in SU(N), \phi \mapsto U\phi$)

$$\mathcal{L} = (\partial_\mu \phi)^\dagger (\partial^\mu \phi) - m^2 \phi^\dagger \phi. \quad (1.13)$$

We could require the theory to be invariant under the gauge symmetry $SU(N)$. However, the fact that we have taken derivatives of the field ϕ in the Lagrangian spoils the gauge symmetry as, although we have suppressed the dependence for brevity, $U = U(x)$. In order to write a gauge-invariant Lagrangian, we must introduce $N^2 - 1$ new fields A_μ^a , one for each generator of the group, known as gauge bosons. Combining the new fields A_μ^a into a single object $A_\mu = A_\mu^a T_F^a$, they transform in the *adjoint representation* in the following way:

$$A_\mu = A_\mu^a T_F^a \mapsto U \left(A_\mu + \frac{1}{g} \partial_\mu \right) U^\dagger, \quad (1.14)$$

with g the coupling constant of the group.

One can then construct a gauge-invariant Lagrangian,

$$\mathcal{L} = (D_\mu\phi)^\dagger(D_\mu\phi) - m^2\phi^\dagger\phi, \quad (1.15)$$

where D_μ is the covariant derivative defined as:

$$D_\mu \equiv \partial_\mu - igA_\mu^a T_F^a, \quad (1.16)$$

which now transforms as $D_\mu\phi \mapsto UD_\mu\phi$.³ With one problem solved, another emerges in its place: the field's A_μ^a are non-dynamical. Luckily, this is easily fixed by introducing a field-strength tensor

$$F_{\mu\nu} = F_{\mu\nu}^a T^a = \partial_\mu A_\nu - \partial_\nu A_\mu - ig[A_\mu, A_\nu] \quad (1.17)$$

and the term

$$-\text{Tr}(F_{\mu\nu}F^{\mu\nu}) = -\frac{1}{4}F_{\mu\nu}^a F^{a,\mu\nu} \quad (1.18)$$

into the Lagrangian. One can show the field strength tensor transforms as $F_{\mu\nu} \mapsto UF_{\mu\nu}U^\dagger$ and as such this term is gauge invariant.

The particles we have detected experimentally make up the Standard Model Lagrangian, which are listed along with how they transform under each symmetry in table 1.1. Writing down all possible renormalisable, gauge-invariant terms involving these particles make up the Standard Model Lagrangian. From now on in this thesis, we focus primarily on the electroweak sector of the Standard Model (i.e. $SU(2)_L \times U(1)_Y$).

However, there is a subtlety to this. Note that the fermions which appear in the SM are Weyl fermions (i.e. they have distinct anti-particles). Left- and right-

³Note in this example ϕ transforms in the fundamental representation and so the generators are simply the generators of the group. In general, however, one constructs the covariant derivative so that the generators are the generators of the group in the representation under which the field transforms.

	q_L	q_R	l_L	l_R	H
$SU(3)_c$	3	3	-	-	-
$SU(2)_L$	2	-	2	-	2
$U(1)_Y$	$\frac{1}{6}$	$\frac{1}{6} + \frac{\sigma_3}{2}$	$-\frac{1}{2}$	$\frac{1}{2} + \frac{\sigma_3}{2}$	$\frac{1}{2}$

Table 1.1: Table showing the gauge transformations of SM matter fields (quarks, q , leptons, l , and the Higgs boson, H) under the SM gauge group. Note there are three generations of quarks and leptons in the SM. For the non-abelian groups, the number shown is the dimension of the representation the field transforms in. In particular, the **2,3** are the fundamental representations of $SU(2)_L, SU(3)_c$ respectively. For the abelian group $U(1)_Y$ we give the charge of the field under this group. The subscripts R and L distinguish left- and right-handed fermion fields. The left-handed quarks can be split into up-type (u, c, t) and down-type (d, s, b) types as $q_L = (u_L, d_L)$. One for each generation. The leptons pair (e, μ, τ) with their corresponding neutrino ($\nu_{e, \mu, \tau}$) as $l_L = (\nu, e)$. We have also grouped the right-handed fermions into a ‘doublet’ form $q_R = (u_R, d_R)$ and $l_R = (0, e_R)$. However, we emphasise that *the right-handed particles transform as singlets under $SU(2)_L$ and grouping them as above is simply for notational convenience* and not to do with their transformation under $SU(2)_L$. The $\sigma_3 = \text{Diag}(1, -1)$ is the third Pauli matrix. The hypercharge of, for example, the right-handed down quark is from extracting the lower component from $(\sigma_3 q_R)$, $1/6 + (-1)/2 = -1/3$.

handed fermions transform differently under the $SU(2)_L$ gauge group. For example, the left-handed fermion doublet q_L transforms in the following way under $SU(2)_L$ group action:

$$SU(2)_L : q_L = \begin{pmatrix} u_L \\ d_L \end{pmatrix} \mapsto U q_L, \quad (1.19)$$

where $U \in SU(2)_L$. Yet right-handed fermions u_R, d_R are $SU(2)_L$ singlets (i.e. they do not transform under $SU(2)_L$ action). Naively, we can write down a Dirac-type mass term for fermions of the form

$$m^2 \bar{\psi} \psi = \begin{pmatrix} \psi_R^\dagger & \psi_L^\dagger \end{pmatrix} \begin{pmatrix} \psi_L \\ \psi_R \end{pmatrix} = \psi_R^\dagger \psi_L + \psi_L^\dagger \psi_R \quad (1.20)$$

where $\bar{\psi} = \gamma^0 \psi^\dagger$. However, this term is clearly not $SU(2)_L$ invariant, as the left- and

right-handed components mix. Note that we can still write down a kinetic term,

$$i\bar{\psi}\not{D}\psi = i\bar{\psi}_L\not{D}\psi_L + i\bar{\psi}_R\not{D}\psi_R \quad (1.21)$$

where $\not{D} = \gamma^\mu D_\mu$ is the covariant derivative, which doesn't mix left and right-handed terms and so is gauge invariant.

The same argument applies for the leptons.

Fortunately, the Standard Model is still able to generate mass terms for the fermions through a mechanism known as Spontaneous Symmetry Breaking, which we will now introduce.

1.1.1 Spontaneous Symmetry Breaking

The Standard Model electroweak sector is a spontaneously broken Yang-Mills theory. It is based on the non-abelian $SU(2)_L \times U(1)_Y$ gauge symmetry, which breaks under the Higgs mechanism to $U(1)_{\text{em}}$. The field responsible for the symmetry breaking is the Higgs field H : a two-dimensional complex vector field that transforms as a doublet under $SU(2)$, and with hypercharge $Y = 1/2$. The scalar sector of the SM consists of the particles within the Higgs doublet and has the following Lagrangian:

$$\mathcal{L}_H = (D_\mu H)^\dagger (D^\mu H) - V(H^\dagger H). \quad (1.22)$$

The first term includes kinetic and gauge boson interactions, and the second term $V(H^\dagger H)$ is the potential of the Higgs. The covariant derivative D_μ is constructed from all groups the Higgs boson transforms under (see table 1.1):

$$D_\mu H = \partial_\mu H + i(gW_\mu^a T_F^a + g' B_\mu/2)H \quad (1.23)$$

where g is the coupling constant associated with the group $SU(2)_L$ and g' with $U(1)_Y$. The vector fields $W_\mu^{1,2,3}$ are the three gauge bosons of $SU(2)_L$ and B_μ the one gauge boson of $U(1)_Y$. Recall the $T_F^a = \sigma^a/2$ are the generators of the group $SU(2)_L$ in the fundamental rep. with σ^a the three Pauli matrices. Implicitly we have included the generator for $U(1)_Y$ as well, which is simply $1/2$.

The most general renormalisable potential we can write down is:

$$V(H^\dagger H) = -\mu^2 H^\dagger H + \lambda(H^\dagger H)^2, \quad (1.24)$$

with μ, λ free parameters. Notice if $\mu^2 < 0$, then this potential is minimal when $H^\dagger H = 0$, however, if $\mu^2 > 0$ then the potential is minimal when $H^\dagger H = \frac{\mu^2}{2\lambda}$. The latter is the case in the Standard Model and gives the Higgs boson what is known as a vacuum expectation value or vev which we denote $v = \sqrt{\frac{\mu^2}{\lambda}}$ wherein the vacuum the Higgs boson takes a non-zero value. There are infinitely many possible vacua for this potential. This can be seen by writing the Higgs doublet in terms of its constituent fields ϕ^a , $a = 1, 2, 3, 4$:

$$H \equiv \frac{1}{\sqrt{2}} \begin{pmatrix} \phi^1 + i\phi^2 \\ \phi^4 - i\phi^3 \end{pmatrix}, \quad (1.25)$$

where any $\phi_1^2 + \phi_2^2 + \phi_3^2 + \phi_4^2 = \frac{\mu^2}{\lambda}$ minimises the potential. All such possible vacua are connected by a gauge transformation, and so are equivalent. By convention and without loss of generality choosing only ϕ^4 to have a nonzero vev, which breaks electroweak symmetry to $U(1)_{\text{em}}$:

$$H = \frac{1}{\sqrt{2}} \begin{pmatrix} \phi^1 + i\phi^2 \\ (\mathfrak{h} + v) - i\phi^3 \end{pmatrix} \quad (1.26)$$

where we have redefined the field $\phi^4 \equiv \mathfrak{h} + v$ such that the field \mathfrak{h} now has a zero vacuum expectation value. This particle is commonly known as the Higgs scalar. The other fields, ϕ^1, ϕ^2, ϕ^3 we dub ‘Goldstone bosons’ [23, 24] although technically, the symmetries involved are gauged, therefore they are not true Goldstone bosons.

We can perform a gauge transformation which leaves the doublet with the following form in what is known as the unitary gauge:

$$H = \frac{1}{\sqrt{2}} \begin{pmatrix} 0 \\ \mathfrak{h} + v \end{pmatrix}. \quad (1.27)$$

Just as with the Dirac fermions, it was impossible to write down a gauge-invariant mass term for the Gauge bosons $W_\mu^{1,2,3}$. Now consider the Higgs kinetic term post symmetry breaking, evaluated at the vacuum

$$(D_\mu H)^\dagger (D^\mu H)|_{\eta=0} = \frac{1}{2} \left(\frac{gv}{2} \right)^2 (|W_\mu^+|^2 + |W_\mu^-|^2) + \frac{1}{2} \left(\frac{v\sqrt{(g^2 + g'^2)}}{2} \right)^2 |Z_\mu^0|^2 \quad (1.28)$$

$$\equiv \frac{1}{2} m_W^2 (|W_\mu^+|^2 + |W_\mu^-|^2) + \frac{1}{2} m_Z^2 |Z_\mu^0|^2 \quad (1.29)$$

where we have defined the fields

$$W^\pm \equiv \frac{1}{\sqrt{2}} (W_\mu^1 \pm iW_\mu^2) \quad (1.30)$$

$$Z_\mu^0 \equiv \frac{1}{\sqrt{g^2 + g'^2}} (gW_\mu^3 - g'B_\mu) \quad (1.31)$$

$$A_\mu \equiv \frac{1}{\sqrt{g^2 + g'^2}} (gW_\mu^3 + g'B_\mu) \quad (1.32)$$

which are the propagating fields, such that there are no mixed terms such as $\sim v^2 W^1 W^2$ in the Lagrangian. The gauge bosons now have masses $m_w = \frac{gv}{2}$ and $m_Z = \frac{v\sqrt{g^2 + g'^2}}{2}$ (as does the Higgs $m_h^2 = 2\lambda v^2$). This is the so-called Higgs mechanism: the Goldstone bosons have become the Longitudinal polarisations of the now massive W^\pm and Z bosons. Note A_μ here is the QED photon which remains massless.

Similarly, it is possible to write down Yukawa terms which generate a mass for the fermions. For the first-generation:

$$\mathcal{L}_Y^{\text{quarks}} = -y_d \bar{q}_L H d_R - y_u \bar{q}_L \tilde{H} u_R + h.c. \quad (1.33)$$

where $\tilde{H} = i\sigma^2 H^*$ and h.c. stands for hermitian conjugate. The y_u, y_d are up and down type Yukawa couplings. Writing down the Yukawa terms for the other two generations is completely analogous. For the leptons,

$$\mathcal{L}_Y^{\text{leptons}} = -y_e \bar{l}_L H e_R + h.c., \quad (1.34)$$

where y_e is the electron Yukawa coupling. Note there is only one term as neutri-

nos are massless in the Standard Model. Substituting in the Higgs doublet post-symmetry breaking eq. (1.27) and evaluating at the vacuum ($\mathfrak{h} = 0$), the Yukawa terms look like a Dirac mass term with,

$$m_f = \frac{1}{\sqrt{2}} y_f v. \quad (1.35)$$

Putting this all together, the SM Lagrangian is (without the QCD theta parameter)

$$\mathcal{L}_{\text{SM}} = -\frac{1}{4} G_{\mu\nu}^\alpha G^{\alpha,\mu\nu} - \frac{1}{4} W_{\mu\nu}^a W^{a,\mu\nu} - \frac{1}{4} B_{\mu\nu} B^{\mu\nu} \quad (1.36)$$

$$+ (D_\mu H)^\dagger (D^\mu H) - V(H^\dagger H) \quad (1.37)$$

$$+ i\bar{q}_L \not{D} q_L + i\bar{q}_R \not{D} q_R + i\bar{l}_L \not{D} l_L + i\bar{l}_R \not{D} l_R \quad (1.38)$$

$$- \left(Y_u \bar{q}_L \tilde{H} u_R + Y_d \bar{q}_L H d_R + h.c. \right) - \left(Y_l \bar{l}_L \tilde{H} e_R + h.c. \right). \quad (1.39)$$

where the first line has the kinetic terms for the gauge bosons: the gluons, and the electroweak gauge bosons in the form of eq. (1.18). The second line has the Higgs kinetic and potential terms. The third line has the kinetic terms for the fermions as eq. (1.21), and the fourth their couplings to the Higgs. Implicit is the sum over all generations of quarks and leptons.

Having solved the fermion mass problem by finding a Higgs-like boson at the LHC [25, 26], which also agrees well with experimental results so far [27, 28], one might be tempted to say that the electroweak sector is complete. However, the Higgs doublet as constructed in the SM is not the only choice for spontaneous symmetry breaking still consistent with experiment (see e.g. [18, 29, 30]). In this thesis, we are interested in classifying these choices and exploring how key experimental signals, still at low energies, may soon be able to narrow down the choices. To do this, we will find it useful to introduce Effective Field Theory (EFT) which will allow us to classify low energy signals in a (mostly) model independent way.

As a final aside in this section, later in this thesis, we will find it useful to

parameterise the Higgs doublet in polar coordinates as:

$$H = \frac{v+h}{\sqrt{2}} \mathbf{U} \begin{pmatrix} 0 \\ 1 \end{pmatrix}, \quad \mathbf{U} = e^{i\sigma_a \varphi^a / v}, \quad (1.40)$$

where the coordinates h, φ^a are not the same as \mathfrak{h}, ϕ^a but are related by a field-redefinition which leaves all physical observables invariant. Nevertheless, upon expanding \mathbf{U} ,

$$H = \frac{1}{\sqrt{2}} \begin{pmatrix} i\varphi^1 + \varphi^2 \\ (h+v) - i\varphi^3 \end{pmatrix} + \mathcal{O}((\varphi^a)^2), \quad (1.41)$$

which looks remarkably similar to eq. (1.26), but with corrections $\mathcal{O}((\varphi^a)^2)$. This is exactly as is required for a valid field redefinition as we will see. Furthermore, either parameterisation will excite the same particle from the vacuum as, e.g.,

$$\langle 0 | \mathfrak{h} | p \rangle = \langle 0 | h | p \rangle. \quad (1.42)$$

As a result, we can treat either particle as our Higgs boson.

1.2 Effective Field Theory

Effective theories underpin the study of physics. This is the reason why, for example, astronomers can study extragalactic solar systems without worrying about every individual rock which makes up each planet and moon.

Throughout physics, the key requirement for an effective description to be appropriate, is a separation of scales. The same is true of particle physics. If we assume that our current theory (the SM) is incomplete insofar as there are new,

undiscovered particles at a mass scale Λ much heavier than the electroweak scale v ,⁴

$$\Lambda \gg v, \tag{1.43}$$

then the SM is only valid at energy scales well below Λ (as such Λ is sometimes called a ‘cut-off’). At the energy levels of current generating scattering experiments, such as the LHC, we are far below the mass-shell of these new particles. Hence they only appear for a short time as virtual particles (and not as external particles), travelling only a short characteristic distance $1/\Lambda$ before decaying. However, their effects are not entirely invisible, and could still be measurable in low-energy observables.

If such heavy particles exist, when viewed at low energies (i.e. at the characteristic distances $1/v$ of current scattering capabilities) the non-local, virtual interactions of such particles look local. Given our low-energy, ‘local’ theory, we can build an effective Lagrangian (which is only valid for energies $\ll \Lambda$) by taking a Taylor expansion of the non-localities as a series of local operators. Denoting the local operators $Q_i^{(d)}$ which are built out of only SM particles, and required to obey the SM gauge group $SU(3)_c \times SU(2)_L \times U(1)_Y$, we obtain an effective Lagrangian of the form:

$$\mathcal{L}_{\text{EFT}} = \mathcal{L}_{\text{SM}} + \sum_{d=4}^D \sum_{i=1}^{n_d} \frac{C_i^{(d)}}{\Lambda^{d-4}} Q_i^{(d)}. \tag{1.44}$$

The $C_i^{(d)}$ are known as Wilson coefficients; d is the integer mass dimension of terms appearing in the operators $Q_i^{(d)}$. n_d is the number of effective operators at dimension d , where i runs over each of these operators. D is the highest dimension operator of the EFT. In principle, taking $D \rightarrow \infty$ recovers the full theory with only SM particles (i.e. wlight particles) as the external states. In practice, taking D to be finite gives an approximation, valid to order $\sim 1/\Lambda^{D-4}$. This EFT is known as the Standard Model EFT or SMEFT.

The approach from Eq. (1.44) to EFTs is (mostly) model independent: the

⁴Strictly speaking, we also make the assumption that no new particles exist at energy levels below Λ which indeed may not be the case. However, we will also make the assumption that if such particles do exist their effects are likely to be minimal, otherwise we would have expected to have already detected them.

Wilson coefficients $C_i^{(d)}$ are left arbitrary, to be constrained by experiment. But they are theory dependent - we may compare the Wilson coefficients from a given theory to experimental data to place bounds on which models might be allowed in nature.

1.2.1 The Decoupling Theorem

A key assumption in the construction of EFTs is that the operator expansion is converging below the cutoff. In SMEFT this is enforced by explicitly suppressing each term by powers of a heavy mass scale Λ . Here we shall see why this approach is not just an arbitrary choice but is motivated in field-theory by the decoupling theorem.

The decoupling theorem [31] explores the infrared behaviour of gauge theories.

In the original paper, Appelquist and Carazzone considered the following scenario: a set of massless gauge fields $A_{\alpha,\mu}(x)$ coupled to a set of massive spin- $\frac{1}{2}$ fields (fermions) $\Psi_n(x)$ with the following Lagrangian:

$$\mathcal{L}(x) = -\frac{1}{4}F_{\alpha\mu\nu}F_{\alpha}^{\mu\nu} - \bar{\Psi}\gamma_{\mu}D^{\mu}\Psi - \bar{\Psi}m\Psi - \delta m\bar{\Psi}\Psi, \quad (1.45)$$

where

$$F_{\mu\nu}^a = \partial_{\mu}A_{\nu}^a - \partial_{\nu}A_{\mu}^a - gf^{abc}A_{\mu}^bA_{\nu}^c, \quad (1.46)$$

$$(D_{\mu}\Psi)_n = \partial_{\mu}\Psi_n + i[T^a, A_{\mu}^a]_n. \quad (1.47)$$

and g is the coupling of the gauge group, and the quantity m is the mass of the heavy particles. The mass counterterm (from renormalisation) is explicitly included and is denoted as δm . This parameter is explicitly adjusted such that the one-particle-irreducible (1PI) fermion self-energy vanishes at the point $\not{p} = m$ at each order in perturbation theory. The conclusion of [31] is the following:

Take any 1PI Feynman diagram with external (light) vector mesons only but containing internal (heavy) fermions. When all external momenta (i.e. p^2) are small relative to m^2 , the diagram will be suppressed by some power of the mass m

compared to a diagram with the same number of external (light) vector mesons but without any internal (heavy) fermions or absorbed into renormalisation parameters of the low energy theory.⁵

This so-called ‘decoupling theorem’, while originally proven only for this particular (simple) theory, turns out to be very general. And, as mentioned, it is the principle by which we are able to suppress SMEFT by powers of Λ . This is because SMEFT is decoupling: all heavy physics above the scale Λ has been integrated out leaving only the SM fields. We are free to take the limit $\Lambda \rightarrow \infty$ to recover the SM Lagrangian.

Note, however, there is a caveat to the decoupling theorem. One must integrate out full representations in order for it to apply. By this we mean that if a low energy state in the IR (infrared) is part of a full representation where the rest of which has been integrated out, the theory is so-called ‘non-decoupling’. The symmetry in the IR is then realised non-linearly.

This is pointing strongly towards a key question about the electroweak sector. Whether the broken symmetry group $SU(3)_c \times U(1)_{\text{em}}$ with electroweak symmetry realised non-linearly is a result of either:

- Standard Model-style symmetry breaking of the form $SU(3)_c \times SU(2)_L \times U(1)_Y \rightarrow SU(3)_c \times U(1)_{\text{em}}$ caused by the Higgs doublet taking a non-zero vev.
- Some decoupling new physics, which spontaneously breaks the symmetry, and gives rise to a scalar Higgs-like boson.
- Some non-decoupling new physics spontaneously breaks the symmetry, and gives rise to a scalar Higgs-like boson.

Only the first two of these can be adequately captured by SMEFT. We require a new, more general EFT which can capture these non-decoupling effects. This is known as Higgs EFT or HEFT.

⁵This paragraph is strongly paraphrased from the original paper [31] for clarity.

1.2.2 HEFT

The most general⁶ leading-order (LO) EFT Lagrangian with $SU(3)_c \times U(1)_{\text{em}}$ linearly and electroweak symmetry non-linearly realised we can write down is

$$\mathcal{L}_{\text{HEFT}} = -\frac{1}{4}G_{\mu\nu}^\alpha G^{\alpha,\mu\nu} - \frac{1}{4}W_{\mu\nu}^a W^{a,\mu\nu} - \frac{1}{4}B_{\mu\nu}B^{\mu\nu} \quad (1.48)$$

$$+ \frac{1}{2}\partial_\mu h \partial^\mu h + \frac{v^2 F(h)^2}{4} \text{Tr}[D_\mu \mathbf{U} D^\mu \mathbf{U}^\dagger] - V(h) \quad (1.49)$$

$$+ i\bar{q}_L \not{D} q_L + i\bar{q}_R \not{D} q_R + i\bar{l}_L \not{D} l_L + i\bar{l}_R \not{D} l_R \quad (1.50)$$

$$- \frac{v}{\sqrt{2}} (\bar{q}_L \mathbf{U} \mathcal{Y}_q(h) q_R + h.c.) - \frac{v}{\sqrt{2}} (\bar{l}_L \mathbf{U} \mathcal{Y}_l(h) l_R + h.c.). \quad (1.51)$$

Summation over all generations of fermions is implied, and the QCD theta term and neutrino mass terms are not included. The complete NLO HEFT Lagrangian along with the inclusion of these missing terms can be found in [33], along with a more detailed derivation of eq. (1.48).

There are many things to unpack here. First of all, the familiar terms from the SM: the first line being the kinetic terms of the gauge bosons, the third line being the kinetic terms for the fermions.

The Higgs field, h ,⁷ which we identify as the experimentally detected neutral scalar particle of mass 125 GeV, transforms as a singlet under the non-linear electroweak symmetry realisation. The Lagrangian has been canonically normalised such that the coefficient of the Higgs kinetic term is 1/2.

On the fourth line, the Yukawa couplings have been promoted to functions of h ,

$$\mathcal{Y}_q(h) = \text{Diag}(Y_u(h), Y_d(h)) \quad \mathcal{Y}_l(h) = \text{Diag}(0, Y_e(h)) \quad (1.52)$$

where $Y_i(h)$ is a (3×3) matrix running over each generation of fermion. Setting $Y_i(h=0)$ recovers the i^{th} fermion mass. The \mathbf{U} is a unitary matrix which contains the Goldstone bosons and has some subtleties involved.

⁶There is disagreement about this, boiling down to the difficulty in choosing an appropriate power counting for HEFT. See e.g. [32].

⁷Note this is a different field to \mathfrak{h} before in e.g. eq. (1.26), though we identify them both with the ~ 125 GeV neutral scalar particle found at the LHC. In the cases of SMEFT or the SM, h can be reached from \mathfrak{h} by a field redefinition.

We can describe the Goldstone bosons as a dimensionless unitary matrix transforming under the global custodial symmetry group $SU(2)_L \times SU(2)_R$:

$$\mathbf{U}(x) = e^{i\sigma_a \varphi^a(x)/v} \quad \mathbf{U}(x) \mapsto L\mathbf{U}(x)R^\dagger \quad (1.53)$$

where L, R are the $SU(2)_{L,R}$ transformations. The Goldstone covariant derivative is given by

$$D_\mu \mathbf{U}(x) = \partial_\mu \mathbf{U}(x) + ig \frac{\sigma_a}{2} W_\mu^a \mathbf{U}(x) - \frac{ig'}{2} B_\mu \mathbf{U}(x) \sigma_3 \quad (1.54)$$

which transforms as $D_\mu \mathbf{U} \mapsto L(D_\mu \mathbf{U})e^{-i\sigma_3 \theta_3/2}$. The custodial symmetry is broken to $SU(2)_L \times SU(2)_R \rightarrow SU(2)_V$ by gauging the hypercharge symmetry $U(1)_Y$ contained in $SU(2)_R$ and the fermion mass splittings. To break the symmetry explicitly, we need to include another operator with the kinetic term

$$\mathcal{L}_{\mathcal{C}} = c_T \frac{v^2}{8} \text{Tr}(\mathbf{T} \mathbf{U} D_\mu \mathbf{U}^\dagger) \text{Tr}(\mathbf{T} (D^\mu \mathbf{U}) \mathbf{U}^\dagger) \quad (1.55)$$

where $\mathbf{T} = \mathbf{U} \sigma_3 \mathbf{U}^\dagger$ is not invariant under $SU(2)_R$ and is sometimes called a custodial breaking spurion. The coefficient c_T is, however, strongly bounded $c_T \leq 10^{-2}$, which means assuming custodial symmetry is often a good approximation.

It will be convenient to parameterise the Goldstone matrix U by

$$\mathbf{U} = \frac{i}{v} \sigma_a \varphi^a + \sqrt{1 - \frac{\varphi^2}{v^2}}, \quad (1.56)$$

where $\varphi^2 = \varphi^a \delta_{ab} \varphi^b$ for $a = 1, 2, 3$ and φ^a are now the Goldstone fields. The ungauged Goldstone kinetic term is:

$$\frac{v^2}{4} \text{Tr}[\partial_\mu \mathbf{U} \partial^\mu \mathbf{U}^\dagger] = \frac{1}{2} \left(\partial_\mu \varphi^a \delta_{ab} \partial^\mu \varphi^b + \frac{(\varphi^c \delta_{ca} \partial_\mu \varphi^a)(\varphi^d \delta_{db} \partial^\mu \varphi^b)}{v^2 - \varphi^2} \right) \quad (1.57)$$

$$= \frac{1}{2} \partial_\mu \varphi^a \left(\delta_{ab} + \frac{\varphi_a \varphi_b}{v^2 - \varphi^2} \right) \partial^\mu \varphi^b \quad (1.58)$$

$$= \frac{1}{2} \partial_\mu \varphi^a g_{ab}(\varphi) \partial^\mu \varphi^b, \quad (1.59)$$

we shall see later, the $g_{ab}(\varphi)$ here we can identify as a metric.

Finally, the function $F(h)$ encodes the couplings of the Higgs to the Goldstone bosons. It must have that $F(0) = 1$ but otherwise is a generic function of h . Indeed without the decoupling theorem in our tool belt, what we do not have now is a clear expansion parameter (recall in SMEFT we had $\sim E/\Lambda$). In this work, at times we will use the naive expansion:

$$F(h) = 1 + a\frac{h}{v} + b\frac{h^2}{v^2} + \dots \quad (1.60)$$

However, the HEFT expansion is much more subtle and indeed taking (a finite number of terms in) different expansions has been shown to yield different observable results [34]. We will discuss this in the following subsection.

1.2.3 Power Counting in HEFT

In order to make (many) physical predictions with HEFT, one must construct an expansion of operators in some small parameter. However, in order for such predictions to be physically meaningful one must first establish a hierarchy of the most physically relevant terms. This will mean it is possible to make approximate predictions taking only a finite number of terms from the expansion. Establishing the ordering of terms in the Lagrangian is what is known as ‘power counting’.

A simple theory which demonstrates this idea of power counting is Fermi theory where the heavy scale M_W which suppresses higher order terms. For example, the four-fermion interaction is a mass dimension-6 term which only appears in the effective description at low energies ($E \ll M_W$). It has a coupling proportional to the Fermi constant, $G_F = \frac{g^2}{4\sqrt{2}M_W^2}$, i.e. the W mass suppresses the coupling.

This same idea extends to the SMEFT. We work under the assumption that it is a weakly-coupled EFT, i.e. the Wilson coefficients are of order ~ 1 . The power counting is simply the canonical mass dimension of the operators in the expansion. As with Fermi theory, higher dimension operators are weighted by inverse scales of the heavy new physics scale Λ .

Strongly coupled theories, on the other hand, follow a different power counting. An example of this is Chiral Perturbation Theory (ChPT) of low energy QCD. Its

power counting follows Weinberg's approach based on renormalisation [35]. Consider what we will call the leading order Chiral Lagrangian:

$$\mathcal{L}_2 = \frac{f^2}{4} \text{Tr}(\partial_\mu U^\dagger \partial^\mu U), \quad (1.61)$$

where $U = e^{2i\Phi/f}$ is a dimensionless, unitary matrix containing the mesons in the matrix Φ , and f the meson decay constant. Notice this looks remarkably similar to the Goldstone kinetic term from eq. (1.48). Now at one-loop order, the meson loops bring with them factors of $(1/4\pi f)^n$ with e.g. for the pions $4\pi f_\pi \sim 1.2$ GeV, and polynomial factors of the loop momenta p^n , stemming from derivative couplings. These loops require renormalising: the four-derivative ChPT operators act as the counter-terms to the two derivative ChPT operators. This provides an iterative basis to organise the expansion: each order must contain at least the operators required to act as counter-terms for the preceding order. This is why we previously called eq. (1.61) the leading order term.

Ultimately, HEFT may be strongly-coupled (e.g. composite Higgs models) or weakly-coupled (e.g. SMEFT theories, or some Loryons [18]). Remaining ambivalent as to which leads to the ambiguity in its power counting. One must therefore consider it as a fusion of power countings. The Goldstone bosons and the Higgs both follow enter the Lagrangian in dimensionless functions similarly to the pions, and so follow a ChPT-like power counting. The remaining longitudinal components of the gauge bosons, and the fermions follow a SMEFT-like power counting. The LO HEFT Lagrangian, therefore, contains terms with up to four derivatives (from the gauge boson kinetic terms) and yet some two-derivative operators are relegated to NLO [33].

Naive Dimensional Analysis (NDA) provides a formula to keep track of the many pieces at play. Following [32], if Λ is the cutoff of the EFT then the terms are normalised to the following formula:

$$\frac{\Lambda^4}{16\pi^2} \left[\frac{\partial_\mu}{\Lambda} \right]^{N_p} \left[\frac{4\pi\phi}{\Lambda} \right]^{N_\phi} \left[\frac{4\pi A}{\Lambda} \right]^{N_A} \left[\frac{4\pi\psi}{\Lambda^{3/2}} \right]^{N_\psi} \left[\frac{g}{4\pi} \right]^{N_g} \left[\frac{y}{4\pi} \right]^{N_y} \quad (1.62)$$

where ϕ represents both the Higgs and Goldstone bosons, ψ is a generic fermion,

A a generic gauge field, g a gauge coupling and y a Yukawa coupling. N_i , $i = p, \phi, \psi, A, g, y$ counts the number of insertions of the relevant piece. This formula ensures that operators belonging to higher-orders in the expansion are suppressed by powers of 4π respecting the normalisation of the Chiral sector, and powers of Λ from new physics contributions.

1.2.4 A Note on Renormalisability and EFTs

The Standard Model Lagrangian is obtained by restricting the dimensionality of operators to be ≤ 4 , out of a requirement of (power-counting) renormalisability. Having a renormalisable Lagrangian means that all UV divergences can be cancelled with a finite number n of counterterms. These must be fixed by n measurements, such that the theory will be predictive. However, by allowing these higher dimensional operators into the Lagrangian in e.g. eq. (1.44), we seem to have cast renormalisability and the prospect of a predictive theory aside: in attempting to renormalise the Lagrangian and remove UV divergences, we would expect to end up with infinitely many parameters to the theory, for which we will need infinitely many measurements to fix. Luckily, this is not a devastating problem. If we probe the EFT Lagrangian at an energy $E \ll \Lambda$, higher dimension terms will be suppressed relative to the lower dimension terms. If we ignore terms beyond some power of d in eq. (1.44), there will be a finite number of terms allowed to a given order in $1/\Lambda$ and hence a finite number of corrections necessary for renormalisation. And, as such, it is still possible to have an EFT which is (approximately - truncating at higher values of d allows for more precision) predictive.

These same arguments apply in HEFT, provided higher-dimensional operators in the expansion are subleading [36, 37].

1.3 Geometry of Scalar Particles

Many recent works [1, 2, 38–44] have considered treating scalar particles in terms of differential geometry. In particular, this approach has proved beneficial in the study of HEFT. First and foremost, however, we will discuss the geometric space in which

HEFT can be considered to reside.

Recall the scalar sector of the SM is considered to consist of the Higgs boson, and three Goldstone bosons.

We refer the reader to [39] for a more detailed derivation.

Note that in the literature, the HEFT and SMEFT Lagrangians are often referred to as the non-linear and linear Effective Field Theory Lagrangians, referring to how the scalar sector transforms under the $\mathcal{O}(4)$ custodial symmetry.

1.3.1 Summary of Differential Geometry

In this subsection, we will briefly review the necessary differential geometry for the remainder of this thesis. For a more complete and substantial overview of differential geometry, see [45].

We begin by identifying the metric in field-space. If we have some ‘coordinates’ on an n -dimensional space, which we will denote ϕ^i with $i \in \{0, \dots, n - 1\}$ that we identify with n scalar fields, then we can write down an infinitesimal distance-element ds on the space as the following

$$ds^2 = G_{ij}(\phi)d\phi^i d\phi^j \tag{1.63}$$

where we identify $G_{ij}(\phi)$ as the field-space metric, i.e. a rank 2 tensor field which satisfies the same properties as a normal metric, in that it is both

- Symmetric: $G_{ij} = G_{ji}$,
- Non-degenerate: in essence this is the requirement, if treating the metric as a matrix, that no complete rows or columns of the metric are zero. This follows from the requirement that the scalar fields are dynamical.

We can also construct the tangent vector field to the manifold. This is simply done by parameterising the field ϕ^i by some parameter t . We can define the components to the tangent vector field at the point p as

$$\Phi_p^i \equiv \frac{d\phi^i(t)}{dt}. \tag{1.64}$$

However, we have a complication here. Of course the field ϕ does not just depend on some single parameter t , but actually the set of space-time coordinates x^μ which themselves must obey the usual properties of general relativity. I.e. they also lie on a manifold in space-time which is distinct from the field-space manifold. So we generalise our tangent vector field from eq. (1.64) to the following

$$(\Phi_p^i)_\mu \equiv \frac{\partial \phi^i(x)}{\partial x^\mu}. \quad (1.65)$$

Under a field-space redefinition of the form $\phi^i = \phi^i(\tilde{\phi})$, the components of the tangent vector field transforms in the following way:

$$(\tilde{\Phi}_p^i)_\mu = (\Phi_p^j)_\mu \left(\frac{\partial \tilde{\phi}^i}{\partial \phi^j} \right) \quad \text{or} \quad \partial_\mu \tilde{\phi}^i = \left(\frac{\partial \tilde{\phi}^i}{\partial \phi^j} \right) \partial_\mu \phi^j \quad (1.66)$$

and the components of a 2-tensor ⁸ T^{ij} , such as the metric, transforms as

$$\tilde{T}^{ij} = \left(\frac{\partial \tilde{\phi}^i}{\partial \phi^k} \right) \left(\frac{\partial \tilde{\phi}^j}{\partial \phi^l} \right) T^{kl}. \quad (1.68)$$

We then want to write down an action, which we want to be invariant under

- 1 Lorentz transformations.
- 2 Space-time coordinate redefinitions.
- 3 Field-space redefinitions.

We are interested in only terms with two-derivatives as before, so combining the two objects we have (the metric and the tangent vector field) the action we *have* to write down is

$$S = \int d^4x \sqrt{|g|} \frac{1}{2} \partial_\mu \phi^i G_{ij}(\phi) \partial^\mu \phi^j. \quad (1.69)$$

⁸The full tangent vector field and 2-tensor including the basis are defined as

$$(\Phi_p)_\mu = \frac{\partial \phi^i(x)}{\partial x^\mu} \cdot \frac{\partial}{\partial \phi^i} \quad \text{and} \quad T = T^{ij} \frac{\partial}{\partial \phi^i} \frac{\partial}{\partial \phi^j} \quad (1.67)$$

respectively.

where the spacetime metric is $g_{\mu\nu}$ and $|g| = |\det(g_{\mu\nu})|$. Looking back at our list:

- 1 This action obeys Lorentz invariance, as we have summed over all Lorentz indices.
- 2 We can perform a space-time coordinate redefinition $x^\mu \rightarrow y^\mu(x)$ which will leave the action invariant as we have included the factor $\sqrt{|g|}$ (i.e. the metric of space-time).
- 3 Non-derivative field-space redefinitions (see section 1.5.2) of the form $\phi = \phi(\tilde{\phi})$ should leave the action invariant. Indeed they do as, using the chain rule,

$$S = \int d^4x \sqrt{|g|} \frac{1}{2} \partial_\mu \phi^i G_{ij}(\phi) \partial^\mu \phi^j \quad (1.70)$$

$$= \int d^4x \sqrt{|g|} \frac{1}{2} \partial_\mu \tilde{\phi}^k \frac{\partial \phi^i}{\partial \tilde{\phi}^k} G_{ij}(\phi(\tilde{\phi})) \frac{\partial \phi^j}{\partial \tilde{\phi}^l} \partial^\mu \tilde{\phi}^l \quad (1.71)$$

$$= \int d^4x \sqrt{|g|} \frac{1}{2} \partial_\mu \tilde{\phi}^k \tilde{G}_{kl}(\tilde{\phi}) \partial^\mu \tilde{\phi}^l \quad (1.72)$$

which is exactly as expected from the construction of the action.

From the above action, a field-space invariant path integral can also be constructed:

$$Z[0] = \int [d\phi] \sqrt{\det G(\phi)} e^{iS[\phi]}. \quad (1.73)$$

As usual, we can construct Christoffel symbols Γ and the Riemann tensor R for the manifold

$$\Gamma_{jk}^i = \frac{1}{2} G^{il} (\partial_j G_{kl} + \partial_k G_{lj} - \partial_l G_{jk}) \quad (1.74)$$

$$R_{ijkl}^i = \partial_k \Gamma_{lj}^i - \partial_l \Gamma_{kj}^i + \Gamma_{lj}^m \Gamma_{km}^i - \Gamma_{jk}^m \Gamma_{lm}^i \quad (1.75)$$

which will come in useful later.

We can also construct a geometric covariant derivative \mathcal{D} (technically \mathcal{D}_X where

$X = X^i \frac{\partial}{\partial \phi^i}$) whose components \mathcal{D}_i act on a scalar V as:

$$\mathcal{D}_i V = \partial_i V \quad (1.76)$$

$$\mathcal{D}_i \mathcal{D}_j V = \frac{\partial^2 V}{\partial \phi^i \partial \phi^j} - \Gamma_{ij}^k \frac{\partial V}{\partial \phi^k}. \quad (1.77)$$

1.3.2 Geometry and HEFT

Rewriting the (ungauged) scalar sector of eq. (1.48), we can see that its dynamics are captured by differential geometry.

Making use of the fact that $\mathcal{O}(4) \sim SU(2)_L \times SU(2)_R$, which is spontaneously broken from $\mathcal{O}(4) \rightarrow \mathcal{O}(3)$ in the gauged case, we can parameterise the Goldstone bosons into the unit 4-vector,

$$\mathbf{n} = \frac{1}{v} \begin{pmatrix} \varphi^1 \\ \varphi^2 \\ \varphi^3 \\ \sqrt{v^2 - |\varphi|^2} \end{pmatrix} \quad (1.78)$$

where $|\varphi|^2 = \varphi^a \varphi^a$, where the Higgs and Goldstones transform under the $\mathcal{O}(4)$ symmetry as

$$h \mapsto h \quad \mathbf{n} \mapsto \mathcal{O} \mathbf{n} \quad (1.79)$$

where $\mathcal{O} \in \mathcal{O}(4)$. Explicitly, the Goldstones are transforming non-linearly under the symmetry as a result of the fourth component of \mathbf{n} .

We can rewrite the ungauged kinetic part of the HEFT Lagrangian in this parameterisation as

$$\mathcal{L}_{G,\text{kinetic}} = \frac{v^2}{2} (\partial_\mu \mathbf{n}) \cdot (\partial^\mu \mathbf{n}) \quad (1.80)$$

$$= \frac{1}{2} (\partial_\mu \varphi^a) v^2 \left(\frac{\partial \mathbf{n}(\varphi)}{\partial \varphi^a} \right) \cdot \left(\frac{\partial \mathbf{n}(\varphi)}{\partial \varphi^b} \right) (\partial^\mu \varphi^b). \quad (1.81)$$

Were one to expand out the Lagrangian, one would find exactly the same result as using Weinberg's parameterisation. In going from the first to the second line we

have used that, via the chain rule,

$$\partial_\mu \mathbf{n} = (\partial_\mu \varphi^a) \frac{\partial \mathbf{n}(\varphi)}{\partial \varphi^a}. \quad (1.82)$$

From eq. (1.80) we can define the Goldstone metric as

$$g_{ab}(\varphi) \equiv v^2 \left(\frac{\partial \mathbf{n}(\varphi)}{\partial \varphi^a} \right) \cdot \left(\frac{\partial \mathbf{n}(\varphi)}{\partial \varphi^b} \right) \quad (1.83)$$

which is exactly the metric for the 3-sphere.

Extending to include the Higgs kinetic term as well,

$$\mathcal{L}_{\text{HEFT,kinetic}} = \frac{1}{2} \partial_\mu h \partial^\mu h + \frac{1}{2} F(h)^2 \partial_\mu \varphi^a g_{ab}(\varphi) \partial^\mu \varphi^b \quad (1.84)$$

$$= \frac{1}{2} \partial_\mu \phi^i G_{ij} \partial^\mu \phi^j \quad (1.85)$$

where $\phi = (h, \varphi^a)$ and $i = h, 1, 2, 3$. We can see that HEFT has the following metric on the manifold \mathcal{M} :

$$G_{ij} \equiv \begin{pmatrix} 1 & 0 \\ 0 & F(h)^2 g_{ab}(\varphi) \end{pmatrix}. \quad (1.86)$$

Comparing this with the Lagrangian (extracted from the integrand of the action) from eq. (1.69), in flat space-time we can identify: a 4-dimensional, real analytic field-space manifold \mathcal{M} , with coordinates on the manifold being the fields h, \mathbf{n} .⁹

It also helps to define an inverse metric G^{ij} using that $G^{ij} G_{jk} = \delta_k^i$ so we can raise and lower indices,

$$G^{ij} \equiv \begin{pmatrix} 1 & 0 \\ 0 & \frac{g^{ab}(\varphi)}{F(h)^2} \end{pmatrix}, \quad (1.87)$$

where $g^{ab} g_{bc} = \delta_c^a$.

Notice the top-right and bottom-left components of eq. (1.86) are zero. This is a result of the $\mathcal{O}(4)$ symmetry acting non-linearly on the Goldstones, but leaving the

⁹Note analyticity of the manifold is required such that it is possible to take power series expansions of the field. This is important such that limits of the field theory can be taken safely.

Higgs untouched.

The function $F(h)$ is heavily related to the curvature of the scalar manifold. The Christoffel symbols eq. (1.74), for example, are [41]:

$$\Gamma_{ab}^h = -F'(h)F(h)g_{ab}(\varphi) \quad (1.88)$$

$$\Gamma_{hb}^a = \Gamma_{bh}^a = \frac{F'(h)}{F(h)}\delta_{ab} \quad (1.89)$$

$$\Gamma_{bc}^a = \frac{\varphi_a}{v}g_{bc}(\varphi). \quad (1.90)$$

with all other components being zero and $F'(h)$ being a shorthand for $\partial F(h)/\partial h$.

Then the nonzero components of the Riemann tensor eq. (1.75)

$$R_{ahb}^h = -v^2F(h)F''(h)g_{ab}(\varphi) \quad (1.91)$$

$$R_{hhb}^a = \frac{F''(h)}{F(h)}\delta_{ab} \quad (1.92)$$

$$R_{abc}^c = -2 \left[1 - (vF'(h))^2 \right] g_{ab}(\varphi). \quad (1.93)$$

Looking at these, it is clearly useful to define what we will call ‘sectional curvatures’

$$R_h \equiv -\frac{F''(h)}{F(h)} \quad (1.94)$$

$$R_\varphi \equiv \frac{1}{(vF(h))^2} - \frac{(F'(h))^2}{F(h)^2}. \quad (1.95)$$

These will re-appear frequently.

1.3.3 Re-gauging the Symmetry

We have treated electroweak symmetry as global to derive the metric, and compute curvatures. It turns out in the high-energy scattering limit, this is a good approximation section 1.4. However, it is possible to re-gauge the theory following [39].

To do this, we need to relate the mathematics of symmetries in field-space to symmetries of the scalar manifold. Geometrically, symmetries must be captured by the metric: for example, if there is a rotational symmetry to the manifold, the metric should look identical as you rotate the manifold along the symmetry axis.

This we should formulate mathematically.

We begin by considering global symmetries on the manifold, then generalise to local symmetries later.

Global Symmetries

Consider a *flow* along the manifold. A flow is a single-parameter family of maps which give rise to streamlines on the manifold.¹⁰

We can identify a vector field which is the tangent to the streamlines at each point, which has the components

$$t^i = \frac{d\phi^i}{d\Theta}. \quad (1.96)$$

This vector field can also be thought of as generating a *flow* along the manifold. Infinitesimally, the flow generated by t^i is

$$\delta_\Theta \phi^i = \Theta t^i(\phi) + \mathcal{O}(\Theta^2). \quad (1.97)$$

The flow is said to be an *isometry* if the metric looks the same at each point along the flow line. If there are multiple isometries, we will label these by α . Then, mathematically, this means our α isometries must satisfy

$$\mathcal{L}_{t_\alpha} g = 0 \quad \text{or} \quad \mathcal{D}_i t_j + \mathcal{D}_j t_i = 0. \quad (1.98)$$

where \mathcal{L}_{t_α} is the Lie derivative for the vector t_α^i , and \mathcal{D}_i our usual geometric covariant derivative on the manifold.¹¹ This is the *Killing equation*, and t_α^i are *Killing vectors*.

Then the Killing vectors t_α^i of the manifold generate the infinitesimal field transformations

$$\delta_\theta \phi^i = \theta^\alpha t_\alpha^i(\phi) \quad (1.99)$$

¹⁰In particular, a flow along a manifold \mathcal{M} is single-parameter family of diffeomorphisms $\sigma_\theta : \mathcal{M} \rightarrow \mathcal{M}$ labelled by $\theta \in \mathbb{R}$. These maps have the properties: $\sigma_{\theta=0}$ is the identity map; and $\sigma_{\theta_1} \circ \sigma_{\theta_2} = \sigma_{\theta_1+\theta_2}$. Streamlines are the curves generated by the flow.

¹¹Note technically the Lie derivative of the potential must also vanish, i.e. $\mathcal{L}_{t_\alpha} V = 0$.

with θ^α being infinitesimal parameters. Then, using the chain rule, the components of the tangent vector field (or the gradient of ϕ^i) transform as

$$\delta_\theta(\partial_\mu\phi^i) = \theta^\alpha \left(\frac{\partial t_\alpha^i}{\partial\phi^j} \right) (\partial_\mu\phi^j). \quad (1.100)$$

Killing vectors form the symmetry algebra

$$[t_\alpha, t_\beta]^i = f_{\alpha\beta}^\gamma t_\gamma^i. \quad (1.101)$$

where the $[t_\alpha, t_\beta]^i$ is a Lie bracket which evaluates to

$$[t_\alpha, t_\beta]^i = t_\alpha^k \frac{\partial t_\beta^i}{\partial\phi^k} - t_\beta^k \frac{\partial t_\alpha^i}{\partial\phi^k}. \quad (1.102)$$

and $f_{\alpha\beta}^\gamma$ are structure constants of a Lie algebra, i.e. we can identify this with a Lie algebra as in eq. (1.5).

Ultimately, *the global symmetries of the scalar kinetic energy term are the isometries of the manifold.*

Local Symmetries

Generalising to local symmetries is as simple as replacing the infinitesimal parameters θ^α by functions of spacetime $\theta^\alpha(x)$

$$\delta_\theta\phi^i(x) = \theta^\alpha(x)t_\alpha^i(\phi(x)) \quad (1.103)$$

and the gauge covariant derivative on the manifold

$$(\mathbf{d}_\mu\phi(x))^i \equiv \partial_\mu\phi^i(x) + A_\mu^\beta t_\beta^i(\phi(x)) \quad (1.104)$$

where $A_\mu^\beta(x)$ is the gauge field associated with the Killing vector $t_\beta^i(\phi)$, into which we have absorbed a factor of i as well as the gauge coupling. The gauge covariant

derivative transforms as

$$\delta_\theta (d_\mu \phi)^i = \theta^\alpha(x) \left(\frac{\partial t_\alpha^i}{\partial \phi^j} \right) (d_\mu \phi)^j \quad (1.105)$$

and the gauge fields as

$$\delta_\theta A_\mu^\alpha = -\partial_\mu \theta^\alpha + f_{\beta\gamma}^{\alpha} \theta^\beta A_\mu^\gamma. \quad (1.106)$$

Now the gauged version of eq. (1.84) is just

$$\mathcal{L}_{\text{HEFT,kinetic}} = \frac{1}{2} d_\mu \phi^i G_{ij}(\phi) d^\mu \phi^j. \quad (1.107)$$

In the case of HEFT, $A_\mu^\alpha = \{W_\mu^I, B^\mu\}$ where $I = 1, 2, 3$. The associated Killing vectors which we quote here from [39] are

$$\frac{t_I^a}{v^2} = i \frac{g}{4} g^{ab}(\varphi) \text{Tr} \left(\mathbf{U} \frac{\partial \mathbf{U}^\dagger}{\partial \varphi^b} \sigma_\alpha \right) \quad \frac{t_Y^a}{v^2} = i \frac{g_Y}{4} g^{ab}(\varphi) \text{Tr} \left(\mathbf{U}^\dagger \frac{\partial \mathbf{U}}{\partial \varphi^b} \sigma_3 \right). \quad (1.108)$$

1.3.4 SMEFT as a Special Case of HEFT

SMEFT is a special case of HEFT in which electroweak symmetry is realised linearly. In the usual formulation of the SMEFT, this is clear to see as the Lagrangian is a gauge invariant analytic function of the Higgs doublet H . However, by taking a field-redefinition, it is possible to make the Lagrangian *look* like it realises the symmetry non-linearly. Contrastly, however, if there is no way to re-define the fields in your Lagrangian such that it is analytic in H at $H = 0$, then electroweak symmetry is non-linearly realised [46].

For example, take the SM case which is the low-energy limit in which the Goldstone bosons and Higgs re-form a multiplet and the curvature of the manifold becomes flat (i.e. if one were to calculate the Ricci scalar it would be zero):

$$F_{\text{SM}}(h) = F_{\text{flat}}(h) = 1 + \frac{h}{v}. \quad (1.109)$$

In this case, it is possible to re-write eq. (1.84) (and the Higgs potential) in terms

of the 4-vector

$$\phi = (v + h)\mathbf{n}(\varphi) \tag{1.110}$$

as

$$\mathcal{L}_{\text{SM, scalar}} = \frac{1}{2}\partial_\mu\phi \cdot \partial^\mu\phi - \frac{\lambda}{4}(\phi \cdot \phi - v^2)^2. \tag{1.111}$$

which, under a field-redefinition,

$$\phi \rightarrow \begin{pmatrix} \phi^1 \\ \phi^2 \\ \phi^3 \\ v + \mathfrak{h} \end{pmatrix} \tag{1.112}$$

looks exactly like the fields from the Higgs doublet eq. (1.22) but re-packaged in a 4-vector, allowed by the group symmetry $\mathcal{O}(4) \sim SU(2)_L \times SU(2)_R$. We can see this field now transforms linearly under the symmetry.

Furthermore, we will see that it is possible to map a HEFT Lagrangian onto a SMEFT in the case that an $\mathcal{O}(4)$ invariant fixed point exists on the scalar manifold. Therefore, we may write that:

$$\text{SM} \subset \text{SMEFT} \subset \text{HEFT}.$$

The case in which the electroweak EFT does not admit a linear representation we denote in this thesis $\text{HEFT} \setminus \text{SMEFT}$ where backslash is the mathematical symbol for the difference of sets. A schematic picture is displayed in fig. 1.1.

An $\mathcal{O}(4)$ Invariant Fixed Point

It is shown in [39, 41] that there exists a choice of coordinate system for a scalar manifold \mathcal{M} where the Higgs transforms linearly under the \mathcal{O} symmetry iff there also exists an $\mathcal{O}(4)$ invariant fixed point. This is as a result of the Linearisation Lemma, Coleman, Wess & Zumino [47]. More precisely, the result of the Linearisation Lemma

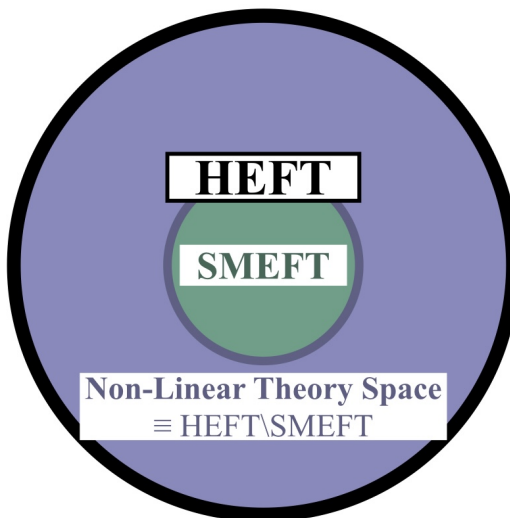


Figure 1.1: Visual depiction of the space of HEFT theories. There is some evidence for the boundary between non-linearly realised electroweak theories and SMEFT theories belonging to the former, see e.g. Ref. [6].

is that there exists a field redefinition in which the fields transform linearly under $\mathcal{O}(4)$ transformations in some representation of $\mathcal{O}(4)$ *if* there is an $\mathcal{O}(4)$ -invariant fixed point. As mentioned in [39], if this representation contains the 4-dimensional vector representation (eq. (1.112)), which in our case of a 4d manifold is generally true, then it is possible to combine the fields into the complex scalar doublet H as in eq. (1.26).

For example, in the case of the Standard Model, we see from eq. (1.111), the vector ϕ has the transformation property $O : \phi \mapsto O\phi$, $O \in \mathcal{O}(4)$ therefore the point $\phi = 0$ is an $\mathcal{O}(4)$ invariant fixed point. In such a case, it will be possible to write the HEFT Lagrangian in eq. (1.48) in terms of ϕ , i.e. as a SMEFT.

Furthermore, the reverse statement is clearly satisfied. If the coordinates ϕ form a multiplet and transform linearly under the action of the group $\mathcal{O}(4)$ then it is clear that the group action leaves the origin $\phi = 0$ invariant. I.e. the origin is the $\mathcal{O}(4)$ -invariant fixed point.

Note in theories without the custodial symmetry, the fixed point is instead $SU(2)_L \times U(1)_Y$ invariant.

As an aside, in general these field redefinitions can be hard to spot. A further use of the geometric formulation of HEFT is that geometry can tell you if a theory has

electroweak symmetry linearly or non-linearly realised, via a simple formula in [41].

1.4 Longitudinal Vector Boson Scattering Amplitudes

In the high-energy limit, the Goldstone boson that was eaten by a gauge boson during the Higgs mechanism (to become massive) will control the scattering of that gauge boson in its longitudinal polarisation state. Schematically this is shown in Fig. 1.2. Calculating scattering amplitudes of longitudinal gauge bosons is therefore an important test of the scalar sector.

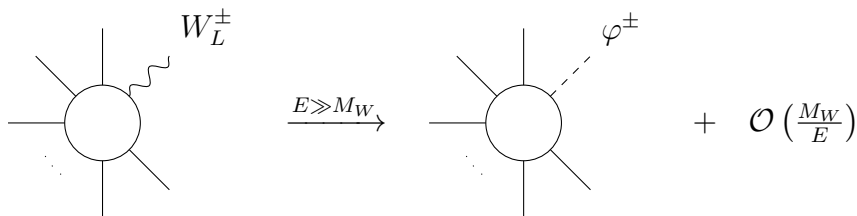


Figure 1.2: Schematic representation of the Equivalence Theorem [7–10]. The external longitudinal gauge boson e.g. W_L^\pm can be approximated to be its corresponding Goldstone boson φ^\pm in the high-energy scattering limit, i.e. if the characteristic energy E of the process is much greater than the gauge boson mass.

This is behaviour required by the equivalence theorem [7–10]: at an energy E much higher than the vector boson mass M , the leading order scattering amplitude of the (external) longitudinally polarised vector bosons on-shell, V_L , is given by the amplitude in which the on-shell vector bosons have been replaced by their corresponding Goldstone boson φ :

$$\mathcal{A}(V_L^a, V_L^b, \dots) \rightarrow \mathcal{A}(\varphi^a, \varphi^b, \dots) + \mathcal{O}\left(\frac{M_W}{E}\right).$$

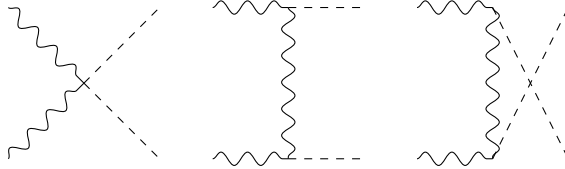
For example, this is $(\varphi^1 + i\varphi^2)/\sqrt{2}$ for the W^+ boson.

In particular, we are interested in the two scattering amplitudes $W_L^+ W_L^+ \rightarrow W_L^+ W_L$ and $W_L^+ W_L^- \rightarrow hh$, which pertain to the Higgs and Goldstone boson couplings. To do this, we begin by taking the expansion eq. (1.60) with the Goldstones packaged as in eq. (1.53). Keeping only the relevant parts of the HEFT Lagrangian

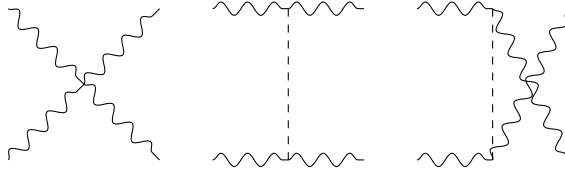
at high energy,

$$\mathcal{L} = \frac{1}{2} \partial_\mu h \partial^\mu h + \frac{1}{2} v^2 \left(1 + 2F'(0) \frac{h}{f} + (2F''(0) + F'(0)^2) \frac{h^2}{f^2} + \dots \right) \text{Tr} [\partial_\mu \mathbf{U}^\dagger \partial^\mu \mathbf{U}] \quad (1.113)$$

where we have Taylor expanded $F(h)$ about $h = 0$ to make the coupling terms more explicit. Note that again we have ignored the potential piece, as its contributions to amplitudes are subleading in the Mandelstam invariant $s \sim E_{\text{CM}}^2$ and therefore less relevant at high-energies.



(a) $W_L^+ W_L^- \rightarrow hh$



(b) $W_L^+ W_L^+ \rightarrow W_L^+ W_L^+$

Figure 1.3: Feynman diagrams contributing to tree-level scattering in the high-energy limit for the process $W_L^+ W_L^- \rightarrow hh$ in a), and $W_L^+ W_L^+ \rightarrow W_L^+ W_L^+$ in b). All external gauge boson snaking lines correspond to the appropriate W-boson. The dashed lines correspond to the Higgs boson.

The Feynman diagrams in Fig. 1.3 contribute towards the scattering amplitudes: $\mathcal{A}(W_L^+ W_L^+ \rightarrow W_L^+ W_L^+)$ and $\mathcal{A}(W_L^+ W_L^- \rightarrow hh)$ respectively at tree level. In the high energy limit, we have the following amplitudes as a result:

$$\mathcal{A}(W_L^+ W_L^+ \rightarrow W_L^+ W_L^+) = s \left[\frac{1}{F(h)^2} \left(\frac{1}{v^2} - (F'(h))^2 \right) \right]_{h=0} + \mathcal{O}(g^2, t/s) \quad (1.114)$$

$$\mathcal{A}(W_L^+ W_L^- \rightarrow hh) = s \left[\frac{F''(h)}{F(h)} \right]_{h=0} + \mathcal{O}(g^2, t/s) \quad (1.115)$$

where the s, t are Mandelstam invariants of the $2 \rightarrow 2$ scattering process, and particle

masses are neglected since $s \gg M_H^2, M_W^2$. Recall the R_h, R_φ defined from looking at the Riemann tensor eq. (1.94), evaluated at $h = 0$, are these same amplitudes:

$$\mathcal{A}(W_L^+ W_L^+ \rightarrow W_L^+ W_L^+) = sR_\varphi(0) + \mathcal{O}(g^2, t/s) \quad (1.116)$$

$$\mathcal{A}(W_L^+ W_L^+ \rightarrow hh) = -sR_h(0) + \mathcal{O}(g^2, t/s) \quad (1.117)$$

This is a very handy consequence of the geometric formulation of the scalar sector. It turns out (see chapter 2 and [41]) that taking geometric covariant derivatives of these curvatures give higher point amplitudes.

1.5 Effective Field Theory and the S-Matrix

The S-matrix¹² in quantum field theory is the operator which time-evolves an initial state particle into a final state:

$$\langle i|S|f\rangle \quad (1.118)$$

It is usually decomposed in the following way:

$$S = 1 + iT \quad (1.119)$$

where \mathcal{T} is known as the transfer matrix and relates the S-matrix to matrix elements \mathcal{M} .

$$\langle f|\mathcal{T}|i\rangle = (2\pi)^4 \delta^4(p_i - p_f) \mathcal{M}(i \rightarrow f) \quad (1.120)$$

The matrix elements \mathcal{M} we get from summing Feynman graphs and this tells you about transitioning from one particle to another. The identity element 1 is essentially requiring that if the initial and final states are exactly the same, there is always a Feynman graph you can write down where the particles do not interact. In which

¹²Different to the action also, confusingly, denoted as S . In section 1.5.2 we shall see how to compute matrix elements (i.e. components of the S-matrix) from the action.

case, the state must be left alone. We require that the S-matrix is unitary, i.e. that if we time-evolve two identical states identically, their norm must be preserved:

$$\langle p|S^\dagger S|p\rangle = \langle p|p\rangle. \quad (1.121)$$

which is equivalent to requiring conservation of probability.

There are many interesting properties of the S-matrix, such as [48]. In this work, we will consider the consequences of unitarity on the perturbative series (perturbative unitarity) which will place bounds on our theory as in [49]. We will also make use of the LSZ formula, which relates time-ordered scattering amplitudes with the path integral. These we introduce below.

1.5.1 Perturbative Unitarity

Consider the definition of the transfer matrix in eq. (1.122). Unitarity ($S^\dagger S = 1$) implies that

$$i(\mathcal{T}^\dagger - \mathcal{T}) = \mathcal{T}\mathcal{T}^\dagger. \quad (1.122)$$

Extracting a component of eq. (1.122) matrix for the states $|f\rangle, |i\rangle$, we can rewrite this in terms of a cross-section in the following method:

$$\langle f|\mathcal{T}\mathcal{T}^\dagger|i\rangle = \sum_X \int d\Pi_X \langle f|\mathcal{T}^\dagger|X\rangle \langle X|\mathcal{T}|i\rangle \quad (1.123)$$

$$= \sum_X (2\pi)^4 \delta^4(p_f - p_X) (2\pi)^4 \delta^4(p_i - p_X) \int d\Pi_X \mathcal{M}(i \rightarrow X) \mathcal{M}^*(f \rightarrow X) \quad (1.124)$$

where we have used the completion relation that $\sum_X |X\rangle \langle X| = \mathbb{I}$. This leaves us with the optical theorem for inelastic scattering:

$$\mathcal{M}(i \rightarrow f) - \mathcal{M}^*(f \rightarrow i) = i(2\pi)^4 \sum_X \int d\Pi_X \delta^4(p_i - p_X) \mathcal{M}(i \rightarrow X) \mathcal{M}^*(f \rightarrow X). \quad (1.125)$$

In the case where the initial and final states are the same, $|i\rangle = |f\rangle = |A\rangle$, where $|A\rangle$ is a two-particle state in the centre-of-mass frame,

$$2\text{Im}\mathcal{M}(A \rightarrow A) = \sum_X (2\pi)^4 (2\pi)^4 \delta^4(p_A - p_X) \int d\Pi_X |\mathcal{M}(X \rightarrow A)|^2 \quad (1.126)$$

$$= 2E_{CM} |\vec{p}_i| \sum_X \sigma(A \rightarrow X) \quad (1.127)$$

where E_{CM} is the centre of mass energy and \vec{p}_i the momenta of an initial state particle. In the second line, we have noticed the line above is exactly a sum over cross-sections $\sigma(A \rightarrow X)$. This is the optical theorem.

The optical theorem is a hugely powerful theorem, one consequence of which is perturbative unitarity which we will now consider.

Consider a two-to-two elastic scattering process in the centre of mass frame of the particles A and B , the optical theorem eq. (1.125) gives, noting that the initial and final states must be identical i.e. we require θ , the angle of one of the final-state particles to the incoming beam axis, to be zero

$$\text{Im}\mathcal{M}(AB \rightarrow AB, \theta = 0) = 2E_{CM} |\vec{p}_i| \sum_X \sigma_{\text{tot}}(AB \rightarrow X) \quad (1.128)$$

$$\geq 2E_{CM} |\vec{p}_i| \sigma_{\text{tot}}(AB \rightarrow AB) \quad (1.129)$$

Then the general cross-section for this process is given by the following formula,

$$\sigma_{\text{tot}}(AB \rightarrow AB) = \frac{1}{32\pi E_{CM}^2} \int d\cos\theta |\mathcal{M}(\theta)|^2. \quad (1.130)$$

If we decompose the amplitude into partial waves,

$$\mathcal{M}(\theta) = 16\pi \sum_{j=0}^{\infty} a_j (2j+1) P_j(\cos\theta) \quad (1.131)$$

where $P_j(\cos\theta)$ are the Legendre polynomials normalised such that $P_j(1) = 1$ and

$$\int_{-1}^1 P_j(\cos\theta) P_k(\cos\theta) d\cos\theta = \frac{2}{2j+1} \delta_{jk} \quad (1.132)$$

such that, when combining with eq. (1.130), we get the following formula

$$\sigma_{\text{tot}} = \frac{16\pi}{E_{\text{CM}}} \sum_{j=0}^{\infty} (2j+1) |a_j|^2 \quad (1.133)$$

and therefore, via eq. (1.128),

$$\sum_{j=0}^{\infty} (2j+1) \text{Im}(a_j) \geq \frac{2|\vec{p}_i|^2}{E_{\text{CM}}} \sum_{j=0}^{\infty} (2j+1) |a_j|^2. \quad (1.134)$$

This is a *partial wave unitarity bound*: it is saying that since $|a_j| \geq \text{Im}(a_j)$, we are essentially balancing two sides of an inequality.

We can further simplify eq. (1.128) for specific cases, which we do for those relevant to this work. Working in the high-energy limit such that we can neglect particle masses, $|\vec{p}_i| = E_{\text{CM}}/2$, if the total cross-section is well approximated by the elastic one, then:

$$\text{Im}(a_j) \simeq |a_j|^2, \quad (1.135)$$

therefore

$$0 \leq \text{Im}(a_j) \leq 1 \quad \text{and} \quad |\text{Re}(a_j)| \leq \frac{1}{2}. \quad (1.136)$$

If the scattering is not elastic we will have to take extra care.

The two relevant examples of perturbative unitarity bounds for this thesis are the following:

1 Elastic $W_L^+ W_L^+ \rightarrow W_L^+ W_L^+$

As the amplitude does not depend on the scattering angle θ , matching to eq. (1.131),

$$|a_0| = \frac{s |R_\varphi(0)|}{16\pi} \quad (1.137)$$

and all other $a_j = 0$ for $j > 0$. Around the energy scale $\sim v$ of current

scattering experiments, we get the following restriction on R_φ as

$$v|R_\varphi(0)|^{1/2} \leq 4\sqrt{\pi}. \quad (1.138)$$

2 Inelastic $W_L^+W_L^- \rightarrow hh$

For this now inelastic scattering process, we cannot use the optical theorem directly, but instead we can use the optical theorem for the process $W_L^+W_L^- \rightarrow W_L^+W_L^-$ i.e. from eq. (1.128),

$$\text{Im } \mathcal{M}(W_L^+W_L^- \rightarrow W_L^+W_L^-, \theta = 0) \simeq \quad (1.139)$$

$$2E_{\text{CM}}|\vec{p}_i| \left(\sigma_{W_L^+W_L^- \rightarrow W_L^+W_L^-} + \sigma_{W_L^+W_L^- \rightarrow hh} \right) \quad (1.140)$$

Using crossing symmetry,

$$\mathcal{M}(W_L^+W_L^- \rightarrow W_L^+W_L^-) = (s+t)R_\varphi(0) \quad (1.141)$$

where now t does indeed have dependence on θ a

$$t = -\frac{E_{\text{CM}}^2}{4} (1 + \cos \theta) = -\frac{s}{2} (1 + \cos \theta). \quad (1.142)$$

Denoting the partial wave coefficients from this elastic process as $a_{\text{elastic},j}$,

$$|a_{\text{elastic},0}| = \frac{s|R_\varphi(0)|}{32\pi} \quad (1.143)$$

$$|a_{\text{elastic},1}| = \frac{s|R_\varphi(0)|}{96\pi}, \quad (1.144)$$

with all others zero. We will also need the coefficients from the inelastic $W_L^+W_L^- \rightarrow hh$ process which we denote $a_{\text{inelastic},j}$ and identify the only one which is nonzero as

$$|a_{\text{inelastic},0}| = \frac{s|R_h(0)|}{16\pi}. \quad (1.145)$$

Then substituting the partial waves expansions into eq. (1.148) again,

$$\sum_{j=0}^{\infty} (2j+1) \operatorname{Im}(a_{\text{elastic},j}) = \frac{2|\vec{p}_i|}{E_{\text{CM}}} \sum_{j=0}^{\infty} (2j+1) \left(|a_{\text{elastic},j}|^2 + \frac{1}{2} |a_{\text{inelastic},j}|^2 \right), \quad (1.146)$$

where the factor $\frac{1}{2}$ of $|a_{\text{inelastic},j}|^2$ is as a result of the final state containing indistinguishable particles. We can focus individually on the j^{th} component [50] by considering scattering of only one angular momentum eigenstate, rather than a plane wave. This allows us to just consider, e.g., the zeroth component which gives the relevant bound in the high energy limit:

$$\operatorname{Im}(a_{\text{elastic},0}) = |a_{\text{elastic},0}|^2 + \frac{1}{2} |a_{\text{inelastic},0}|^2 \quad (1.147)$$

or,

$$\left(\frac{R_{\varphi}(0)_s}{16\pi} \right)^2 + \frac{1}{2} \left(\frac{R_h(0)_s}{8\pi} \right)^2 \leq 1. \quad (1.148)$$

To apply this result to the case of HEFT, we see that unitarity restricts its range of validity.¹³

1.5.2 LSZ Formula and Field-Redefinitions

We have, up to this point, hailed the path integral as being the holy grail of quantum field theory, and yet have demonstrated nothing of its usefulness. The LSZ reduction formula is one such use. A detailed derivation of the LSZ formula can be found in many textbooks (such as [51, 52]). We will review it in this subsection. The LSZ formula, as we shall see, is so powerful as it relates the path integral to time-ordered scattering amplitudes. These essentially assign a probability in a given theory for an external state $|i\rangle$ to, over time, evolve into an external state $|f\rangle$. In order to do this, we need both:

¹³Note that partial wave unitarity bounds also apply to SMEFT, restricting $E_{\text{CM}} < 4\sqrt{\pi}\Lambda$, however it already has a more stringent cutoff of Λ .

- Some idea of external and internal states. We know that external states, as they are free particles far from the interaction point, must be on-shell ($\vec{p}^2 = m^2$).
- (Time-ordered) correlation functions which can be thought of the overlap of the time-evolved initial state and the final state. The magnitude of this correlation gives the probability for $|i\rangle$ to have evolved into $|f\rangle$.

We begin by retrieving the appropriate correlation functions from the path integral.

Correlation Functions from the Path Integral

Following a similar derivation found in [53], recall the path integral eq. (1.11). If we add to it a source term J , for simplicity only considering one scalar field, η .

$$Z[J] \equiv e^{iW[J]} \equiv \int \mathcal{D}\eta e^{iS[\eta] + i \int d^4x \eta(x) J(x)} \quad (1.149)$$

From now on we will often use the simplified notation that $\eta(x) = \eta^x$, $J(x) = J_x$. The spacetime integral can be abbreviated as a sum over a dummy-index

$$\int d^4x J(x) \eta(x) = J_x \eta^x. \quad (1.150)$$

We can obtain time-ordered, n-point correlation functions in the presence of the source $\langle 0|T\{\eta(x_1) \dots \eta(x_n)\}|0\rangle_J = \langle \eta^{x_1} \dots \eta^{x_n} \rangle$ by taking functional derivatives with respect to the source term. For this reason it is known as the correlator generating functional:

$$\langle \eta^{x_1} \dots \eta^{x_n} \rangle_J \equiv \frac{1}{Z[J]} (-i)^n \frac{\delta^n Z}{\delta J_{x_1} \dots \delta J_{x_n}} = \frac{\int \mathcal{D}\eta e^{iS[\eta] + i\eta^x J_x} \eta(x_1) \dots \eta(x_n)}{\int \mathcal{D}\eta e^{iS[\eta] + i\eta^x J_x}}. \quad (1.151)$$

Then setting $J(x) = 0$ returns us the original theory

$$\langle \eta^{x_1} \dots \eta^{x_n} \rangle_{J=0} = \left(\frac{1}{Z[J]} (-i)^n \frac{\delta^n Z}{\delta J_{x_1} \dots \delta J_{x_n}} \right) \Big|_{J=0} = \frac{\int \mathcal{D}\eta e^{iS[\eta]} \eta(x_1) \dots \eta(x_n)}{\int \mathcal{D}\eta e^{iS[\eta]}}. \quad (1.152)$$

It turns out that the function $W[J]$, which was introduced in eq. (1.149), is the generating functional for connected amplitudes only,

$$\langle \eta^{x_1} \dots \eta^{x_n} \rangle_{J,\text{connected}} = (-i)^n \frac{\delta^n(iW)}{\delta J_{x_1} \dots \delta J_{x_n}}, \quad (1.153)$$

and taking the Legendre transformation of $W[J]$ yields the one-particle-irreducible (1PI) effective action, $\Gamma[\phi]$. This is the set of all diagrams which cannot be split into two diagrams (with one or more external legs) by cutting only one propagator. We will need these to construct amplitudes later. Notice the Legendre transform is a function of the fields $\phi(x)$ rather than $\eta(x)$,

$$\phi^x[J] \equiv \frac{\delta W}{\delta J_x} \propto \langle \eta^x \rangle_J \quad (1.154)$$

where the piece in brackets follows from eq. (1.153). Finally the Legendre transformation is defined as

$$\Gamma[\phi] \equiv W[J[\phi]] - \phi^x J_x[\phi]. \quad (1.155)$$

Then $i\Gamma[\phi]$ is the generating functional for the 1PI correlation functions:

$$\langle \eta^{x_1} \dots \eta^{x_n} \rangle_{J,1\text{PI}} = (-1)^n \frac{\delta^n(i\Gamma)}{\delta \phi(x_1) \dots \delta \phi(x_n)} \quad \text{for } n \geq 3. \quad (1.156)$$

The Two-Point Function

The connected two-point function is the propagator for an internal state:

$$D^{xy}[J] \equiv \langle \eta^x \eta^y \rangle_{J,\text{connected}} = -\frac{\delta^2(iW)}{\delta J_x \delta J_y} = -\left[\frac{\delta^2(i\Gamma)}{\delta \phi^x \delta \phi^y} \right]^{-1} \quad (1.157)$$

where taking $J = 0$ gives the propagator for the original field theory. The second equality in eq. (1.157) is a general property of the Legendre transformation. Taking the Fourier transform, we get the usual momentum-space 1PI propagator:

$$\int d^4x_1 d^4x_2 e^{ip_1x_1} e^{ip_2x_2} D^{x_1x_2}[J=0] = (2\pi)^4 \delta^4(p_1 + p_2) \Delta(p_1) \quad (1.158)$$

where

$$\Delta(p_1) = \frac{i}{p^2 - m^2 - \Sigma(p^2) + i\epsilon} \quad (1.159)$$

with $-i\Sigma(p^2)$ the 1PI two-point function.

Recall that external states were required to be on-shell, i.e. sitting directly at the pole of the propagator when $p_{\text{ext}}^2 = m_{\text{pole}}^2 = m^2 + \text{Re } \Sigma(m^2)$. Or,

$$\int d^4x e^{ip_{\text{ext}}x} \left. \frac{\delta^2 \Gamma}{\delta \phi^x \delta \phi^y} \right| = 0. \quad (1.160)$$

The LSZ Formula

Now that we have both ingredients (external states, and time-ordered correlation functions) we can derive the LSZ formula.

From the definition of an external state eq. (1.160), we would like to ‘pick out’ the on-shell component of the external states of our correlation functions. This is known as amputating the propagators, and the J-dependent amputated correlation functions are given by

$$\left(D_{x_1 y_1}^{-1} \right) \cdots \left(D_{x_n y_n}^{-1} \right) \langle \eta^{y_1} \cdots \eta^{y_n} \rangle_{J, \text{connected}}. \quad (1.161)$$

The momentum space amplitudes \mathcal{A} follow by taking the Fourier transform

$$(2\pi)^4 \delta^4(p_{\text{ext},1} + \cdots + p_{\text{ext},n}) i \mathcal{A}(p_{\text{ext},1}, \dots, p_{\text{ext},n}) = \quad (1.162)$$

$$\int \left[\prod_{i=1}^n d^4x_i e^{ip_{\text{ext},i}x_i} \right] (-i) \left(\left(D_{x_1 y_1}^{-1} \right) \cdots \left(D_{x_n y_n}^{-1} \right) \langle \eta^{y_1} \cdots \eta^{y_n} \rangle_{J, \text{connected}} \Big|_{J=0} \right), \quad (1.163)$$

which is the fabled LSZ formula. While here we have only considered the scalar field case, these same arguments generalise to bosonic and fermionic fields. See e.g. sec. 10 of [54].

It follows from here why field redefinitions must leave amplitudes invariant, which was the basis for geometric formulation of scalar particles section 1.3.1. This we will now show.

Field Redefinition Invariance

Consider a local field redefinition

$$\phi(x) = F[\phi'(x)] \quad (1.164)$$

where the field redefinition $F[\phi'(x)]$ can contain integer powers of $\phi'(x)$ and finitely many derivatives.

The new Lagrangian \mathcal{L}' is

$$\mathcal{L}[\phi(x)] = \mathcal{L}[F[\phi'(x)]] = \mathcal{L}'[\phi'(x)] \quad (1.165)$$

The path integral is now

$$Z'[J] = \int \mathcal{D}\phi' e^{i \int (\mathcal{L}'[\phi'] + J\phi')} = \int \mathcal{D}\phi e^{i \int (\mathcal{L}'[\phi] + J\phi)}. \quad (1.166)$$

where the integral in the exponent can be understood to be over the four usual space-time dimensions. Here, ϕ' is just a dummy integration variable so can be replaced by ϕ for free.

Comparing to the old path integral which, under the change of variables eq. (1.164), is

$$Z[J] = \int \mathcal{D}\phi' \left| \frac{\delta F}{\delta \phi'} \right| e^{i \int (\mathcal{L}'[\phi'] + JF[\phi'])} \quad (1.167)$$

where the Jacobian piece, $|\delta F/\delta \phi'| = 1$ in Dimensional Regularisation, except for the case of a fermionic chiral transformation in which case there is an anomaly [55]. Neglecting such anomalies, and returning the dummy variable to ϕ ,

$$Z[J] = \int \mathcal{D}\phi e^{i \int (\mathcal{L}'[\phi] + JF[\phi])} \quad (1.168)$$

We see that the only difference between $Z[J]$ and $Z'[J]$ is the source term:

$$\int JF[\phi] \quad \text{v.s.} \quad \int J\phi. \quad (1.169)$$

Following [56, 57], amplitudes following from the LSZ procedure do not care about this difference so long as

$$\langle p|F[\phi]|0\rangle \neq 0. \quad (1.170)$$

As such, a field-redefinition leaves the S-matrix and amplitudes invariant.

For a detailed derivation of how amplitudes transform under generic field-redefinitions (including e.g. derivatives), see [53].

1.5.3 Integrating Out a Particle

Beginning with an action S of heavy fields (Φ) and light (ϕ) fields (i.e. a UV complete model)

$$S_{\text{UV}}[\phi, \Phi] \quad (1.171)$$

we would like to obtain an ‘effective’ action of the light fields only

$$S_{\text{eff}}[\phi] \quad (1.172)$$

which only focuses on the relevant degrees of freedom, but nonetheless has limited validity. Writing this into the partition function,

$$Z = \int \mathcal{D}\phi \mathcal{D}\Phi \exp\{iS_{\text{UV}}[\phi, \Phi] + iJ_x \eta^x\} \quad (1.173)$$

$$= \int \mathcal{D}\phi \exp\{iS_{\text{eff}}[\phi] + iJ_x \eta^x\} \quad (1.174)$$

where J is again a source term which we shall set to zero later. We cannot, in general, exactly integrate out the field Φ , otherwise we would have already done it. But we can instead approximate the path integral.

At one-loop order, we can compute the effective action by the following method. First the EoM (equation of motion) for the heavy field (Φ_c) is given when

$$\frac{\delta S}{\delta \Phi}(\phi, \Phi_c[\phi]) = 0. \quad (1.175)$$

If we expand Φ about this minimum value $\Phi = \Phi_c + \eta$,

$$S[\phi, \Phi_c + \eta] = S[\Phi_c] + \frac{1}{2} \frac{\delta^2 S}{\delta \Phi^2} \Bigg|_{\Phi_{EoM}} \eta^2 + \mathcal{O}(\eta^3) \quad (1.176)$$

where the term $\mathcal{O}(\eta)$ disappears due to eq. (1.175). Then we can substitute this into eq. (1.173). We can freely shift the functional integration variables from $\mathcal{D}\Phi$ to $\mathcal{D}\eta$ as the function Φ_c is constant, and perform the integral to second order in η which leaves

$$\int \mathcal{D}\eta \exp(iS_{UV}[\phi, \Phi_c + \eta]) \approx \exp(iS[\phi, \Phi_c]) \left[\det \left(-\frac{\delta^2 S}{\delta \Phi^2} \Bigg|_{\Phi_c} \right) \right]^{-1/2} = \exp(iS_{\text{eff}}[\phi]) \quad (1.177)$$

from which we identify the standard result for the effective action

$$S_{\text{eff}} \approx S[\phi, \Phi_c] + \frac{i}{2} \text{Tr} \log \left(-\frac{\delta^2 S}{\delta \Phi^2} \Bigg|_{\Phi_c} \right) \quad (1.178)$$

where the first term is the tree-level result, and the second the one-loop result. This is known as the *background field method* as the light fields ϕ are held constant while integrating over Φ .

We will be interested in the one-loop result later in this thesis. Focusing on that piece for a moment, the Tr here is understood to be evaluated by inserting a complete set of momentum and spatial states

$$S_{\text{eff}}^{\text{one-loop}} = \frac{i}{2} \int d^4x \int \frac{d^4q}{(2\pi)^4} \text{tr} e^{iq \cdot x} \log \left(-\frac{\delta^2 S}{\delta \Phi^2} \Bigg|_{\Phi_c} \right) e^{-iq \cdot x} \quad (1.179)$$

where the remaining trace tr is a trace over internal indices, e.g. spin, gauge, etc.

Higher loops are generally computed using the covariant derivative expansion. It will also require careful treatment of renormalisation group running. The entire procedure is documented in detail in [58].

At times in this thesis, we will only be interested in the tree-level effective action at up to two-derivative order. In general, simply substituting Φ_c into S_{UV} will leave

us with non-local terms. However, following [41] we assume that S_{UV} nevertheless has a quasi-local derivative expansion

$$S_{\text{UV}}[\phi, \Phi] = S_{\text{UV}}^{(0)}[\phi, \Phi] + S_{\text{UV}}^{(2)}[\phi, \Phi] + \dots = \sum_{p=0}^{\infty} S_{\text{UV}}^{(2p)}[\phi, \Phi] \quad (1.180)$$

where $S_{\text{UV}}^{(2p)}$ is a local, analytic function of ϕ, Φ containing $2p$ derivatives. Additionally, writing the EoM for the heavy field as a derivative expansion

$$\Phi_c[\phi] = \sum_{k=0}^{\infty} \Phi^{(2k)}[\phi] \quad (1.181)$$

where, for example the zero-derivative term solves

$$\frac{\partial V}{\partial \Phi}(\phi, \Phi_c^{(0)}) = 0 \quad \text{where} \quad S_{\text{UV}}^{(0)} = - \int d^4x V \quad (1.182)$$

In principle, we can reconstruct $\Phi_c^{(2k)}$ by expanding order by order, but as we are only interested in two derivatives,

$$S_{\text{eff}}^{(0)}[\phi] + S_{\text{eff}}^{(2)}[\phi] = S_{\text{UV}}^{(0)}[\phi, \Phi_c^{(0)} + \Phi_c^{(2)}] + S_{\text{UV}}^{(2)}[\phi, \Phi_c^{(0)}] \quad (1.183)$$

$$= S_{\text{UV}}^{(0)}[\phi, \Phi_c^{(0)}] + \Phi_c^{(2)} \frac{\delta S_{\text{UV}}^{(0)}}{\delta \Phi}[\phi, \Phi_c^{(0)}] + S_{\text{UV}}^{(2)}[\phi, \Phi_c^{(0)}] + \dots \quad (1.184)$$

$$= S_{\text{UV}}^{(0)}[\phi, \Phi_c^{(0)}] + S_{\text{UV}}^{(2)}[\phi, \Phi_c^{(0)}] + \dots \quad (1.185)$$

where in the second line we have set $\delta S_{\text{UV}}^{(0)}/\delta \Phi = 0$ at the two-derivative order to zero using the EoM.

Therefore, at the two-derivative level at leading order, we can simply substitute the zero-derivative EoM into the original action to recover the effective action. This procedure is best illustrated with an example, which will aid to tie-together the topics covered in this chapter.

1.5.4 Example of Integrating Out a Particle

We conclude this chapter with an example of the procedure to integrate out a particle, leaving us with an EFT. This example, from [6, 41], shows this procedure and

how a UV model can realise electroweak symmetry either linearly or non-linearly, ultimately, as we will see, depending on a choice of the model parameters.

Our model is the Standard Model plus a singlet S with a Z_2 symmetry (i.e. $Z_2 : S \rightarrow -S$). The relevant UV Lagrangian is the following

$$\mathcal{L}_{\text{UV}} = (D_\mu H)^\dagger (D^\mu H) + \frac{1}{2} \partial_\mu S \partial^\mu S - V(H, S) \quad (1.186)$$

where the potential is

$$V(H, S) = -m_1^2 H^\dagger H - \frac{m_2^2}{2} S^2 - \frac{\tilde{\lambda}}{4} H^\dagger H S^2 + \frac{\lambda_S}{8} S^4 + \frac{\lambda_H}{2} (H^\dagger H)^2. \quad (1.187)$$

In particular, the new parameters m_1, m_2 are the masses of the Higgs doublet and new scalar respectively, and $\tilde{\lambda}, \lambda_S, \lambda_H$ are coupling constants. For all of these being positive, S and H will both get a vev. The mass of the Singlet S is useful to compute as well, i.e.

$$m_S^2 = \left. \frac{\partial^2 V}{\partial S^2} \right|_{S=v_s} = \lambda v_S^2 = 2 \left(\tilde{\lambda} \frac{v_H^2}{4} + m_2^2 \right) \quad (1.188)$$

where v_S, v_H are the vevs of S and H respectively. The zero-derivative EoM of S is the solution to eq. (1.182), i.e. the solution to

$$S \left(-m_2^2 - \frac{\tilde{\lambda}}{2} H^\dagger H + \frac{\lambda_S}{2} S^2 \right) = 0 \quad (1.189)$$

is, explicitly,

$$S_c^{(0)} = \sqrt{\frac{2}{\lambda_S} \left(m_2^2 + \frac{\tilde{\lambda}}{2} H^\dagger H \right)}. \quad (1.190)$$

This we can substitute directly into eq. (1.183) to find the two-derivative effective Lagrangian. We are interested only in the kinetic pieces here, although the potential pieces are also interesting to consider, which is done in detail in [41]. The relevant

term is

$$\frac{1}{2}\partial_\mu S\partial^\mu S \xrightarrow{S \rightarrow S_c^{(0)}} \frac{1}{2} \frac{\left(\frac{2}{\lambda_S} \left(\frac{\tilde{\lambda}}{2}\partial_\mu(H^\dagger H)\right) \frac{2}{\lambda_S} \left(\frac{\tilde{\lambda}}{2}\partial^\mu(H^\dagger H)\right)\right)}{\frac{2}{\lambda_S} \left(m_2^2 + \frac{\tilde{\lambda}}{2}H^\dagger H\right)} \quad (1.191)$$

leaving the effective Lagrangian to be

$$\mathcal{L}_{\text{eff}}^{(2)} = \frac{1}{4} \frac{\tilde{\lambda}}{\lambda_S} \frac{\partial_\mu(H^\dagger H)\partial^\mu(H^\dagger H)}{\left(m_2^2 + \frac{\tilde{\lambda}}{2}H^\dagger H\right)} + (D_\mu H)^\dagger(D^\mu H). \quad (1.192)$$

The question we must now ask is: does this Lagrangian realise electroweak symmetry linearly or non-linearly? It is still written in terms of the Higgs doublet H which might naively suggest linear. However, as mentioned, we require the Lagrangian to be an analytic function of H which might not be the case depending on the sign of m_2^2 . It will be illuminating to write the (ungauged) effective Lagrangian, using the polar parameterisation in eq. (1.40), in terms of h, \mathbf{U} :

$$\mathcal{L}_{\text{eff}}^{(2)} = \frac{1}{2} \left[1 + \frac{\tilde{\lambda}^2(v+h)^2}{\lambda_S(8m_2^2 + 2\tilde{\lambda}(v+h)^2)} \right] (\partial_\mu h\partial^\mu h) + \frac{(v+h)^2}{4} \text{Tr} [\partial_\mu \mathbf{U}^\dagger \partial^\mu \mathbf{U}]. \quad (1.193)$$

Then the sectional curvatures are

$$R_\varphi = \frac{\tilde{\lambda}^2}{8\lambda_S m_2^2 + \tilde{\lambda}(\tilde{\lambda} + 2\lambda_S)(v+h)^2} \quad (1.194)$$

$$R_h = \frac{8\tilde{\lambda}^2\lambda_S m_2^2}{\left(8\lambda_S m_2^2 + \tilde{\lambda}(\tilde{\lambda} + 2\lambda_S)(v+h)^2\right)^2}. \quad (1.195)$$

Indeed the two cases depending on the sign of the mass-squared m_2^2 yield the following results, with all other parameters positive:

$m_2^2 \gg 0$ In this case, the Lagrangian is SMEFT as it is analytic in $H^\dagger H$. We can see this explicitly by taking an expansion of eq. (1.192) in powers of $m_2^2 \gg v^2$:

$$\mathcal{L}_{\text{eff}}^{(2)} \sim \frac{1}{4} \frac{\tilde{\lambda}}{\lambda_S} \frac{1}{m_2^2} \partial_\mu(H^\dagger H)\partial^\mu(H^\dagger H) + (D_\mu H)^\dagger(D^\mu H) + \mathcal{O}(\text{dim-8}). \quad (1.196)$$

I.e. we have the original SM kinetic term for the Higgs doublet, with an additional dimension six, SMEFT operator. Indeed taking the decoupling limit, $m_2^2 \rightarrow \infty$, yields the SM Lagrangian and is well-behaved.

$m_2^2 \ll 0$ In the negative mass-squared case, the Lagrangian has a pole when $8m_2^2 = -2\tilde{\lambda}(v+h)^2$. Some ‘spurious’ singularities can be removed by a field-redefinition [41], but this pole cannot as indeed the sectional curvature R_φ which maps directly onto an amplitude also has a singularity. As a result, this manifold must belong to HEFT\SMEFT. We can also employ the aforementioned unitarity bounds. Recall this is the mass of the particle we integrate out. Now if we consider the simpler case of eq. (1.138), as generally both bounds are similar though eq. (1.138) slightly less restrictive,

$$v^2|R_\varphi(0)| = \frac{v^2\tilde{\lambda}^2}{\tilde{\lambda}^2v^2 + 4\lambda_S m_S^2} \leq 16\pi \quad (1.197)$$

Naively it looks like we can increase m_S to our heart’s content. However, notice that $m_S^2 = 2\left(\tilde{\lambda}\frac{v^2}{4} + m_s^2\right)$ and we must have $m_S^2 > 0$. Since $m_2^2 < 0$, in order to increase m_S one must increase $\tilde{\lambda}$. Unitarity bounds, however, computed by the same method as section 1.5.1 also restrict $\tilde{\lambda} \leq 8\pi$. It is not possible to simply increase the mass of the singlet indefinitely while keeping a consistent theory and thus it is *non-decoupling*.

$m_2^2 = 0$ In the massless case $m_2^2 = 0$ there is also a singularity at $h = -v$ where the curvature blows up, and is indeed itself in HEFT\SMEFT.

All this to say, one can see that by changing m_2^2 , one can vary between SMEFT and HEFT\SMEFT. We also see some evidence here that non-decoupling UV physics can result in a HEFT\SMEFT theory.

With this model, we have seen how even a simple new physics model can result in a non-linear realisation of electroweak symmetry. We have also seen how unitarity of the S-matrix restricts the model parameters. In the following section, making use of these same principles, we will see how amplitude space in the neighbourhood of the SM can provide us with hints towards a linear or non-linear realisation.

CHAPTER 2

Roads to the Standard Model

Experimental data collated and compared with predictions of theories of EWSB (electroweak symmetry breaking) has narrowed down the range possibilities; many a casualties lie indeed now discarded having been disproven by the progress in our measurements. The Higgs boson discovery, coming up on a decade old, was the main stroke in our map, subsequent data giving a profile that resembles the one heralded by the Standard Model (SM). Theory considerations have long pointed out the SM case for EWSB to be unstable under higher scale corrections and indicated that new physics should lie in wait at the electroweak scale. Whether these considerations should be revisited and our theory perspective profoundly changed, or if instead patience is all that is needed, the pressing question at present posed by experimental data is to characterize the theory ‘neighbourhood’ of the SM. The claim that one observes nothing but the SM at the LHC is indeed only as good our characterization of what else we could observe; it is here we find value in the aforementioned casualties. The aim in this work is to explore the consistent theory neighbourhood of the Standard Model.

A long known and studied approach, or ‘trajectory’, to the SM is a linearly realized Effective Field Theory (SMEFT), see [59] for a review, this road being pointed

at by the decoupling theorem [31] introduced in section 1.2.1. The integration of any heavy particle whose mass can be arbitrarily larger than the EWSB vev ($M > v$) in a perturbative linear realization will yield the SMEFT; supersymmetry or composite Higgs models fall into this category. Is this the only road to the Standard Model, i.e. are there other consistent limits to obtain the SM couplings for the known spectrum of elementary particles? As fundamental as this topic is, on its present formulation the candidate preceded the question; Higgs Effective Theory [60,61] is an EFT that encompasses the SMEFT but extends beyond it and might offer new roads. In HEFT, a linear realisation is not assumed (though admissible in certain limit) and is indeed the most general Lorentz and gauge invariant theory with the known spectrum of particles (which suggests it should be possible to formulate it in terms of amplitudes). The theories that this EFT describes but fall out of SMEFT, which will be called here non-linear theory space HEFT\SMEFT or simply non-linear EFTs¹, could contain a path to the SM other than via SMEFT. Recall this non-linear space is characterised as missing a point in field space which is left invariant under an $O(4)$ transformation [38,39] section 1.3.4, be it because it is not present or because the would be invariant point is singular [41]. The geometric formalism of HEFT section 1.3.1 was used to derive this result and also aids in exploring the properties of theories without field redundancies, as introduced in [38,39], and followed up in [40,41,62] - it is also adopted here. Some theories in HEFT\SMEFT non-linear space have been formulated while having a perturbative expansion [41]; they have been found to have a cut-off of $\sim 4\pi v$ and no limit can be taken within them that yields the SM. It has been suggested that *all* of this this non-linear space shares this property of a finite v -bound cut-off [46] with further evidence provided in [40], which means in turn that they all could be casualties of our exploration with present and future machines. This question has been explored so far with perturbative unitarity bounds, while here it is looked at with semi-classical arguments.

This chapter is structured as follows. Section 2.1 extends geometry from amplitudes as in section 1.4, and sec. 2.1.1 presents the basis in Riemann normal coor-

¹This terminology is used to imply that theories in non-linear space do not admit a linear representation. Note also, in other works these are called, with a slight abuse of notation, HEFT.

dinates; results which can also be found in [40] although are derived independently here. Section. 2.1.2 presents theory and experimental bounds on the curvature plane while 2.2 characterises SMEFT on this plane. In sec. 2.3, example models of linear and non-linear theory space are presented and characterised in the curvature plane. Sec. 2.4 presents theories in non-linear theory space arising from geometry rather than explicit models and finds candidate non-linear theories that seem to approach the SM. A semi-classical argument for the finite cut-off of theories in non-linear space is given in 2.5.

2.1 Geometry and Amplitudes

For simplicity, $O(4) \supset SU(2) \times U(1)$ invariance in the EWSB sector is assumed. We take the high energy limit and make use of the equivalence theorem. The Higgs singlet field is denoted h , and the Goldstones swallowed by the W and Z bosons as φ^a , $a = 1, 2, 3$.

Let us start by defining our geometry from the scattering-matrix S in order to depart from a common-place, basis-invariant magnitude in particle physics. Following the line-integral definition for general amplitudes valid also in the UV, we have ($S = 1 - i\mathcal{A}$):

$$-R_{h+h-} = \frac{1}{2\pi i} \oint \frac{1}{s_{12}^2} \mathcal{A}_{W_1^+ W_2^- \rightarrow hh} \quad (2.1)$$

$$-R_{+--+} = \frac{1}{2\pi i} \oint \frac{1}{s_{12}^2} \mathcal{A}_{W_1^+ W_2^+ \rightarrow W+W+} \quad (2.2)$$

$$-\nabla_h R_{+h-h} = \frac{1}{2\pi i} \oint \frac{1}{s_{12}^2} \mathcal{A}_{W_1^+ W_2^- \rightarrow hhh} \quad (2.3)$$

$$-\nabla_h R_{+--+} = \frac{1}{\pi i} \oint \frac{1}{s_{12}^2} \mathcal{A}_{W_1^+ W_2^+ \rightarrow W_3^+ W_4^+ h} \quad (2.4)$$

$$= \frac{1}{\pi i} \oint \frac{1}{s_{34}^2} \mathcal{A}_{W_1^+ W_2^+ \rightarrow W_3^+ W_4^+ h} \quad (2.5)$$

where $s_{ij} = (p_i + p_j)^2$. Indices in the Riemann tensor run through $h, a = 1, 2, 3$ and the \pm entries are given by contracting an a -index with the projector $(\delta_1^a \pm i\delta_2^a)/\sqrt{2}$,

for example

$$R_{h+h-} = R_{hahb} \frac{(\delta_1^a + i\delta_2^a)}{\sqrt{2}} \frac{(\delta_1^b - i\delta_2^b)}{\sqrt{2}} \quad (2.6)$$

While the above definition is useful to include UV models and derive positivity bounds [63], in practice we will work with the low energy EFT. In which case the correspondence is taking our geometry from the order $\mathcal{O}(s)$ coefficients in a Taylor expansion. What's more is they capture all terms to this order. Being explicit,

$$\mathcal{A}_{W_1^+ W_2^- \rightarrow hh} = -s_{12} R_{+h-h} \quad (2.7)$$

$$\mathcal{A}_{W_1^+ W_2^+ \rightarrow WW} = -s_{12} R_{+--+} \quad (2.8)$$

$$\mathcal{A}_{W_1^+ W_2^- \rightarrow hhh} = -s_{12} \nabla_h R_{+h-h} \quad (2.9)$$

$$\mathcal{A}_{W_1^+ W_2^+ \rightarrow W_3^+ W_4^+ h} = -\frac{s_{12} + s_{34}}{2} \nabla_h R_{+--+} \quad (2.10)$$

where we have neglected masses assuming $s \gg M_W^2, M_Z^2, m_h^2$.

This starting point makes evident that our tensor, R , and its derivatives are physical and field redefinition (coordinate) invariant. Even if intuitive, this last statement should be qualified. On the geometry side, having defined tensor entries rather than invariants, one has that these change under coordinate transformations - albeit with well defined properties. Recall (section 1.5.2) they are nonetheless the same for local (defined around the vacuum) transformations of our fields which leave the amplitudes the same [64]:

$$\hat{\phi}^i = \left(\delta_j^i + \sum_{k=1} c_j^k \phi^k \right) \phi^j \quad (2.11)$$

so that after quantization both fields produce a particle out of the vacuum,

$$\langle p | \phi^i | 0 \rangle = \langle p | \hat{\phi}^i | 0 \rangle \quad (2.12)$$

with $|p\rangle$ the state associated with the field. It is for this type of transformation that the S matrix will be left invariant, and tensors evaluated at the vacuum transform

trivially, since:

$$\left. \frac{\partial \phi^i}{\partial \hat{\phi}^j} \right|_{\phi=0} = \delta_j^i \quad (2.13)$$

Still, from where we stand the definition of Riemann tensor components in terms of amplitudes seems arbitrary and potentially inconsistent. So let us now turn to the Lagrangian theory which yields such relations.

2.1.1 Riemann Normal Coordinates

Take the metric that the Riemann tensor derives from in eqs. (2.1-2.5) as $G_{ij}(\phi)$, with $i, j = h, 1, 2, 3$, $\phi = (h, \varphi^a)$ $a = 1, 2, 3$. The amplitudes in eqs. (2.1-2.5) follow from the action

$$\begin{aligned} S &= \frac{1}{2} \int d^4x \partial_\mu \phi^i G_{ij} \partial^\mu \phi^j \\ &= \frac{1}{2} \int d^4x (\partial_\mu h \partial^\mu h + F(h)^2 g_{ab} \partial^\mu \varphi^a \partial_\mu \varphi^b) \end{aligned} \quad (2.14)$$

In matrix notation, our parametrization of the metric reads

$$G_{ij} = \begin{pmatrix} 1 & \\ & F^2 g_{ab} \end{pmatrix} \quad (2.15)$$

where off-diagonal entries are forbidden by symmetry and g_{ab} is the metric on the 3-sphere which we find useful to represent via the unit vector $u(\varphi)$:

$$g_{ab} = \frac{\partial u(\varphi)}{\partial \varphi^a} \cdot \frac{\partial u(\varphi)}{\partial \varphi^b} \quad u \cdot u = 1 \quad (2.16)$$

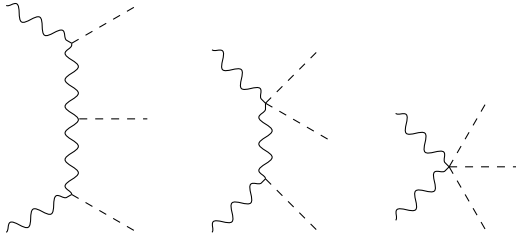


Figure 2.1: Diagrams for the $\mathcal{O}(s)$ contribution to the $WW hhh$ amplitude in the basis of eq. (2.14).

with u transforming as a vector under $O(4)$. It follows that the non-vanishing elements of the Riemann tensor and its first covariant derivative are

$$R_{abcd} = \left(\frac{1}{v^2} - (F')^2 \right) F^2 g_{a[c} g_{bd]} \quad (2.17)$$

$$R_{ahbh} = -F'' F \tilde{g}_{ab} \quad (2.18)$$

$$\nabla_h R_{ahbh} = F^2 \left(-\frac{F''}{F} \right)' g_{ab} \quad (2.19)$$

$$\nabla_h R_{abcd} = F^4 \left(\frac{1}{v^2 F^2} - \frac{(F')^2}{F^2} \right)' g_{a[c} g_{bd]} \quad (2.20)$$

$$\nabla_a R_{hbcd} = \frac{F^4}{2} \left(\frac{1}{v^2 F^2} - \frac{(F')^2}{F^2} \right)' g_{a[c} g_{bd]} \quad (2.21)$$

where prime denotes differentiation with respect to h and it is useful to define

$$R_h \equiv -\frac{F''}{F} \quad R_\varphi \equiv \frac{1}{v^2 F^2} - \frac{(F')^2}{F^2} \quad (2.22)$$

Verifying that these tensor entries appear as coefficients in the 4- and 5-point amplitudes is a matter of computing amplitudes: expanding our metric around the vacuum and adding over the various diagrams, e.g. see fig. 2.1 for those contributing to $WW \rightarrow hhh$, relations (2.1-2.5) are recovered. The $O(4)$ symmetry in our system reduces the number of independent components and amplitudes to R_h , R_φ and its derivatives.

Geometry does tell us however, that there is a frame where this computation is particularly simple: the frame where our coordinates follow geodesics, i.e. Riemann normal coordinates (RNC).

Let us then go into a brief outline of RNC. One can solve iteratively the Geodesic

equation:

$$\frac{d^2\phi^i}{d\sigma^2} + \Gamma_{jk}^i(\phi) \frac{d\phi^j}{d\sigma} \frac{d\phi^k}{d\sigma} = 0 \quad (2.23)$$

in an expansion which assumes the dependence on ϕ of Γ admits a Taylor expansion and introduces new coordinates ϕ' defined to second order as

$$\phi'^i = \phi^i + \frac{1}{2}\Gamma_{jk}^i(0)\phi^j\phi^k + \mathcal{O}(\phi^3)$$

Together with a metric in the new coordinates and to ϕ'^3 order [65]:

$$G(\phi')_{ij} = G(0)_{ij} + \phi'^k\phi'^l\frac{1}{3}R_{iklj} + \frac{1}{6}\phi'^k\phi'^l\phi'^m\nabla_m R_{iklj}$$

For concreteness, one can work out this transformation for our metric to find:

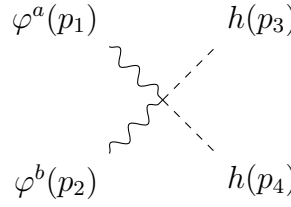
$$\begin{pmatrix} h' \\ \varphi' \end{pmatrix} = \begin{pmatrix} h - FF'\varphi^2/2 \\ \varphi^a + F'h\varphi^a/F + \Gamma_{bc}^a\varphi^b\varphi^c/2 \end{pmatrix} + \mathcal{O}(\phi^3)$$

The use of RNC is the reduction to parametrization independent magnitudes, i.e. Riemann tensor and its derivatives with the Christoffel symbols absent in our frame. In an analogy with general relativity, this is the free-falling frame where tidal effects reveal the geometry of the space-time manifold. In practice, there are no 3-point amplitudes ² and the interacting Lagrangian for 4-point reads:

$$\begin{aligned} \mathcal{L}_4^{\text{RNC}} = & \frac{1}{6}R_{hahb} (2h\partial h\varphi^a\partial\varphi^b - (\partial h)^2\varphi^a\varphi^b - h^2\partial\varphi^a\partial\varphi^b) \\ & + \frac{1}{6}R_{abcd}\partial\varphi^a\varphi^b\varphi^c\partial\varphi^d \end{aligned} \quad (2.24)$$

²They are reinstated however once we account for massive states.

The first line gives the Feynman rule



$$\frac{iR_{ahbh}}{3} \begin{pmatrix} (p_1 + p_2)(p_3 + p_4) \\ +2p_1p_2 + 2p_3p_4 \end{pmatrix}$$

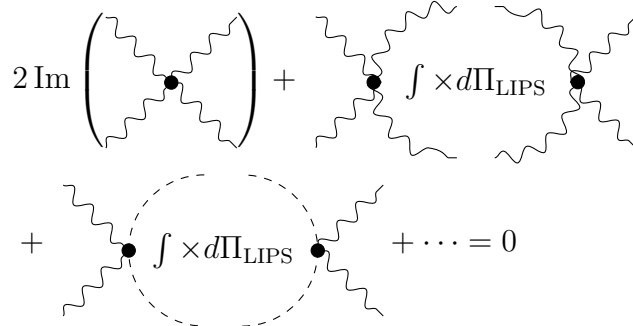
which evaluated on-shell is the sole diagram needed to compute $A_{WW \rightarrow hh}$ in this frame. For 5-point vertexes, we have

$$\begin{aligned} \mathcal{L}_5^{\text{RNC}} = & \frac{1}{12} (\nabla_h R_{\partial\varphi h h \partial\varphi} + \nabla_h R_{\partial h \varphi \varphi \partial h} + 2\nabla_h R_{\partial h \varphi h \partial\varphi}) \\ & + \frac{1}{12} (\nabla_h R_{\partial\varphi\varphi\varphi\partial\varphi} + 2\nabla_\varphi R_{\partial\varphi h \varphi \partial\varphi}) \end{aligned} \quad (2.25)$$

where the term $\nabla_\varphi R_{dh\varphi\varphi d\varphi}$ cancels due to the Riemann tensor asymmetry; and with abuse of notation $V_\varphi = V_a \varphi^a$, similarly for h . For the 5-point amplitude, again due to the absence of 3-point vertexes, evaluating the Feynman rule that follows from the 5-point action yields the result (i.e. in this frame there is only the last diagram in fig. 2.1 to compute). Amplitudes for six or more particles in total do require a sum over diagrams and contain, in addition, poles which nevertheless can be derived from lower-point amplitudes, see [40].

2.1.2 Experimental and Theory Constraints on Curvature

Unitarity constrains the magnitude of curvature, and its derivatives, for a given c.m. energy s , to the 4-point level. Symbolically



$$2 \text{Im} \left(\text{loop diagram} \right) + \text{tree diagram} \int d\Pi_{\text{LIPS}} + \text{tree diagram} \int d\Pi_{\text{LIPS}} + \dots = 0$$

where the first partial wave for W^+W^- gives, as we have computed in eq. (1.148),

$$\left(\frac{R_\varphi s}{16\pi}\right)^2 + \frac{1}{2}\left(\frac{R_h s}{8\pi}\right)^2 \leq 1 \quad (2.26)$$

where we have accounted for the amplitude being real. One can also select the W^+W^+ channel, but the emphasis in here is on bounds which are sensitive to both curvatures simultaneously which helps to better close some corners in the curvature plane.

One can use these constraints to determine the theory cut-off in terms of curvature; however, here we turn this around to note that given that we have explored energies up to $s \sim v^2$ and no new states have showed up, we can set an upper limit on curvature.

This limit is super-seeded by experimental bounds from LHC which bound Higgs couplings. In the conventional parametrization, one has:

$$F(h)^2 = 1 + 2a\frac{h}{v} + b\frac{h^2}{v^2} + \mathcal{O}(h^3) \quad (2.27)$$

which gives a curvature around the origin

$$v^2 (R_\varphi(0), R_h(0)) = (1 - a^2, -(b - a^2)) \quad (2.28)$$

itself related to amplitudes as, substituting (2.22,2.17,2.18) on (2.7,2.8),

$$\mathcal{A}_{W_1^+ W_2^+ \rightarrow WW} = s_{12} R_\varphi \quad (2.29)$$

$$\mathcal{A}_{W_1^+ W_2^- \rightarrow hh} = -s_{12} R_h \quad (2.30)$$

Translating bounds on the coefficients from present and future measurements into curvature, we present the plot in fig. 2.2. The value in both sets of constraints is to put into context how much of the theory-consistent curvature space have we explored experimentally.

From the outer-most to inner-most region of fig. 2.2: the (outer-most) grey region is excluded due to unitarity; up to the blue region is excluded by current LHC

bounds (the region is translated from bounds on a in [66], and b in [67]); finally, up to the green and orange (inner-most) regions we present expected exclusion limits for HL-LHC and FCC respectively. The projected bounds on R_φ, R_h are derived using sensitivity predictions of a (HL-LHC, [68]; FCC-ee, [69]); and b ([17] for both HL-LHC and FCC-hh), around their SM values. All uncertainties and projected sensitivities are displayed at the 95% confidence level; where multiple sensitivity estimates are given, the most conservative is selected. Note that HL-LHC bounds used here predate the LHC ones so that the seemingly marginal improvement is likely an underestimation.

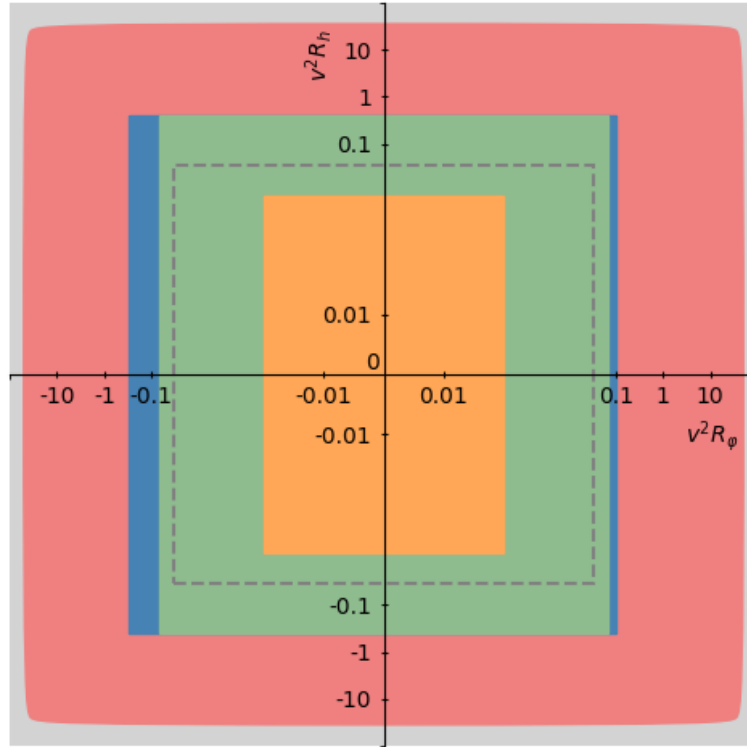


Figure 2.2: Theoretically (grey) and experimentally (up to blue) excluded (up to 95% confidence level) regions of the curvatures R_h, R_φ which are related to electroweak amplitudes as in eqs (2.30,2.29): and sensitivity limits of future colliders (HL-LHC, up to green; FCC, up to orange), also up to 95% confidence level. See text for detail. The plot scales linearly within the dashed box and logarithmically outside.

2.2 Correlation of curvature in SMEFT

In the linear realization and to first order (with our assumption of $O(4)$ invariance) we have:

$$R_\varphi = R_h \tag{2.31}$$

Which is to say the coefficients of s in the 4-point amplitudes for W^+W^+ scattering and $W^+W^- \rightarrow hh$ in eqs (2.30,2.29) are anti-correlated. Correlations do appear in the linear parametrization of SMEFT in HEFT [70] in line with what we find here, nonetheless in this section we go into some length of how this can be derived to display the utility of a geometric language.

A simple argument to show there is a correlation, if a bit more abstract, is to use Riemann normal coordinates and custodial symmetry around the $O(4)$ -symmetric point - which admits Cartesian coordinates. In this frame, the metric reads

$$G_{ij}(\phi) = \delta_{ij} + \frac{1}{3}R_{iklj}\phi^k\phi^l + \mathcal{O}(\phi^3) \tag{2.32}$$

and a linear realization of $O(4)$ symmetry dictates that the Riemann tensor be of the form $R(\delta_{il}\delta_{kj} - \delta_{kl}\delta_{ij})$, with a single unknown R . A transformation from Cartesian to polar coordinates then reveals $R_h = R_\varphi$.

The collapse of the two curvatures into a single one can also be derived matching the two EFTs:

$$\begin{aligned} \frac{(\partial h^2 + F^2\partial\varphi^2)}{2} = & K \left(\frac{H^\dagger H}{M^2} \right) (\partial H^\dagger H)^2 \\ & + G \left(\frac{H^\dagger H}{M^2} \right) D_\mu H^\dagger D^\mu H \end{aligned} \tag{2.33}$$

where it should be understood from a general SMEFT action, we transformed to a basis where the Higgs singlet is canonically normalized.

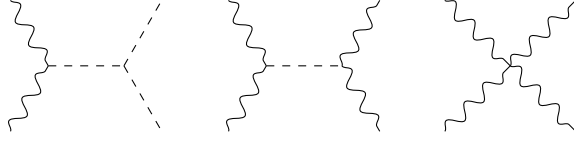


Figure 2.3: A selection of diagrams for the $WWhh$ and $WWWW$ amplitudes with the action in eq. (2.36)

This exercise yields, to order M^{-4}

$$R_\varphi = -3\frac{G'(0)}{M^2} + \frac{H^\dagger H}{M^4} \left(2(G'(0))^2 - \frac{5}{2}G''(0) \right) \quad (2.34)$$

$$R_h = -3\frac{G'(0)}{M^2} + \frac{H^\dagger H}{M^4} (4(G'(0))^2 - 5G''(0)) \quad (2.35)$$

which also reveals the correlation is lost at order M^{-4} .

Finally, and in a direct connection with observables, one can compute the amplitude which has been used to define our curvature, the computation itself getting rid of any field redundancy. Take the non-canonically normalized action

$$\mathcal{L} = \frac{1}{2} \frac{c_{H\Box}}{M^2} (\partial_\mu H^\dagger H)^2 + \frac{c_{HDD}}{M^2} H^\dagger H D_\mu H^\dagger D^\mu H \quad (2.36)$$

After normalization of the theory, computation of diagrams such as those shown in fig. 2.3, where we note that in this frame there is a h^3 coupling that scales with s and must be accounted for, yields

$$\mathcal{A}_{W^+W^+ \rightarrow W^+W^+} = \frac{s}{M^2} (c_{H\Box} - c_{HDD}) \quad (2.37)$$

$$\mathcal{A}_{W^+W^- \rightarrow hh} = -\frac{s}{M^2} (c_{H\Box} - c_{HDD}) \quad (2.38)$$

and hence the direct connection with SMEFT geometry as

$$(R_\varphi, R_h) = \frac{1}{M^2} (c_{H\Box} - c_{HDD}, c_{H\Box} - c_{HDD}) . \quad (2.39)$$

2.3 Models as Probes into HEFT

Recent study of EFT has shown that UV completion might impose extra constraints on an otherwise seemingly valid EFT, as is the case of positivity constraints [48]. It should be said that these constraints on the curvatures themselves R_h and R_φ do not restrict their sign, but reveal the need for doubly-charged states if the curvature is negative [63]. It is for these reasons that this section looks at models and introduces two new representations under $O(4)$ as

$$\mathbf{h} : 4 \text{ of } O(4) \tag{2.40}$$

$$\Phi : 9 \text{ of } O(4) \text{ (traceless symmetric)} \tag{2.41}$$

$$S : 1 \text{ of } O(4) \tag{2.42}$$

with the results of positivity constraints suggesting S and Φ will produce positive and negative curvature respectively. Note that \mathbf{h} is the Higgs doublet H in a real representation as

$$\left(\tilde{H}, H \right) = \hat{\sigma}_I \frac{\mathbf{h}^I}{\sqrt{2}} \tag{2.43}$$

with $\tilde{H} = \epsilon H^*$ and $\sigma^I = (\sigma^i, 1)$ with σ^i the Pauli matrices. We consider the addition of a 9 and a 1 separately with respective actions

$$\mathcal{L}_S = \frac{1}{2} D_\mu \mathbf{h}^T D_\mu \mathbf{h} + \frac{1}{2} (\partial S)^2 - V(\mathbf{h}, S^2) \tag{2.44}$$

$$\mathcal{L}_\Phi = \frac{1}{2} D_\mu \mathbf{h}^T D_\mu \mathbf{h} + \frac{1}{2} \text{Tr} (D_\mu \Phi D^\mu \Phi) - V(\mathbf{h}, \Phi) \tag{2.45}$$

The key distinction is whether $\langle \Phi \rangle = 0$ or not, which depends on the sign of its mass term and its mixing as induced by the potential.

2.3.1 Only h acquires a vev, SMEFT case

In this subsection we momentarily restrict the $O(4)$ symmetry to $SO(4)$ to allow for tri-linear couplings. First for the singlet S case, we take a potential as

$$V = -\frac{g_* m_S}{2} S \mathbf{h}^2 + \frac{m_S^2}{2} S^2 + \frac{m_{\mathbf{h}}^2}{2} \mathbf{h}^2 \quad (2.46)$$

extra terms allowed by the symmetry will give controlled corrections to the result and we neglect them. Integrating the field S at tree level returns

$$\mathcal{L}_{\text{eff}} = \frac{1}{2} \frac{g_* m_S}{2} \mathbf{h}^2 \frac{1}{\partial^2 + m_S^2} \frac{g_* m_S}{2} \mathbf{h}^2 \quad (2.47)$$

$$= \frac{g_*^2}{2} (H^\dagger H)^2 + \frac{g_*^2}{2m_S^2} (\partial(H^\dagger H))^2 + \mathcal{O}(\partial^4) \quad (2.48)$$

then via eq. (2.39)

$$(R_\varphi, R_h) = \left(\frac{g_*^2}{m_S^2}, \frac{g_*^2}{m_S^2} \right) \quad (2.49)$$

i.e. positive curvature for the singlet case, as expected.

Along the same lines, the potential for the symmetric representation is

$$V = -\frac{g_* m_\Phi}{2} \mathbf{h}^T \Phi \mathbf{h} + \frac{m_\Phi^2}{2} \Phi^2 + \frac{m_{\mathbf{h}}^2}{2} \mathbf{h}^2 \quad (2.50)$$

The integration now returns, to dimension six:

$$\begin{aligned} \mathcal{L}_{\text{eff}} &= \frac{g_*^2}{8} \text{Tr} \left[\left(\mathbf{h} \mathbf{h}^T - \frac{\mathbf{h}^2}{4} \right) \frac{m_\Phi^2}{\square + m_\Phi^2} \left(\mathbf{h} \mathbf{h}^T - \frac{\mathbf{h}^2}{4} \right) \right] \\ &= \frac{3g_*^2}{8} (H^\dagger H)^2 + \frac{g_*^2}{m_\Phi^2} \left(H^\dagger H D H^\dagger D H + \frac{(\partial H^\dagger H)^2}{8} \right) \end{aligned} \quad (2.51)$$

where $\square = D_\mu D^\mu$ and one has that the operator does yield negative curvature:

$$(R_\varphi, R_h) = \left(-\frac{3g_*^2}{4m_\Phi^2}, -\frac{3g_*^2}{4m_\Phi^2} \right). \quad (2.52)$$

2.3.2 Both Φ and \mathbf{h} break the symmetry, HEFT\SMEFT non-linearly realised theory space

As we will show, this case does not belong in SMEFT and stands as a representative of non-linearly realised electroweak theory space. We take the extension of a mexican hat potential for two fields as:

$$V(\Phi) = -\frac{\vec{m}^2}{2} \cdot \begin{pmatrix} \mathbf{h}^2 \\ \Phi^2 \end{pmatrix} + \begin{pmatrix} \mathbf{h}^2 \\ \Phi^2 \end{pmatrix}^T \frac{\lambda}{8} \begin{pmatrix} \mathbf{h}^2 \\ \Phi^2 \end{pmatrix} - \frac{\tilde{\lambda}}{8} \mathbf{h}^T \Phi \Phi \mathbf{h} + \frac{\tilde{\lambda}_\Phi}{8} \text{Tr}(\Phi \Phi \Phi \Phi) \quad (2.53)$$

with \vec{m}^2 a 2-vector and λ a 2×2 symmetric matrix. Since Φ acquires a vev, we take $\tilde{\lambda} > 0$ which triggers $O(4) \rightarrow O(3)$ and preserves custodial symmetry. Linear terms in the fields are absent, contrary to the previous case which since we restore $O(4)$ in place of $SO(4)$. The key question as will be shown is to consistently compute particle couplings and masses from an explicit potential.

The Goldstone boson Lagrangian and couplings to the radial singlet modes δh , $\delta\Phi$ read:

$$\mathcal{L} = \frac{1}{2} ((v_{\mathbf{h}} + \delta h)^2 + C_9(v_\Phi + \delta\Phi)^2) \frac{g_{ab}}{v^2} D^\mu \varphi^a D_\mu \varphi^b \quad (2.54)$$

where

$$C_9 = \frac{2 \times 4}{4 - 1}, \quad v^2 = v_{\mathbf{h}}^2 + C_9 v_\Phi^2, \quad \sin \beta = \sqrt{C_9} \frac{v_\Phi}{v}, \quad (2.55)$$

and

$$\langle \mathbf{h} \rangle = \begin{pmatrix} 0 \\ 0 \\ 0 \\ v_{\mathbf{h}} \end{pmatrix} \quad \langle \Phi \rangle = \frac{v_\Phi}{2\sqrt{3}} \begin{pmatrix} 1 \\ 1 \\ 1 \\ -3 \end{pmatrix} \quad (2.56)$$

the generalization of C_9 to $SO(N)$ being $C_{N(N+1)/2-1} = 2N/(N-1)$. Take the

mixing for the singlet radial modes $\delta\mathbf{h}$ and $\delta\Phi$ as (note that no other field in Φ or \mathbf{h} is a singlet of $SO(3)$ so we know these two only mix among each other):

$$\begin{pmatrix} \delta\mathbf{h} \\ \delta\Phi \end{pmatrix} = \begin{pmatrix} \cos\omega & -\sin\omega \\ \sin\omega & \cos\omega \end{pmatrix} \begin{pmatrix} h \\ \tilde{h} \end{pmatrix} \quad (2.57)$$

Putting the above back in the Lagrangian for the Goldstones and taking h to be the lightest singlet, one obtains in our basis of eq. (2.14,2.27)

$$a = c_\omega c_\beta + \sqrt{C_9} s_\beta s_\omega \quad b = c_\omega^2 + C_9 s_\omega^2 \quad (2.58)$$

Note that the limit of no mixing gives $b = 1$ and a parametrization of the curvature $R_h = -R_\varphi$ orthogonal to the SMEFT with a potential new road to the SM. The question to be answered is then: can one take $\omega = \beta = 0$ while keeping $m_{\tilde{h}} \gg m_h$ and maintaining perturbativity?

To answer this question we should express ω and β in terms of physical masses and couplings, then use eq. (2.28) to substitute and find curvature as a function of physical masses and couplings. In practice we have to solve for the potential. The value of the fields that minimize V can be read off after rearranging as

$$V(v_{\mathbf{h}}, v_\Phi) = \left(\vec{v}^2 - 2\hat{\lambda}^{-1}\vec{m}^2 \right)^T \frac{\hat{\lambda}}{8} \left(\vec{v}^2 - 2\hat{\lambda}^{-1}\vec{m}^2 \right) \quad (2.59)$$

with

$$\vec{v}^2 = 2\hat{\lambda}^{-1}\vec{m}^2 \quad \hat{\lambda} = \lambda + \begin{pmatrix} & -3\tilde{\lambda}/8 \\ -3\tilde{\lambda}/8 & 7\tilde{\lambda}_\Phi/12 \end{pmatrix} \quad (2.60)$$

Next, expanding around the vevs we find the mass matrix for the singlets $\delta\mathbf{h}, \delta\Phi$ as

$$M^2 = \text{Diag}(v) \hat{\lambda} \text{Diag}(v) = U \text{Diag}(m_h^2, m_{\tilde{h}}^2) U^T \quad (2.61)$$

with $\text{Diag}(v) = \delta^{ij}v_j$. The aim is to express ω, β as $\omega(m_h, m_{\tilde{h}}, \hat{\lambda}, v), \beta(m_h, m_{\tilde{h}}, \hat{\lambda}, v)$,

which can be done by taking the determinant of the mass matrix

$$\det(M^2) = v_{\mathbf{h}}^2 v_{\Phi}^2 \det(\hat{\lambda}) = m_h^2 m_{\tilde{h}}^2 \quad (2.62)$$

and combining the eigenvector equations into

$$\sin(2\omega) = \frac{2v_{\mathbf{h}}v_{\Phi}}{m_h^2 - m_{\tilde{h}}^2} \hat{\lambda}_{\mathbf{h}\Phi} \quad (2.63)$$

to obtain

$$\sin(2\omega) = \frac{2m_h m_{\tilde{h}}}{m_h^2 - m_{\tilde{h}}^2} \frac{\hat{\lambda}_{\mathbf{h}\Phi}}{\sqrt{\det(\hat{\lambda})}} \quad (2.64)$$

$$\sin(2\beta) = \sqrt{C_9} \frac{2m_h m_{\tilde{h}}}{v^2 \sqrt{\det \hat{\lambda}}} \quad (2.65)$$

No obstacle prevents taking $\omega \rightarrow 0$ with $\hat{\lambda}_{\mathbf{h}\Phi} \rightarrow 0$, but it is evident that β cannot be arbitrarily close to zero while keeping \tilde{h} massive and respecting unitarity. Qualitatively then, we have a minimum attainable curvature as:

$$\left(v^2 R_{\varphi} \geq \frac{3m_h^2 m_{\tilde{h}}^2}{8\pi^2 v^4}, \quad v^2 R_h \leq -\frac{3m_h^2 m_{\tilde{h}}^2}{8\pi^2 v^4} \right) \quad (2.66)$$

where we took the unitarity bound on $\hat{\lambda}$ that follows from the 4-pt amplitude for δh and $\delta\Phi$, see e.g. [8]. This result, being proportional to the extra state mass, yields a naive cut-off $R = \frac{4\pi}{\Lambda^2}$ with inverse dependence on the new physics scale:

$$\frac{\Lambda^2}{v^2} \sim \frac{(4\pi)^3 v^2}{\lambda_{\text{SM}} m_h^2} \quad (2.67)$$

so that the largest cut-off, or the closest to the SM couplings one can get, is attained for the lowest new physics scale. How low this scale can be while still being able to assume an EFT applies can be estimated from the amplitude for W scattering,

mediated by the singlets in the full theory

$$-\mathcal{A} = \frac{s}{v^2} \left(1 - c_\beta^2 \frac{s}{s - m_h^2} - s_\beta^2 \frac{s}{s - m_{\tilde{h}}^2} \right) + (s \rightarrow t) \quad (2.68)$$

The plot in fig. 2.4 shows the region in the curvature plane that the models discussed in this section cover. In particular for the minimum mass of the extra singlet we take the limit of $m_{\tilde{h}} \gtrsim 350$ GeV from [71] as reference.

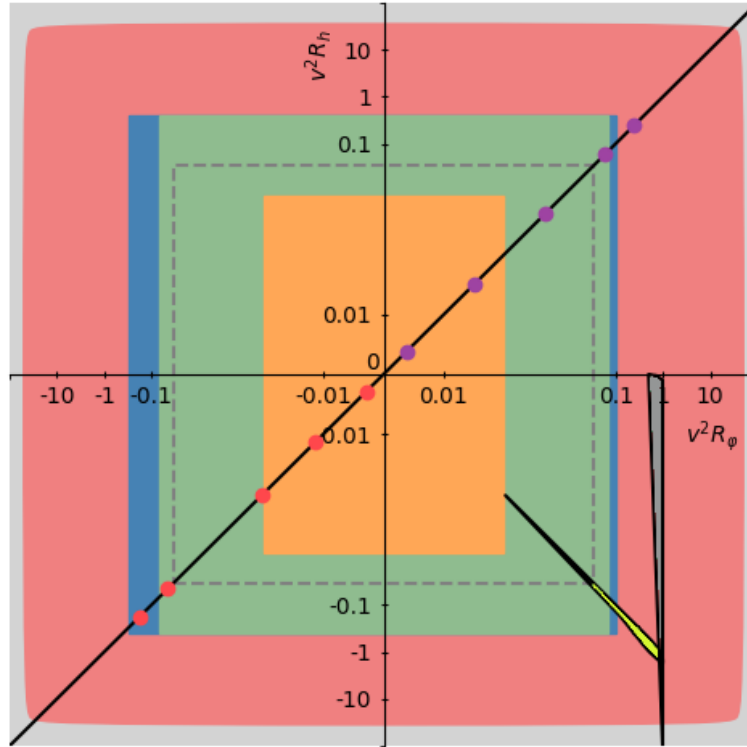


Figure 2.4: Range of curvature for SMEFT and non-linearly realised theories, on the same background as Fig. 2.2. Two non-linearly realised theories are plotted: the yellow region shows curvature for the symmetric representation with $\langle \Phi \rangle \neq 0$, and the dark-grey region shows a hyperbolic manifold (see sec. 2.4). The black line shows SMEFT curvature: the purple and red dots represent the singlet and the symmetric representation with $\langle \Phi \rangle = 0$ examples from sec. 2.3 respectively. The outer-most to inner-most dots are evaluated with coupling $g_* = 1$ and heavy singlet mass: 500 GeV, 1 TeV, 1.5 TeV, 2 TeV and 4 TeV.

2.4 Manifolds

The above HEFT cases fall into the category of manifolds with a singularity, as one can see by integrating out heavy states [41]. In contrast, one can also have that no $O(4)$ -symmetric point is present and the manifold is smooth at every point. This section visualizes both types of manifolds, together with those that admit a SMEFT description. Consider (higher dimensional) cylindrical coordinates, the gauge symmetry acts rotating along the axis and orthogonal to this rotation we have a cylindrical radial coordinate ρ and a ‘height’ z . Our manifolds are hypersurfaces within this 5d space parametrized by h and φ^a

$$(\rho(h)u(\varphi), z(h)) \tag{2.69}$$

With a line element:

$$d\ell^2 = \left(\left(\frac{d\rho}{dh} \right)^2 \pm \left(\frac{dz}{dh} \right)^2 \right) dh^2 + \rho(h)^2 du^2 \tag{2.70}$$

which defines the 4-d metric, where the plus sign is for Euclidean 5d space and the minus for the metric with a $(-1, 1, 1, 1, 1)$ signature. In our basis, eq. (2.14), dh^2 has unit coefficient which can always be attained by a field redefinition. This line element we can then identify with that from eq. (1.63). In terms of geometry, the singlet Higgs field h equals distance in field space for fixed u . From the equation above and our basis it also follows that $F(h) = \rho(h)/v$ with $F(0) = 1$ giving $\rho(0) = v$. For convenience let us define $\theta \equiv (h + h_0)/f$ with f a new physics scale.

The most symmetric manifolds are S^4 , R^4 & \mathcal{H}^4 which are parametrized in our basis as

$$S^4 \quad (f \sin(\theta)u, f \cos(\theta)) \tag{2.71}$$

$$R^4 \quad ((h + v)u, 0) \tag{2.72}$$

$$\mathcal{H}^4 \quad (f \sinh(\theta)u, f \cosh(\theta)) \tag{2.73}$$

and yield constant (field-independent) curvature:

$$S^4, \mathcal{H}^4 \quad R_\varphi, \quad R_h \quad \pm \frac{1}{f^2}, \quad \pm \frac{1}{f^2} \quad (2.74)$$

while the $f \rightarrow \infty$ limit yields R^4 which corresponds to the SM. Indeed these manifolds can be described in SMEFT and correspond to Composite Higgs Models [72] or negative curvature models [73].

2.4.1 Non-linearly Realised Theories with a Singularity

A one-parameter deformation of the manifolds above takes us into non-linearly realised theory space with a singularity at the origin:

$$\text{deformed } S^4 \quad \left(f s_{\gamma\theta} u, \int dh \sqrt{1 - \gamma^2 c_{\gamma\theta}^2} \right) \quad (2.75)$$

$$\text{deformed } \mathcal{H}^4 \quad \left(f s h_{\gamma\theta} u, \int dh \sqrt{\gamma^2 c h_{\gamma\theta}^2 - 1} \right) \quad (2.76)$$

where $s_{\gamma\theta} = \sin(\gamma\theta)$ and the singularity is made evident by the curvature

$$\text{deformed } S^4 \quad R_\varphi \quad R_h \quad \frac{1 - \gamma^2}{f^2 s_{\gamma\theta}^2} + \frac{\gamma^2}{f^2}, \quad \frac{\gamma^2}{f^2} \quad (2.77)$$

$$\text{deformed } \mathcal{H}^4 \quad \frac{1 - \gamma^2}{f^2 s h_{\gamma\theta}^2} - \frac{\gamma^2}{f^2}, \quad - \frac{\gamma^2}{f^2} \quad (2.78)$$

since the origin, and would-be- $O(4)$ invariant point, $\theta = 0$, returns $R_\varphi = \infty$. This singularity is present for any $\gamma \neq \pm 1$ which seemingly presents a way to approximate the SM by sending first $f \rightarrow \infty$ while keeping $f s_{\gamma\theta_0} (f s h_{\gamma\theta_0}) = v$ constant, then $\gamma \rightarrow 1$. Indeed in this limit, $\partial^n R \propto (1 - \gamma^2)$ and contributions to amplitudes of an arbitrary number of particles cancel. Nonetheless and quite relevantly in this limit, the singularity is just a field distance v/γ from the vacuum $h = 0$. The model in the section above with a symmetric representation taking a vev also belongs to the non-linearly realised theories with singularities, yet it showed that the SM point cannot

be reached. So it could be that the deformed manifolds have no UV completion, yet from low energy we see no indication for it. This highlights the need for a bound based purely in the EFT perspective to comprise all possibilities.

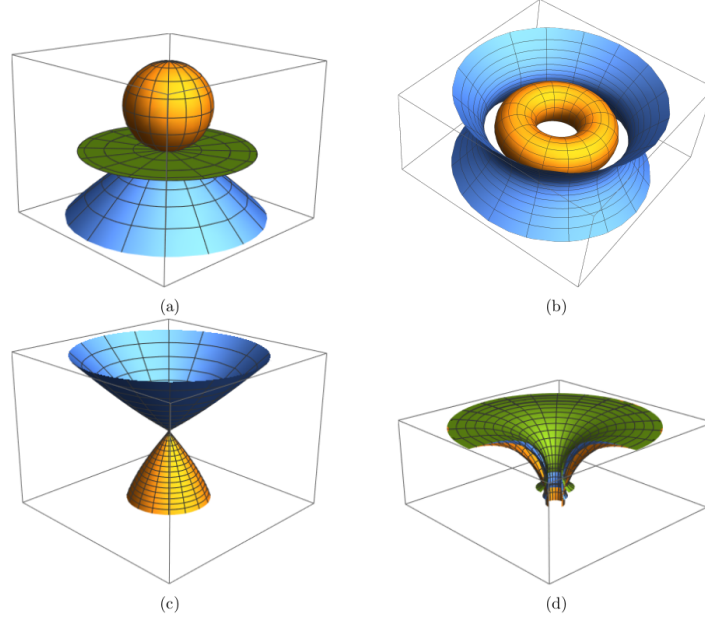


Figure 2.5: Examples of manifolds which belong in SMEFT (a), or in non-linearly realised theory space (b,c,d) with the gauge symmetry action being rotation around the z axis. SMEFT manifolds in (a) correspond to: Composite models (yellow), the SM (green), and negative curvature models (blue). Manifolds representing non-linearly realised theories (b,d) are smooth, while (c) presents a singularity and both (c,d) are in a class which resembles the SM around the vacuum. For (d), part of the manifolds have been cut out for better visualization.

2.4.2 Smooth Non-linearly Realised Theories

On the other hand, one could have smooth manifolds in non-linearly realised theory space, $\rho \neq 0 \forall h$; we take here as examples a torus and a hyperbola (in Euclidean space)

$$\text{torus} \quad ((\rho_0 + fc_\theta)u, fs_\theta) \quad (2.79)$$

$$\text{hyperbola} \quad ((\rho_0 + fch_{\hat{\theta}})u, fsh_{\hat{\theta}}) \quad (2.80)$$

where $\hat{\theta} = (\hat{h}(h) + \hat{h}_0)/f$ with $(dh/d\hat{h})^2 = sh_{\hat{\theta}}^2 + ch_{\hat{\theta}}^2$ as follows from our normalization in Euclidean 5d. In terms of curvature, these manifolds give:

$$\begin{array}{ccc} & R_{\varphi} & R_h \\ \text{Torus} & \frac{\cos(\theta)^2}{v^2}, & \frac{\cos(\theta)}{fv} \end{array} \quad (2.81)$$

$$\text{Hyperbola} \quad \frac{ch_{\hat{\theta}}^2}{(ch_{\hat{\theta}}^2 + sh_{\hat{\theta}}^2)v^2}, \quad \frac{-ch_{\hat{\theta}}}{(ch_{\hat{\theta}}^2 + sh_{\hat{\theta}}^2)^2fv} \quad (2.82)$$

We see that the hyperbola does not go through the zero curvature point for any value of f, θ , always keeping a distance as the explicit model in the previous section did. The torus however for $\theta = \pi/2$ does have both curvatures vanish, yet by construction the manifold is not R^4 . Visually, for this point we are sitting atop of the torus and for its first two derivatives it does resemble a plane, but its third derivative is non-vanishing and indeed $R'_h = 1/f^2v$ which is bounded from below given $\rho_0 > f$ and for $\theta = \pi/2$, $v = \rho_0$.

This nonetheless illustrates the possibility of manifolds that do look locally like the SM to the n th derivative, yet do not go through the origin. Let us take on such set of manifolds labelled by n

$$F_{(n)}(h) = 1 + \frac{h}{v} + c_n \left(\frac{h}{v}\right)^n \quad |c_n| > \frac{(n-1)^{n-1}}{n^n} \quad (2.83)$$

The manifolds associated with these F_n for $n = 3, 4, 5$ are plotted in fig. 2.5 and they resemble a plane and hence the SM ever more accurately for increasing n around $h = 0$.

2.5 Obstacles in the Road to the SM

We have encountered HEFT\SMEFT non-linearly realised theories which either come from smooth manifolds with no $O(4)$ -invariant point, or manifolds which get arbitrarily close to the would be $O(4)$ -invariant point, but the point itself is singular.

A number of UV complete theories yield non-linearly realised theories with singularities at the origin. From working out an explicit example, we have seen that

these can only get within a finite distance of the SM point. This explicit computation relied on knowledge of the full theory, but here we attempt to give an argument as to why non-linearly realised theories are not a road to the SM model in purely low energy grounds.

Let us turn to semi-classical arguments. Consider the Higgs field as sourced by a probe particle i localized in a region σ_x and with a mass $m_i > m_h$. This configuration is, of course, short lived yet for times smaller than the decay rates one might consider such system. The renormalizable linear realization gives an equation of motion ³,

$$(-\square - m_h^2)h(x) = \frac{m_i}{v}J_i(x) \quad (2.84)$$

where

$$\text{Spin } 1/2 \quad J_i = \langle i | \bar{\psi} \psi | i \rangle \quad (2.85)$$

$$\text{Spin } 1 \quad J_i = -\langle i | m_i V_\mu V^\mu | i \rangle \quad (2.86)$$

and the particle state is

$$|i\rangle = \int \frac{d^3p}{(2\pi)^3} \Psi(p) \frac{a_{i,p}^\dagger}{\sqrt{2E_p}} |0\rangle \quad (2.87)$$

Away from the localised source the field is

$$h(r > \sigma_x) = \frac{m_i}{v} \int \frac{d^4x d^4q}{(2\pi)^4} \frac{e^{iq(x-y)} \hat{J}_i(\vec{x})}{q^2 - m^2} \quad (2.88)$$

$$\simeq -\frac{m_i}{v} \frac{e^{-m_h r}}{4\pi r} \quad (2.89)$$

where in the second line we assumed that the current J_i is the same as the probability density, as we shall see justified in the non-relativistic limit.

Consider now the candidate non-linearly realised theories that resemble the Standard Model to a high degree, examples given in the previous section are the functions

³The spin 0, 1 case has an extra h/v times the source which we have dropped.

$F_{(n)}$ as given in (2.83) or the deformed S^4, \mathcal{H}^4 theories (2.77,2.78). The solution above should be a good first approximation certainly for large distances $r > 1/m_h$ where the field value is exponentially close to the vacuum value. However, at shorter distances if our candidate theories truly present a limit in which the SM couplings are recovered, the solution should still be a good approximation. The field value nonetheless increases with decreasing distance and if there is a singularity, in this SM limit, it is just a distance $v/\gamma \simeq v$ away in field space. Conversely, for smooth non-linearly realised theories, even if our series example $F_{(n)}$ resembles the SM locally around the vacuum, the corrections in eq. (2.84) read $1 + nc_n(h/v)^n$ with $nc_n \sim 1$ for $n \gg 1$ and would dominate over the SM for $h \sim v$. This is indeed the same condition for both types of theories and yields a naive minimum distance or cut-off

$$\frac{h(\sigma_x < r < m_h^{-1})}{v} \simeq \frac{m_i}{v} \frac{1}{4\pi v r} \quad (2.90)$$

$$\frac{h(r_0)}{v} \sim 1 \quad \text{for} \quad \frac{1}{r_0} \equiv \Lambda \sim 4\pi v \frac{v}{m_i} \quad (2.91)$$

This points at a cut-off an inverse coupling factor higher than other estimates based on perturbative unitarity. Nevertheless, quantum mechanics has something to say about our implicit assumption $\sigma_x < r_0$. Indeed $r_0 \sim (m_i^2/4\pi v^2)m_i^{-1}$ is smaller than the inverse mass of a particle for perturbative couplings (which is the case for the SM) but in order to localize the particle in a distance smaller than the inverse mass, the uncertainty principle dictates a range of momenta that extends to the relativistic regime. In this high energy limit, our current J_i suffers a relativist factor m/E suppression as explicit evaluation of the matrix elements shows when going beyond the non-relativistic approximation. For a fermion, one has

$$J_i(x) = \int \frac{d^3p d^3k}{(2\pi)^6} \frac{\bar{u}(k)u(p)}{\sqrt{2E_p 2E_k}} e^{i(p-k)x} \Psi^*(k) \Psi(p) \quad (2.92)$$

which implies that the space-integral over the source J_i is suppressed and the field

value at a distance $r > \sigma_x$ is

$$\frac{h(\sigma_x < r)}{v} = \frac{N(m_i \sigma_x) m_i}{4\pi v r v^2} = \frac{N(\sigma_x m_i)}{r m_i} \alpha_i \quad (2.93)$$

$$N(m_i, \sigma_x) = \frac{\int d^3 k (m_i/E_p) |\Psi(p)|^2}{\int d^3 k |\Psi(p)|^2} \quad \alpha_i = \frac{m_i^2}{4\pi v^2} \quad (2.94)$$

which is the same result for spin 1/2 and 1. This suppression implies that the pre-factor of α_i in the eq. (2.93) is at most order one, which would then require an order one α_i to probe $(h/v) \sim 1$. Note that this α_i will be at the edge of perturbative unitarity, although loop corrections will be suppressed by $\sim 1/(4\pi)$.

As an estimate, we take a Gaussian distribution $\Psi \sim e^{-(p\sigma_x)^2/2}$ and evaluate the potential at a distance $r = 2\sigma_x$ which encloses 95% of the probability density to find that with $\alpha_i \sim 2$ the cut-off, or inverse distance, where we would probe $h \sim v$ would be $r_0 = 0.6m_i^{-1}$,

$$\Lambda \sim \sqrt{\frac{8\pi\sigma_x m_i}{N(\sigma_x m_i)}} \Big|_{m_i \sigma \sim 0.3} \quad v \simeq 2 \text{ TeV}. \quad (2.95)$$

The nature of EWSB and the question of whether a symmetric $O(4)$ point exists should be independent of the introduction of our probe particle i , although admittedly the fact that one would require couplings on the perturbative edge makes the above a rough estimate.

The naive scaling from eq. (2.90) does, however, point towards the typical scale for non-perturbative effects. This is indeed the natural scale for answering non-local questions about our theory. For instance, this scaling is like that of the electroweak Sphaleron, whose energy scales as

$$E_{\text{sph}} \sim \frac{4\pi v}{g}. \quad (2.96)$$

This is one such non-local probe which we will study in the following chapter.

2.6 Summary

This work studied the non-linearly realised theory space HEFT\SMEFT, and the potential limits to recover the SM other than via SMEFT with the use of a geometric formulation. Explicit examples, which include perturbative UV complete models, can and will be told apart from the SMEFT case by future experiments via projection of measurements on the curvature plane defined from the WW scattering and $WW \rightarrow hh$ amplitudes (see fig. 2.4). These examples of non-linearly realised theory space HEFT\SMEFT do not offer a limit to recover the SM and possess a finite cut-off. In contrast to these, non-linearly realised theories were formulated in sec. 2.4 which resemble the SM amplitudes for arbitrary precision and number of particles. While these theories look like the SM model around the vacuum, at a Higgs-singlet-distance of $\sim v$ they reveal their nature of electroweak symmetry realised non-linearly. Making use of semi-classical arguments to displace the Higgs field by $\sim v$, we find an argument for general theories in non-linearly realised theory space to be distinguishable from the SM when probing the theory at an energy (inverse distance) of at most $4\pi v/g_{\text{SM}}$. Our discussion applies to non-linearly realised theories both with and without singularities (non-analyticities). The most pressing outstanding question is the characterization of experimental signatures that follow from the semi-classical arguments given here. This we address in the following chapters.

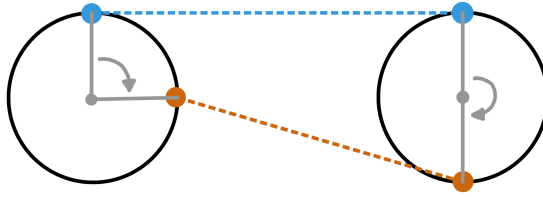
Sphalerons in Non-Linearly Realised Theories

Non-perturbative dynamics depend generically on extended field configurations which hence probe theories globally in field space. As such, these would be sensitive even to theories that locally resemble the SM. One of the prominent, phenomenologically relevant examples of such non-perturbative dynamics is B- and L-number violating sphaleron processes.

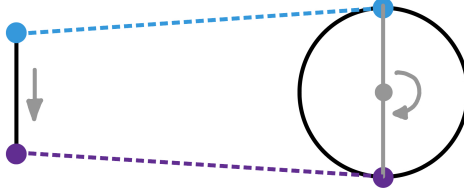
A sphaleron is a static, classical tunnelling solution of finite energy between two topologically distinct vacua in our system. As described in [74], we consider a loop in field-configuration space which begins and ends at the vacuum parameterised by a new coordinate-like variable $\alpha \in [0, \pi]$. If the loop is non-contractible, these two vacua are topologically distinct which is marked by a change in the topological winding number by an integer. We would, therefore, expect a tunnelling solution between two vacua of winding numbers n and $n + 1$ to itself have winding number $n + 1/2$.

In fig. 3.1 shows how a winding number can result from a non-trivial map between two distinct manifolds. Later, we will introduce how to compute the winding number for a sphaleron.

Consider an $SU(2)$ gauge theory. Requiring a finite, static (semi-classical) action



(a) A hypothetical map from $S^2 \rightarrow S^2$. Notice that traversing the whole circle on the left must return the original, starting point. However, the circle on the right has been traversed twice. This map is said to be non-trivial and has winding number of 1.



(b) A hypothetical map from a straight line to S^2 . Note that the start and end points of the line are distinct, else we have the identical case to fig. 3.1a. Traversing along the line maps directly to a single point on S^2 . This is a trivial map and has no winding.

Figure 3.1: Demonstration of trivial fig. 3.1a and non-trivial fig. 3.1b maps.

requires itself that fields tend towards such vacuum configurations at spatial infinity. Spatial infinity can be thought of as a 2-sphere, S_2 . The vacuum configuration for the three $SU(2)$ gauge fields A_μ^a where $a = 1, 2, 3$ can be derived in the following way. Consider the time-independent action for the Gauge fields:

$$S = \int d^3x F_{\mu\nu}^a F_a^{\mu\nu} \quad (3.1)$$

integrating over \mathbb{R}^3 and with the non-Abelian field strength

$$F_{\mu\nu}^a = \partial_\mu A_\nu^a - \partial_\nu A_\mu^a + g\epsilon^{abc} A_\mu^b A_\nu^c. \quad (3.2)$$

In order to have a finite action, we must have that

$$F_{\mu\nu}^a \xrightarrow{|\vec{x}| \rightarrow \infty} 0 \quad (3.3)$$

which, naively from eq. (3.2), implies that

$$A_\mu^a \xrightarrow{|\vec{x}| \rightarrow \infty} 0. \quad (3.4)$$

However, we still have the freedom to take a gauge transformation of the form

$$A_\mu = i\frac{g}{2}A_\mu^a\sigma^a \xrightarrow{|\vec{x}|\rightarrow\infty} U_\infty\partial_\mu U_\infty^\dagger \quad (3.5)$$

where $U_\infty = U_\infty(\theta, \phi)$ is an $SU(2)$ matrix, and σ^a are the usual three Pauli matrices. (θ, ϕ) are the angular coordinates at spatial infinity. These solutions are called *pure gauge* and the set of all infinitely many solutions (as $SU(2)$ is continuous) is known as the *vacuum configuration*.

We can think of the functions U_∞ as a mapping between points at spatial infinity, to elements of the gauge group $SU(2)$ which is topologically equivalent to the 3-sphere. Finite, static action configurations are, as such, associated with mappings from a 2-sphere S_2 to a 3-sphere S_3 which is the gauge group.

These mappings are trivial, and as a result have no associated winding number and no topologically distinct vacua. However, if we use the variable α to define a family of maps from $S^2 \rightarrow S^3$ which vary continuously with α . As shown in [74], this is topologically equivalent to a single map:

$$S_2 \times \alpha \sim S_3 \rightarrow S_3 \quad (3.6)$$

which is a non-trivial mapping, and as such when traversing non-contractible loops in field-space between vacua, the winding number changes. Therefore, in order to tunnel between topologically distinct vacua, one needs an extended field configuration. I.e. it needs to leave one vacuum state to enter another, and the parameter α one can think of as ‘tracking’ this process. This extended field configuration is the sphaleron.

3.1 Sphalerons in the Standard Model

Sphalerons were first predicted in the electroweak sector of the Standard Model in two successive papers [74, 75]. They showed the Standard Model sphaleron would have a winding-number of 1/2 and an energy of ~ 10 GeV which we will review in this subsection. We will work in the approximation, along with [74, 75], that

the weak mixing angle vanishes, so that the $U(1)$ gauge fields may be set to zero. Hence we can approximately consider the SM electroweak sphaleron to be the $SU(2)$ sphaleron. This is valid up to corrections of order g'/g .

The Sphaleron Ansatz

Loosely following N. Manton, [74], an ansatz for the sphaleron is composed in the following way.

We must have that the sphaleron energy E_{sph} is finite to have a sensible solution, i.e.

$$E_{\text{sph}} = \int d^3x \left[\frac{1}{2} \text{Tr}[F_{ij}F^{ij}] + (D_i H)^\dagger (D^i H) + V(H) \right] \quad (3.7)$$

where H is the Higgs doublet, and F_{ij} the $SU(2)$ field-strength tensor with $i, j = 1, 2, 3$. For the energy to be finite, the Higgs doublet must asymptotically go to a minimum of $V(H)$ at spatial infinity, i.e. the vacuum. Assuming a spherically symmetric ansatz, at $r \rightarrow \infty$ we can construct a limiting field depending only on two angles θ, ϕ (lower case ϕ here is a spatial angle):

$$H^\infty(\theta, \phi) = \lim_{r \rightarrow \infty} H(r, \theta, \phi) \quad (3.8)$$

where we are welcome to choose that

$$H^\infty(\theta = 0) = \frac{v}{\sqrt{2}} \begin{pmatrix} 0 \\ 1 \end{pmatrix} \quad (3.9)$$

as the limiting field is spherically symmetric. This perfectly (by design) aligns with our choice of the Higgs vacuum,

$$H^{\text{vacuum}} = \frac{v}{\sqrt{2}} \begin{pmatrix} 0 \\ 1 \end{pmatrix}. \quad (3.10)$$

Therefore, we can consider the limiting field H^∞ as a map from spatial infinity to the vacuum manifold of the Higgs doublet, exactly the $S^2 \rightarrow S^3$ trivial mapping we

saw earlier.

Recall that introducing the variable $\alpha \in [0, \pi]$ which parameterises a family of such maps, i.e. $H^\infty = H^\infty(\mu, \theta, \phi)$, where the loop must start and end ($\alpha = 0, \pi$) at the vacuum configuration. Manton then parameterises the limiting field as

$$H^\infty(\mu, \theta, \phi) = \frac{v}{\sqrt{2}} \begin{pmatrix} \sin \mu \sin \theta e^{i\phi} \\ e^{-i\mu} (\cos \mu + i \sin \mu \cos \theta) \end{pmatrix} = \frac{v}{\sqrt{2}} U_\infty \begin{pmatrix} 0 \\ 1 \end{pmatrix} \quad (3.11)$$

which is shown in [74] to be topologically equivalent to the map $H^\infty : S^3 \rightarrow S^3$. The matrix U_∞ has the form

$$U_\infty = \frac{\sqrt{2}}{v} \begin{pmatrix} (H_2^\infty)^* & H_1^\infty \\ (-H_1^\infty)^* & H_2^\infty \end{pmatrix} \quad (3.12)$$

which we will need shortly, where $H_{i=1,2}$ are the components of the Higgs doublet.

¹ It is proposed in [75] for the Standard Model case to use the Higgs field as a ‘wrapper’ to keep the field-configuration well-defined. I.e. at the point where $r = 0$, the angles θ, ϕ are undefined therefore for a fully defined field configuration, there cannot be any residual dependence on them at the origin. Therefore Higgs doublet we give the following spherically symmetric ansatz:

$$H(r, \theta, \phi) = \tilde{h}(r) H^\infty(\theta, \phi) + (1 - \tilde{h}(r)) \frac{v}{\sqrt{2}} \begin{pmatrix} 0 \\ e^{-i\mu} \cos \mu \end{pmatrix} \quad (3.13)$$

where H^∞ is the limiting field at infinity (the vacuum). Notice the (smooth) function \tilde{h} takes the radial dependence and can be thought of as the Higgs field contribution. The fields then take the following boundary conditions:

$$\lim_{r \rightarrow 0} \tilde{h}(r) = 0 \qquad \lim_{r \rightarrow \infty} \tilde{h}(r) = 1 \quad (3.14)$$

Notice \tilde{h} is defined to be dimensionless and chosen to have a non-zero vev. The first

¹The reason for this choice of U_∞ is such that if one calculates the covariant derivative of H^∞ , $D_i H$, one will find it is zero. Again, this conspires to keep the sphaleron energy finite.

boundary condition ensures that at spatial infinity, the Higgs and Goldstones take their vacuum configuration. The second ensures the Higgs doublet is single-valued at $r = 0$, and therefore well-defined everywhere.

Now the gauge field. At spatial infinity we must also have that A_μ^a is pure-gauge (i.e. eq. (3.5)). A suitable ansatz for the remainder gauge field at infinity is then

$$\frac{ig\sigma^a}{2}A_i^a|_{r=\infty} = +U_\infty\partial_iU_\infty^\dagger = A_i^\infty. \quad (3.15)$$

with $A_0 = 0$ being our gauge choice. Extending the ansatz to all space with a smooth function $f(r)$, the remaining pieces of the gauge field are given the following ansatz

$$A_i(r, \mu, \theta, \phi) = f(r)A_i^\infty(\mu, \theta, \phi). \quad (3.16)$$

The function $f(r)$ obeys the following boundary conditions:

$$\lim_{r \rightarrow 0} \frac{1}{r}f(r) = 0 \quad \lim_{r \rightarrow \infty} f(r) = 0, \quad (3.17)$$

again, intended to keep the sphaleron energy finite.

Given these boundary conditions, one must numerically solve for the functions $f(r), \tilde{h}(r)$ [76] by proposing a suitable ansatz with tun-able parameters [74] which minimise the sphaleron energy. The energy is (generally) maximal at $\mu = \pi/2$ (i.e. the height of the barrier). The SM sphaleron energy has ultimately been found to be [76]

$$E_{\text{sph}} = 1.948 \frac{g}{4\pi v} = 9.11 \text{ TeV}. \quad (3.18)$$

The Winding Number

The topological charge q for the mapping $S^3 \rightarrow S^3$ can be written in terms of the non-Abelian field strength eq. (3.2):

$$q = \frac{g^2}{32\pi^2} \int_{t=-\infty}^{+\infty} dt \int d^3x \frac{1}{2} \epsilon^{\mu\nu\rho\sigma} F_{\mu\nu}^a F_{\rho\sigma}^a. \quad (3.19)$$

where q always takes integer values. It is well-known that the integrand above can be written as a total derivative, $\frac{1}{2}\epsilon^{\mu\nu\rho\sigma}F_{\mu\nu}F_{\rho\sigma} = \partial_\mu K^\mu$ with

$$K^\mu = \epsilon^{\mu\nu\rho\sigma} \left(F_{\nu\rho}^a A_\sigma^a - \frac{g}{3}\epsilon^{abc} A_\nu^a A_\rho^b A_\sigma^c \right) \quad (3.20)$$

Using Stoke's theorem, we can express the topological charge as

$$q(t_0) = \int d^3x K^0 \Big|_{t=-\infty}^{t=t_0} + \int_{-\infty}^{t_0} \int_S \vec{K} \cdot d\vec{S} \quad (3.21)$$

for S a surface at $r \rightarrow \infty$. By setting $t_0 = \infty$, we recover q as in eq. (3.19). The last integral on the right will vanish if \vec{K} decreases fast enough at large distances. The remaining term is the Chern-Simons number N_{CS} :

$$N_{\text{CS}} = \int d^3x K^0 \Big|_{t=-\infty}^{t=t_0} \quad (3.22)$$

Note that eq. (3.22) has lost gauge invariance. As a result, we must take extra care, nevertheless, the term that remains is the so-called *winding number* of the sphaleron [77].

We can think of α as a time-dependent quantity [76], where $\alpha(t = -\infty) = 0$ and $\alpha(t = t_0) = \alpha$. We'll use a different choice of gauge to before to compute the winding number. Following [75], we choose

$$U_\infty(\alpha, r, \theta, \varphi) = e^{i\alpha\sigma_3/2} (\cos(\alpha) + i \sin(\alpha) \hat{x} \cdot \vec{\sigma}) e^{i\alpha\sigma_3/2}. \quad (3.23)$$

And to keep the Higgs doublet in the unitary gauge far from the origin, a further gauge transformation² is needed:

$$A'_i(\mu, r, \theta, \varphi) = \tilde{U}^\dagger A_i \tilde{U} + \frac{i}{g} \tilde{U}^\dagger \partial_i \tilde{U} \quad (3.24)$$

$$\tilde{U}(\alpha, r, \theta, \varphi) = \exp(i\mu\Omega(r)\hat{x} \cdot \vec{\sigma}) \quad \Omega(0) = 0 \quad \Omega(r \rightarrow \infty) \rightarrow 1 \quad (3.25)$$

²As in [78], by interpreting α to be a variable that depends on time, this is technically not a true gauge transformation. But proceeding nonetheless.

with $A'_0 = 0$ still, and $\Omega(r)$ some function obeying the above boundary conditions which must approach 1 rapidly as $r \rightarrow \infty$ such that \vec{K} vanishes at spatial infinity. Therefore we are in the correct gauge to compute the winding number [75]. Then substitution of eq. (3.16) yields, after some calculation,

$$N_{\text{CS}} = \int d^3x K^0 \Big|_{t=-\infty}^{t=t_0} = \frac{2\alpha - \sin 2\alpha}{2\pi}. \quad (3.26)$$

Exactly as we had hoped, the winding number (or N_{CS}) changes by 1 between the two vacua at $\alpha = 0$ and $\alpha = \pi$:

$$N_{\text{CS}}(\alpha = 0) = 0 \quad (3.27)$$

$$N_{\text{CS}}(\alpha = \pi) = 1 \quad (3.28)$$

and that mid-way between the two vacua, at $\alpha = \pi/2$

$$N_{\text{CS}}(\alpha = \pi/2) = \frac{1}{2}. \quad (3.29)$$

Note that in linearly realised theories, such as those in [79], the situation is similar with an altered sphaleron energy.

3.2 Modification of Sphaleron Solutions

Recall from section 2.4 the absence of a $O(4)$ -symmetric point in the HEFT\SMEFT leads to manifolds topologically different from the SMEFT case. Thus, one may be able to differentiate both theories, even when they appear to be the same locally (and hence inseparable by processes described by the perturbative S -matrix), by studying the physics of field configurations that depend on the global properties of this manifold. In this section, we focus on the sphaleron configurations which, in principle, rely on the existence of $O(4)$ -symmetric point to exist.

As we have discussed, a sphaleron is the maximum-energy point in a minimal-energy non-contractible loop through scalar and gauge field space. This loop can be approximated by a family of static field configurations depending on the parameter

$\alpha \in [0, \pi]$. Previously we considered the Higgs field to be part of the usual doublet as eq. (3.13). Now in the HEFT case, considering the Higgs h and Goldstone matrix U to transform independently, the field configuration we consider is

$$h = h(r), \quad U = e^{i\alpha\sigma_3/2} (\cos(\alpha) + i \sin(\alpha) \hat{x} \cdot \vec{\sigma}) e^{i\alpha\sigma_3/2}, \quad (3.30)$$

$$W_0 = 0, \quad W_j = -\frac{i}{g} a(r) U \partial_j U^\dagger \quad (3.31)$$

where $\hat{x} = \vec{x}/|x|$ is the unit vector in space, U and W are the $SU(2)$ Goldstone and gauge fields³, and $h(r)$ and $a(r)$ are radial functions that minimise the energy and satisfy the boundary conditions

$$h(0) = h_\odot, \quad a(0) = 0, \quad \lim_{r \rightarrow \infty} h(r) = 0, \quad \lim_{r \rightarrow \infty} a(r) = 1, \quad (3.32)$$

with $h = h_\odot$ being the $O(4)$ -invariant point if it exists. That $U|_{\alpha=0} = U|_{\alpha=\pi} = 1$ ensures that the curve described in field space by varying α is indeed a loop.

The sphaleron is the configuration at the midpoint of the loop, with $\alpha = \pi/2$. In order for it to be well-defined everywhere in space, it is crucial that $h(0) = h_\odot$. This is because $U|_{\alpha \neq 0, \pi}$ is singular at the origin. Indeed, taking the limit $r \rightarrow 0$ from different spatial directions will yield different U matrices. This makes the field configuration undefined at $r = 0$, unless all values of U can be identified and collapsed into a single point, making it single-valued. This can only be done if there is a $O(4)$ -invariant point h_\odot where $F(h_\odot) = 0$.⁴ Therefore, fully well-defined sphaleron configurations cannot exist in HEFT\SMEFT theories which have $F(h) > 0$ for all h .

One can nevertheless work with the definition we have given for U away from the origin, and see if the singularity there has physical consequences. In particular, in order for it to be physically meaningful, the sphaleron solution must have finite

³The effects of the $U(1)$ sector are neglected here which is an approximation valid up to corrections of order g'/g , see Ref. [75].

⁴See Ref. [79] for a study of sphalerons in non-SM theories with this property.

energy, using an ansatz as that of Eqs. (3.30) with $\alpha = \pi/2$:

$$E = \int d^3x \left[\frac{4}{g^2 r^2} \left(\frac{da}{dr} \right)^2 + \frac{8a^2(1-a)^2}{g^2 r^4} + \frac{1}{2} \left(\frac{dh}{dr} \right)^2 + \frac{v^2 F(h)^2}{r^2} (1-a)^2 + V(h, \Phi) \right]. \quad (3.33)$$

While the energy density around $r = 0$ would diverge as $1/r^2$ if $F(h) \neq 0$, the volume integral cancels this divergence for a finite result. Another road to reach the same finiteness conclusion is to remember that the sphaleron energy remains finite when $\lambda \rightarrow \infty$ in the SM, i.e. we freeze the Higgs field value on its vacuum and take the particle out of the spectrum. It should be noted nonetheless that had we been dealing with a 2-dimensional theory, the solutions would have indeed disappeared. Notice that additionally the same computation can be performed to compute the winding number as the Standard Model case. Topologically, these are still distinct vacua.

The question that follows is then how is the sphaleron energy, which we now know to be finite, modified. This energy does know about the Higgs manifold non-locally and is, as such, qualitatively different from, say, scattering experiments. In particular, the relevant question (even if just theoretical) as posed in chapter 2 is whether a non-linearly realised theory locally SM-like around the vacuum but globally different can be told apart by the sphaleron energy.

A smooth set of functions F_n for non-linearly realised theories that look locally ever more SM like for increasing integer n were proposed in Ref. [1], here we rewrite them as

$$F_n = 1 + \frac{h}{v} + c_n \left(\frac{h}{v} \right)^n, \quad c_n = (-1)^n \frac{(n-1)^{n-1}}{n^n (1-F_\star)^{n-1}}. \quad (3.34)$$

These functions have a minimum F_\star at $f_\star = -v_\star/v = -n(1-F_\star)/(n-1)$, we take $0 < F_\star < 1$ with the lower limit in particular to keep a non-linearly realised type A theory. We use them as a probe for approaching the SM while in non-linearly realised theory space. As the origin boundary condition for the Higgs, we take as $h(0) = -v_\star$ where $F'(-v_\star) = 0$.

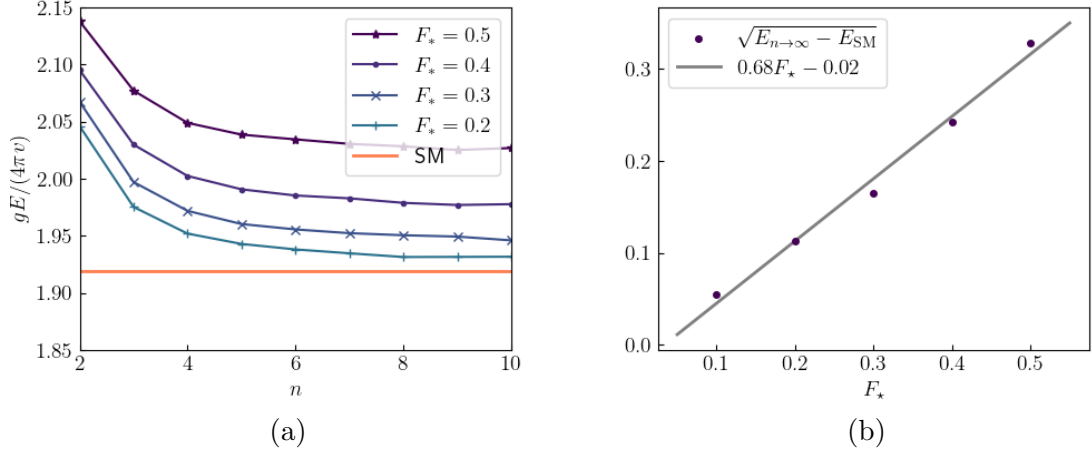


Figure 3.2: Fig. 3.2a: sphaleron energy as a function of n for different values of F_* . Fig. 3.2b: square root of the difference between the limit value of the energy as $n \rightarrow \infty$ (taken from $n = 10$) and the SM energy as a function of F_* , together with a linear fit.

Ansatz			n					
			1(SM)	2	3	4	5	6
A)	Eqs. (3.38), (3.39)	E_{Sph}	1.948	2.079	1.991	1.971	1.966	1.966
		ζ_a	1.4	1.2	1.4	1.4	1.4	1.4
		ζ_h	1.6	2.4	2.0	1.8	1.7	1.6
B)	Neural network	E_{Sph}	1.919	2.053	1.976	1.952	1.943	1.938

Table 3.1: Values of the sphaleron energy in units of $g/4\pi v$ (and corresponding radii ζ_a and ζ_h) at $F_* = 0.2$ and varying n , as computed with methods **A)** and **B)**.

The dimensionless radius $\zeta = gvr$ simplifies the energy to read

$$E = \frac{4\pi v}{g} \int d\zeta \left[4\dot{a}^2 + \frac{8a^2(1-a)^2}{\zeta^2} + \frac{\zeta^2}{2} \dot{f}^2 + F(vf)^2(1-a)^2 + \zeta^2 \frac{\lambda}{8g^2} (f^2 + 2f)^2 \right], \quad (3.35)$$

with $f = h/v$. The sphaleron is obtained by minimising this energy as a function of the profiles $a(\zeta)$ and $f(\zeta)$. We use two different approaches to minimize it for different values of n in the F_n functions defined above:

A) Analytical ansatz. While, due to their non-linear character, one cannot solve the Euler-Lagrange equations that follow from the variational principle for the energy E :

$$-8\ddot{a} + 16 \frac{a(1-1)(1-2a)}{\zeta^2} - 2(1-a)F(f)^2 = 0, \quad (3.36)$$

$$-\zeta^2 \ddot{f} - 2\zeta \dot{f} + 2FF'(f)(1-a)^2 + \zeta^2 \frac{\lambda}{g^2} f(1+f/2)(1+f) = 0, \quad (3.37)$$

one can solve their asymptotic form in the limits $\zeta \rightarrow 0, \infty$. Following Ref. [75], we devise an ansatz as a piece wise function with the solutions to the asymptotic equations which we join at a radius ζ_a (ζ_h for the Higgs function). Such a function has therefore 4 integration constants, two of which are fixed by the boundary conditions, while the other two are found by imposing the same value for the function and its first derivative at ζ_a (ζ_h). This leads to

$$\hat{a}(\zeta) = \begin{cases} \zeta^2 \left(\frac{\zeta_a F_*^2 + 6}{6\zeta_a(4+\zeta_a)} - \frac{F_*^2}{12} \log(\zeta/\zeta_a) \right) & \zeta < \zeta_a \\ 1 - \frac{4-F_*^2\zeta_a^2/6}{4+\zeta_a} e^{-(\zeta-\zeta_a)/2} & \zeta > \zeta_a \end{cases}, \quad (3.38)$$

$$\hat{f}(\zeta) = \begin{cases} f_* \left(1 - \frac{p+\sigma\zeta_h}{2p+\sigma\zeta_h} \left(\frac{\zeta}{\zeta_h} \right)^p \right) & \zeta < \zeta_h \\ f_* \frac{p\zeta_h}{2p+\sigma\zeta_h} \frac{1}{\zeta} e^{-\sigma(\zeta-\zeta_h)} & \zeta > \zeta_h \end{cases}, \quad (3.39)$$

where $\sigma = m_h/(2m_W)$, $2p = (\sqrt{1 + 8F_*''F_*} - 1)$. Substituting this ansatz back in the energy expression Eq. (3.36) allows for minimisation in two variables ζ_a, ζ_h which we do numerically. This semi-numerical method will not yield the true minimum energy since the ansatz are not solutions to the full equations,

but it does have the advantage of treating boundary conditions analytically. Results are shown in Tab. 3.1.

B) Numerical ansatz. Directly minimise E numerically, employing a small neural network as an ansatz for f and a . We use the Elvet package [80] for this purpose. The neural network is densely connected, with 1 input (ζ), two outputs (f and a) and 2 hidden layers with 5 units each.

Both approaches lead to similar results, shown in Fig. 3.2, with **B)** giving slightly lower energies than **A)** as expected. From these results, it is clear that, as $n \rightarrow \infty$, the sphaleron energies tend to a value differing from the SM one, provided $F_\star \neq 0$. We find that the difference between this value and the SM one is approximately proportional to F_\star^2 , as displayed in Fig. 3.2b. This non-perturbative phenomenon is hence sensitive to non-linearly realised theories that would be indistinguishable for perturbative scattering.

The prospects for observation of zero-temperature sphaleron-mediated processes rely on $B + L$ violation and involve all three families of fermions. Such a process might be initiated by, e.g., the impact of an energetic neutrino and the production of a multiparticle flavourful final state on IceCube [76,81], or by a high-energy collision at LHC and future colliders [82,83], although exponential suppression factors might make it unobservable in practice [84,85]. At finite temperature, the sphaleron energy is to be computed with the temperature-dependent effective potential and processes that are sensitive to it include the decoupling temperature for $B + L$ violating effects in baryogenesis, see e.g. [86].

3.3 Summary

Ultimately, we find that sphalerons can exist in HEFT/SMEFT theories, albeit with a field-configuration which is not fully defined. This is, however, a similar situation to the Higgs freeze-out limit ($\lambda \rightarrow \infty$) considered in [75] which also leads to a finite sphaleron energy. The energy of the sphaleron is modified from the Standard Model one, which may be observable experimentally. However the deviation could be very small, perhaps around the percent level: unlike the situation for amplitudes

of chapter 2, the sphaleron does indeed appear to approach the Standard Model energy. While it could still be possible to measure sphaleron energy deviations at the percent level, the sphaleron is phenomenologically difficult to pin-down as [83] have shown. As we shall see, phase transitions on the other hand offer a more promising avenue.

CHAPTER 4

The Cosmology of HEFT

The direct experimental exploration of the electroweak (EW) scale is in full swing at the LHC, and we are closing in on the answers to questions historically central to particle physics: the hierarchy problem, the mechanism for electroweak symmetry breaking, and mass generation. Looking out into the cosmos, on the other hand, has proven to be a source of invaluable input to our theories of Nature, the latest potential window into early cosmology—possibly including electroweak transitions—being gravitational waves.

At the front line of this exploration is the Higgs scalar and its properties. Given the absence of particles beyond the Standard Model (SM) spectrum thus far, the formalism of Effective Field Theories (EFTs) provides a general, model independent framework to characterise the Higgs particle. This formalism presents a dichotomy in that the electroweak EFT might or might not admit a linear representation. These two options are dubbed SMEFT and $\text{HEFT} \setminus \text{SMEFT}$ where backslash is the mathematical symbol for the difference of sets. The HEFT is the most general gauge and Lorentz invariant EFT we can write, and thus it includes both options. However, the literature often refers to the $\text{HEFT} \setminus \text{SMEFT}$ simply as HEFT. Here, we use non-linearly realised theory space $\equiv \text{HEFT} \setminus \text{SMEFT}$ to make it clear that

we are referring to EFT's that do not admit a linear representation.

The characterisation of these theories has been laid out [38, 39, 41], examples of UV completions and general results for certain classes have been derived [1, 18, 40, 43, 87, 88] and new features continue to emerge and be explored [5, 42, 44, 89–96]. A pertinent remark is that the SMEFT vs HEFT\SMEFT characterisation is an IR one, and there are known cases in which the UV description that completes a non-linearly realised HEFT\SMEFT theory presents linear scalar representations; what sets apart such linearly realised UV theories is that they are non-decoupling with an upper bound on the mass of new states of $\sim 4\pi v$. If such a contrast of UV and IR descriptions seems counter-intuitive, an example in nature is QCD and its natural low energy description using the chiral Lagrangian. Fully comprehensive characterisations are nonetheless elusive, in essence because the question is non-local in field space. Scattering experiments can only probe our theory around the vacuum to higher terms in our Taylor expansion of the Lagrangian in fields, incrementally improving our knowledge of the theory with more particles involved in the scattering process, yet still inherently local. It is here that cosmology offers a global view of our theory and the possibility of testing it non-locally via phenomena such as phase transitions or topological defect formation. It is the aim of this work to examine the window that cosmology opens on HEFT\SMEFT theories, especially those hardest to distinguish locally from the SM, and chart its complementarity with LHC data.

The elementary result for EFT characterisation is the presence or absence of a point in scalar field space which is invariant, i.e. stays fixed, under the gauge group action. A useful visualisation in a two-dimensional field space with rotation as the gauge group has the fixed point at the origin. The extension to the electroweak theory led to naming it an $O(4)$ fixed point with $SU(2)_L \times U(1)_Y \subset O(4)$. If this fixed point is present, it is possible to cast the EFT as a SMEFT, and if absent the EFT is non-linearly realised. This absence can arise in two broad forms:

- type A, theories entirely without a fixed point,
- type B, theories with a singularity at the would-be fixed point in scalar space.

This distinction with SMEFT and within non-linearly realised theories is one about

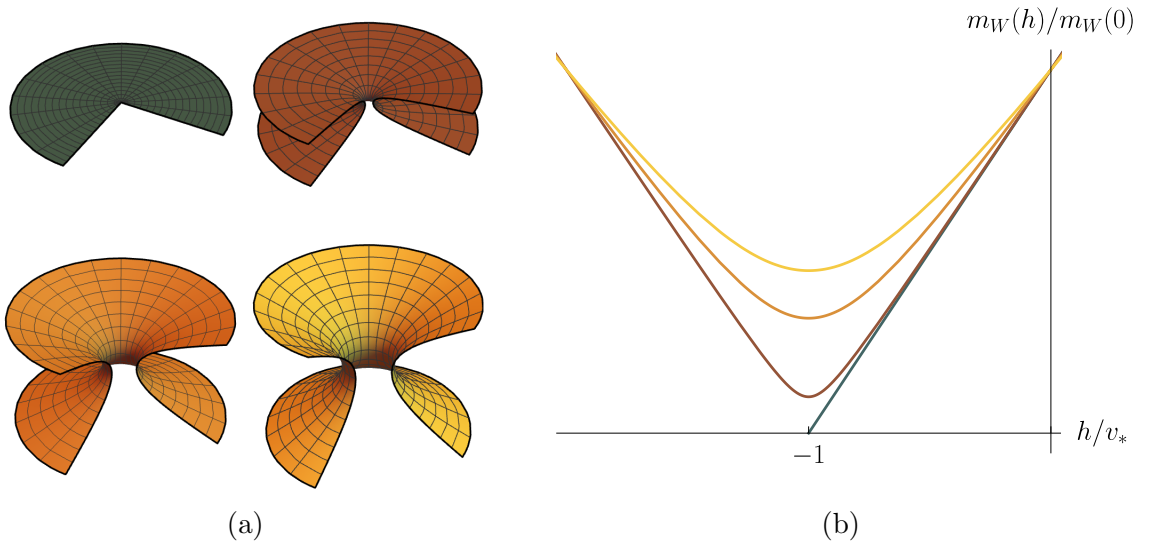


Figure 4.1: In Fig. 4.1a, from top to bottom and left to right, 2D representations of the 4D scalar manifold for the SM case (top left) and type A theories with the metric of Eqs. (4.34, 4.39) and $\sin^2 \chi = 0.01, 0.1$, and 0.2 . The Goldstone bosons correspond to the angle around the z axis, while the Higgs h parametrises the surface in the orthogonal direction to them. Fig. 4.1b shows $M_W(h)/M_W(0)$ for the SM and the type A theories in Fig. 4.1a with the same colour coding.

the possible realisation of the symmetry, and therefore one can expect the electroweak phase transition epoch of the universe to shed light on the question—we do not consider here low energy inflation or other scenarios that bypass a universe at T_{ew} . The cosmology of ultraviolet completions giving rise to theories with a singularity, i.e. type B, has in fact been studied already in Ref. [97] (see also [98]); this work focuses on type A. For a discussion of possible UV completions of type A theories see [6], and the example UV model provided in appendix A.

The absence of a fixed point in type A theories requires, in turn, a revision of the behaviour of the theory at high temperature. Indeed strictly speaking, electroweak symmetry cannot be restored at high temperature since there is not a point in the manifold for such restoration. One can still talk about discrete symmetry restoration nonetheless; a type A theory does not present a fixed point where the electroweak gauge boson masses would vanish, but it might contain a point where they reach their *minimum*. Let us suppose this point is a field distance v_* away from our current vacuum. One can then define reflection around this point: if h is the Higgs fluctuation around the vacuum, let us define $\phi \equiv h + v_*$, and the reflection as

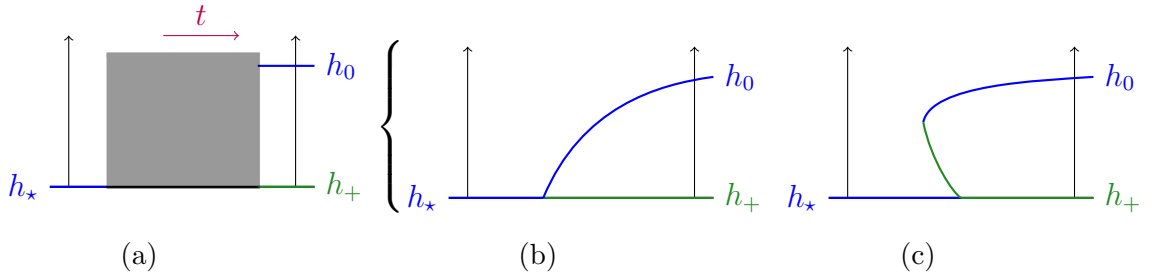


Figure 4.2: The possible extrema histories in SMEFT, minima in blue and maxima in green.

$\phi \mapsto -\phi$. The case of SMEFT has no such possible symmetry: v_* can be taken instead to be the distance to the fixed point, and by definition ϕ , a radius, is always positive. The geometric approach helps visualise such theory. The possibility of extending a ‘radius’ to negative values leads to a wormhole-like structure as shown in Fig. 4.1a.

Even with this discrete parity introduction, one might not have symmetry restoration at high temperature. In fact, given the variety of possibilities for minima in these theories, it is convenient to consider the history of extrema of the finite temperature potential in this extended range for the Higgs field including ‘negative’ values. We represent such histories as diagrams where time flows from left to right and the Higgs field value increases upwards, with lines showing the evolution, emergence and disappearance of extrema of the effective potential, see for example Fig. 4.2. For reference, the characterisation of possibilities for the extrema history in the case of the Standard Model with variable Higgs mass are well known but still useful to cast in this diagrammatic approach. One can have a transition from the symmetry-restored high temperature phase –with a potential of a single minimum at h_* – to the broken low temperature phase – with a minimum at h_0 and a maximum h_+ sitting where h_* used to be– via either (i) the splitting of the original minimum into a maximum and minimum (Fig. 4.2b), or (ii) the formation of a maximum-minimum pair at a finite distance and with a barrier between the new minimum and the symmetric minimum (Fig. 4.2c). The latter gives rise to a first order phase transition while the former contains the case of the SM with its measured couplings, yielding a cross-over phase transition. The extension to SMEFT allows for changing the EW transition to possibility (ii), see e.g. Ref. [99], but still not changing the qualitative picture of

possibilities as drawn above.

In non-linearly realised theories by contrast, the range for h need not have bounds, and the symmetric minimum might lose its natural extrema status (see Ref. [100]) but further, new minima arise from small deviations to SM couplings. The extension of the Higgs manifold shown in Fig. 4.1 is symmetric under the discrete reflection ($\phi \rightarrow -\phi$), which introduces a doubling of the minima, with a new one arising on the other side of the wormhole. This symmetric limit with Higgs parity restoration at high temperature – i.e. a single minimum h_{\star} – is shown in Fig. 4.3b, history P, and without parity restoration in Fig. 4.4. For no high temperature symmetry restoration we can find high and low temperature configurations as in Fig. 4.5.

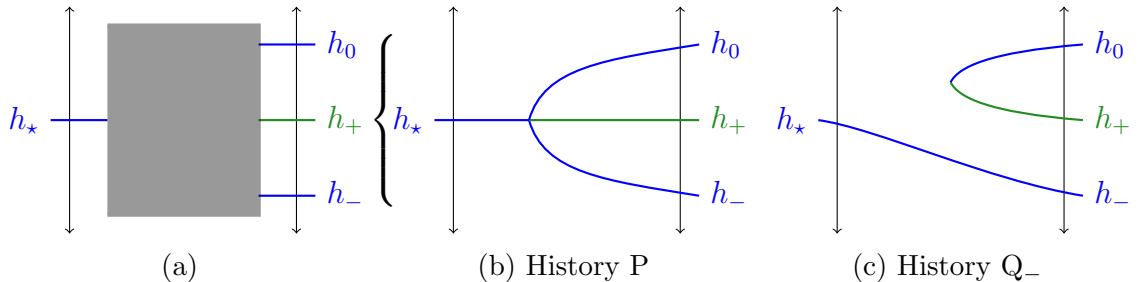


Figure 4.3: Extrema histories we encounter in non-linearly realised theories with one extrema at high temperature and three at low temperature.

All the diagrams shown in Figs. 4.3–4.5, are selected not by an artistic whim but rather because they do occur in the theories here considered. Generically one needs the further input of potential difference between extrema or barrier height to determine the phenomenology, but certain diagrams do however necessarily lead to processes markedly distinct from the SM. An example is Fig. 4.4b with a single minimum for all history and hence no phase transition; while this in itself is a qualitative difference from the SM case, it is not one easily testable. History R in Fig. 4.4c by contrast does necessarily lead to a phase transition before the original minimum meets a sudden end encountering a maximum. Histories P,Q and R—Fig. 4.3 shows Q₋, while Q₀ is the parity-reflected case—will be the main cases of this study since they leave potentially observable traces or are partially ruled out.

In Figs. 4.3–4.5 we have also introduced notation to label extrema; we will use h_0 for the minimum of the potential we find ourselves in today, h_{+} and h_{-} for possible

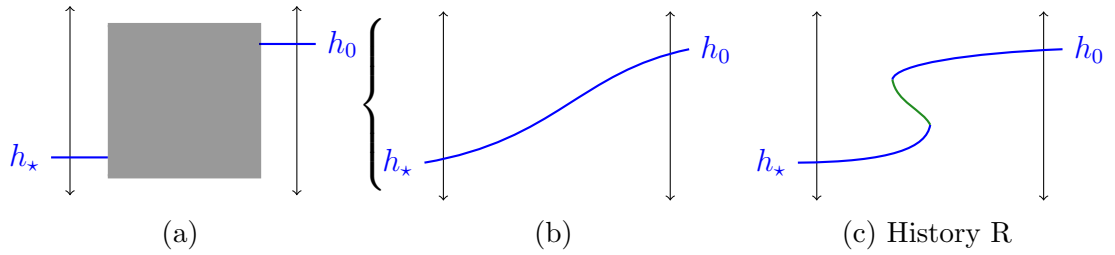


Figure 4.4: Possible extrema histories for a single minimum at high and low temperature

maximum and minimum in the $T = 0$ potential. Note that our definition of h_0 as our vacuum today, –around which we have e.g. measured the mass of the Higgs to be 125 GeV– while conventional, does mean that any evolution of the universe that leads to the vacuum at h_- today is discarded, without loss of generality.

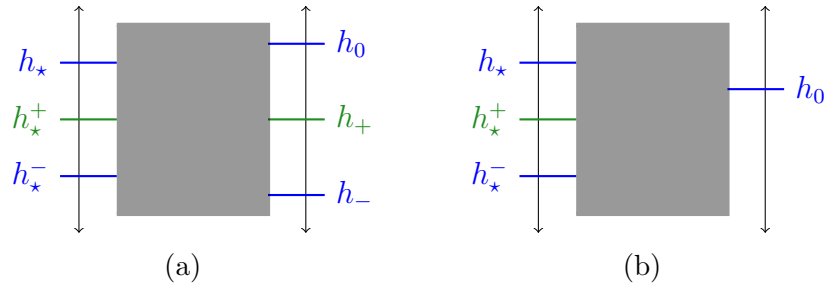


Figure 4.5: Initial and $T = 0$ extrema we find as realisations in non-linearly realised theories without high-temperature symmetry restoration.

4.1 The Thermal Effective Potential

In order to study phase transitions in the early universe we must construct the thermal effective potential. A full, detailed derivation can be found in numerous works such as [101–103]. Here, we outline the procedure via the imaginary time formalism, highlighting key features.

The Thermal Partition Function

A familiar principle from thermodynamics is that many thermodynamical properties of a system can be determined using the partition function. For a quantum mechanical system in the grand canonical ensemble, who's dynamics are governed

by the Hamiltonian operator \hat{H} at temperature $T = 1/\beta$:

$$\mathcal{Z} = \text{Tr} \left\{ e^{-\beta \hat{H}} \right\} = \sum_a \int d\phi_a \langle \phi_a | e^{-\beta \hat{H}} | \phi_a \rangle \quad (4.1)$$

is the partition function. The trace is taken over the full Hilbert space, on the right hand side the states $|\phi_a\rangle$ are in the Schroedinger picture, and all are summed over. It will help to write the partition function as a path integral. It is possible to, making use of the completion relations for the states $|\phi_a\rangle$, write the partition function as (neglecting irrelevant pre-factors)

$$\mathcal{Z} = \int \mathcal{D}\phi \exp \left\{ \int_0^\beta d\tau \int d^3x \mathcal{L}_E \right\} \quad (4.2)$$

where \mathcal{L}_E is the Lagrangian for the system in Euclidean space (which is related to the Lagrangian in Minkowsky space \mathcal{L}_M by $\mathcal{L}_E = -\mathcal{L}_M|_{\tau=it}$). We will not detail the procedure here, but refer the reader to e.g. [101].

It is important to note that one of the features that arises in this path integral is that the field ϕ is periodic in τ : $\phi(0, x) = \phi(\beta, x)$, and $\tau \in \{0, \beta\}$. Consequently, it is possible to expand ϕ into Fourier modes

$$\phi(x) = T \sum_{n=-\infty}^{\infty} \int \frac{d^3\mathbf{k}}{(2\pi)^3} e^{ik \cdot x} \phi(k) = T \sum_{n=-\infty}^{\infty} \int \frac{d^3\mathbf{k}}{(2\pi)^3} e^{i(\omega_n \tau - \mathbf{k} \cdot \mathbf{x})} \phi(k) \quad (4.3)$$

$$\omega_n = 2n\pi T \quad (4.4)$$

for $k = (\omega_n, \mathbf{k})$. These are known as Matsubara modes, and ω_n are the Matsubara frequencies.

The partition function eq. (4.2) is the same for fermionic fields with spin-1/2. In this case, we restrict the field to be anti-periodic ($\psi(0, x) = -\psi(\beta, x)$), where the Matsubara frequencies are now odd $\omega_n = (2n + 1)\pi T$.

Following the simplest case of a real and free scalar field with Lagrangian

$$\mathcal{L}_E = \frac{1}{2} \partial_\mu \phi \partial^\mu \phi + \frac{1}{2} m^2 \phi^2 \quad (4.5)$$

we can write, after substituting in the Matsubara modes and writing $\omega^2 = \mathbf{k}^2 + m^2$,

$$\mathcal{Z}(T) = \int \mathcal{D}\phi \exp \left\{ -\frac{1}{2}T \sum_{n=-\infty}^{\infty} \frac{1}{V} \sum_{\mathbf{k}} (\omega^2 + \omega_n^2) |\phi(\omega_n, \mathbf{k})|^2 \right\} \quad (4.6)$$

where $\phi(\omega_n, \mathbf{k})^* = \phi(-\omega_n, -\mathbf{k})$ such that $\phi(\omega_n, \mathbf{k})\phi(-\omega_n, -\mathbf{k}) = |\phi(\omega_n, \mathbf{k})|^2$. Notice that the momenta k_i have become discrete, $k_i = 2\pi n_i/L_i$. This is because we have chosen to compute this expression over a discrete volume V and take the continuum limit later, for ease of computation.¹ In order now to integrate over the fields, we need to change integration variables to the Matsubara modes, i.e.:

$$\mathcal{D}\phi(x) = \det \left| \frac{\delta\phi(x)}{\delta\phi(k)} \right| \underbrace{d\phi(0, \mathbf{k})}_{\text{Zero Mode}} \times \underbrace{\prod_{n \geq 1} d\phi(\omega_n, \mathbf{k})}_{\text{Non-Zero Mode}} \quad (4.8)$$

The result for the determinant from e.g. [101] is:

$$\det \left| \frac{\delta\phi(x)}{\delta\phi(k)} \right| = \left(\underbrace{\frac{T}{2\pi} \sqrt{\frac{2\pi T}{V}}}_{\text{Zero Mode}} \underbrace{\prod_{m \geq 1} \frac{T\omega_m^2}{\pi V}}_{\text{Non-Zero Mode}} \right). \quad (4.9)$$

Splitting the Matsubara modes into a zero and a non-zero mode is a choice whose usefulness will become clear later. Changing the integral measure results in the

¹Recall taking the infinite volume limit for the \mathbf{k} integral involves the replacement

$$\frac{1}{V} \sum_{\mathbf{k}} \xrightarrow{V \rightarrow \infty} \int \frac{d^3\mathbf{k}}{(2\pi)^3} \quad (4.7)$$

or vice versa in a finite volume.

following

$$\begin{aligned}
\mathcal{Z}(T) &= \int \mathcal{D}\phi \exp \left\{ -\frac{1}{2}T \sum_{n=-\infty}^{\infty} \frac{1}{V} \sum_{\mathbf{k}} (\omega^2 + \omega_n^2) \right\} \\
&= \int \mathcal{D}\phi \prod_{\mathbf{k}} \exp \left\{ -\frac{T}{2V} \sum_{n=-\infty}^{\infty} (\omega^2 + \omega_n^2) |\phi(\omega_n, \mathbf{k})|^2 \right\} \\
&= \prod_{\mathbf{k}} \det \left| \frac{\delta\phi(x)}{\delta\phi(k)} \right| \int d\phi(0, \mathbf{k}) \prod_{n \geq 1} d\phi(\omega_n, \mathbf{k}) \\
&\quad \exp \left\{ -\frac{T\omega^2}{2V} |\phi(0, \mathbf{k})|^2 - \frac{T}{V} \sum_{n=1}^{\infty} (\omega^2 + \omega_n^2) |\phi(\omega_n, \mathbf{k})|^2 \right\} \\
&= \prod_{\mathbf{k}} \det \left| \frac{\delta\phi(x)}{\delta\phi(k)} \right| \sqrt{\frac{2\pi V}{T\omega^2}} \times \prod_{n \geq 1} \frac{\pi V}{T(\omega^2 + \omega_n^2)}
\end{aligned}$$

where as usual we have split the Matsubara modes into zero and non-zero modes.

Using eq. (4.9),

$$\mathcal{Z}(T) = \prod_{\mathbf{k}} \frac{T}{\omega} \prod_{n \geq 1} \frac{\omega_n^2}{\omega^2 + \omega_n^2} \quad (4.10)$$

$$\begin{aligned}
&\xrightarrow{V \rightarrow \infty} \exp \left\{ -\frac{V}{T} \int \frac{d^3\mathbf{k}}{(2\pi)^3} \left(\frac{\omega}{2} + T \ln(1 - e^{-\omega/T}) \right) \right\}. \quad (4.11)
\end{aligned}$$

Free Energy

The free energy $F = -T \ln \mathcal{Z}$ is used to determine how much thermodynamic work a system can produce. And as such is the relevant quantity for phase transitions.

For scalar particles:

$$\lim_{V \rightarrow \infty} \frac{F}{V} = \int \frac{d^3\mathbf{k}}{(2\pi)^3} \left(\frac{\omega}{2} + T \ln(1 - e^{-\omega/T}) \right) \quad (4.12)$$

$$\equiv J_0(m) + \tilde{J}_B(m, T) \quad (4.13)$$

The second term we can simplify further to

$$\tilde{J}_B(m, T) = T \int \frac{d^3\mathbf{k}}{(2\pi)^3} \ln \left(1 - e^{\sqrt{m^2 + \mathbf{k}^2}/T} \right) \quad (4.14)$$

$$= \frac{T^4}{2\pi^2} \int dx x^2 \ln \left(1 - e^{-\sqrt{(m/T)^2 + x^2}} \right) \quad (4.15)$$

We use the subscript B to indicate that, although we derived this for scalar fields, all bosonic fields contribute to the free energy in the same way. Fermions, however, contribute differently as the Matsubara frequencies are odd:

$$\lim_{V \rightarrow \infty} \frac{F}{V} = \int \frac{d^3 \mathbf{k}}{(2\pi)^3} \left(\frac{\omega}{2} + T \ln (1 + e^{-\omega/T}) \right) \quad (4.16)$$

$$\equiv J_0(m) + \tilde{J}_F(m, T). \quad (4.17)$$

Again, simplifying further,

$$\tilde{J}_F(m, T) = \frac{T^4}{2\pi^2} \int dx x^2 \ln \left(1 + e^{-\sqrt{(m/T)^2 + x^2}} \right) \quad (4.18)$$

In this derivation, we have considered a free theory. In practice, we would like to also include interactions. This is done following the so-called *background field method* which was introduced in section 1.5.3. Essentially, it involves computing the procedure having shifted $\phi \rightarrow \bar{\phi} + \eta$ where $\bar{\phi}$ is a constant field. Unfortunately, the functional integral we computed no longer has a closed-form solution, but we can employ perturbation theory to yield an approximate expression for the effective potential. Indeed the one-loop result we can obtain easily by replacing the mass m with an *effective mass* which is now field-dependent

$$m_{\text{eff}}^2(\bar{\phi}) = \left. \frac{\partial^2 V(\phi)}{\partial \phi^2} \right|_{\phi=\bar{\phi}}, \quad (4.19)$$

where V is some potential. Note as long as couplings are small, this can contain other fields as well.

Relation to the Coleman Weinberg Potential

The first, temperature-independent terms in eqs. (4.12) and (4.16) are just the Coleman-Weinberg potential. We can see this by computing the one-loop effective

action for an interacting scalar field from eq. (1.179), which is

$$V_{\text{eff}}^{\text{one-loop}} = -\frac{i}{2} \int \frac{d^4 k}{(2\pi)^4} e^{ik \cdot x} \log(-\partial_\mu \partial^\mu + m_{\text{eff}}^2(\phi)) e^{-ik \cdot x} \quad (4.20)$$

$$= -\frac{i}{2} \int \frac{d^4 k}{(2\pi)^4} \log(-k^2 + m_{\text{eff}}^2(\phi)) \quad (4.21)$$

$$= -\frac{i}{2} \int \frac{d^4 k}{(2\pi)^4} \log(-(k^0)^2 + (\mathbf{k})^2 + m_{\text{eff}}^2(\phi)). \quad (4.22)$$

which, upon integrating over k^0 , gives [104]:

$$V_{\text{eff}}^{\text{one-loop}} = \frac{1}{2} \int \frac{d^3 \mathbf{k}}{(2\pi)^3} \omega \quad (4.23)$$

apart from an infinite constant which can be ignored, i.e. exactly the temperature independent terms in eqs. (4.12) and (4.16). As such, one usually considers the temperature dependent terms to be ‘thermal corrections’ to the Coleman Weinberg effective potential, and the sum of both to be the ‘thermal effective potential’.

The Bounce Action

In a finite temperature phase transition for a system, we have the case where, at high temperatures, the system is in some absolute vacuum state. However, as the system cools, a new vacuum state begins to manifest, which is energetically favourable.

If the ground state of the system evolves continuously, this is a second order phase transition. I.e. the ground state can simply ‘roll’ down the potential well into the true vacuum. In a first order phase transition, the transition between the false and true vacua is discontinuous because there is a barrier in the potential between them.

The transition occurs through quantum tunnelling between the vacua. Initially the phase transition occurs only some regions of space, known as bubbles, which grow and coalesce until the new phase completely replaces the old.

In the case in which the first order phase transition is strong, the process of bubble nucleation can produce a significant, and realistically observable, gravitational wave signal.

At finite temperature, the tunnelling rate for a first order phase transition from

a false vacuum to a true vacuum is given by [105]

$$\Gamma[\beta] \sim -2 \operatorname{Im}(F). \quad (4.24)$$

Indeed following on from the thermal partition function eq. (4.2), to compute the tunnelling rate, we can again employ the background field method, $\phi = \bar{\phi} + \eta$. If we choose $\bar{\phi}$ to minimise the Euclidean action, it will dominate the path integral. Then we can write

$$\mathcal{Z} = \int \mathcal{D}\phi e^{-S_E[\phi]} = \int \mathcal{D}\eta e^{-S_E[\bar{\phi}] - \frac{1}{2} S_E''[\bar{\phi}] \eta^2 + \dots} \quad (4.25)$$

where $S_E''[\bar{\phi}] = \left. \frac{\delta^2 S_E}{\delta \phi^2} \right|_{\phi=\bar{\phi}}$. Then the tunnelling rate is

$$\Gamma[\beta] = 2T \operatorname{Im} \left[\ln \left(\mathcal{Z}_0 + \int \mathcal{D}\eta e^{-S_E[\bar{\phi}] - \frac{1}{2} S_E''[\bar{\phi}] \eta^2 + \dots} \right) \right] \quad (4.26)$$

$$\sim 2T \operatorname{Im}[\ln \mathcal{Z}_0] + 2 \frac{T}{\mathcal{Z}_0} \operatorname{Im} \left[\int \mathcal{D}\eta e^{-S_E[\bar{\phi}] - \frac{1}{2} S_E''[\bar{\phi}] \eta^2 + \dots} \right] \quad (4.27)$$

$$\equiv A(T) e^{-S_E[\bar{\phi}]} \quad (4.28)$$

where \mathcal{Z}_0 is the contribution from the solution in which the system remains in the false vacuum which we would expect to dominate. Note the remaining path integral is subject to the boundary conditions that $\phi_{T=0}(r=0) = \phi_{\text{true}}$ and $\phi_{T=0}(r=\infty) = \phi_{\text{false}}$, where ϕ_{true} and ϕ_{false} refer to the true and false vacua respectively, assuming the field is spherically symmetric. The function $A(T)$ we can compute by evaluating the path integral to second order and absorbing \mathcal{Z}_0 , to

$$A(T) = \frac{T}{\mathcal{Z}_0} \operatorname{Im}[(\det S_E[\bar{\phi}])^{-1/2}], \quad (4.29)$$

however it is a very difficult computation, and nonetheless it is the exponential suppression that is more important for phase transitions.

In the thermal case, when length scales are large compared to β one can take

the high-temperature limit where $\beta \ll 1$,

$$\int_0^\beta d\tau \sim \beta \qquad \frac{\partial\phi}{\partial\tau} \sim 0, \quad (4.30)$$

the Euclidean action is approximately

$$S_E \approx \beta \int d^3\mathbf{x} \left[\frac{1}{2}(\nabla\phi)^2 + V(\phi) \right] \quad (4.31)$$

$$\equiv \beta S_3[\phi] \quad (4.32)$$

where S_3 is the three-dimensional action. Now the tunnelling rate looks like

$$\Gamma[\beta] \sim e^{-S_3/T}. \quad (4.33)$$

The argument of the exponential, S_3/T , is called the *bounce action* and is the relevant thermal action to compute for early universe phase transitions [106], which we will refer to in later sections.

4.2 Classical Action

The tree level Lagrangian for the electroweak sector we use here to model non-linear theories reads

$$\mathcal{L} = \frac{1}{2}\partial h^2 + \frac{F^2(h)}{2}v^2\frac{1}{2}\text{Tr} [D_\mu U D^\mu U^\dagger] - V(h) - \left[\frac{F_\psi(h)v}{\sqrt{2}}\bar{\psi}_L Y U \psi_R + \text{h.c.} \right] \quad (4.34)$$

$$\equiv \frac{1}{2}d_\mu\Phi^i G_{ij}d^\mu\Phi^j - V(h) - \left[\frac{F_\psi(h)v}{\sqrt{2}}\bar{\psi}_L Y U \psi_R + \text{h.c.} \right], \quad (4.35)$$

where $F(0) = F_\psi(0) = 1$ and $v = 246$ GeV. Here, U is a special unitary 2×2 matrix parameterised by 3 scalar degrees of freedom φ^a , the Nambu-Goldstone bosons, which, together with the Higgs degree of freedom h , span a four-dimensional manifold with coordinates $\Phi^i = (\varphi^a, h)$. We have used the latin letters i, j, k for the components of Φ , running from 1 to 4, and a, b, c for Nambu-Goldstone bosons running from 1 to 3. The gauged covariant derivative $d_\mu\Phi = \partial_\mu\Phi + t_C A_\mu^C$, with electroweak bosons $A_\mu^C = \{W_\mu^I, B^\mu\}$, where $I = 1, 2, 3$ and t_C are the killing vectors [39]

defined as, together with the metric

$$\tilde{g}_{ab} = \frac{v^2}{2} \text{Tr} \left(\frac{\partial U}{\partial \varphi^a} \frac{\partial U^\dagger}{\partial \varphi^b} \right) = v^2 \frac{\partial u^T}{\partial \varphi^a} \frac{\partial u}{\partial \varphi^b}, \quad G_{ij} = \begin{pmatrix} F^2 \tilde{g}_{ab} & \\ & 1 \end{pmatrix}, \quad (4.36)$$

$$\frac{t_I^a}{v^2} = \frac{ig\tilde{g}^{ab}}{4} \text{Tr} \left(U \frac{\partial U^\dagger}{\partial \varphi^b} \sigma_I \right) \quad \frac{t_Y^a}{v^2} = \frac{ig_Y\tilde{g}^{ab}}{4} \text{Tr} \left(U^\dagger \frac{\partial U}{\partial \varphi^b} \sigma_3 \right) \quad (4.37)$$

$$= \frac{g\tilde{g}^{ab}}{2} u^T T_I \frac{\partial u}{\partial \varphi^b}, \quad = \frac{g_Y\tilde{g}^{ab}}{2} u^T T_Y \frac{\partial u}{\partial \varphi^b}, \quad (4.38)$$

where u is a real four vector of norm one, $u^T u = 1$, and σ are the Pauli matrices. We use T to stand for a subset of the generators of $SO(4)$ such that $T^T = -T$, $\text{Tr}[TT] = -4$. There are a number of relations these objects obey due to unitarity such as $(\partial U)U^\dagger = -U\partial U^\dagger$. For simplicity we will take a universal F , $F_\psi = F$ with no flavour structure, which for concreteness will read, as a function of the Higgs field,

$$F(h) = \sqrt{s_\chi^2 + c_\chi^2(1 + h/v_\star)^2} = \sqrt{s_\chi^2 + c_\chi^2(1 + \gamma_a h/v)^2}, \quad (4.39)$$

where one has $\gamma_a = v/v_\star$. In the general formulation of the HEFT, $F^2(h)$ can be an arbitrary analytic function $F^2(h) = 1 + \sum_{n=1}^{\infty} f_n h^n$. Our choice corresponds to setting

$$f_1 = \frac{2 \cos^2 \chi}{v_\star}, \quad f_2 = \frac{\cos^2 \chi}{v_\star^2}, \quad f_{n>2} = 0, \quad (4.40)$$

which just amounts to imposing that $F^2(h)$ is quadratic in h with generic coefficients. This is enough to model the main feature of our non-linearly realised theory: a scalar manifold with a double sheet structure, connected by a throat at a distance v_\star from our vacuum $h = 0$. It is at the narrowest point of this throat where F reaches its minimum, and so do electroweak particle masses. For $\chi > 0$, $\text{Min}[F(h)] > 0$ which we maintain throughout, a limit of decreasing χ is depicted in Fig. 4.1 for both F and the shape of the manifold. The field-dependent mass term for gauge bosons then reads

$$m_W(h) = \frac{gv}{2} F(h), \quad m_Z(h) = \frac{v}{2} F(h) \sqrt{g^2 + g_Y^2}, \quad (4.41)$$

with $F \geq \sin \chi$ over the full range of h , and the minimum is achieved for

$$\text{Min}[m_W(h)] \equiv \frac{gv}{2} F(-v_\star) = \frac{gv \sin \chi}{2}. \quad (4.42)$$

We dub the reflection transformation introduced in the previous section Higgs parity—not to be confused with other acceptations [107]—whose action on ϕ , the distance to the throat of the manifold, reads

$$\phi = h + v_\star \equiv h + v\gamma_a^{-1}, \quad (4.43)$$

$$\boxed{\text{Higgs Parity}} \quad \phi \rightarrow -\phi, \quad (4.44)$$

which as remarked in the introduction is not a symmetry applicable to SMEFT.

A scalar manifold and metric differing from the SM flat case will imply different couplings and deviations in observables. Scattering matrix elements are given in terms of tensors in field space projected on the different directions with vierbeins; in particular, the tensor that dictates scalar couplings to order p^2 is the curvature tensor and its covariant derivatives [38, 41]. One has in our case a Riemann tensor \mathcal{R} that follows from the metric G as

$$\mathcal{R}_a{}^b{}_c{}^d = R_\varphi(\tilde{g}_{ac}\tilde{g}^{bd} - \delta_a^d\delta_c^b), \quad \mathcal{R}_{ah}{}^{bh} = R_h\delta_a^b, \quad (4.45)$$

and the only two independent functions

$$v^2 R_\varphi(h) \equiv \frac{1}{F^2} - v^2 [(\log F)']^2 = \frac{c_\chi^2(1+h/v_\star)^2(1-c_\chi^2\gamma_a^2) + s_\chi^2}{(s_\chi^2 + c_\chi^2(1+h/v_\star)^2)^2}, \quad v^2 R_\varphi(0) = 1 - c_\chi^4\gamma_a^2, \quad (4.46)$$

$$v^2 R_h(h) \equiv -\frac{v^2 F''}{F} = -\frac{\gamma_a^2 s_\chi^2 c_\chi^2}{(s_\chi^2 + c_\chi^2(1+h/v_\star)^2)^2}, \quad v^2 R_h(0) = -\gamma_a^2 s_\chi^2 c_\chi^2, \quad (4.47)$$

where we also present curvature evaluated at the origin because this is what LHC is sensitive to and can set bounds on, as in Ref. [1].

Lastly the tree level potential, which might generate new extrema, is a quartic

potential accommodating the Higgs mass but with free cubic and quartic terms

$$V(h) = \frac{m_h^2}{2}h^2 + \frac{m_h\sqrt{\lambda}}{2}\gamma_4(1-\epsilon)h^3 + \frac{\lambda}{8}\gamma_4^2h^4, \quad (4.48)$$

with the SM limit $\gamma_4 \rightarrow 1, \epsilon \rightarrow 0$. We have defined $\sqrt{\lambda} \equiv m_h/v \simeq 125/246$ as a way to parametrise our system, but note this does not imply an SM-like quartic coupling.

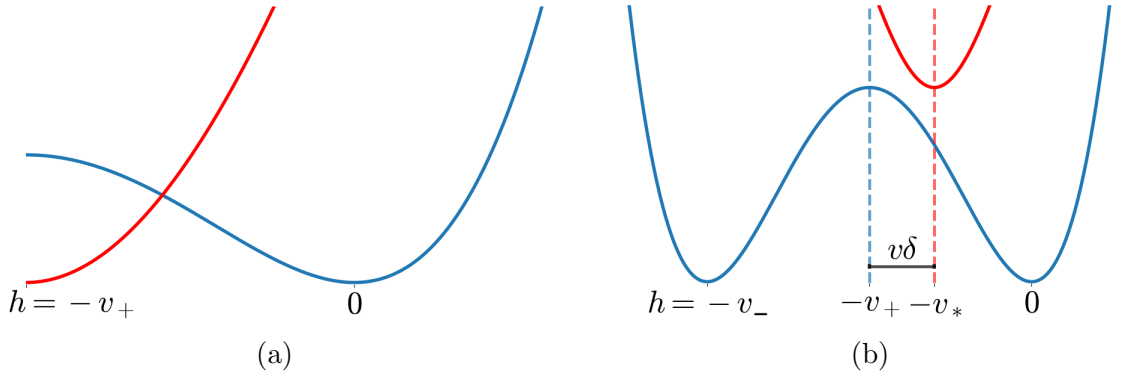


Figure 4.6: Schematic diagram of the tree level Higgs potential $V(h)$ in blue and in red the Higgs-dependent W mass, $v^2 m_W^2(h)$, in arbitrary units to set our conventions. Along the horizontal axis runs the Higgs field h . Fig. 4.6a shows the SM and SMEFT case, with $h \in [-v_+, \infty)$, and Fig. 4.6b shows the non-linearly realised theory case where $h \in (-\infty, \infty)$. The quantities v_\pm, v_* and δ are defined in Eqs. (4.49), (4.39) and (4.53) respectively.

The tree-level potential has a minimum by design at $h = 0$, where we define the vacuum we inhabit today. There are two other possible extrema at a distance v_\pm which read, in terms of γ_4, ϵ :

$$h_{\mp}(T=0) \equiv -v_{\mp} \equiv -v\gamma_4^{-1} \frac{3(1-\epsilon) \pm \sqrt{1+9(\epsilon^2-2\epsilon)}}{2} \equiv \begin{cases} -2v\gamma_4^{-1}\gamma_\epsilon^{-1} \\ -v\gamma_4^{-1}\gamma_\epsilon \end{cases}, \quad (4.49)$$

where we have defined

$$\gamma_\epsilon \equiv \begin{cases} \frac{3(1-\epsilon) - \sqrt{1+9(\epsilon^2-2\epsilon)}}{2} & \epsilon \leq 1 - \sqrt{8/9} \\ \sqrt{2} & \epsilon > 1 - \sqrt{8/9} \end{cases}. \quad (4.50)$$

Only in the former range of ϵ are two other extrema present because for the solutions

to be real one needs

$$9(1 - \epsilon)^2 \geq 8. \quad (4.51)$$

That is, numerically, $\epsilon \leq 1 - \sqrt{8/9} \simeq 0.057$. At the upper limit of this inequality $\gamma_\epsilon = \sqrt{2}$, and the two extrema meet at $h/v = -\sqrt{2}\gamma_4^{-1}$ to form an inflection point, which informs our definition of γ_ϵ for the upper interval. It should be stressed that this small range for positive ϵ where two extrema are present does not guarantee an expansion in small epsilon is viable, in particular not when close to the upper limit.

The values of the potential at the different extrema are

$$V(-v_\mp) = \frac{\lambda v^4 \gamma_4^{-2}}{4} \left(\frac{v_\mp}{v \gamma_4^{-1}} \right)^2 \left(1 + \frac{1 - \epsilon}{2} \left(\frac{-v_\mp}{v \gamma_4^{-1}} \right) \right) = \begin{cases} \gamma_4^{-2} \gamma_\epsilon^{-2} \lambda v^4 (1 - \gamma_\epsilon^{-1} (1 - \epsilon)) \\ \gamma_4^{-2} \gamma_\epsilon^2 \lambda v^4 (2 - \gamma_\epsilon (1 - \epsilon)) / 8 \end{cases}. \quad (4.52)$$

Note that only differences in these values are significant, and so we have chosen $V(0) = 0$ in the definition of the potential in Eq. (4.48). It is useful to define the distance between the local maximum of the potential and the minimum value of electroweak masses as

$$\delta \equiv \begin{cases} \frac{v_+ - v_*}{v} = \gamma_4^{-1} \gamma_\epsilon - \gamma_a^{-1} & \epsilon \leq 1 - \sqrt{8/9} \\ \gamma_4^{-1} \sqrt{2} - \gamma_a^{-1} & \epsilon > 1 - \sqrt{8/9} \end{cases}, \quad (4.53)$$

and a visual definition of δ in the presence of two tree-level minima is given in Fig. 4.6.

In the limit of small deviation from (local) SM couplings $\epsilon, \delta \ll 1$, we have— noting that this expansion is in the $\epsilon < 1 - \sqrt{8/9}$ interval,

$$\gamma_\epsilon \simeq 1 + 3\epsilon, \quad V(h_\mp) \simeq \begin{cases} 4\gamma_4^{-2} \lambda v^4 \epsilon + \mathcal{O}(\epsilon^2) \\ \gamma_4^{-2} \lambda v^4 / 8 + \mathcal{O}(\epsilon) \end{cases}. \quad (4.54)$$

Now through the definition of v_* in Eq. (4.43), those of v_\pm in Eq. (4.49) and the above, we can write the theory in terms of 4 free parameters δ, χ, ϵ and γ_4 which control respectively,

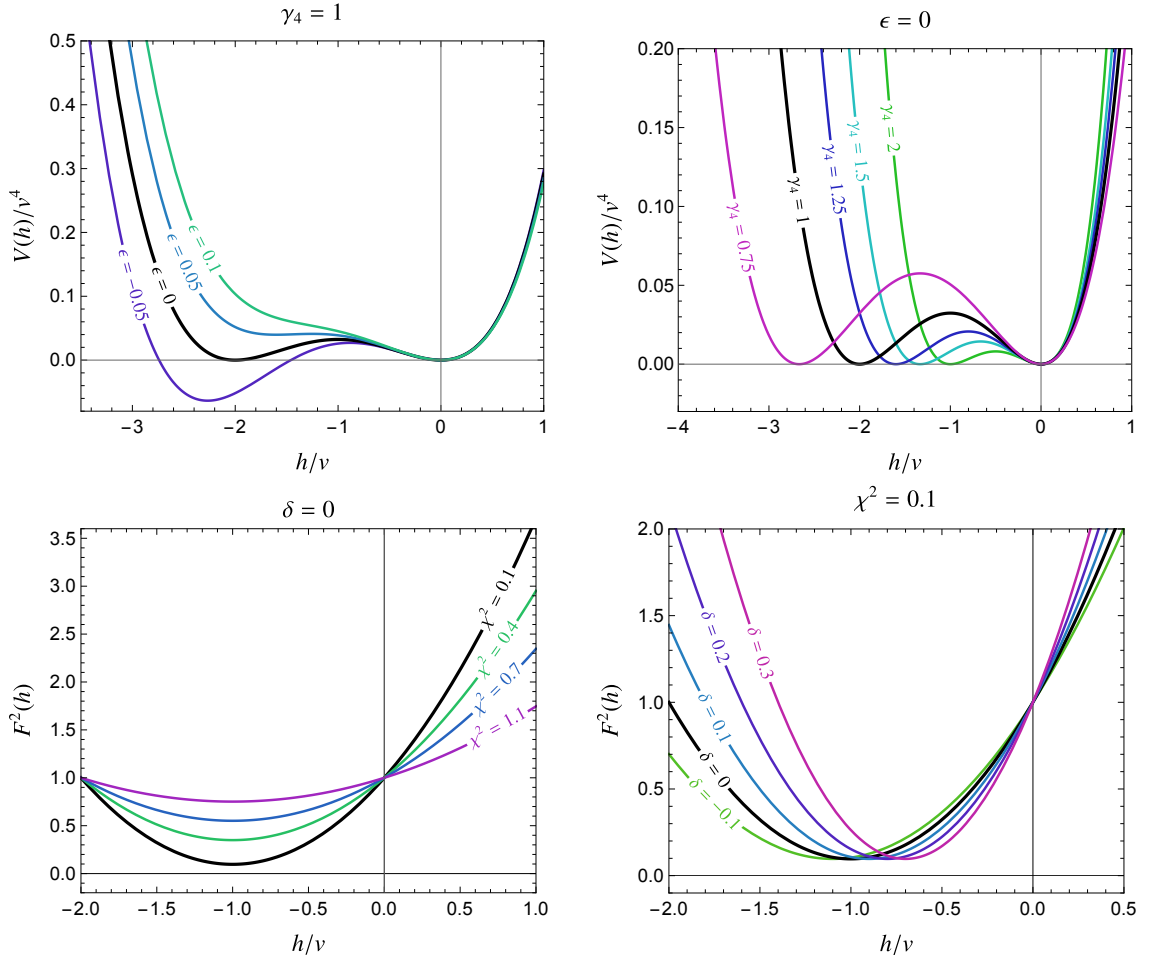


Figure 4.7: The effect of the 4 free parameters of our effective Lagrangian on the tree-level potential $V(h)$ and the $F(h)$ function. Top: variation of the potential $V(h)$ with ϵ (left) and γ_4 (right). Bottom: variation of the $F(h)$ function with χ (left) and δ (right).

χ the width of the throat, defined in Eq. (4.39) and depicted in Figs. 4.1 and 4.7.

ϵ the energy difference between the two tree-level minima and the Higgs triple coupling; this is defined in Eq. (4.48), and its effect depicted in Fig. 4.7.

γ_4 the distance between the two tree level minima and the triple and quartic Higgs coupling, defined in Eq. (4.48), and depicted in Fig. 4.7.

δ the distance between the throat and the potential tree level maximum, defined in Eqs. (4.39) and (4.53) and depicted in Figs. 4.6 and 4.7.

As we shall see, this modelling of non-linearly realised theories is versatile enough to unveil a rich phenomenology of which here we purport to show what we believe to be a representative sample.

4.3 The Thermal Effective Potential in Non-Linear Realised Theory Space

The key quantity to study phase transitions and defect formation is the effective potential at finite temperature. The computation of this potential is not without obstacles, long since identified and discussed in the literature extensively, see e.g. Ref. [108] for a review. In such context, here we opt for laying out our derivation with all assumptions and choices explicit while emphasising the limit of applicability of our results. In addition by facing old problems from a new theory, we believe this work might bring novel approaches and perspective.

The effective potential will be computed to one loop at finite temperature. This suffices to chart possible new phenomena that HEFT brings to the electroweak phase transition. Before proceeding to the computation, however, let us first discuss its limitations. The potential estimate here is not valid in all the field domain since perturbation theory breaks down in thermal field theory for gauge theories in the limit of vanishing transverse mode mass (i.e. the infrared problem [109])—for the EW theory this occurs around the $O(4)$ fixed point. While the perturbative expansion can be supplemented with resummation techniques and dimensional reduction as

detailed in Ref. [103, 108],² the deciding say lies in lattice. Rather than attempting to extend the potential computation to this domain beyond perturbativity, we will mark its limits and base our conclusions on results outside of it. It is worth noting already that the IR problem arises as the masses of gauge bosons approach zero and the presence of a lower bound on such masses in our theory ameliorates the problem.

A second relevant consideration is that our potential, since it is computed in an EFT, is not valid to arbitrarily high temperatures. The amplitude for longitudinal boson scattering scales as $R s$, where s is the square of the centre of mass energy. This points to a cutoff where new states would appear at $\Lambda \sim 4\sqrt{\pi}|R(0)|^{-1/2}$ (see eq. (2.26) and [1]), see also [40] where unitarity leads to an estimate of $\Lambda \sim 4\pi v$. Experimental data from LHC constrains the curvature around the EW vacuum at zero temperature to be small so that the cut-off is above the TeV. In the evolution of the universe, however, the electroweak vacuum changes position in field space and scans over a range of values. Approximating as customary the thermally averaged cross-section in this environment as the zero temperature result convoluted with the thermal distributions, one can expect the cut-off estimation outlined above for $h = 0$ to be extended to different manifold values $\Lambda(h) \sim 4\sqrt{\pi}|R(h)|^{-1/2}$. This naive extension of the cut-off estimate to thermal field theory ignores the extra Boltzmann suppression that the contribution of heavy states receive (indeed UV divergences in thermal field theory are much softened with respect to zero temperature), but doing so is erring on the conservative side. We therefore consider the cut-off for the whole range that the Higgs field explores, and one has that it would be lowest at the highest curvature, i.e. the throat, see Fig. 4.8. At the throat one has $\Lambda \sim 4\sqrt{\pi}[R_\varphi(h = -v_\star)]^{-1/2} = 4\sqrt{\pi}v \sin(\chi) = 1.7 \sin(\chi)$ TeV, imposing a minimum value for χ for our EFT to be applicable, and we impose a similar expression for R_h . In the following phenomenological study it is ensured that the cut-off is at least 450 GeV at the throat for the allowed parameter space.

²Another promising direction using nonperturbative methods is presented in [110].

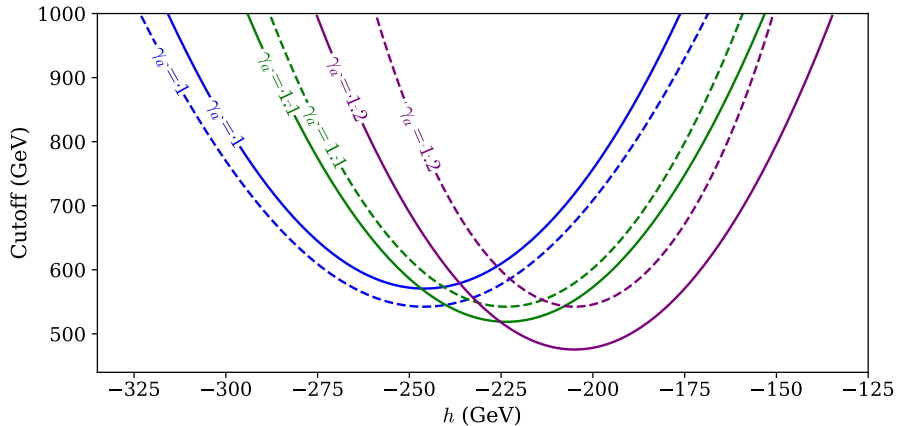


Figure 4.8: Field-dependent cut-off as estimated from perturbative unitarity to be $4\sqrt{\pi} |R_I(h)|^{-1/2}$ for sectional curvatures $R_\varphi(h)$ (solid) and $R_h(h)$ (dashed) as defined in Eqs. (4.46) and (4.47). The parameter $\chi = \sqrt{0.1}$ and the following $\gamma_a = v/v_*$ values are chosen as those that lead to domain walls, $\gamma_a = 1$ (see Sec. 4.4); the doom scenario, $\gamma_a = 1.1$ (see Sec. 4.5.2 and Fig. 4.25 in Sec. 4.7); and $\gamma_a = 1.2$ a conservative value for the observable bubble region shown in Fig. 4.24. For comparison, the nucleation temperature in phase transitions studied here is around 100 GeV.

4.3.1 Calculation of the one-loop finite-temperature potential

The geometric description presents relevant differences with the standard computation of one loop corrections for the effective potential, so let us sketch them here in some length. Path integral methods allow us to write one loop corrections in a few lines of algebra, while the notation is abstract enough to encompass both the finite and zero temperature case which we discuss simultaneously. In this functional computation one expands around a background value for the fields $\bar{\Phi}$, which satisfy the EoM at one loop order, along geodesics if the field space has curvature. This expansion reads, with $\delta\Phi$ being the field variation we will integrate over,

$$\Phi^i[\delta\Phi] = \bar{\Phi}^i + \delta\Phi^i - \frac{1}{2}\Gamma_{jk}^i(\bar{\Phi})\delta\Phi^j\delta\Phi^k + \mathcal{O}(\delta\Phi)^3, \quad A^\mu = \bar{A}^\mu + \delta A^\mu, \quad (4.55)$$

with Γ the connection derived from the metric G . An expansion for fermions can be similarly derived to that for gauge bosons.

The path integral for the effective action Γ_{eff} to one loop reads

$$e^{i\Gamma_{\text{eff}}} = e^{iS[\Phi, \bar{A}]} \int \sqrt{G} [\mathcal{D}\delta\Phi][\mathcal{D}\delta A] e^{i\frac{1}{2}\delta_{\Phi}^2 S + i\frac{1}{2}\delta_A^2 S + i\delta_{\Phi}\delta_A S}, \quad (4.56)$$

where \sqrt{G} is the scalar metric inserted for an invariant volume element and the second variation around the background field for gauge bosons is a standard result, whereas for the scalars we have, when applied to the action in Eq. (4.34),

$$\delta_{\Phi}^2 S = \int d^4x \delta\Phi^i (-G_{ij} D^2 - \nabla_i \nabla_j V) \delta\Phi^j, \quad \nabla_i \nabla_j V = \begin{pmatrix} V'' & 0 \\ 0 & FF'V'\tilde{g}_{ab} \end{pmatrix}, \quad (4.57)$$

with ∇ the covariant derivative w.r.t. field coordinates and D the covariant space-time derivative acting in the scalar manifold tensor space [39], which hereafter setting the background field to a constant equals the ordinary derivative. The extension to higher loop order can be found in Ref. [5]. It is well worth remarking that the mass term for Goldstones, $FF'V'$, (which vanishes at the vacuum) will be altogether missed in this coordinate system if not doing a covariant treatment. This non-covariant treatment would lead to inconsistency as one can realise by resorting to the SM with linear scalar coordinates where all 4 d.o.f. have a mass term away from the vacuum; in essence the point is that even in flat space, when in spherical coordinates, one has to use a covariant formulation. The mixed term in gauge and scalar fields one can borrow from Ref. [37]:

$$\delta_{\Phi}\delta_A S = \int d^4x [-\delta A_B D_{\mu} t_{B,i} \delta\Phi^j]. \quad (4.58)$$

This term can be absorbed in a redefinition of the path-integral fields without changing the measure as done in Ref. [37], but here instead as is more common practice in thermal field theory we cancel it out with the introduction of a gauge fixing term

$$\mathcal{L}_{g.f.} = -\frac{1}{2\xi} \sum_B (\xi t_B^i G_{ij} \delta\varphi^j + D_{\mu} \delta A_B^{\mu})^2, \quad (4.59)$$

which puts our gauge bosons in the R_{ξ} gauge while producing an extra mass term

for the scalars as

$$\delta_{\Phi}^2(S + S_{g.f.}) = -\delta\Phi(D^2 + \nabla^2V + \xi m_{gf}^2)\delta\Phi, \quad (4.60)$$

with the additional gauge dependent term

$$[m_{gf}^2]_j^i = \sum_B t_B^i t_{j,B} = \frac{(Fv)^2}{4} \begin{pmatrix} g^2\delta_a^b + g_Y^2\tilde{g}^{ac}v^2u^T T_Y \frac{\partial u}{\partial\varphi^c} u^T T_Y \frac{\partial u}{\partial\varphi^b} & 0 \\ 0 & 0 \end{pmatrix}, \quad (4.61)$$

with $\text{Tr}[m_{gf}^2] = 2m_W^2(h) + m_Z^2(h)$. We note that the last term does depend on the angular degrees of freedom, the Goldstones φ ; this does not mean they will feature in the effective potential (which could only come about via explicit breaking) but that the final result, when all tensors have had their indices contracted, will make any Goldstone boson dependence disappear. The second variation of the action for gauge bosons on the other hand is

$$\delta_A^2(S + S_{g.f.}) = \delta A^\mu (\eta_{\mu\nu}D^2 - (1 - \xi^{-1})D_\mu D_\nu + m_A^2) \delta A^\nu. \quad (4.62)$$

When it is only the effective potential one is after, derivatives of the background field can be neglected, and we obtain loop corrections as, for the scalar correction

$$-i \int d^4x V_{h\Phi} = -\frac{1}{2} \text{Tr} [\log (G\partial^2 + \nabla^2V + \xi m_{gf}^2)] + \frac{1}{2} \text{Tr} \log(G) \quad (4.63)$$

$$= -\frac{T}{2} \text{Tr} [\log (\delta_i^j \partial^2 + \nabla_i \nabla^j V + \xi [m_{gf}^2]_i^j)]. \quad (4.64)$$

The trace is over internal indexes, position and momentum, and for the full one loop corrections one adds over fermions and gauge bosons. This trace can now be made specific to thermal (with periodic time of interval $1/T$) and $T = 0$ corrections as (with momentum in Euclidean space)

$$V_{1\text{-loop}} = \frac{1}{2} \int \frac{d^4\ell}{(2\pi)^4} \text{tr} [\log (\ell^2 + \nabla^2V + \xi m_{gf}^2)], \quad (4.65)$$

$$V_{\text{Th}} = \frac{T}{2} \sum_n \int \frac{d^3\ell}{(2\pi)^3} \text{tr} [\log (E_n^2 + \ell^2 + \nabla^2V + \xi m_{gf}^2)], \quad (4.66)$$

where the trace is now over scalar indexes, and the 0 components of the momenta are the Matsubara frequencies [102] in V_{Th} . While the first term requires counterterms, the second only has a field independent divergence that one can leave aside. Let us renormalise the corrections in vacuo next by dividing our effective potential into

$$V_{\text{eff}}(h, T) = V(h) + \Delta V_{CW}(h) + \Delta V_{\text{Th}}(h, T), \quad (4.67)$$

where the one loop correction at $T = 0$, ΔV_{CW} has the form, with cut off regularisation,

$$\Delta V_{CW} = \sum_i [\Delta V_{1\text{-loop},i} + \Delta V_{1\text{-loop},i}^{c.t.}], \quad (4.68)$$

$$\Delta V_{1\text{-loop},i} = \frac{1}{64\pi^2} n_i \left(m_i^4 \left(\log(m_i^2/\Lambda^2) - \frac{1}{2} \right) + 2\Lambda^2 m_i^2 \right), \quad (4.69)$$

where i runs over Φ scalars, electroweak gauge bosons, ghosts and fermions, for the latter for practical purposes, as all other fermions contribute negligibly, only the top. There are three types of masses as far as the field dependence is concerned which will dictate the number of counterterm operators needed

$$F^2(h), \quad V''(h), \quad \frac{V'(h)F'(h)}{F(h)}. \quad (4.70)$$

The counterterms needed are of the form either of the three above or their square and due to functional dependence similarities they amount to 6 terms; 4 could be taken as the tree level terms present in the Higgs potential and the other two from (VF'/F) are rational rather than polynomial and require an additional two counterterms. Equivalently here we take

$$V_{1\text{-loop},i}^{c.t.} = a_i m_i^4(h) + b_i m_i^2(h), \quad \text{Counter-terms} \quad (4.71)$$

Which are fixed by the renormalisation conditions here imposed as

$$\left. \frac{dV_{CW,h}}{dh} \right|_{h=0} = \left. \frac{d^2V_{CW,h}}{dh^2} \right|_{h=0} = \left. \frac{dV_{CW,\varphi}}{dh} \right|_{h=0} = \left. \frac{d^2V_{CW,\varphi}}{dh^2} \right|_{h=0} = 0, \quad (4.72)$$

$$\sum_{A,B,t} \left. \frac{dV_{CW,i}}{dh} \right|_{h=0} = \sum_{A,B,t} \left. \frac{d^2V_{CW,i}}{dh^2} \right|_{h=0} = 0. \quad (4.73)$$

These imply that $h = 0$ will stay a minimum of the potential with mass m_h . The vanishing of the field dependent mass for φ conflicts with these renormalisation conditions in Landau's gauge. While one can, as in Ref. [111], approach this problem by resummation, here we avoid this gauge and rather in the following select for concreteness *Feynman's gauge*, $\xi = 1$.

The thermal contributions on the other hand are

$$\Delta V_{\text{Th}} = \frac{T^4}{2\pi^2} \sum_i n_i J_{S_i} \left(\frac{m_i(h)^2}{T^2} \right), \quad (4.74)$$

with n_i the number of degrees of freedom and S_i identifying the statistics, Bose-Einstein (b), or Pauli-Dirac (f); explicitly

$$J_{b/f}(x^2) = \int_0^\infty y^2 dy \log \left(1 \mp \exp \left\{ -\sqrt{x^2 + y^2} \right\} \right). \quad (4.75)$$

All the above leads to the 1-loop finite temperature potential

$$V_{\text{eff}} = V(h) + \sum_i n_i \left\{ \frac{m_i^2(h)}{64\pi^2} \left(m_i^2(h) \left[\log \left(\frac{m_i^2(h)}{m_i^2(0)} \right) - \frac{3}{2} \right] + 2m_i^2(0) \right) + \frac{T^4}{2\pi^2} J_{S_i} \left(\frac{m_i^2(h)}{T^2} \right) \right\}. \quad (4.76)$$

Each term in this sum, in our Feynman gauge, is

$$m_t^2(h) = m_t^2(0)F(h)^2, \quad n_t = -12, \quad m_h^2(h) = V''(h), \quad n_h = 1, \quad (4.77)$$

$$m_{W_T}^2(h) = m_W^2(0)F(h)^2, \quad n_{W_T} = 4, \quad m_{W_L}^2(h) = \frac{F'V'}{F} + m_{W_T}^2(h), \quad n_{W_L} = 2, \quad (4.78)$$

$$m_{Z_T}^2(h) = m_Z^2(0)F(h)^2, \quad n_{Z_T} = 2, \quad m_{Z_L}^2(h) = \frac{F'V'}{F} + m_{Z_T}^2(h), \quad n_{Z_L} = 1. \quad (4.79)$$

In the following, to avoid cluttered notation, a mass with no argument (m_W) is to be understood as a constant, the mass measured at the vacuum; for a field-dependent mass the dependence will be made explicit, e.g. $m_W(\phi)$. It is useful to extend the extrema defined in Sec. 4.2 to be the extrema of the finite temperature effective potential, $h_{\pm}(T)$, $h_0(T)$ so that the end-point of the temperature ‘trajetory’ returns $h_0(0) = 0$, $h_{\pm}(0) = -v_{\pm}$. On the other hand, potential differences and barriers read

$$\Delta V(T) = V_{\text{eff}}(h_-(T), T) - V_{\text{eff}}(h_0(T), T), \quad (4.80)$$

$$U_0(T) = V_{\text{eff}}(h_+(T), T) - V_{\text{eff}}(h_0(T), T), \quad (4.81)$$

$$U_-(T) = V_{\text{eff}}(h_+(T), T) - V_{\text{eff}}(h_-(T), T). \quad (4.82)$$

At high temperatures, given the importance of electroweak particle corrections, the relevant point in field space is to be found around $h = -v_{\star}$ rather than our vacuum at $h = 0$. For this reason, we will write in the following the potential as a function of ϕ as in Eq. (4.43) where e.g.

$$\phi_{\pm} = h_{\pm} + v_{\star}, \quad \phi_0 = h_0 + v_{\star}. \quad (4.83)$$

4.3.2 Limitations of the calculation

Were one to aim at more precision, the present approximation can be improved by higher zero temperature or thermal loop corrections. These however suffer from an infrared illness as outlined in the beginning of this section. This problem is identified

when the expansion parameter controlling the IR divergences

$$\varepsilon_{IR} \equiv \frac{g^2 T}{\pi m_W(\phi)}, \quad (4.84)$$

ceases to be small.³ While some amelioration can be provided by daisy resummation [112], the ‘magnetic modes’ stay massless in perturbation theory and make these divergences unavoidable [109]. Whenever the expansion parameter is larger than one, we simply cannot trust perturbation theory and must resort instead to non-perturbative methods in the form of lattice. Luckily, we do not need access to this non-perturbative region of the parameter space to unveil a range of novel phenomenology. We address the IR problem by identifying the region of the field values ϕ that possess a controlled expansion $\varepsilon_{IR}(\phi) < 1$, and only there do we trust the analytically and perturbatively computed potential. The expression that determines this region in ϕ reads

$$\left(\frac{\phi}{T}\right)^2 > \gamma_a^{-2} \left[\left(\frac{2g}{c_\chi \pi}\right)^2 - \tan^2 \chi \frac{v^2}{T^2} \right], \quad \boxed{\text{IR Bound}} \quad (4.85)$$

where we note that for temperatures below $T_{IR} = \pi s_\chi v / (2g)$, the RHS is negative and this constraint disappears for a controlled expansion in the entire range of ϕ . Above T_{IR} nonetheless the bound applies, and it implies that for small values of ϕ the computation of the potential is unreliable.

Let us exemplify how this IR bound is used here in practice by taking the SM as a case study. The SM potential for high temperature is a 4th degree polynomial in the fields and the extrema can be solved for analytically, for a pedagogical exposition see Sec. 4.1 of [102]. One finds that a minimum-maximum pair appears at a temperature T_1 as an inflection point at a distance $\phi_0(T_1)/T_1 = 3(2m_W^3 + m_Z^3)/(4\pi\lambda v^3) \propto 1/m_h^2$ from the origin. This minimum becomes degenerate in potential energy with the origin at the critical temperature T_c and sits at a distance $\phi_0(T_c)/T_c = (4/3)\phi_0(T_1)/T_1$ from it. After T_c , we would naively expect to have a first order phase transition. For this perturbative argument to be trustworthy, however, one should require the

³A similar effective expansion parameter to Eq. (4.84) exists for both the Z and h bosons.

new minimum to be in the region $\varepsilon_{IR}(\phi_0) < 1$. The region $\varepsilon_{IR}(\phi) > 1$ is an interval around the origin ($\phi = 0$) which shrinks with time and disappears at T_{IR} , whereas the distance of ϕ_0 to $\phi = 0$ generally increases monotonically. It suffices then to specify the earliest time/highest temperature at which this condition is imposed: if satisfied at a temperature T , lower temperatures will continue to respect the bound. We distinguish two possibilities:

- **Weak IR constraint.** The new minimum should be at a position where the IR expansion is under control at the critical temperature, that is

$$\varepsilon_{IR}(\phi_0(T_c)) < 1, \quad (4.86)$$

which when applied to the SM returns

$$\text{SM: } \frac{g}{\pi} \leq \frac{(2m_W^3 + m_Z^3)}{2\pi\lambda v^3}, \quad m_h \leq \sqrt{\frac{(2m_W^3 + m_Z^3)}{2gv^3}}v \simeq 75 \text{ GeV}, \quad (4.87)$$

which translates into an upper bound on the Higgs mass for a reliable first order phase transition prediction, a well known qualitative condition here made quantitative as outlined.

- **Strong IR constraint.** The new minimum should be at a position where the IR expansion is under control already at the temperature when it first appears, that is

$$\varepsilon(\phi_0(T_1)) < 1, \quad (4.88)$$

which applied to the SM gives

$$\text{SM: } \frac{g}{\pi} \leq \frac{3(2m_W^3 + m_Z^3)}{8\pi\lambda v^3}, \quad m_h \leq \sqrt{\frac{3(2m_W^3 + m_Z^3)}{8gv^3}}v \simeq 65 \text{ GeV}. \quad (4.89)$$

This a stronger demand and as such demands a smaller allowed ranged of the

Higgs field.

None of these bounds, however, are satisfied in the SM given the measured Higgs mass, and one cannot affirm there is a first order phase transition; in fact lattice computations reveal that the SM with the measured couplings presents instead a crossover transition [113, 114]. The bounds we obtain are not far from the actual value for the first order phase transition (1OPT) endpoint as determined by lattice 72 ± 7 GeV [115] and are also in line with more explicit estimates of the loop expansion breakdown [116].

In our scenario with an extended range for ϕ the application is analogous, and we abstain from making predictions at temperatures where the minima fall in the $\varepsilon_{IR} > 1$ region. To be explicit and consistent across cases, *we demand that in a 1OPT, the minimum ϕ_0 satisfies $\varepsilon_{IR}(\phi_0) < 1$ at the critical temperature, T_c , (weak constraint) or the temperature when the minima first appears, T_1 (strong constraint).* The diagrams for the histories of extrema allow for a visualisation of the strong IR constraint, as shown in Fig. 4.9.

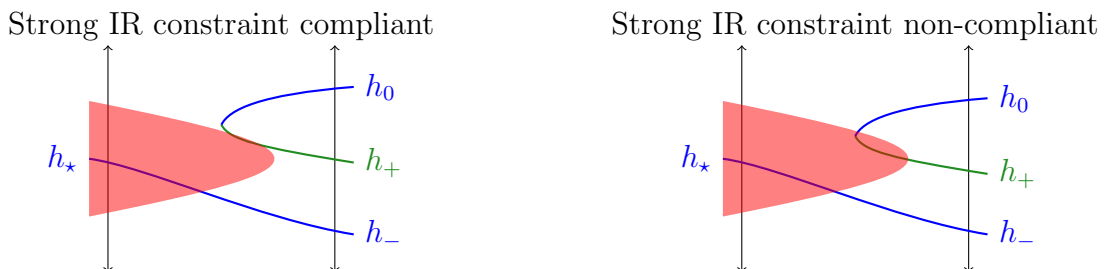


Figure 4.9: Schematic representation of thermal histories for the extrema of the effective potential satisfying (left) and violating (right) the strong IR constraint.

Lastly, the large field regime of the $T = 0$ potential might suffer from the same instability as the SM [117] but in some instances is aggravated. One has, in the theory under study

$$\begin{aligned}
 V_{\text{eff}}(\phi \gg v) &\simeq \frac{\lambda\gamma_4^2}{8}\phi^4 \left(1 + \frac{3L(\phi)}{8\pi^2\gamma_4^2} \left[\frac{2m_W^4 + m_Z^4 - 4m_t^4}{m_h^2 v^2} \gamma_a^4 c_\chi^4 + \frac{m_h^2}{v^2} \gamma_4^4 + \frac{2m_W^2 + m_Z^2}{3v^2} \gamma_a^2 c_\chi^2 \gamma_4^2 \right] \right), \\
 &\equiv \frac{\lambda\gamma_4^2}{8}\phi^4 (1 + a_{\text{loop}}L(\phi))
 \end{aligned} \tag{4.90}$$

with $L(\phi) = \log(\phi^2/v^2)$. In the SM case, top quark contributions drive the effective

quartic coupling towards negative values and the electroweak minimum is metastable when field values are extended to the Planck mass. In the present case we will address the same problem with two prescriptions, *perturbativity* and *boundedness-from-below*.

The constraint that we denote perturbativity follows from demanding a loop correction subleading to the tree level one;⁴ given the dependence in Eq. (4.90) this demand is strongest at the edges of the field range, and it explicitly reads $a_{\text{loop}}L(4\pi v) < 1$. These edges should be chosen to capture a large enough domain of the potential to resolve the features of both minima, which roughly fall around $-v \leq \phi \leq v$. We require that this constraint holds instead over the field range $-4\pi v \leq \phi \leq 4\pi v$, about an order of magnitude larger in field space, which should safely capture the important features and ensure the probability of tunneling in some destabilized direction outside this range is considerably suppressed.

A related but independent constraint arises from demanding the potential be bounded from below in the range we consider, which again we choose to be field values within $4\pi v$ of the origin $\phi = 0$. To be conservative, we required that the potential does not start to turn downwards at high field values. We first checked whether the potential was concave up or concave down at the $\pm 4\pi v$ boundaries. A concave up potential passes the test. If the potential was concave down at the boundary, however, we required that the potential was increasing (decreasing) with ϕ at the positive (negative) $4\pi v$ boundary. Lastly, we note that the 1-loop contribution to Eq. (4.76) is complex for some values of the field value ϕ –e.g. when V'' changes sign for a concave to convex tree-level potential. However it is the real part of the effective potential that is relevant for phase transitions [118,119], given the imaginary component of ΔV_{CW} is very small relative to the real part, which is found to hold in all cases studied here. It is therefore the real part of the effective potential which will be considered in the following for numerical computations.

⁴Please note this constraint differs from unitarity bounds since we demand a convergent loop expansion rather than an effective coupling value below the unitarity limit, which in this study would be a subdominant constraint to perturbativity as here defined.

4.3.3 Symmetry (non)restoration and roads to the SM

The study of phenomenology will make use of numerical methods guided by analytical estimates; here we present some of the latter. Much in the way of the well studied electroweak phase transition in the SM for small Higgs mass, here a high temperature expansion helps draw the features of the problem and provide an understanding of the underlying dynamics. In addition, it also sheds some light on the question of limits in non-linearly realised theories that might lead to the SM.

At high temperatures, the thermal corrections can be approximated by polynomials in the masses provided we are in the regime [101]:

$$\frac{m_i(\phi)}{\pi T} < 1, \quad (4.91)$$

and hence this high temperature approximation is *valid* for a neighbourhood around the point $\phi = 0$ which shrinks with decreasing temperature. We note that (4.85) *excludes* a neighbourhood around the origin as opposed to the above; these two exclusion regions fortunately do not overlap.

The field coordinate $\phi = h + v_*$ as outlined above is convenient to write thermal corrections in terms of which

$$\begin{aligned} V_{\text{eff}}^{\text{HT}} = & G_o v^3 \phi - D_o v^2 \phi^2 + E_o v \phi^3 + \frac{\lambda \gamma_4^2}{8} \phi^4 \\ & + \sum_B n_i \left(\frac{m_i^2(\phi)}{8\pi^2} \left[\frac{m_i^2}{4} + \frac{\pi^2 T^2}{3} \right] - \frac{T(m_i^2(\phi))^{3/2}}{12\pi} - \frac{m_i^4(\phi)}{64\pi^2} \log \left(\frac{m_i^2}{T^2 A_B} \right) \right) \\ & + \sum_F n_i \left(\frac{m_i^2(\phi)}{16\pi^2} \left[\frac{m_i^2}{2} - \frac{\pi^2 T^2}{3} \right] - \frac{m_i^4(\phi)}{64\pi^2} \log \left(\frac{m_i^2}{T^2 A_F} \right) \right), \end{aligned} \quad (4.92)$$

where keeping up with our notation masses with no arguments are constants, the values measured at the vacuum, n_i are given in Eqs. (4.77)–(4.79) whereas

$$\log(A_B) = 5.4076 - 3/2, \quad \log(A_F) = 2.6351 - 3/2, \quad (4.93)$$

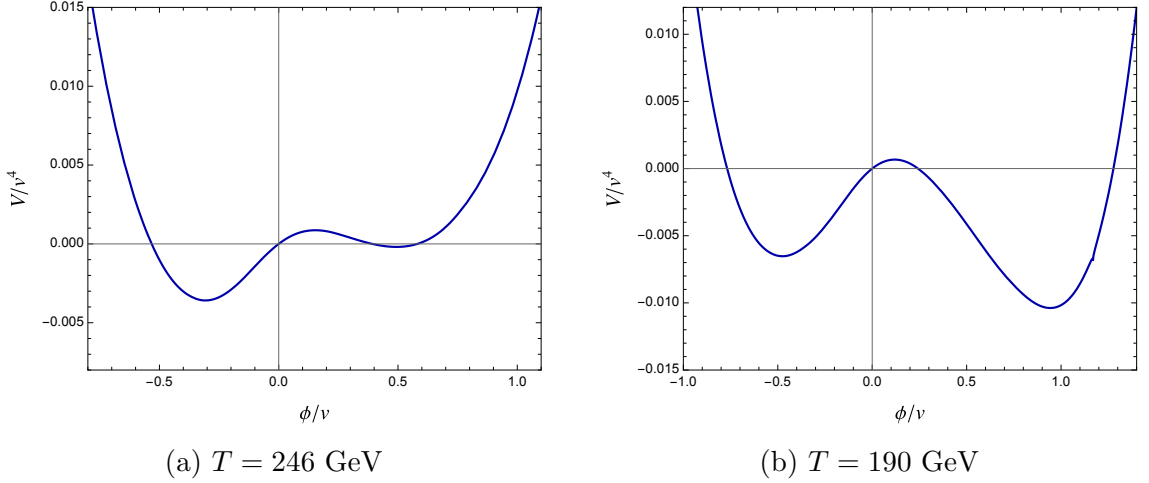


Figure 4.10: One-loop effective potential plotted for $\chi = \sqrt{0.1}$, obeying the high-temperature symmetry restoration bound in Eq. (4.109). The benchmarks chosen here are $\gamma_4 = 1$, $\epsilon = 0.02$, $\delta = -0.1$. Fig. 4.10a and Fig. 4.10b show the potential evolution with temperature for $T = 246$ GeV and $T = 190$ GeV, respectively. Notice, in particular, the large χ smooths the potential around $\phi/v = 0$ in contrast to Fig. 4.11.

$$G_o = -\frac{\lambda\delta\gamma_\epsilon^2}{2}(1 - \gamma_\epsilon^{-1}\gamma_4\delta)(1 + \gamma_\epsilon^{-1}\gamma_4\delta + 3((1 - \epsilon)\gamma_\epsilon^{-1} - 1)) \quad (4.94)$$

$$= -\frac{\lambda\gamma_4\gamma_a^{-1}\gamma_\epsilon^{-1}}{2}(\gamma_4^{-1}\gamma_\epsilon - \gamma_a^{-1})(2 - \gamma_\epsilon\gamma_a^{-1}\gamma_4), \quad (4.95)$$

$$D_o = \frac{\lambda}{4}(6(1 - \epsilon)\gamma_4\gamma_a^{-1} - 3(\gamma_a^{-1}\gamma_4)^2 - 2), \quad (4.96)$$

$$E_o = -\frac{\lambda}{2}\gamma_4\gamma_a^{-1}(\gamma_4 - \gamma_a(1 - \epsilon)). \quad (4.97)$$

It is useful for phenomenological purposes to highlight the terms that break Higgs parity. Couplings to the electroweak bosons and top quark are symmetric so that all asymmetry is sourced by the potential either at tree level, or through the effective masses of Goldstones and the Higgs. Note that, as in the SM case, a cubic term would arise from thermal loops of gauge bosons, but this would be parity symmetric as $(\phi^2)^{3/2}$. All sources of parity violation are turned off for ϵ and δ vanishing which aligns the maximum of the tree level potential with the throat of the manifold and sets the energy difference between minima to zero. This limit of vanishing δ and ϵ simplifies eqs. (4.94)–(4.97) so that the coefficients of parity violating terms are linear in ϵ and δ as $G_o \simeq -\lambda\delta/2$ and $E_o \simeq \lambda\delta\gamma_4^2/2 - 2\lambda\gamma_4\epsilon$.

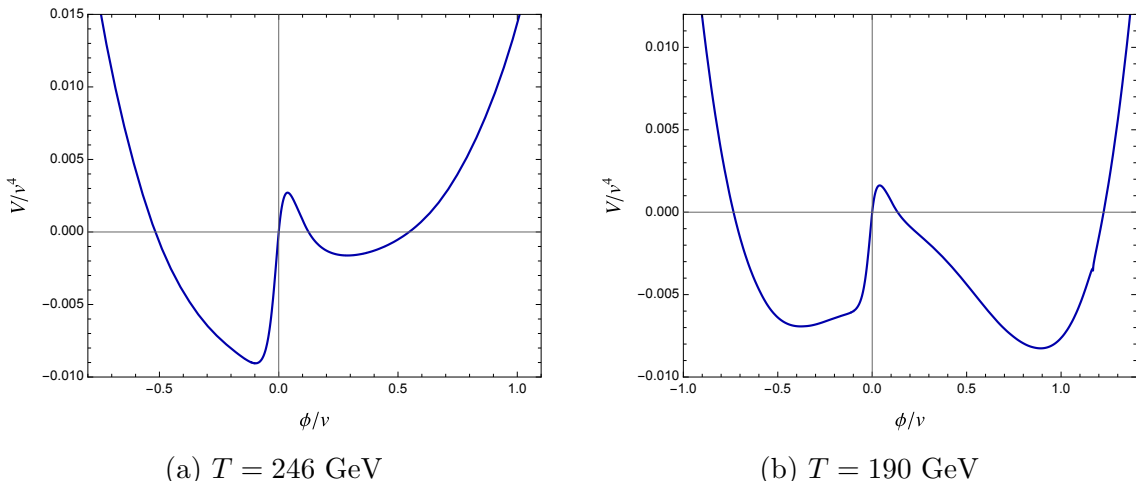


Figure 4.11: One-loop effective potential plotted for $\chi = 0.05$, which unlike Fig. 4.10, does not satisfy the high-temperature symmetry restoration bound in Eq. (4.109). The benchmarks chosen here are $\gamma_4 = 1$, $\epsilon = 0.02$, and $\delta = -0.1$. Fig. 4.11a and Fig. 4.11b show the potential evolution with temperature for $T = 246$ GeV and $T = 190$ GeV respectively. For this choice of χ , the potential is sharply peaked around $\phi/v = 0$ in contrast to Fig. 4.10.

While the high energy expansion yields a potential as a polynomial in the fields and is amenable to analysis in SMEFT, in our non-linearly realised theory the potential is instead a rational function of the fields due to the Goldstones contribution, $V'F'/F \propto (c_\chi^2 \gamma_a^2 \phi^2 + s_\chi^2)^{-1}$. Naively recovering a polynomial, as in the SM and SMEFT case, would require taking $\chi \rightarrow 0$ while having the numerator polynomial start at ϕ^2 to avoid poles, attainable by $\delta \rightarrow 0$. Such a limit, in the direction of recovering the SM, is in fact a discontinuous one in what is a distinguishing feature of this non-linearly realised theory. This feature is hinted at in the small χ limit with $\delta \neq 0$, where plots of the potential in Fig. 4.11 show a sharp rise around the throat ($\phi = 0$).⁵

This feature can be understood analytically if we inspect the very high temper-

⁵We have checked that the sharp features of this potential around the origin come primarily from the shape of the manifold. The imaginary parts of the potential are still much smaller than the real parts here.

ature potential while still keeping in mind $T < 4\pi v$:

$$V_{\text{eff}}^{\text{HT}}(\phi) = \sum_B n_i \frac{T^2 m_i^2(\phi)}{24} - \sum_F n_i \frac{T^2 m_i^2(\phi)}{48} + \mathcal{O}(T^0) \quad (4.98)$$

$$= \frac{T^2}{24} \left((6m_W^2 + 3m_Z^2 + 6m_t^2) F^2(\phi) + V''(\phi) + 3V'(\phi) \frac{F'(\phi)}{F(\phi)} \right) + \mathcal{O}(T^0) \quad (4.99)$$

$$= V_{\text{eff}}^{\text{HT}'}(0)\phi + \frac{V_{\text{eff}}^{\text{HT}''}(0)}{2}\phi^2 + \mathcal{O}(\phi^3, T^0), \quad (4.100)$$

with

$$V_{\text{eff}}^{\text{HT}'}(0) = T^2 v \left(\frac{E_o}{4} + \frac{G_o c_\chi^2 \gamma_a^2}{8s_\chi^2} \right), \quad (4.101)$$

$$\frac{V_{\text{eff}}^{\text{HT}''}(0)}{2} = T^2 \left(\frac{2m_W^2 + m_Z^2 + 2m_t^2}{8v^2} c_\chi^2 \gamma_a^2 + \frac{\lambda \gamma_4^2}{16} - \frac{D_o c_\chi^2 \gamma_a^2}{4s_\chi^2} \right). \quad (4.102)$$

This expansion around the Higgs parity symmetric field value $\phi = 0$ allows one to discuss symmetry restoration in analytic but approximate terms as follows.

- $V_{\text{eff}}^{\text{HT}'}(0) \neq 0$. The linear term in ϕ breaks Higgs parity and will prevent $\phi = 0$ from being an extremum, its sign for small δ, ϵ determining if this extremum has shifted to positive or negative values. Assuming $V_{\text{eff}}'' > 0$ and that the minimum is in a neighbourhood of the throat ($\phi = 0$), one has a minimum shifted to negative ϕ values for positive slope, a condition expressed in terms of the model parameters as when substituting in Eq. (4.101) as

$$-\frac{\lambda}{8} \gamma_4 \gamma_a^{-1} (\gamma_4 - \gamma_a (1 - \epsilon)) - \frac{\lambda c_\chi^2 \gamma_4 \gamma_a \gamma_\epsilon^{-1}}{16s_\chi^2} (\gamma_4^{-1} \gamma_\epsilon - \gamma_a^{-1}) (2 - \gamma_\epsilon \gamma_a^{-1} \gamma_4) > 0, \quad (4.103)$$

and the opposite inequality for a minimum in the positive ϕ axis. In the limit

of small ϵ and δ we can simplify the expression to derive

$$\delta \frac{c_\chi^2 - 2s_\chi^2}{16s_\chi^2} < -\frac{\epsilon}{2\gamma_4} \quad \begin{array}{l} \text{high } T \text{ min at } \phi < 0 \\ \text{History } Q_- \end{array} \quad (4.104)$$

$$\delta \frac{c_\chi^2 - 2s_\chi^2}{16s_\chi^2} > -\frac{\epsilon}{2\gamma_4} \quad \begin{array}{l} \text{high } T \text{ min at } \phi > 0 \\ \text{History } Q_0 \end{array} \quad (4.105)$$

$$\delta \frac{c_\chi^2 - 2s_\chi^2}{16s_\chi^2} \simeq -\frac{\epsilon}{2\gamma_4} \quad \begin{array}{l} \text{high } T \text{ min at } \phi \simeq 0 \\ \text{History } P \end{array} . \quad (4.106)$$

The equivalence with histories is not exact given that this analytic approximation does only hold for small ϵ and δ , but it is useful in sketching the possibilities. This result divides the (ϵ, δ) plane in half with a negative slope line that goes through the origin as in Fig. 4.14: above this line one would find history Q_0 , below it Q_- .

- $V_{\text{eff}}^{\text{HT}'}(0) = 0$. If the linear term vanishes, which is the case for $\epsilon, \delta \rightarrow 0$, $\phi = 0$ is an extremum: a minimum for $V_{\text{eff}}^{\text{HT}''}(0) > 0$ and maximum for $V_{\text{eff}}^{\text{HT}''}(0) < 0$. The sign of the second term, s_0 , will hence determine if Higgs parity is restored or not so

$$s_0 \equiv \text{Sign}[V_{\text{eff}}^{\text{HT}''}(0)] \quad (4.107)$$

$$= \text{Sign} \left[\frac{2m_W^2 + m_Z^2 + 2m_t^2}{8} c_\chi^2 \gamma_a^2 - \frac{m_h^2 \gamma_4^2}{16} (\gamma_a^2 \gamma_4^{-2} t_\chi^{-2} (6(1-\epsilon)\gamma_4 \gamma_a^{-1} - 3(\gamma_a^{-1} \gamma_4)^2 - 2) - 1) \right], \quad (4.108)$$

which to first order in an ϵ, δ expansion returns

$$s_0 \simeq \text{Sign} \left(\frac{(\sin 2\chi)^2}{\cos(2\chi)} - \frac{m_h^2}{m_W^2 + m_t^2 + m_Z^2/2} \right), \quad (4.109)$$

$$\begin{cases} s_0 > 0 \Rightarrow \chi > 0.3, & \text{Symmetry restoration at high } T \\ s_0 < 0 \Rightarrow \chi < 0.3, & \text{Symmetry stays broken at high } T. \end{cases}$$

The small χ limit leading to no symmetry restoration leads to an apparent contra-

diction: one expects this limit to yield SM-like couplings and with it the symmetry should naively be restored at high temperature. This finding sheds light on the question posed in Ref. [1] of whether non-linearly realised theories have a limit in which the SM is recovered. Approaching SM-like couplings from our non-linearly realised theory, we obtain a locally identical theory around $h = 0$ which nonetheless does not have symmetry restoration at high temperature for any infinitesimally small value of χ since the theory is different at $\phi = 0$. This discontinuous limit can be spotted opening up the term $V'F'/F$ in Eq. (4.100)

$$V_{\text{eff}}^{\text{HT}} \supset V_{\text{peak}} = -\frac{T^2 D_o}{4} \frac{\phi^2}{\phi^2/v^2 + s_\chi^2/(c_\chi^2 \gamma_a^2)} \quad (4.110)$$

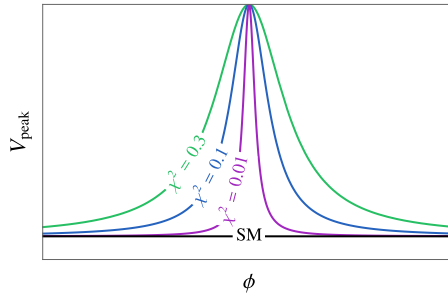


Figure 4.12: Contribution V_{peak} of the $V'F'/F$ term to the effective potential.

This same limit of $\chi \rightarrow 0$ would give an ever smaller cut-off at the throat as the curvature increases as outlined in the discussion at the beginning of Sec. 4.3. New light states would be accessible in the thermal history which would change our EFT to a theory with extra degrees of freedom. This suggests that for a consistent theory, the functions in our manifold should be sufficiently smooth. The exploration of this interplay in the $\chi \rightarrow 0$ limit and its phenomenology, however, we leave for future work on the connection of UV models and HEFT\SMEFT.

Fig. 4.12 plots the contribution for different values of χ and the SM, and shows that at no finite stage is the SM limit (a constant for all field range, in black) reached. Sign of an anomalous limit is also present in the linear term of Eq. (4.100) since it reads in this expansion $G_o/s_\chi^2 \sim \delta/\chi^2$, giving a different result depending on the order of limits that one takes to the SM. Unlike the behaviour in Eq. (4.110) however, the SM can be approached by first taking $\delta \rightarrow 0$.

4.4 Domain Walls

The finite temperature effective potential is symmetric under Higgs parity in the limit $\epsilon, \delta \rightarrow 0$. This limit contains couplings that are locally those of the SM yet the doubling of the Higgs domain implies two degenerate minima at low temperature. One has different possible phases for the discrete symmetry in the universe history and, although this theory might locally resemble the SM, the cosmological dynamics change drastically. As the most salient new possible feature, one has spontaneous breaking of Higgs parity and the creation of domain walls. The formation of domain walls in the Higgs field is, to the best of our knowledge, a unique feature of non-linearly realised theories. In this section we describe and identify the conditions for this approximate symmetry to lead to walls with the assumption, validated below, that δ, ϵ are small enough to expand on.

Sec. 4.3.3 showed that for $\chi > 0.3$ and small ϵ and χ there will be symmetry restoration in the form of a single minimum at high energies, whereas the zero temperature potential presents two parity reflected minima. This well studied case of cosmological spontaneous breaking of discrete symmetry leads in general to the formation of walls and will be the focus of our study here. The late time phenomenology of walls is quite insensitive to whether the transition is first or second order, but let us sketch how it occurs in both cases for illustration. For a first order PT, different patches in the universe will bubble to one of the two vacua, and after the bubbles collide and lose energy to the bath a network of walls will form, the characteristic size of this network dependent on the transition properties.

For a second order PT, depicted in Fig. 4.3b (history P), shortly after the critical temperature the small separation and barrier between minima implies that thermal fluctuations for correlation-volume (l^3 with $l^{-2} = V''(h_0) \simeq V''(h_-)$) patches allow for transitions from one vacuum to another. As temperature decreases, the probability of these jumps will decrease with the Boltzmann factor, $\sim e^{-l^3 U/T}$ where U is the potential barrier given our approximate degeneracy assumption $U = U_0 = U_-$ with $U_{0,-}$ in Eq. (4.81), until this suppression is effective enough to in practice forbid the transitions. At this time patches of the correlation volume will be stuck in whichever vacuum they happened to be at, and the network of walls will form.

Formation is marked by Ginzburg's temperature defined as the temperature when the the negative of the exponent in Boltzmann's factor equals one,

$$T_G \equiv [V_{\text{eff}}''(h_0(T_G), T_G)]^{-3/2} U(T_G). \quad (4.111)$$

This description allows for a qualitative picture of the symmetry non-restoration case for $\chi < 0.3$. In this instance two minima survive until high temperature, but noting that the barrier scales like $v^2 T^2$ and naively correlation the length is T^{-1} , one can expect that above $T \sim v$ the Boltzmann factor is large enough to allow for these jumps. If this is so, even without symmetry restoration, the Ginzburg temperature is well defined and one can expect formation of walls. This must be the case at least in a neighbourhood below $\chi = 0.3$, but we leave its detailed study for future work.

The definition of the Ginzburg temperature is implicit; in practice however it is well approximated by the zero temperature potential, in our case

$$T_G \simeq \frac{\lambda v^4}{8\gamma_4^2 m_h^3} \sim 60\gamma_4^{-2} \text{GeV}, \quad (4.112)$$

where we have expanded on ϵ, δ and kept only the first term. The probabilities P_0 and P_- to find a patch of each vacua h_0 and h_- at the Ginzburg temperature can then be estimated as

$$\frac{P_0}{P_-} \sim \exp\left(\frac{l^3 V_{\text{eff}}(h_-, T)}{T_G} - \frac{l^3 V_{\text{eff}}(h_0, T)}{T_G}\right) = \exp\left(\frac{\Delta V(T_G)}{U(T_G)}\right), \quad (4.113)$$

where ΔV is as defined in Eq. (4.80). A large $\Delta V/U$ ratio would imply one vacuum is selected predominantly and very few walls form. We instead assume this ratio, which depends only on ϵ , is small, which implies small ϵ according to Eq. (4.54). This translates into $\Delta V/U = 32\epsilon \ll 1$.

We note that regardless of how the network formed and the typical scale of structure, both types of phase transition have a large wall stretching out to the horizon. One can realise this in a 2D case by rolling a dice to fill each correlation patch inside a causal box with either of the two vacua. Once the filling is done, a zoom out to see the global structure will reveal the presence of this large wall.

Let us then continue taking l as the typical scale of the network regardless of how it was formed. The small scale structure dynamics is ruled by the balance of pressure $p = \Delta V(T_G)$ and tension μ . The tension is well approximated by the zero temperature potential and to first non-vanishing order in small ϵ, δ

$$\mu = \int_{-\infty}^{\infty} d\ell T_0^0(h_w(\ell)) = \int d\ell \left(\frac{1}{2} (\nabla h_w)^2 + V(h_w) \right) = \frac{2\sqrt{\lambda}v^3}{3\gamma_4^2}, \quad (4.114)$$

where the profile function is found as a solution to the static field equations and reads $\gamma_4\sqrt{\lambda}h_w(\ell)/m_h = \tanh(m_h\ell) - 1$.

The potential energy difference, Eq. (4.80), vanishes in the parity symmetric limit and here it suffices to estimate it to linear order in δ and ϵ . On top of this expansion, we also perform a loop expansion, with minima at $h_- = h_-^{(0)} + \kappa h_-^{(1)}$, $h_0 = h_0^{(0)} + \kappa h_0^{(1)}$ and $\kappa = (4\pi)^{-2}$ to find the energy difference ($V_{\text{eff}} = V + V_\kappa$, $V_\kappa = V_{CW} + V_{\text{Th}}$)

$$\Delta V = V(h_-^{(0)}) + V_\kappa(h_-^{(0)}) + \frac{dV(h_-^{(0)})}{dh} \kappa h_-^{(1)} + \mathcal{O}(\kappa^2) \quad (4.115)$$

$$- \left[V(h_0^{(0)}) + V_\kappa(h_0^{(0)}) + \frac{dV(h_0^{(0)})}{dh} \kappa h_0^{(1)} + \mathcal{O}(\kappa^2) \right] \quad (4.116)$$

$$= V(h_-^{(0)}) + V_\kappa(h_-^{(0)}) - [V(h_0^{(0)}) + V_\kappa(h_0^{(0)})] + \mathcal{O}(\kappa^2), \quad (4.117)$$

where the derivative term cancels since it is evaluated at a minimum to the given approximation. One can now use that $h_i^{(0)}$, the minima of the tree level potential, do not depend on δ and are the Higgs parity conjugate of one another to write

$$h_-^{(0)} = -2v\gamma_4^{-1} + \epsilon h_{a,-}^{(1)} + \mathcal{O}(\epsilon^2), \quad (4.118)$$

whereas we recall by definition and for all values of the tree level potential $h_0^{(0)} = 0$.

The expanded energy difference is then

$$\Delta V = \epsilon \left(\frac{\partial V(-2v\gamma_4^{-1})}{\partial \epsilon} - \frac{\partial V(0)}{\partial \epsilon} \right) \Big|_{\epsilon=0} + \epsilon h_{a,-}^{(1)} \left(\frac{dV(-2v\gamma_4^{-1})}{dh} \right) \Big|_{\epsilon=0} \quad (4.119)$$

$$+ \delta \left(\frac{\partial V_\kappa(-2v\gamma_4^{-1})}{\partial \delta} - \frac{\partial V_\kappa(0)}{\partial \delta} \right) \Big|_{\epsilon, \delta=0}, \quad (4.120)$$

where the potential derivative w.r.t. the field will cancel once more given it is evaluated at a minimum to the given approximation. The leading ϵ contribution comes at tree level and is straightforward to obtain. For δ , a number of intermediate steps leads to

$$\delta \left(\frac{\partial}{\partial \delta} [V_\kappa(-2v\gamma_4^{-1}) - V_\kappa(0)] \right) \Big|_{\delta, \epsilon=0} = \delta \sum_i \left[\frac{\partial m_i^2(-2v\gamma_4^{-1})}{\partial \delta} - \frac{\partial m_i^2(0)}{\partial \delta} \right] \frac{\partial V_\kappa}{\partial m_i^2} \quad (4.121)$$

$$= \frac{T^2}{2\pi^2} \frac{\partial F^2(-2v\gamma_4^{-1})}{\partial \delta} \sum n_i m_i^2(0) J'_i(m_i^2(0)/T^2) \quad (4.122)$$

$$= \frac{6\gamma_4 \delta c_\chi^2 T^2}{\pi^2} \left(2m_W^2(0) J'_b \left(\frac{m_W^2(0)}{T^2} \right) + m_Z^2(0) J'_b \left(\frac{m_Z^2(0)}{T^2} \right) - 4m_t^2(0) J'_f \left(\frac{m_t^2(0)}{T^2} \right) \right) \quad (4.123)$$

$$\equiv \lambda v^4 \gamma_4^{-2} \delta (b(x)x^{-2}), \quad (4.124)$$

where $x = v/T$, and we used that our renormalisation conditions of Eq. (4.73) imply the variation w.r.t. the mass vanishes so that the linear term in δ comes from the thermal J functions, which are F -dependent (and F is δ -dependent). The result is the potential energy difference to leading order in ϵ, δ ,

$$p_V(T) = \Delta V(T) = 4\lambda v^4 \gamma_4^{-2} (\epsilon + b(x)x^{-2}\delta/4) + \mathcal{O}(\kappa\epsilon, \delta^2). \quad (4.125)$$

Wall dynamics will be determined by the balance of the volume pressure $p_V = \Delta V$ and an equivalent tension pressure $p_T = \mu/l$. Volume pressure ΔV domination at T_G means the lowest energy vacuum patches will quickly expand against the other vacuum patches and make the l size structure of walls disappear shortly after formation. The opposite case, approximately given by $(\epsilon + b(x)x^{-2}\delta/4) < 1/6$ [120], has that tension would drive dynamics together with the friction of the thermal bath. Indeed in vacuo, the tension would make the walls oscillate converting potential energy stored in tension into kinetic energy and back. The thermal bath however introduces friction with a pressure $T^4 v_w$ with v_w the wall velocity which dissipates the energy of the walls efficiently back into the bath, some of it in the form of gravitational radiation. Both instances then lead to the disappearance of the l size

network shortly after formation.

The dynamics of the large wall are dictated by the horizon rather than l and one can translate the above discussion by $l^{-1} \rightarrow H$. As long as $\mu H \geq p_V(T)$, structure of size H^{-1} will enter the horizon, oscillate and radiate as controlled by tension and friction leaving a potentially detectable trace. The opposite case wipes even this large wall away leaving virtually no trace. Focusing on detectable phenomenology, we restrict to the condition for long lived large walls, which is $p_T > p_V$ as outlined above, and reads explicitly

$$p_T(H(T_G)) = \mu H(T_G) > p_V = \Delta V(T_G), \quad (4.126)$$

$$|\epsilon + b(x_G)x_G^{-2}\delta/4| \lesssim \frac{x_G^{-2}v^2}{6m_h M_{\text{pl}}} \sqrt{\frac{4\pi^3 g_\star}{45}}, \quad (4.127)$$

where $x_G^2 = v^2/T_G^2$. This condition can be met by a cancellation of ϵ and δ , however, if they themselves are individually much larger than the RHS of the inequality above, the temperature dependence would mean that the condition will, shortly after T_G , not be satisfied. For this reason we also impose a condition on the logarithmic derivative w.r.t. temperature of the LHS; explicitly the change after an e-fold variation in temperature should also be smaller than the RHS of Eq. (4.127),

$$\left. \frac{d}{d \log x} (b(x)x^{-2}\delta/4) \right|_{x_G} \lesssim \frac{x_G^{-2}v^2}{6m_h M_{\text{pl}}} \sqrt{\frac{4\pi^3 g_\star}{45}}. \quad (4.128)$$

All the above conditions are met for $\epsilon = \delta = 0$, a case in which the perfect degeneracy would make walls endure the history of the universe to be around today. If so, their effect must have been negligible in the cosmological evolution and in particular any anisotropic impact on the CMB less than one part in 10^5 . Given the energy density stored in walls is μH , the bound can be translated into the tension [120]

$$\mu H_0 < M_{\text{pl}}^2 H_0^2 \quad \Rightarrow \quad \mu = \frac{2\sqrt{\lambda} v v_+^2}{3} = \frac{2\sqrt{\lambda} v^3}{3\gamma_4^2} \leq (0.1 \text{ GeV})^3. \quad (4.129)$$

Avoiding this bound would require smaller tension, attainable with larger γ_4 , of order $\gamma_4 \sim 10^4$, yet perturbativity from e.g. $h + h \rightarrow h + h$ scattering demands

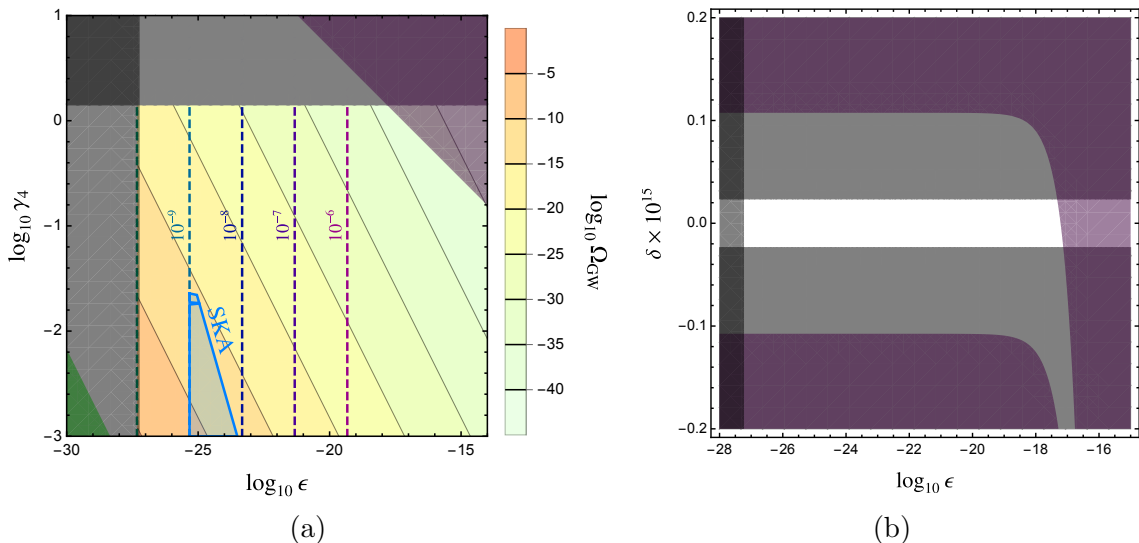


Figure 4.13: Fig. 4.13a shows the (ϵ, γ_4) plane with excluded regions in darker green (from the upper bound on walls energy density, Eq. (4.132)), light gray horizontal (perturbativity, Eq. (4.90)), dark gray (wall annihilation before BBN, (4.131)). The region in dark purple is discarded if one is to have walls that survive long past the original phase transition (Eq. (4.126)). Also shown is the gravitational wave spectrum value at peak frequency $\Omega_{\text{GW}}(f_{\text{peak}})$ in the yellow gradient, see Eq. (4.155) and Sec. 4.6. Dashed lines for the peak frequencies run from $f_{\text{peak}} = 10^{-6}$ Hz on the far right to 10^{-10} Hz on the far left in intervals of 10, and in blue the region SKA [11] would be sensitive to (this region, however, is excluded by LHC bounds, see Sec. 4.7). Fig. 4.13b shows the (ϵ, δ) excluded by wall annihilation before BBN in dark grey vertical Eq. (4.131), and the regions discarded for long lived walls following from Eq. (4.127) (purple) and Eq. (4.128) (grey horizontal).

$\lambda\gamma_4^2 < 8\pi/3$, and this possibility is ruled out. The avenue of reducing the tension in our degenerate potential means bringing the vacua closer together, which is a modification at small field values only. As a result this conclusion is robust against higher dimensional operator insertions in the potential.

Having ruled out the $\delta = \epsilon = 0$ limit, we now turn to finite but small values of the Higgs parity breaking parameters. We note that the condition that ensures wall survival at the Ginzburg time, Eq. (4.126), is more demanding if translated to later time and larger x ; for finite ΔV it will cease to be satisfied at T_w , i.e.

$$\mu H_w \equiv p_V(T_w) = \Delta V(T_w) \quad \Rightarrow \quad T_w^2 = \sqrt{\frac{45}{4\pi^3 g_\star}} \frac{M_{\text{pl}} \Delta V}{\mu} = \sqrt{\frac{45}{4\pi^3 g_\star}} 6\epsilon m_h M_{\text{pl}}. \quad (4.130)$$

Below this temperature, tension pressure gives way to vacuum pressure and we have

that walls are swept away towards the horizon at a velocity close to the speed of light.

A conservative bound [121] is for this temperature to be higher than our earliest direct evidence of universe history, big bang nucleosynthesis. This constraint can be translated into a lower bound on ϵ :

$$T_w > T_{BBN} \quad \Rightarrow \quad \epsilon \geq \frac{T_{BBN}^2}{6M_{\text{pl}}m_h} \sqrt{\frac{4\pi^3 g_\star}{45}}. \quad (4.131)$$

In addition, the energy density of the walls should always be subdominant if one is to avoid entering an inflationary phase. Given its scaling, this constraint is strongest at the latest time, i.e. T_w

$$\mu H(T_w) \leq g_\star T_w^4 \quad \Rightarrow \quad \epsilon > \frac{m_h^2}{9\lambda\gamma_4^2 M_{\text{pl}}^2}. \quad (4.132)$$

These constraints are put together in Fig. 4.13 for an illustration of the parameter space region compatible with experimental data. We note that the lower bound in ϵ from Eq. (4.132) means a locally SM-like potential (which has $\epsilon = 0$) is excluded, whereas an upper bound follows from the LHC (non)measurement of the triple Higgs coupling, see Eq. (4.173). Nevertheless the large disparity of scales involved leaves the possibility to close this window out of reach.

4.5 Past and Future First Order Phase Transitions

The presence of more than one minimum at a given temperature allows for tunnelling phenomena with potentially detectable imprints in our universe. This requires an evolution of the universe whose dynamics initially puts it in the false vacuum and a tunneling rate large enough to trigger a universe-wide transition, in the past or in the future.

A well studied case that satisfies these conditions is the SM with small Higgs mass. The history for this case is depicted in Fig. 4.2; the high temperature sym-

metric minimum $\phi = 0$ stops being the only extremum after the appearance of a new minimum (and maximum) at a finite (and large enough, see Sec. 4.3.3) field distance. The potential energy difference between minima changes sign at a critical temperature T_c , after which tunneling is energetically viable but suppressed by the negative exponential of the bounce solution action. Given that the $\phi = 0$ symmetric point turns eventually into a maximum, we have that the potential barrier between minima decreases and the energy difference increases, so sooner or later the transition will occur at what is dubbed the nucleation temperature T_N , where $T_N < T_c$.

Non-linearly realised theories allow for first order phase transitions as that in the case of the light SM Higgs but also a set of qualitatively different ones. One could indeed attempt at the equivalent of the light Higgs SM in our non-linearly realised theory; leaving every other parameter SM-like, decreasing γ_4 effectively increases field distances (i.e. decorrelates the quartic coupling and m_h^2 , see Eq. (4.48)) and could yield a first order phase transition. It is the case now, however, that there exist two degenerate true minima, ϕ_0, ϕ_- , given this limit is Higgs parity preserving, and uncorrelated patches of the universe will tunnel into one or the other minimum with equal likelihood. This distribution implies that a network of domain walls would form in the boundary between different-vacua patches, the subsequent phenomenology of domain walls having been studied in Sec. 4.4.

This illustrates the variety of phenomena in non-linearly realised theories. While the picture just described is more convoluted than typical case studies, one can break it down into staged transitions, each of which with a known theory formalism. For this reason we will study in this section scenarios that lead solely to a first order phase transition. Results derived here could be put together with those of Sec. 4.4 for more intricate cases as the one described above with two transitions, however we leave this for future work. Explicitly the cases studied will be histories Q of Fig. 4.3c and R of Fig. 4.4c, where we note that both are far from symmetric under Higgs parity and require sufficiently large ϵ and δ as shown below. For history Q we have two possibilities by flipping the diagram vertically, these are Q_0 and Q_- for a continuous connection of the high temperature with h_0 or h_- respectively. History R

	$\epsilon < 0$		$\epsilon > 0$	
	High T	Low T	High T	Low T
$(\text{ctg}_\chi^2 - 2)\delta > -8\epsilon/\gamma_4$	$h_0(T)$	$h_-(T)$	$h_0(T)$	$h_0(T)$
$(\text{ctg}_\chi^2 - 2)\delta < -8\epsilon/\gamma_4$	$h_-(T)$	$h_-(T)$	$h_-(T)$	$h_0(T)$

Table 4.1: True vacua at high and low temperatures for small ϵ and δ .

leads necessarily to a phase transition given the original minimum disappears, while history Q might not lead to a phase transition if the barrier and separation are never small enough. Following the discussion above we define the nucleation temperature as the temperature when the tunneling rate equals the Hubble 4-volume, which will signal the transition in the early universe

$$v^4 e^{-B(T_N)} \equiv H^4(T_N). \quad (4.133)$$

History Q does not specify which is the true minimum at low energies; this is dictated by the sign of $\Delta V(0)$ and in our parametrisation, ϵ . The two options for the sign of ϵ then have to be put against the two histories $Q_{0,-}$ their selection being in turned mapped to δ . Small χ leads to more than one minimum at high temperature so we choose $\chi > 0.3$ to ensure we remain over the limit of Eq. (4.109).

For exposition purposes, here we use the small ϵ and δ limit to give a connection of history and parameter space through Eq. (4.104); although this expansion does not hold for the whole regime we explore (where we use the full expressions), it does identify possibilities and gives a rough outline of the regions. One has a contrast of high and low energy extrema dependent on the parameters as shown on Tab. 4.1. Note that out of the four, one option is discarded since it never had h_0 , where we are today, as a true vacuum.

It is for a mismatch of high and low temperature minima that transitions are likely and that is the case for two out of remaining three options. These conditions are visualised in Fig. 4.14, which schematically displays the different phenomena that may be found in the (ϵ, δ) plane:

- In the first quadrant, both the tree-level potential and the finite-temperature corrections favor the h_0 SMEFT-like vacuum, and so we expect its cosmolog-

ical phenomenology to be similar to that of the SMEFT. Note that a phase transition in this quadrant would require higher powers of h/v (such as dim-6 or higher operators) in the tree-level potential.

- We mark as *unphysical* the region where the thermal history selects the vacuum h_- at present times, because, by definition, h_- does not have the known measured masses and couplings of the SM particles. This is the case for the third quadrant, in which both the tree-level potential and the thermal corrections favor h_- ; but also for part of the second quadrant, where h_- is the tree-level vacuum; and part of the fourth quadrant, where the system may become trapped at h_- and high temperatures, and not decay until after today.
- In the rest of the second quadrant, we find ourselves currently in the false vacuum h_0 , a situation that we refer to as the *doomsday* scenario, since a phase transition could be triggered at any time. However, as we will show in Sec. 4.5.2, the lifetime of the false vacuum we are in is much larger than the age of the universe. Notice that this possibility of the long-term survival of a false vacuum is in sharp contrast with the SM case.
- In the fourth quadrant, the true vacuum is h_0 , but the finite-temperature corrections favor h_- . There will thus be a region where h_- is selected at high temperatures, and a first-order phase transition happens before today. We have labelled this region *bubbles*, since the phase transition will happen through bubble nucleation, as described in Sec. 4.5.1.
- Finally, around the origin, when both ϵ and δ are small, long-lived domain walls are generated, as described in Sec. 4.4.

These considerations have to be put up against the IR problem; Sec. 4.3.3 outlines our treatment of this issue. In summary we will discuss a phase transition *if the new minimum appears in the perturbative regime, $\varepsilon_{IR}(\phi_0(T_1)) < 1$ (strong IR constraint) or if the new minimum is in the perturbative region by the critical temperature $\varepsilon_{IR}(\phi_0(T_c)) < 1$ (weak IR constraint)*

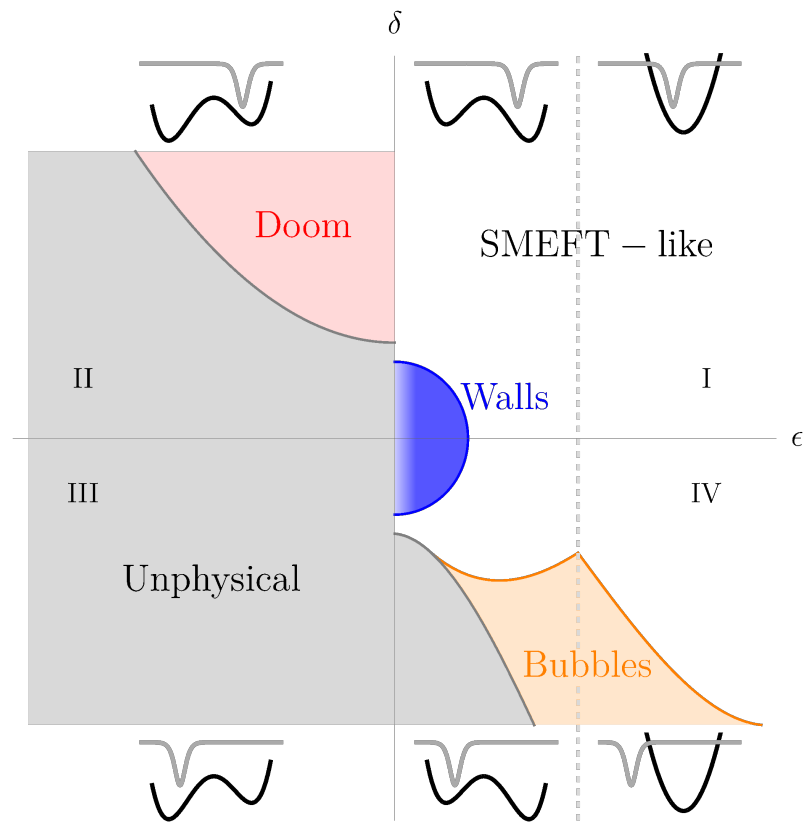


Figure 4.14: Schematic representation of the different cosmological phenomena arising in the (ϵ, δ) plane. The small diagrams at the top and the bottom borders represent the tree-level potential in black, and the finite-temperature corrections in grey.

More complicated histories arise for small χ which we shall comment on but not study in detail. In this case two minima coexist at high temperature and we might have one or more minima at low energy. If the minima coexist above a temperature where thermal fluctuations of correlation-distance-size patches overcome the barrier height (above a Ginzburg temperature, see Sec. 4.4) one has a mixed spatial coexistence of the vacua. Above this temperature either the two minima are degenerate to a good approximation and the evolution is described in Sec. 4.4, or if they have a sizeable energy difference, thermal jumps from the true to the false vacuum will cease first to leave predominantly only the true vacuum. This vacuum might still not be the same as the zero temperature one, in which case a phase transition would be possible. We leave such cases for future study.

4.5.1 First order electroweak phase transition

The possibility of nucleation in the past history of the universe is, given the considerations above, realised in the quadrant $\epsilon > 0$, $\delta < 0$ of the (ϵ, δ) plane so that the true vacuum is today ϕ_0 and at high temperatures ϕ_- . In this quadrant we can find histories Q₋ and R, the latter for $\epsilon > 1 - \sqrt{8/9}$ where there is a single minimum at tree level. For ϕ_- to be the true vacuum at high temperature, however, not only negative but sufficiently sizeable δ is required; we found in a small ϵ, δ expansion that this condition is $\delta < -8s_\chi^2/[\gamma_4(c_\chi^2 - 2s_\chi^2)]\epsilon$. This analytic result is validated around the origin but also extended to large values of the parameters (where one finds history R) by our numerical results in this section.

The determining factor to characterise the transition, once one has arranged for the high temperature vacuum turning into a false one, is the bounce action. In particular it will determine whether the transition took place or whether the probability is too small for it to have occurred yet. At high temperatures this bounce action can be approximated by a 3-space-rotation symmetric action times the small time interval $1/T$

$$B = \frac{S_3}{T}. \quad (4.134)$$

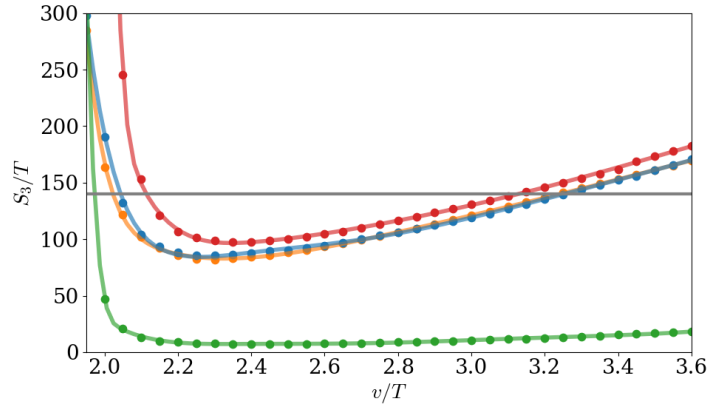


Figure 4.15: Comparison of the four methods to compute the tunnelling bounce action, as described in detail in the text of Sec. 4.5.1. The displayed lines are evaluated for the parameters $\chi = \sqrt{0.1}$, $\epsilon = 0.04$, $\delta = -0.08$, with the results from `CosmoTransitions` in orange, `Anybubble` in blue, the quartic potential approximation in red, and the thin wall approximation in green.

There are no closed formulas for this action but rather a series of approximations of various accuracies and software for numerical solutions of the problem. Here we use both for a better understanding of the process. The software used is `CosmoTransitions` [122] and `Anybubble` [123] whereas the analytic approximations are:

- *Quartic potential.* The formula for the bounce action of a polynomial potential of degree four is known to a good approximation [124]. The formula gives, for a quartic potential with a local minimum at $\phi = 0$, a true minimum at $\phi = \phi_m$, and maximum at ϕ_M as:

$$\bar{V} = \frac{\bar{\lambda}}{2} \left[\frac{\phi^4}{4} - \frac{\phi_m + \phi_M}{3} \phi^3 + \frac{\phi_m \phi_M}{2} \phi^2 \right], \quad (4.135)$$

and a bounce action as:

$$\frac{S_3^L}{T} = 4.85 \sqrt{\frac{8\phi_m \phi_M}{\bar{\lambda} T^2}} \left(\alpha + \frac{\alpha^2}{4} \left[1 + \frac{2.4}{1-\alpha} + \frac{0.26}{(1-\alpha)^2} \right] \right), \quad (4.136)$$

$$\alpha = \frac{9}{2} \frac{\phi_m \phi_M}{(\phi_m + \phi_M)^2}. \quad (4.137)$$

Our effective potential V_{eff} is not a polynomial, but as an approximation it can be modelled as such. We do so by identifying the minimum $\phi_m = \phi_- - \phi_0$

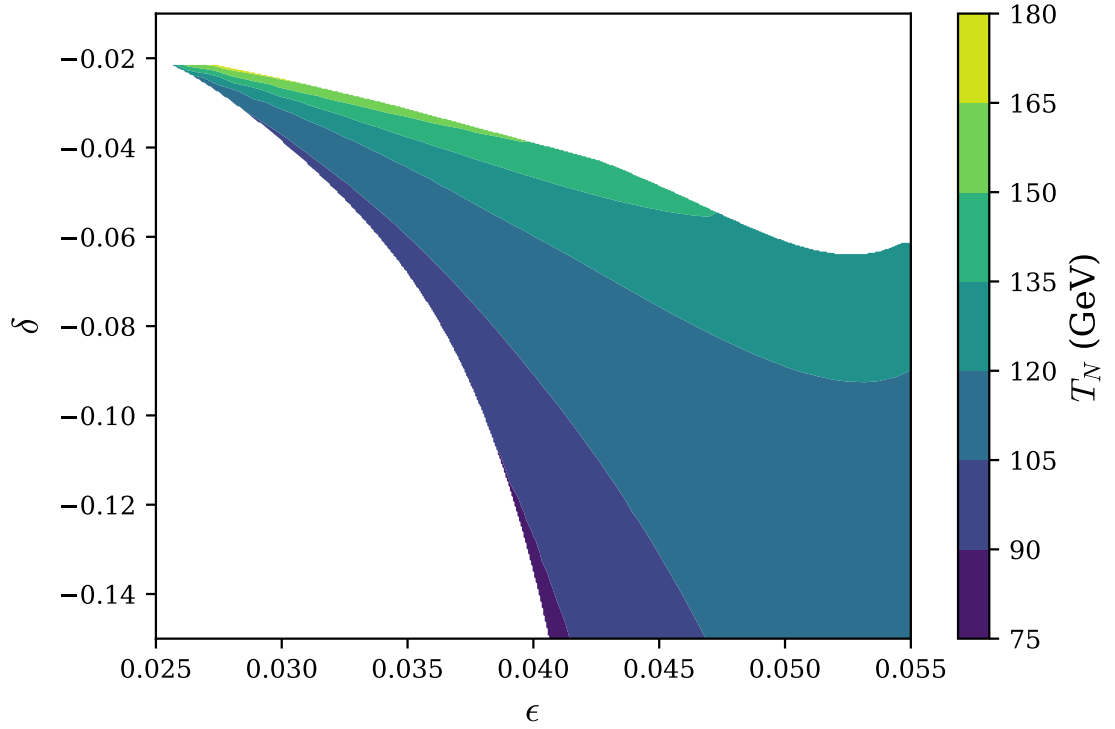


Figure 4.16: A slice of parameter space in ϵ, δ for which the region in colour following history Q_- meets the condition of Eq. (4.142) for some $T = T_N$, the nucleation temperature. For this plot, $\chi = \sqrt{0.1}$ and $\gamma_4 = 1.6$. The blank area in the upper region follows history Q_0 , as the thermal corrections favour the h_0 vacuum, leading to a SMEFT-like cosmological history. In the lower blank region while still following history Q_- , the condition for nucleation, Eq. (4.142), is not met for electroweak scale temperatures and as such we do not predict a first order phase transition in the early universe here. This and Fig. 4.17 occupy roughly quadrant IV of Fig. 4.14.

(if tunneling out of ϕ_-) which leaves still two parameters in the potential, ϕ_M and $\bar{\lambda}$, which are not fixed to the maximum and quartic coupling in Eq. (4.76), but rather are implicitly defined by two conditions of equal energy difference between minima and barrier height, i.e.

$$\bar{V}(\phi_m; \bar{\lambda}, \phi_M) \equiv \Delta V(T), \quad \bar{V}(\phi_M; \bar{\lambda}, \phi_M) \equiv U_-(T). \quad (4.138)$$

These implicit definitions for $\bar{\lambda}$ and ϕ_M that ensure the model potential has the same energy difference and barrier height.

- *Thin wall and triangular approximation.* Shortly after the critical temperature T_c , one has that the thin wall approximation (which assumes a small energy

difference between minima) holds and returns [101]

$$\frac{S_3^{tw}}{T} = \frac{16\pi}{3} \frac{\mu^3}{T(\Delta V)^2}, \quad \mu = \int_{\phi_-}^{\phi_0} d\phi \sqrt{2(V_{\text{eff}}(\phi) - V_{\text{eff}}(\phi_-))}. \quad (4.139)$$

Fitting the potential between minima to a triangle yields

$$\mu_{\Delta} = 2\sqrt{2} \int_{\phi_-}^{\phi_+} \sqrt{(U_-)\phi/(\phi_+ - \phi_-)} = \frac{4\sqrt{2}}{3}(\phi_+ - \phi_-)\sqrt{U_-}, \quad (4.140)$$

and in this approximation

$$\frac{S_3^{tw}}{T} = \left(\frac{4\sqrt{2}}{3}\right)^3 \frac{16\pi}{3} \frac{v}{T} \frac{U_-^{3/2}(\phi_+(T) - \phi_-(T))^3}{\Delta V^2 v}. \quad (4.141)$$

This expression is easy to evaluate, but is only valid for a short time after T_c whereas Eq. (4.137) continues to be valid at lower temperatures.

One can see a comparative plot for the two analytic approximations and the two numerical estimates of the bounce action for the 1-loop thermal effective potential defined in Eq. (4.76) as a function of temperature in Fig. 4.15. The numerical estimates are performed with `Anybubble` [123] and `CosmoTransitions` [122] respectively. For `Anybubble`, the potential has been first fitted to a 9th degree polynomial for technical reasons and then passed into the `Anybubble` code, for `CosmoTransitions` we use the `tunneling1D` module to compute the bounce action.

The curves all start with a very large value of the bounce action as right after the critical temperature, the energy difference between true and false minima is small and the thin wall approximation applies, giving a bounce action inversely proportional to the minima potential energy difference. In the case of history Q_- , as temperature decreases the bounce action decreases and reaches a minimum value after which it grows again. For the case of history R however, the action decreases until it vanishes since the original minimum disappears and so does the barrier between minima. The condition for the transition to occur reads

$$\frac{S_3(T_N)}{T_N} \simeq -\log \frac{H^4(T_N)}{v^4} \simeq 140. \quad (4.142)$$

This condition will be met in history R but not necessarily in history Q_- , where it could be that the bounce action never decreases below 140 and one is stuck in the wrong vacuum. In Fig. 4.16 we show a slice of parameter space where the condition is met for history Q_- , where the gradient marks the nucleation temperature. Additionally Fig. 4.17 extends this slice to encompass history R. As discussed in the next section, if one is stuck in ϕ_- below electroweak temperatures, one stays there until today. Since this conflicts with our definition of ϕ_0 as our vacuum today these instances are excluded; visually that is the lower left white region in Fig. 4.16. On the edge of this region we have a sizeable barrier, but just low enough so that the transition occurs, and it does so strongly. Further away from this lower edge of the wedge in Fig. 4.16, we have smaller barriers and weaker first order phase transitions until at the upper edge one meets the numerical extension of the condition $(\text{ctg}_\chi^2 - 2)\delta < -8\epsilon/\gamma_4$ where the history changes to Q_0 and the universe is always in the true vacuum which is connected continuously at low and high temperatures. For history R with $\epsilon > 1 - \sqrt{8/9}$, this condition changes qualitatively and the edge of the first order phase transition region is found numerically.

4.5.2 Doom: future vacuum decay

The previous section showed that the tunneling rate out of a false vacuum might not be large enough to undergo a transition at temperatures near but below the critical temperature. At later times, the causal 4-volume increases as H^{-4} , and the bounce action is given by the 4d bounce action, well approximated by the potential for $T = 0$. It could be that the growing Hubble volume exceeds both the inverse decay per time and volume at this later time, and vacuum decay would ensue; if so a conservative bound would be to require this to happen before BBN,

$$B \leq 4 \log \frac{v}{H(T_{BBN})} \simeq 4 \log \frac{v M_{\text{pl}}}{T_{BBN}^2} \simeq 250. \quad (4.143)$$

It is the case however, that for all studied cases of history Q_- , if the phase transition does not occur at T_{ew} , it will also not occur before BBN. This means that any point on Fig. 4.16 of Sec. 4.5.1 on the lower left white region, which marked instances

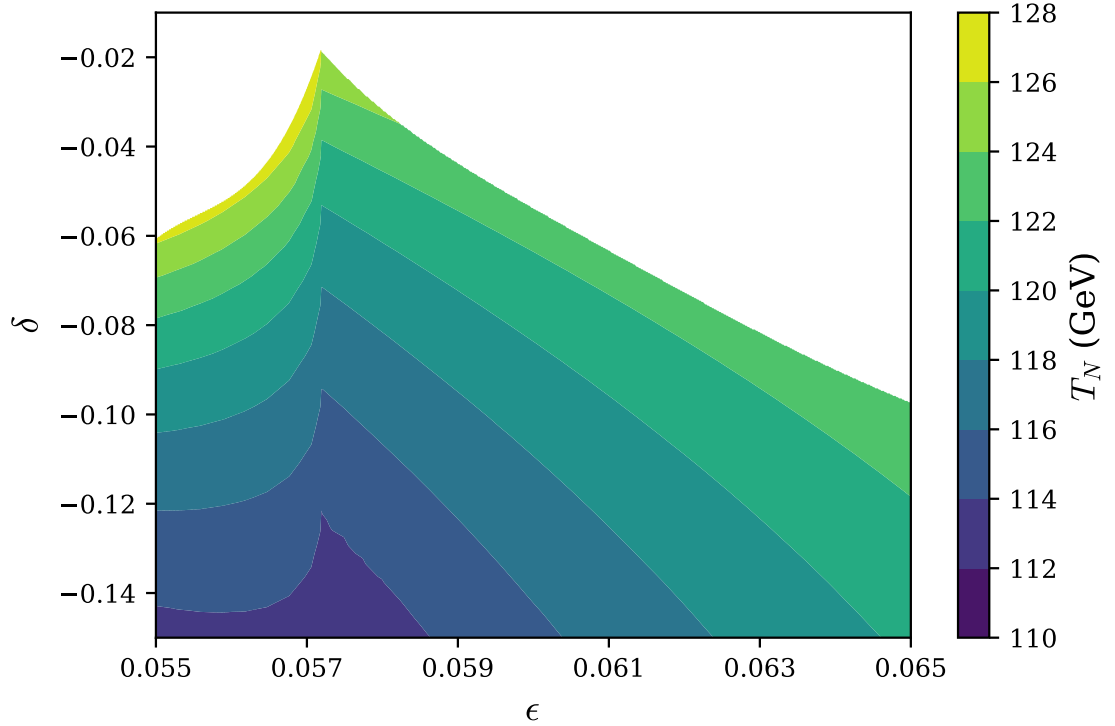


Figure 4.17: Extension of Fig. 4.16 to larger epsilon values and different histories, with $\gamma_4 = 1.6, \chi = \sqrt{0.1}$ as in the previous plot. The plot is discontinuous at $\epsilon = 1 - \sqrt{8/9}$ as a result of Eq. (4.53). For $\epsilon < 1 - \sqrt{8/9}$, the region in colour follows history Q_- and the blank, upper region above this follows history Q_0 as in Fig. 4.16. However, when $\epsilon > 1 - \sqrt{8/9}$, the $T = 0$ potential has a single minimum only and history R is followed for the region in colour. The blank region above only has a single minimum throughout its evolution. We note that the upper boundary from history R to a SMEFT-like history is slightly ambiguous as the potential becomes very flat and difficult to treat numerically.

where the universe remained in the false minimum ϕ_- past the electroweak epoch, the universe will remain in ϕ_- until today. For this reason these points are deemed unphysical.

The situation of being stuck in a false minimum is realised in history Q_0 in the opposite quadrant, $\epsilon < 0$, $\delta > 0$, with the further approximate constraint of $(\text{ctg}_x^2 - 2)\delta \gtrsim -8\epsilon/\gamma_4$ as sketched in Tab. 4.1. In practice, this approximate constraint has to be extended to a numerical search for history Q_0 . In Fig. 4.18, we display in blue the region where the thermal history is that of Fig. 4.5, with two minima at high temperature. Above this region, we have history Q_0 . The infrared problem as sketched in Sec. 4.3.2 casts doubt on histories where extrema are to be found in regions with $\varepsilon_{IR}(\phi_-) > 1$; for such cases we do not trust our perturbative computation, and so we do not discuss the region below the red solid and dashed lines in Fig. 4.18. We also show in gray colour in Fig. 4.18 the regions excluded by the boundedness-from-below and perturbativity criteria described above.

Even when history Q_0 can be perturbatively treated, the fact that at high temperature the only minimum is $h_0(T)$, which turns into a false vacuum at T_c , has to be reconciled with us being at $h_0(T)$ today; this demands that the decay rate be small enough so that the transition has not occurred yet

$$B \geq 4 \log \frac{v}{H_0} \simeq 410. \quad (4.144)$$

This case with negative ϵ is however more restricted from the perturbativity and boundedness from below constraints. This can be understood since for $\epsilon < 0$, $\gamma_\epsilon < 1$ and given $\delta\gamma_4 = \gamma_\epsilon - \gamma_4/\gamma_a$ for positive δ we require small γ_4/γ_a , yet one of the terms in the perturbative bound of Eq. (4.90) scales with $(\gamma_4/\gamma_a)^{-2}$. This perturbative bound then translates into a lower bound on negative ϵ to obtain a bounded from below potential in a range of $\phi \sim 4\pi v$. On the other hand the limit of $\epsilon \rightarrow 0^-$ gives an infinite lifetime and hence is compatible with observation, the question then is if within this allowed window for ϵ decay lifetimes around the age of the universe can be found.

To answer this question we turn to the zero-temperature bounce action; a (eu-

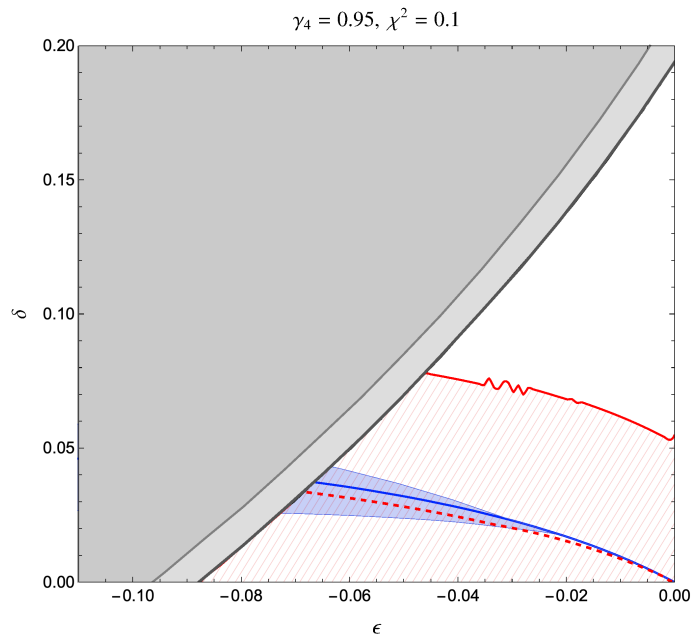


Figure 4.18: Bounds on the (ϵ, δ) parameter space for the doom scenario at $\gamma_4 = 0.95$ and $\chi^2 = 0.1$. The upper-left grey region is excluded by the boundedness-from-below (dark) and perturbativity (light) criteria. The hatched region below the solid red line is excluded by the strong IR constraint, Eq. (4.88), while the dashed red line shows the weak version, Eq. (4.86). There is some noise associated with our method of numerically tracking the temperature evolution of the minima, and this noise is visible in the strong IR constraint curve. The blue region corresponds to the history displayed in Fig. 4.5, in which two minima exist in the high-temperature potential. The blue line separates the regions where the sign of the magnitude defined in Eq. (4.108) is positive or negative and is an estimate for the regions for histories $Q_{-,0}$ respectively

clidean) space-time symmetric solution with the $T = 0$ potential. A quick estimate of the thin wall approximation for our zero temperature potential, which holds if

$$\frac{\Delta V}{3\sigma m_h} = \frac{1}{2\gamma_\epsilon^2}(1 - \gamma_\epsilon^{-1}(1 - \epsilon)) \ll 1, \quad (4.145)$$

gives the tension as in the bubble case expanding in ϵ

$$\sigma = \int_{h_+}^0 dh \sqrt{2V(h)} = \mu + \mathcal{O}(\epsilon) = \frac{2\sqrt{\lambda}v^3\gamma_4^{-2}}{3}, \quad (4.146)$$

and an expression for the bounce action as [125]

$$B = \frac{27\pi^2\sigma^4}{2\Delta V^3} = \frac{3^3\pi^2}{2} \frac{\lambda^2 2^4 \gamma_4^{-8}}{3^4} \frac{1}{2^6 \lambda^3 \epsilon^3 \gamma_4^{-6}} = \frac{\pi^2}{24\lambda\gamma_4^2\epsilon^3}. \quad (4.147)$$

This analytic approximation returns, for $\gamma_4 = 1$, $\epsilon > -0.15$ decay lifetimes longer than today. This is not a particularly accurate result: the use of `CosmoTransitions` and $\gamma_4 = 1$ returns $\epsilon > -0.475$ for a decay after today. All these values are however ruled out by the perturbativity and boundedness bound. These bounds are relaxed for smaller γ_4 allowing for larger $|\epsilon|$ values, so one might expect this limit to allow for shorter universe lifetimes. In this same limit however, the bounce action, while not well approximated by the thin wall, does factor out in the same way for γ_4 , i.e. $B = \lambda^{-1}\gamma_4^{-2}f(\epsilon)$ and so reducing γ_4 actually increases the lifetime exponentially. One concludes then that the lifetime of the universe is in all instances well beyond the current age.

The question that follows is then what are the allowed values for the lifetime. This turns our gaze to the future which changes the estimation qualitatively. Indeed the estimation of the Hubble 4-volume as the relevant spacetime factor is valid in a decelerated expansion with scale factor $a \sim t^p$ but not in an accelerated expansion. In this case revisiting the estimation for the relevant 4-volume, i.e. the past light cone of an observer at time t_f , one obtains for $a \sim e^{H_0 t}$

$$\int_{\text{light cone}} d^4x \sqrt{-\det(g_{\mu\nu})} = \frac{4\pi H_0^{-3} t_f}{3}. \quad (4.148)$$

$$\text{light cone eq.} \quad -a(t)d\chi = dt, \quad \chi(t_F) = 0, \quad (4.149)$$

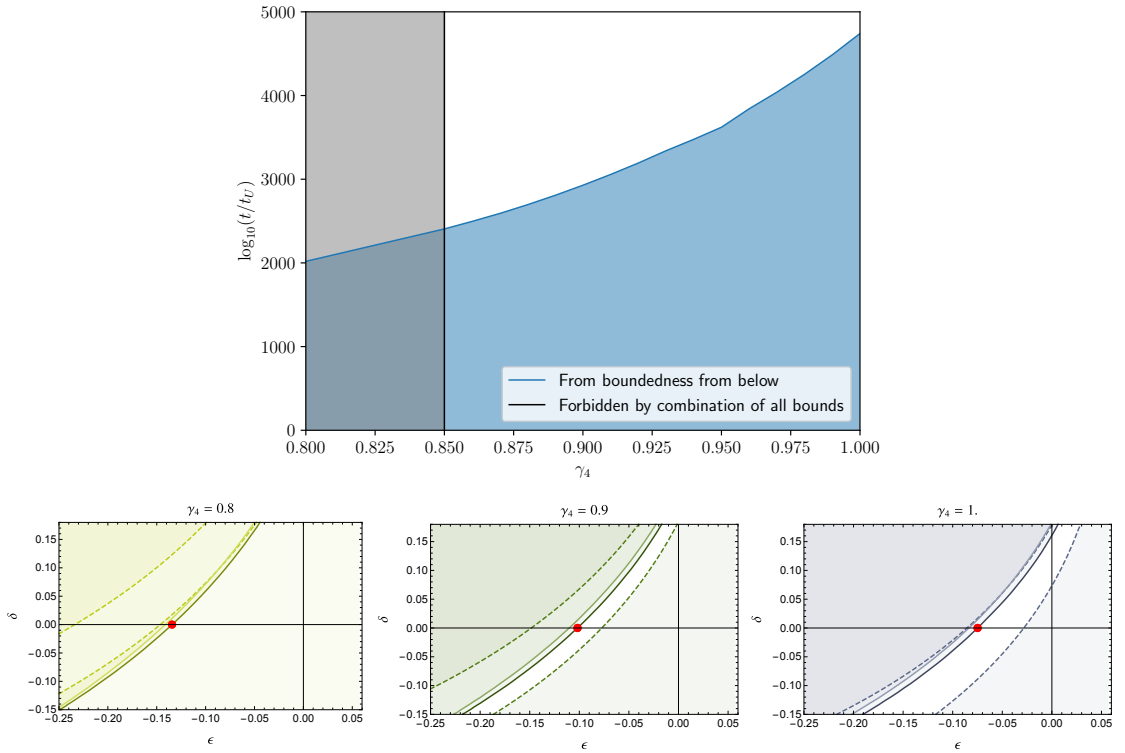


Figure 4.19: Top: excluded values of the lifetime of the universe as a function of γ_4 . Bottom: example points with the minimal lifetime allowed by boundedness from below in the second quadrant of the (ϵ, δ) plane, used to generate the blue line in the top plot. In these three plots, the shaded region is ruled out from various constraints: boundedness from below (darker, solid), perturbativity (lighter, solid), and LHC constraints (dashed). See Sec. 4.7 and Fig. 4.25 for more details on all the bounds shown in these plots.

i.e. an space-time volume which is a sphere of radius H_0^{-1} times time, and one concludes that the accelerated expansion from this perspective is ‘living in a box’, the longtime physicist dream. For a given value of potential parameters we find the lifetime t_f by solving

$$\frac{4\pi H_0^{-3} t_f}{3} v^4 e^{-B} = 1. \quad (4.150)$$

We have used this estimate to generate Fig. 4.19 which further illustrates the point of the lifetime of the universe being much larger than its age. To generate it, we look for the point in the second quadrant of the (ϵ, δ) space that gives the minimal lifetime allowed by the boundedness-from-below criterion, for different values of γ_4 . Such points are shown in red in the 3 plots at the bottom of Fig. 4.19, corresponding to 3 values of γ_4 . We then compute the corresponding lifetime and display it as the blue line in the top plot. The gray region on the left of the top plot is excluded by a combination of all bounds, as described in Sec. 4.7. Thus, the only allowed lifetimes are those in the white region, and are all larger than the age of the universe by a factor $> 10^{2000}$.

4.6 Gravitational Waves

The spectrum of gravitational waves is customarily given as

$$\Omega_{\text{GW}} = \frac{d\rho_{\text{GW}}}{d\log k} = \frac{d\rho_{\text{GW}}}{d\log f}, \quad (4.151)$$

with ρ_{GW} the energy density in gravitational waves, k the wave number and f frequency, in natural units $2\pi f = k$. In our study two sources of gravitational waves have been identified: walls and first order phase transitions. Let us discuss each in turn.

Gravitational emission occurs for domain walls as smaller curvature (larger radius) wall structure enters the causal horizon and starts a damped oscillation in the plasma. While most of the energy goes into the plasma, part of it is emitted as gravitational waves, with the contribution at time t after the big bang for an interval

Δt estimated as $\Delta\rho_{\text{GW}}/\Delta t \simeq G\mu^2/t$. Today the spectrum is redshifted and more so the earlier the emission, so that the peak frequency corresponds to the annihilation time t_w , and one has (see e.g. Ref. [126])

$$f_{\text{peak}} = a_w H_w = \frac{g_0^{1/3} T_0}{g_{\bar{w}}^{1/3} T_w} \sqrt{\frac{4\pi^3 g_w}{45} \frac{T_w^2}{M_{\text{pl}}}} = \frac{g_0^{1/3}}{g_{\bar{w}}^{1/3}} \left(\frac{4\pi^3 g_w}{45} \right)^{1/4} T_0 \sqrt{\frac{6\epsilon m_h}{M_{\text{pl}}}}, \quad (4.152)$$

$$= \frac{g_0^{1/3}}{g_{\bar{w}}^{1/3}} \sqrt{\frac{4\pi^3 g_w}{45} \frac{T_0 T_{\text{BBN}}}{M_{\text{pl}}}} \frac{T_w}{T_{\text{BBN}}} = 1.1 \times 10^{-10} \frac{T_w}{T_{\text{BBN}}} \text{ Hz}, \quad (4.153)$$

where $g_{\bar{w}} = g_w - g_\nu = g_w - 21/4$ and in the last equality we assumed that T_w occurred while $g_w = 10.75$ which is the latest allowed. Correspondingly, the power spectrum value at the peak is given by:

$$\Omega_{\text{GW}}(f_{\text{peak}}) = \frac{G_N \mu^2}{\rho_{\text{cr}}} \left(\frac{T_0}{T_w} \right)^4 = \Omega_\gamma^0 \frac{2^3 \pi g_w}{3^5 g_0} \frac{v^4}{M_{\text{pl}}^4} \frac{1}{\epsilon^2 \gamma_4^4} \quad (4.154)$$

$$= \Omega_\gamma^0 \frac{40}{3\pi^2 g_0} \frac{m_h^2 v^4}{M_{\text{pl}}^2 T_{\text{BBN}}} \frac{T_{\text{BBN}}^4}{T_w^4} \gamma_4^{-4} = 1.4 \times 10^{-17} \frac{T_{\text{BBN}}^4}{T_w^4} \gamma_4^{-4}. \quad (4.155)$$

One can note, when expressed in terms of the ratio of temperatures for the BBN and wall annihilation, that the frequency is bounded to be greater than 0.1 nHz, and the peak in the spectrum increases with decreasing γ_4 and decreasing frequency. These features are shown in Fig. 4.13; given that the strength of the gravitational wave signal is greater for lower frequencies, one finds that the low frequency Square Kilometer Array (SKA) experiment [11] would probe part of the parameter space.⁶ As we shall see in Sec. 4.7, when put against LHC bounds for our model, however, the parameter region that would yield a signal at SKA is already excluded. The shape of the full spectrum can be approximated by k^{-1} , and k^3 right and left of the peak respectively [126], in qualitative agreement with simulations [127].

For a first order phase transition undergoing bubble nucleation, the gravitational wave signal can be estimated using the thermal parameters derived from the tunnelling action: the speed of the transition β/H and the strength of the phase transition α related to the latent heat, both evaluated at the nucleation temperature

⁶We estimate that SKA is sensitive to the GW signal when its power spectrum evaluated at the peak frequency lies above the sensitivity curve.

T_N given in Eq. (4.142).⁷ The thermal parameters are explicitly:

$$\alpha = \frac{1}{\rho_{rad}(T_N)} \left(\Delta V(T_N) - T_N \frac{d\Delta V}{dT} \Big|_{T=T_N} \right), \quad (4.156)$$

$$\frac{\beta}{H_*} = T_N \frac{d(S_3/T)}{dT} \Big|_{T=T_N}, \quad (4.157)$$

where H_* is the Hubble constant at the time of nucleation, $\Delta V(T)$ is defined in Eq. (4.80), and $\rho_{rad}(T_N) = g_* \pi^2 T_N^4 / 30$ is the radiation energy density. The quantity g_* is the effective number of relativistic degrees of freedom in the plasma at T_N , which was calculated by tracking particle decoupling following [129]. The GW signal also depends on the velocity of the bubble wall in the rest-frame of the plasma, v_w , which we calculate following the model-independent prescription in [12].

As demonstrated in Sec. 4.5.1, our non-linearly realised theory model is capable of FOPTs that are qualitatively different than those accessible in SMEFT theories. In particular, we are interested in bubble nucleation that occurs in the parameter space identified in Fig. 4.16. We now present in Fig. 4.20 the behaviour of the associated thermal parameters α , β/H_* along with T_N and v_w as a function of ϵ, δ , using the same slice of parameter space as Fig. 4.16. With these parameters associated with bubble nucleation, we can proceed to estimate the GW signal observable today.

Next, we discuss our calculation of the gravitational wave signal from the thermal parameters. The following discussion is largely pedagogical, and we note that our analysis follows standard techniques. There are three sources of gravitational wave production during bubble nucleation: the bubble collisions, plasma sound waves driven by the expanding bubble wall, and turbulence [106]. The total gravitational wave energy density, Ω_{GW} , is the sum of the signal from each of these sources is

$$\Omega_{\text{GW}} = \Omega_{\text{col}} + \Omega_{\text{sw}} + \Omega_{\text{tu}}. \quad (4.158)$$

The initial source for GW radiation occurs when the bubbles first collide, breaking

⁷More precisely, the relevant temperature is the transition temperature T_* . Here we assume $T_* \approx T_N$ and do not distinguish between them, a safe assumption for fast phase transitions without significant reheating and in the absence of large supercooling [106, 128]

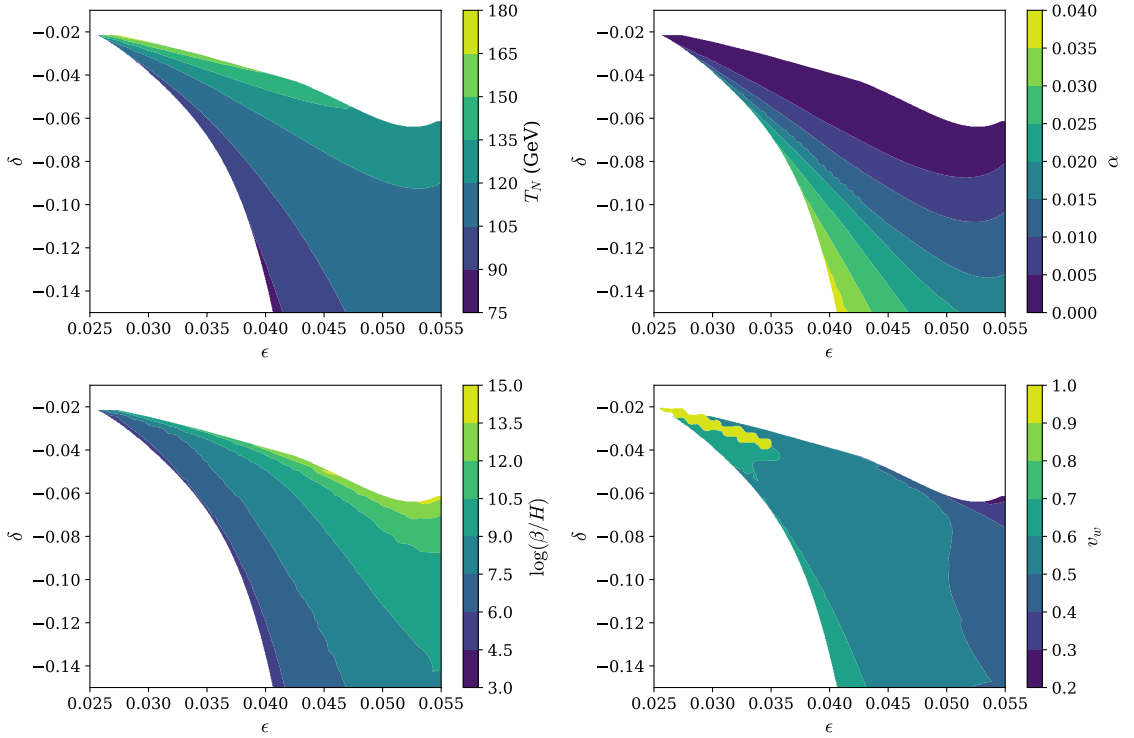


Figure 4.20: The thermal parameters T_N , α , β/H_* , v_w for a slice of ϵ , δ parameter space with $\gamma_4 = 1.6$ and $\chi = \sqrt{0.1}$. The thermal parameters are defined respectively in Eqs. (4.142), (4.156), and (4.157) with the wall velocity estimated using prescription outlined in [12]. Note for a small region of parameter space, runaway bubbles with $v_w \rightarrow 1$ are predicted. However, the region is numerically noisy as a result of finite sampling. Fig. 4.16 is included again on the top left plot.

spherical symmetry. The contribution from bubble collisions, however, is thought to be small (order percent) so long as the walls do not enter the runaway regime [128], so here we do not include them in our estimation of the GW signal.

As the bubbles expand, wave fronts emerge preceding the the bubble walls, forming acoustic sound waves propagating in the plasma. This is typically the dominant contribution to the GW signal near the peak frequency of the gravitational wave power spectrum. Schematically, this power spectrum as measured today can be estimated by redshifting the GW signal at the source,

$$\Omega_{\text{sw}} = F_{\text{redshift}} \times \Omega_{\text{amp}} \times S_{\text{sw}}(f), \quad (4.159)$$

where $S_{\text{sw}}(f)$ is the spectral shape of the GW signal. Accounting for the redshift of GW radiation from the time of production introduces the factor (as outlined in, for

example, Refs. [128, 130, 131])

$$F_{\text{redshift}} = 3.57 \times 10^{-5} \left(\frac{100}{g_*} \right)^{1/3}. \quad (4.160)$$

The GW energy density from the sound waves in the plasma is [132]:

$$\Omega_{\text{sw},0} = 3\Gamma^2 \bar{U}_f^4 (H_* R_*) \tilde{\Omega}_{\text{sw}}, \quad (4.161)$$

where $\Gamma \sim 4/3$ is the adiabatic index, \bar{U}_f is the root mean square (RMS) fluid four-velocity, and R_* is the average separation between bubbles $R_* = (8\pi)^{1/3} v_w / \beta$ [128]. The efficiency factor $\tilde{\Omega}_{\text{sw}}$ stems from converting motion in the fluid to metric perturbations, estimated from simulation to be $\tilde{\Omega}_{\text{sw}} = 0.012$ [132, 133]. The RMS velocity \bar{U}_f is set by the strength of the phase transition α through

$$\bar{U}_f^2 = \frac{3}{4} \kappa_{\text{sw}} \frac{\alpha}{1 + \alpha}. \quad (4.162)$$

The quantity κ_{sw} controls how much of the vacuum energy is transferred into kinetic energy of the plasma. This has been studied in detail in Ref. [134], resulting in numerical fits of $\kappa_{\text{sw}}(v_w, \alpha)$ to approximate full solutions to the relativistic fluid equations of the plasma. The results of these fits are used here and checked against PTPlot [128].

During the phase transition, shock waves will develop, at which point the motion of the plasma is better described by turbulence than acoustic sound waves. If the time scale of shock formation is small compared one Hubble time $\tau_{\text{sh}} < 1/H_*$, the resulting sound wave signal is reduced by a factor $H_* \tau_{\text{sh}} = H_* R_* / \bar{U}_f$. The total Ω_{amp} is then⁸

$$\Omega_{\text{amp}} = 2.061 \Omega_{\text{sw},0} \text{Max}[H_* \tau_{\text{sh}}, 1]. \quad (4.163)$$

⁸The numerical prefactor ensures the total GW power resulting from integrating the power spectrum Ω_{sw} reproduces the total power estimate $\Omega_{\text{sw},0}$ [132]

Putting all of this together gives

$$h^2\Omega_{\text{sw}}(f) = 2.59 \times 10^{-6} h^2 \left(\frac{100}{g_*}\right)^{1/3} \Gamma^2 \bar{U}_{fl}^4 \left(\frac{H_*}{\beta}\right) v_w \text{Max}[H_* \tau_{\text{sh}}, 1] S_{\text{sw}}(f). \quad (4.164)$$

The spectral shape of the sound wave power spectrum is [106]

$$S_{\text{sw}} = \left(\frac{f}{f_{\text{sw}}}\right)^2 \left(\frac{7}{4 + 3(f/f_{\text{sw}})^2}\right)^{7/2}, \quad (4.165)$$

written in terms of the peak frequency as observed today,

$$f_{\text{sw}} = (8.876 \mu \text{ Hz}) \left(\frac{g_{\text{eff}}}{100}\right)^{1/6} \left(\frac{T_N}{100 \text{ GeV}}\right) \left(\frac{1}{v_w}\right) \left(\frac{\beta}{H}\right) \left(\frac{z_p}{10}\right). \quad (4.166)$$

This results from red shifting the frequency profile obtained from numerical simulations, which predict $z_p \sim 10$ [132].

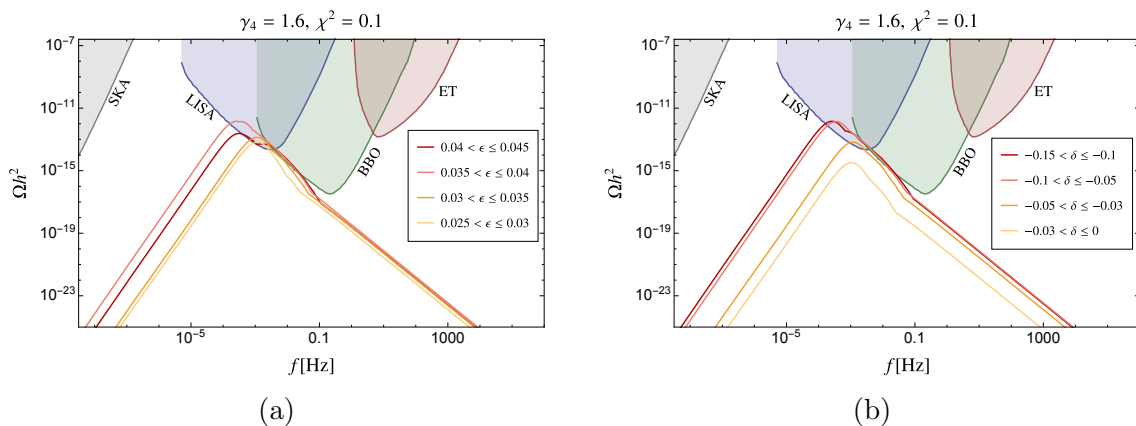


Figure 4.21: The gravitational wave signal for $\gamma_4 = 1.6, \chi^2 = 0.1$. The GW signal curve is the maximal envelope of the power spectra obtained from varying ϵ and δ . To give a sense of the ϵ - and δ -dependence, the parameter space is broken up into subsets, and a resulting maximal envelope power spectrum is drawn for each subset. In Fig. 4.21a, the ϵ -dependence is emphasised by breaking the parameter space up into subsets of ϵ ranges as specified in the legend, while varying over all δ for each curve. In Fig. 4.21b, the δ -dependence is correspondingly emphasised, this time varying over all ϵ for each curve. The GW sensitivity curves are drawn for SKA [11], LISA [13], the Big Bang Observer (BBO) [14], and the Einstein telescope (ET) [15].

The next important contribution to the overall signal is the turbulence term. In this case, the power of the gravitational wave signal at the source is now generated by turbulence in the fluid [131, 135, 136]. While our understanding of turbulence

during cosmological phase transitions is still evolving [131, 137–140], the result used here is:

$$h^2\Omega_{\text{tu}}(f) = 3.35 \times 10^{-4} \left(\frac{H_*}{\beta}\right) \left(\frac{\kappa_{\text{tu}}\alpha}{1+\alpha}\right)^{3/2} \left(\frac{100}{g_*}\right)^{1/3} v_w S_{\text{tu}}(f), \quad (4.167)$$

where the efficiency factor κ_{tu} parameterises how much of the kinetic energy is converted into turbulent motion. Here we use $\kappa_{\text{tu}} = 0.05 \kappa_{\text{sw}}$, as chosen in Ref. [106]. This approximation is based on simulated fluid motion [133], though this simulation does not last long enough to realistically capture turbulence effects. We emphasise that, as noted in the literature, this efficiency factor is not yet well-understood [128, 131, 141, 142]. Finally, the spectral shape of the turbulence signal is [143]:

$$S_{\text{tu}}(f) = \frac{(f/f_{\text{tu}})^3}{[1 + f/f_{\text{tu}}]^{11/3} (1 + 8\pi f/h_N)}, \quad (4.168)$$

where

$$f_{\text{tu}} = 27\mu \text{ Hz} \frac{1}{v_w} \left(\frac{\beta}{H_*}\right) \left(\frac{T_N}{100 \text{ GeV}}\right) \left(\frac{g_*}{100}\right)^{1/6}, \quad (4.169)$$

$$h_N = 16.6\mu \text{ Hz} \left(\frac{T_N}{100 \text{ GeV}}\right) \left(\frac{g_*}{100}\right)^{1/6}. \quad (4.170)$$

The total gravitational wave signal that results from both the sound wave and turbulence contributions is plotted in Fig. 4.21 for a benchmark choice of γ_4 , χ in the nonlinearly realised theory model. We also show the sensitivity curves for planned gravitational wave detectors. Given γ_4 and χ , there is still a range of ϵ and δ that give bubble nucleation and generate a gravitational wave signal. This figure summarizes this parameter space by plotting the maximal envelope of the many power spectra that result from varying ϵ and δ . While no single choice of (ϵ, δ) will reproduce the whole curve, the maximal envelope overlapping with the GW detector sensitivity curves indicates at least one point in (ϵ, δ) parameter space with a power spectrum that exceeds the sensitivity curve. In the remainder of this work, we estimate that a GW signal is within observable reach of a GW detector if there exist some frequencies for which the GW power spectrum exceeds the detector's

sensitivity curve.

4.7 Complementarity with LHC

While measurements at the LHC have opened the door to the electroweak symmetry breaking mechanism and made formidable advances in its exploration, these measurements are also limited to only probe couplings of the electroweak sector around the vacuum. As this work has tried to underline, cosmology has the potential to reach where such scattering experiments cannot, to non-local effects in field space. Here we establish this complementarity quantitatively on a concrete case study by confronting our previous cosmological analysis with LHC bounds.

Local observables correspond to coefficients in a covariant expansion of fields of the action around the vacuum. These can be given in the scalar sector in terms of covariant derivatives of the curvature tensor and scalar potential, reproducing here for simplicity the curvatures of Sec. 4.2:

$$v^2 R_\varphi(0) = 1 - c_\chi^4 \gamma_a^2, \quad v^2 R_h(0) = -\gamma_a^2 s_\chi^2 c_\chi^2, \quad (4.171)$$

which are bounded by ATLAS to a 95% confidence level to be

$$v^2 R_\varphi(0) = -0.080_{-0.13}^{+0.12}, \quad v^2 R_h(0) = +0.080_{-1.1}^{+1.0}, \quad (4.172)$$

where these bounds are derived from [144, 145]. Also relevant will be the element of the third covariant derivative of the potential $(\nabla^3 V)_{hhh} = V'''(0) = 3\lambda\gamma_4(1 - \epsilon)v$, probed by measurements of triple Higgs coupling. Bounds from ATLAS [146] give the following constraints at 95% confidence on the triple-Higgs coupling in the kappa framework (i.e. ratio of the triple-Higgs coupling to the SM expectation)

$$-1.0 < \kappa_\lambda = \frac{V'''(0)}{V_{\text{SM}}'''(0)} = \gamma_4(1 - \epsilon) < 6.6. \quad (4.173)$$

Here, we combine experimental input from the LHC with the cosmological analyses of Secs. 4.4 and 4.5 in order to present a final comprehensive phenomenological

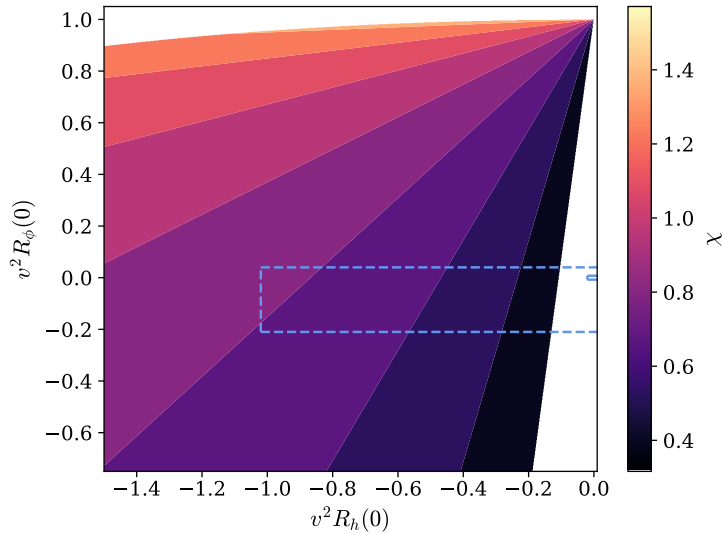


Figure 4.22: The curvature plane $v^2 R_\varphi(0)$ and $v^2 R_h(0)$ as defined in Eq. (4.171). In colour is the region for high-temperature symmetry restoration (see Sec. 4.3.3), i.e. $\pi/2 > \chi > 0.3$. We vary γ_a^2 independently to account for varying $\epsilon, \delta, \gamma_4$. We note for interest but do not show on the plot for clarity that increasing γ_a^2 decreases the curvatures radially originating from $(v^2 R_h(0), v^2 R_\varphi(0)) = (0.0, 1.0)$. The area outside the blue dashed box is excluded by LHC bounds from Eq. (4.172). The FCC would be expected to be sensitive, assuming SM-like couplings, up to the small, inner box [16, 17].

picture. We categorise these results into different different cosmological processes as follows:

- **Symmetry restoration.** The small ϵ, δ limit allows for identification of $\chi > 0.3$ as the region for high temperature symmetry restoration. This does not include the $\chi = 0$ limit which returns SM-like couplings locally; the Standard Model itself presents high temperature symmetry restoration. The feature then arises in this non-linearly realised theory that the non-local phenomenology of the SM is not recovered in the local SM coupling limit. A consequence of this is that the region for high temperature symmetry restoration in our non-linearly realised theory lies a finite distance away in parameter space from the SM couplings limit and as such provides a target for collider experiments. This is illustrated in Fig. 4.22 where said region for small δ, ϵ is depicted and is partially ruled out by LHC bounds and would be explored in full by future experiments such as the FCC.

- **Domain walls.** The wall formation scenario required $\epsilon, \delta < 10^{-15}$, far smaller than collider limits can hope to compete with. LHC constraints therefore will have a relevant impact only in the remaining parameters of the theory, namely γ_4, χ . In the case that $\chi > 0.3$ the theory exhibits symmetry restoration and produces domain walls. As Fig. 4.13 shows, cosmological bounds alone (primarily in the form of wall annihilation before BBN) allow for potentially detectable GW signals at SKA. To produce a signal visible at SKA, one requires small $\gamma_4 < 0.1$ given the parametric dependence in Eq. (4.155). The triple gauge coupling constraint allows very small and even vanishing γ_4 . However, the relevant $\epsilon, \delta \rightarrow 0$ limit implies $\gamma_a = \gamma_4$, and curvature bounds of Eq. (4.172) apply. These constrain γ_4 to a neighbourhood around $1/c_\chi^2$, so that there is a minimum attainable γ_4 well above 0.1. Plugging this value back into eq (4.155) gives a maximum peak of the GW power spectrum resulting from domain walls:

$$\Omega_{\text{g.w.}|_{\text{peak}}}^{\text{max}} = 2.2 \times 10^{-17} \left(\frac{10^{-10} \text{ Hz}}{f_{\text{peak}}} \right)^4 \quad f_{\text{peak}} > 10^{-10} \text{ Hz}. \quad (4.174)$$

Figure 4.23a, shows the impact of LHC bounds and Fig. 4.23b shows the maximal prediction for the peak spectrum in this non-linearly realised theory versus SKA sensitivity, see Eq. (4.174). From this figure, it is clear that the parameter region which sources a domain wall GW signal that SKA is sensitive to is already ruled out by the LHC while the maximum attainable signal in spectrum lies five orders of magnitude below projected sensitivity.

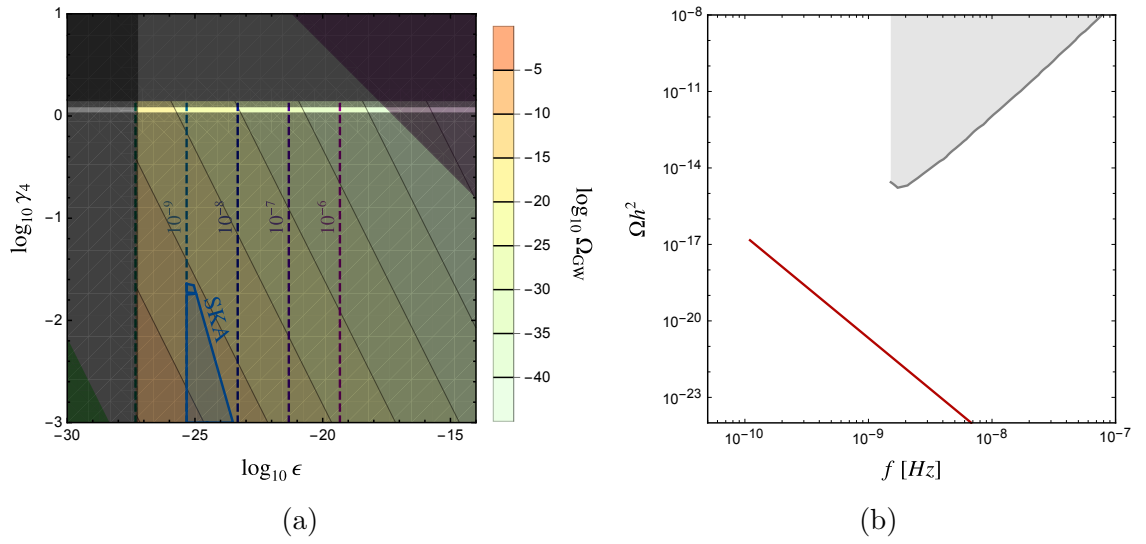


Figure 4.23: (a) The $(\epsilon-\gamma_4)$ plane delineating the wall formation region in parameter space as in Fig. 4.13 with the addition of LHC bounds, Eq. (4.172), in the vertical gray shaded region. (b) Curve for the value of the spectrum at the peak frequency for the allowed region of parameter space taking into account LHC bounds and the sensitivity of SKA [11].

- **First order phase transition.** For first order phase transitions, one requires couplings sizeably different from the SM, which would naively give collider constraints a more prominent role than in the walls case. The main LHC constraint arises again through the bound on R_φ , which constrains $c_\chi^2 \gamma_a$ to lie close to 1. On the other hand we require largish negative δ in this region. Recalling

$$\delta = \gamma_4^{-1} \gamma_\epsilon - \gamma_a^{-1} \quad (4.175)$$

together with $1 < \gamma_\epsilon < \sqrt{2}$ for $\epsilon > 0$ means $\delta < 0$ would require $\gamma_4 > \gamma_\epsilon \gamma_a \simeq \gamma_\epsilon / c_\chi^2 > 1$. The effect of greater than one γ_4 is illustrated in Fig. 4.7; as γ_4 increases, the extrema of the $T = 0$ potential is pushed closer together, which also facilitates nucleation. We plot $\gamma_4 = 1.6$ in Fig. 4.24 to provide an illustrative example of a region in parameter space allowed by current LHC bounds that also predicts a gravitational wave signal detectable at upcoming experiments LISA and BBO, for the region marked in orange and cyan respectively. To estimate the reach of upcoming experiments, we simply check that there exists some range of frequencies such that the GW power spectrum exceeds the detector's sensitivity curve. We leave a full signal-to-noise ratio analysis taking into account possible astrophysical GW backgrounds for later work. Note that, since $\gamma_4 \neq 1, \chi \neq 0$, in the (ϵ, δ) plane of Fig. 4.24 the LHC-allowed region does not go through the origin.

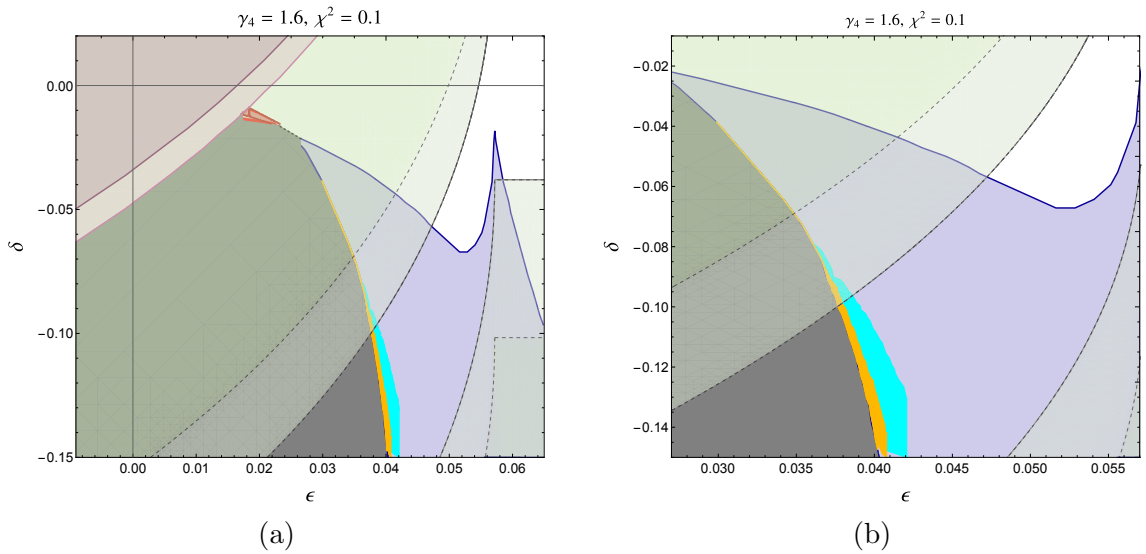


Figure 4.24: Summary of first order phase transition parameter space for $\gamma_4 = 1.6$, $\chi^2 = 0.1$. The region in blue shows the combinations of (ϵ, δ) that we found to admit bubble nucleation while tunnelling from the false vacuum to the true vacuum today. The region in red (dark red) is excluded by the strong (weak) IR constraints. The pink (dark pink) regions are excluded by the boundedness from below (perturbativity) constraint. The light green (green) dashed lines show the LHC constraints on the curvature to the 1σ (2σ) level. The gray region is unphysical, yielding the wrong vacuum today. The regions of first order phase transitions that give a GW signal detectable at LISA (BBO) are shown in orange (cyan). Only a small sliver of parameter space gives signals observable only at BBO, more visible in Fig. 4.24b.

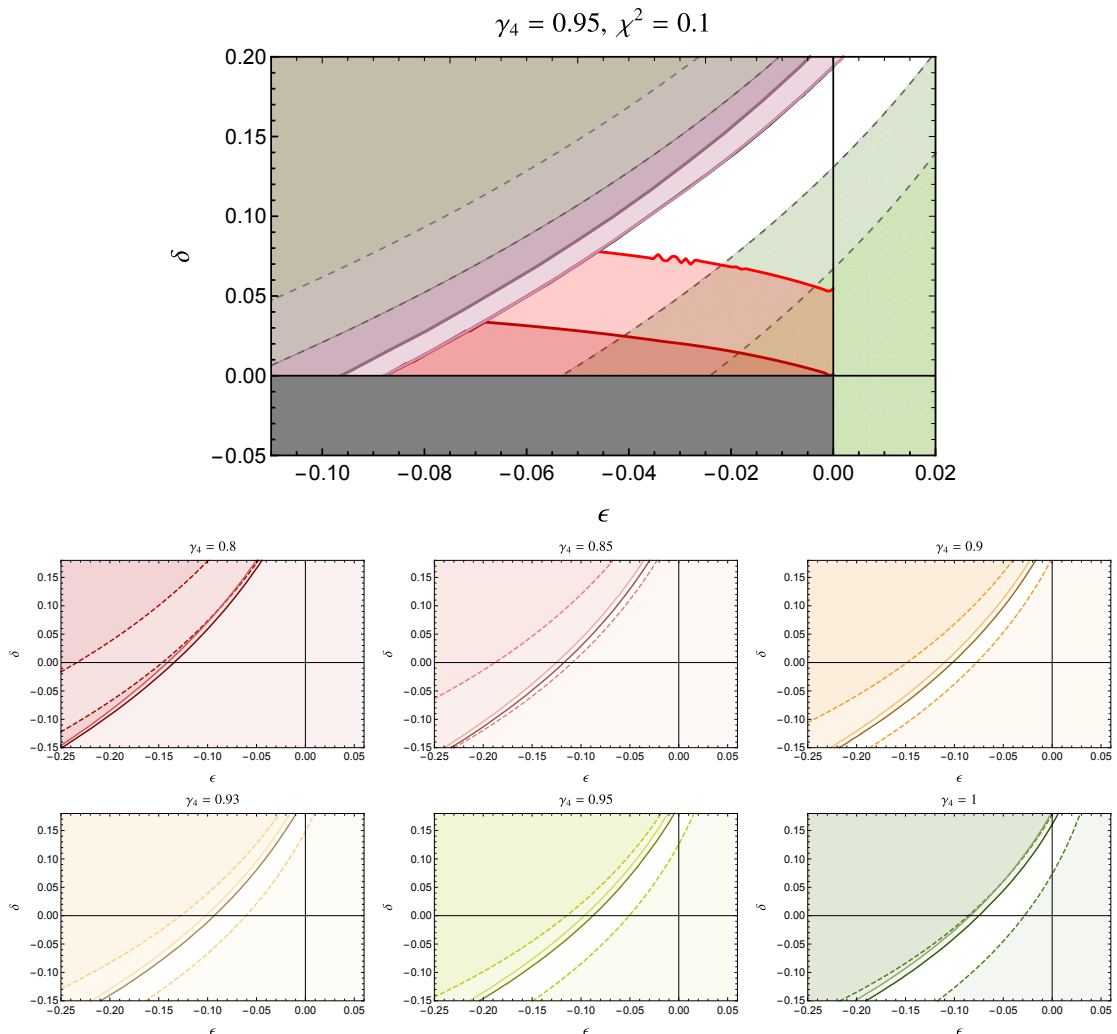


Figure 4.25: Top: Summary of the parameter space that leads to future vacuum decay (the doom scenario). Combination of Fig. 4.18 with LHC bounds in light green (1σ) and darker green (2σ). Bottom: Series of plots with the combination of LHC exclusion regions (delineated with dashed lines) and perturbativity to illustrate that values of $\gamma_4 < 0.85$ are ruled out by a combination of LHC and perturbativity bounds, and therefore discarded in our analysis.

- Doom.** Lastly the quadrant $\epsilon < 0, \delta > 0$ can lead to h_0 as the single high temperature vacuum while the true vacuum today, h_- , having appeared at a distance in field space large enough so that we are currently trapped in a false vacuum. The requirement of $\delta > 0$ in conjunction with LHC bounds with the same reasoning as the one outlined around Eq. (4.175) but now in the opposite direction implies $\gamma_4 < 1$. This limit decreases the Higgs quartic coupling at tree level, increasing the relative contribution of loop effects so that a stronger perturbativity and boundedness from below constraint applies

now. This is illustrated in the lower panel of Fig. 4.25 where one can see that the combination of LHC and perturbativity bounds excludes $\gamma_4 < 0.8$. The reduced range for γ_4 still allows for a region, partially shown in Fig. 4.25 upper panel, where the IR constraint, the LHC and perturbativity constraints are satisfied and we would be currently trapped in a false vacuum. This doom possibility has been found to lead to a lifetime for our universe in excess of 10^{2000} times the lifetime of the universe, see Fig. 4.19.

4.8 Summary

Today the question of whether electroweak symmetry is realised in Nature linearly or non-linearly is within experimental reach. The distinction is non-local in field space and thus calls for non-perturbative phenomena as the unambiguous probe. Such phenomena do arise in cosmology, and this paper has focused on studying the cosmological phenomenology of the non-linear realisation, termed here the *non-linearly realised theory space*, i.e. HEFT\SMEFT which opens qualitatively new features with respect to SMEFT.

Our study has revealed non-decoupling deviations in the sphaleron energy, the possibility of domain wall formation, first order phase transitions at the electroweak scale and vacuum decay in the very distant future, as well as symmetry non-restoration at high temperature. These can be used to answer the EW realisation question because processes such as the formation of electroweak domain walls are, to the best of our current knowledge, exclusive to non-linearly realised theories.

There is evidence to support the statement that non-linearly realised theories are non-decoupling, meaning that no limit can be taken in such theories that returns the SM only. A non-decoupling feature, albeit localised a finite distance away from our vacuum, has been identified with the non-linearly realised theory used here, which has wormhole-like space as the scalar manifold. This feature is to be found in the flat limit that corresponds to the SM locally; the closing of the throat of the wormhole produces a localised singularity in the effective potential that prevents symmetry restoration at high temperature and would likely lead to light new states.

Conversely, away from this local SM limit, there is a region in parameter space that leads to symmetry restoration and presents local couplings around the vacuum which are a ‘finite distance’ away from the SM ones. This minimum size of deviations provides a specific target, and we find that FCC would meet it and rule out the symmetry restoring region. Another non-decoupling effect has been found in the sphaleron energy, although this effect seems difficult to probe. The exploration of its implications for baryogenesis are hitherto unexplored.

The formation of domain walls requires minima that are approximately degenerate, but not exactly so. This requirement sets upper and lower cosmological bounds on ϵ , which is related to the triple Higgs coupling. This window of ϵ is within a range too small to be probed directly by the LHC, although indirect LHC constraints on other parameters of the theory have implications on cosmology. Among them, there is an upper bound on the strength of gravitational waves from walls which lies a few orders of magnitude below the sensitivity of SKA.

The case of a strong first order phase transition is realised in this theory in a way not possible in SMEFT; the extension of the Higgs field range with the wormhole topology considered here contains naturally a second minimum and a barrier such that no large potential corrections are needed. This is qualitatively different from 1OPT’s in the SMEFT, which require the addition of higher dimensional operators to generate a barrier. In order to achieve first order phase transitions in non-linearly realised theories considered here, as opposed to walls, we require sizeable energy difference between minima and hence sizeable deviations from SM couplings. In fact, one has that the region in parameter space that leads to first order transitions is accessible experimentally via the LHC. However, the combination of LHC and current cosmological data does only probe this region partially. It is a promising possibility in fact that non-linearly realised theories could have produced gravitational waves detectable at LISA *and* will give rise to new signals at the HL-LHC.

Lastly, a scenario with vacuum decay in the future is difficult to probe with cosmological observation; the impending annihilation event has been found to be at least 10^{2000} years in the future. The LHC however can probe the possibility of vacuum decay through the determination of Higgs couplings.

This paper has explored a small fraction of the possible cosmological phenomenology of HEFT\SMEFT. It is a fraction which nonetheless included new phenomena not possible in SMEFT and provides the elementary results to attempt a more comprehensive survey. Such exploration, to be complete, should include LHC and cosmological data, but also theory considerations such as perturbativity and the range of validity of an EFT at finite temperature and its relation to curvature. Indeed non-linearly realised theories are constrained from all directions and hence, once these lines are drawn, they will provide specific targets for experiments both on earth and in space, to answer the question of what type of electroweak symmetry realisation is present in Nature.

CHAPTER 5

Summary

This thesis has been concerned with tackling the question of whether electroweak symmetry in the low energy Effective Field Theory regime is realised linearly or non-linearly. This is inherently a question about the geometry of field space as has been understood for some time, coming down to whether or not there is a symmetric fixed-point in field-space. We aim in this thesis to put theory against experiment and highlight where we should look experimentally to see which side of the dichotomy: linear or non-linear, nature falls on.

To this end, we have considered the dimension-6 scalar HEFT operators and their resulting high-energy scattering amplitudes. We uncover some evidence for a minimum-distance in amplitudes between the Standard Model and non-linearly realised theories, consistent with such theories being non-decoupling. This leaves linearly realised theories being the sole route to the SM. At colliders such as HL-LHC and FCC, we are expected to be able to probe around this ‘void’ region in amplitude space between the SM and non-linearly realised theory space which may provide us with some insight into the symmetry realisation.

The question we ask, however, is non-local in field space. Local scattering amplitudes can only tell us so much, and indeed we have made the assumption of

only dimension-6 terms to get there. Non-perturbative physics instead will allow us to probe non-locally in field space, such as sphalerons which are hinted at by semi-classical arguments. However, we find that sphalerons processes, present in non-linearly realised theories despite not being fully-defined, can have energy very similar to the Standard Model. The phenomenology of sphalerons, particularly at colliders, is not currently well-understood. This effect, therefore, may be difficult to probe. However, exploration of its implications for baryogenesis are hitherto unexplored.

Instead, we turn to cosmology, considering first order phase transitions in the early universe or perhaps very far distant future. We study the cases of domain wall formation, which, while possible, is highly constrained by cosmological bounds. Consequently, we find that the strength of a gravitational wave signal from their annihilation will be orders of magnitude below the sensitivity of the upcoming generation of gravitational wave interferometers. Furthermore, fortunately for us, we find that a future vacuum decay is at least 10^{2000} years in the future, and thus also not a viable phenomenological route.

We do find, however, there is the possibility for a strong first order phase transition in non-linearly realised theories of type A which is qualitatively different to SMEFT. In SMEFT, the potential must be configured to generate two minima which requires the addition of higher-dimensional couplings with a low cutoff. As such, with the current formulation of thermal field theory, SMEFT is unable to describe such a phase transition. We avoid such an issue in HEFT\SMEFT where it is possible to extend the range of the Higgs field automatically providing us with a second minima. We find that such a phase transition can produce an observable gravitational wave signal for the upcoming generation of experiments.

It is our expectation that both non-perturbative physics and scattering amplitudes will be required to determine which type of electroweak symmetry realisation exists in nature. Perhaps, with the HL-LHC due to begin operation in 2029 [147] and LISA due to launch in 2034 [148], the resolution is on the horizon.

UV model for non-linearly realised type A theory

In this appendix we present a model that presents the geometry of a type A non-linearly realised theory, i.e. a manifold which does not contain a fixed point, not even a singular one. This model is not meant to be phenomenologically viable or representative. In particular it is built out of linear representations and integration of heavy modes which leaves out the tantalising but hitherto unrealised possibility of starting from non linear representations.

The model is built with an $SU(2)$ doublet ϕ and a singlet h , with vacuum expectation values given by $\langle |\phi|^2 \rangle = v^2/2$ and $\langle h \rangle = 0$. The Lagrangian is

$$\mathcal{L}_{\text{UV}} = \frac{1}{2}(\partial_\mu h)^2 + |\partial_\mu \phi|^2 - V_h(h) - \frac{\lambda_\phi}{2} \left(|\phi|^2 - \frac{v^2}{2} \right)^2 + v^2 G(h) |\phi|^2, \quad (\text{A.0.1})$$

with arbitrary functions $V_h(h)$ and $G(h)$ of the singlet h , with the minimum for $V_h(h)$ at $h = 0$ and $G(0) = 0$, without loss of generality. We employ the usual parametrization of the doublet

$$\phi = \frac{1}{\sqrt{2}} U \begin{pmatrix} 0 \\ v + H \end{pmatrix} \quad (\text{A.0.2})$$

with a radial coordinate H such that $\langle H \rangle = 0$. The Lagrangian becomes

$$\mathcal{L}_{\text{UV}} = \frac{1}{2}(\partial_\mu h)^2 + \frac{1}{2}(\partial_\mu H)^2 + \frac{1}{2}(v + H)^2 \text{Tr} [\partial^\mu U^\dagger \partial^\mu U^\dagger] \quad (\text{A.0.3})$$

$$- V_h(h) - V_H(H) + \frac{v^2}{2} G(h)(v + H)^2. \quad (\text{A.0.4})$$

The H scalar gets a mass $m_H^2 = \lambda_\phi v^2$. Assuming a perturbative $\lambda_\phi \lesssim (4\pi)^2$, we have $m_H^2 \lesssim (4\pi)^2 v^2$. Here, we assume that $m_H^2 \simeq (4\pi)^2 v^2 \gg v^2$ and integrate out H at tree level. This can be done by plugging the solution to the equation of motion for H ,

$$H = \frac{1}{m_H^2} \left\{ v \text{Tr} [\partial^\mu U^\dagger \partial^\mu U^\dagger] + v^3 G(h) \right\} + O\left(\frac{1}{m_H^4}\right), \quad (\text{A.0.5})$$

into the UV Lagrangian, which gives:

$$\mathcal{L}_{\text{eff}} = \frac{1}{2}(\partial_\mu h)^2 + \frac{v^2}{2} \text{Tr} [\partial^\mu U^\dagger \partial^\mu U^\dagger] - V_h(h) + \frac{1}{2m_H^2} \left\{ v \text{Tr} [\partial^\mu U^\dagger \partial^\mu U^\dagger] + v^3 G(h) \right\}^2, \quad (\text{A.0.6})$$

neglecting $O(1/m_H^4)$ terms. In particular, we have

$$F(h)^2 = 1 + \frac{v^2}{m_H^2} G(h), \quad V(h) = V_h(h) - \frac{v^6}{2m_H^2} G(h)^2. \quad (\text{A.0.7})$$

This means that non-linearly realised theories with any $F(h)$ can be achieved with this model. Both type A and B theories can be obtained with an appropriate choice of $G(h)$. In particular, a renormalizable UV completion with

$$G(h) = \frac{c_\chi^2 m_H^2}{v^2} \left(2 \frac{h}{v_\star} + \frac{h^2}{v_\star^2} \right), \quad (\text{A.0.8})$$

$$\begin{aligned} V_h(h) &= V(h) + \frac{v^6}{m_H^2} G(h)^2 \\ &= \left(\frac{m_h^2}{2} + \frac{2c_\chi^4 v^6}{m_H^2 v_\star^2} \right) h^2 + \left(\frac{m_h \sqrt{\lambda}}{2} \gamma_4 (1 - \epsilon) + \frac{2c_\chi^4 v^6}{m_H^2 v_\star^3} \right) h^3 + \left(\frac{\lambda}{8} \gamma_4^2 + \frac{2c_\chi^4 v^6}{2m_H^2 v_\star^4} \right) h^4, \end{aligned} \quad (\text{A.0.9})$$

gives the $F(h)$ and $V(h)$ functions we have used in this work, although additional

terms of the form

$$\mathcal{L}_{\text{eff}} \supset \frac{v^2}{2m_H^2} \left\{ \text{Tr} [\partial^\mu U^\dagger \partial^\mu U^\dagger] \right\}^2 + O\left(\frac{1}{m_H^4}\right), \quad (\text{A.0.10})$$

which we have not considered, are present in the Lagrangian. Corrections to this Lagrangian of order m_H^{-4} can be computed systematically with a functional approach as outlined in [41].

Bibliography

- [1] R. Alonso and M. West, *Roads to the Standard Model*, *Phys. Rev. D* **105** (2022) 096028 [2109.13290]. (document), 1.3, 3.2, 4, 4.2, 4.3, 4.3.3
- [2] R. Alonso, J.C. Criado, R. Houtz and M. West, *Walls, bubbles and doom – the cosmology of HEFT*, 2312.00881. (document), 1.3
- [3] R. Alonso, D. Dimakou and M. West, *Fractional-charge hadrons and leptons to tell the Standard Model group apart*, 2404.03438. (document), 2
- [4] J. Bennett, A. Callison, T. O’Leary, M. West, N. Chancellor and V. Kendon, *Using copies can improve precision in continuous-time quantum computing*, *Quantum Sci. Technol.* **8** (2023) 035031 [2206.02545]. (document)
- [5] R. Alonso and M. West, *On the effective action for scalars in a general manifold to any loop order*, *Phys. Lett. B* **841** (2023) 137937 [2207.02050]. (document), 4, 4.3.1
- [6] R. Alonso, *A primer on Higgs Effective Field Theory with Geometry*, 2307.14301. (document), 1.1, 1.5.4, 4
- [7] M.S. Chanowitz and M.K. Gaillard, *The TeV Physics of Strongly Interacting W’s and Z’s*, *Nucl. Phys. B* **261** (1985) 379. (document), 1.2, 1.4
- [8] B.W. Lee, C. Quigg and H.B. Thacker, *Weak Interactions at Very High-Energies: The Role of the Higgs Boson Mass*, *Phys. Rev. D* **16** (1977) 1519. (document), 1.2, 1.4, 2.3.2
- [9] J.M. Cornwall, D.N. Levin and G. Tiktopoulos, *Derivation of Gauge Invariance from High-Energy Unitarity Bounds on the s Matrix*, *Phys. Rev. D* **10** (1974) 1145. (document), 1.2, 1.4
- [10] G.J. Gounaris, R. Kogerler and H. Neufeld, *Relationship Between Longitudinally Polarized Vector Bosons and their Unphysical Scalar Partners*, *Phys. Rev. D* **34** (1986) 3257. (document), 1.2, 1.4

- [11] A. Weltman et al., *Fundamental physics with the Square Kilometre Array*, *Publ. Astron. Soc. Austral.* **37** (2020) e002 [1810.02680]. (document), 4.13, 4.6, 4.21, 4.23
- [12] W.-Y. Ai, B. Laurent and J. van de Vis, *Model-independent bubble wall velocities in local thermal equilibrium*, *JCAP* **07** (2023) 002 [2303.10171]. (document), 4.6, 4.20
- [13] P. Amaro-Seoane, H. Audley, S. Babak, J. Baker, E. Barausse, P. Bender et al., *Laser interferometer space antenna*, 2017. (document), 4.21
- [14] V. Corbin and N.J. Cornish, *Detecting the cosmic gravitational wave background with the big bang observer*, *Classical and Quantum Gravity* **23** (2006) 2435. (document), 4.21
- [15] B. Sathyaprakash, M. Abernathy, F. Acernese, P. Ajith, B. Allen, P. Amaro-Seoane et al., *Scientific objectives of einstein telescope*, *Classical and Quantum Gravity* **29** (2012) 124013. (document), 4.21
- [16] J. de Blas et al., *Higgs Boson Studies at Future Particle Colliders*, *JHEP* **01** (2020) 139 [1905.03764]. (document), 4.22
- [17] F. Bishara, R. Contino and J. Rojo, *Higgs pair production in vector-boson fusion at the LHC and beyond*, *Eur. Phys. J. C* **77** (2017) 481 [1611.03860]. (document), 2.1.2, 4.22
- [18] I. Banta, T. Cohen, N. Craig, X. Lu and D. Sutherland, *Non-decoupling new particles*, *JHEP* **02** (2022) 029 [2110.02967]. (document), 1.1.1, 1.2.3, 4
- [19] D. Tong, *Line Operators in the Standard Model*, *JHEP* **07** (2017) 104 [1705.01853]. 2
- [20] H.-L. Li and L.-X. Xu, *The Standard Model Gauge Group, SMEFT, and Generalized Symmetries*, 2404.04229. 2
- [21] S. Schafer-Nameki, *ICTP lectures on (non-)invertible generalized symmetries*, *Phys. Rept.* **1063** (2024) 1 [2305.18296]. 1.1
- [22] BOREXINO collaboration, *A test of electric charge conservation with Borexino*, *Phys. Rev. Lett.* **115** (2015) 231802 [1509.01223]. 1.1
- [23] J. Goldstone, *Field Theories with Superconductor Solutions*, *Nuovo Cim.* **19** (1961) 154. 1.1.1
- [24] J. Goldstone, A. Salam and S. Weinberg, *Broken Symmetries*, *Phys. Rev.* **127** (1962) 965. 1.1.1
- [25] ATLAS collaboration, *Observation of a new particle in the search for the Standard Model Higgs boson with the ATLAS detector at the LHC*, *Phys. Lett. B* **716** (2012) 1 [1207.7214]. 1.1.1

- [26] CMS collaboration, *Observation of a New Boson at a Mass of 125 GeV with the CMS Experiment at the LHC*, *Phys. Lett. B* **716** (2012) 30 [1207.7235]. 1.1.1
- [27] ATLAS collaboration, *A detailed map of Higgs boson interactions by the ATLAS experiment ten years after the discovery*, *Nature* **607** (2022) 52 [2207.00092]. 1.1.1
- [28] CMS collaboration, *A portrait of the Higgs boson by the CMS experiment ten years after the discovery.*, *Nature* **607** (2022) 60 [2207.00043]. 1.1.1
- [29] K. Agashe, R. Contino and A. Pomarol, *The Minimal composite Higgs model*, *Nucl. Phys. B* **719** (2005) 165 [hep-ph/0412089]. 1.1.1
- [30] W.D. Goldberger, B. Grinstein and W. Skiba, *Distinguishing the Higgs boson from the dilaton at the Large Hadron Collider*, *Phys. Rev. Lett.* **100** (2008) 111802 [0708.1463]. 1.1.1
- [31] T. Appelquist and J. Carazzone, *Infrared Singularities and Massive Fields*, *Phys. Rev. D* **11** (1975) 2856. 1.2.1, 1.2.1, 5, 2
- [32] B.M. Gavela, E.E. Jenkins, A.V. Manohar and L. Merlo, *Analysis of General Power Counting Rules in Effective Field Theory*, *Eur. Phys. J. C* **76** (2016) 485 [1601.07551]. 6, 1.2.3
- [33] I. Brivio, J. Gonzalez-Fraile, M.C. Gonzalez-Garcia and L. Merlo, *The complete HEFT Lagrangian after the LHC Run I*, *Eur. Phys. J. C* **76** (2016) 416 [1604.06801]. 1.2.2, 1.2.3
- [34] S. Dawson, D. Fontes, C. Quezada-Calonge and J.J. Sanz-Cillero, *Is the HEFT matching unique?*, *Phys. Rev. D* **109** (2024) 055037 [2311.16897]. 1.2.2
- [35] S. Weinberg, *Phenomenological Lagrangians*, *Physica A* **96** (1979) 327. 1.2.3
- [36] G. Buchalla, O. Cata, A. Celis, M. Knecht and C. Krause, *Complete One-Loop Renormalization of the Higgs-Electroweak Chiral Lagrangian*, *Nucl. Phys. B* **928** (2018) 93 [1710.06412]. 1.2.4
- [37] R. Alonso, K. Kanshin and S. Saa, *Renormalization group evolution of Higgs effective field theory*, *Phys. Rev. D* **97** (2018) 035010 [1710.06848]. 1.2.4, 4.3.1, 4.3.1
- [38] R. Alonso, E.E. Jenkins and A.V. Manohar, *A Geometric Formulation of Higgs Effective Field Theory: Measuring the Curvature of Scalar Field Space*, *Phys. Lett. B* **754** (2016) 335 [1511.00724]. 1.3, 2, 4, 4.2
- [39] R. Alonso, E.E. Jenkins and A.V. Manohar, *Geometry of the Scalar Sector*, *JHEP* **08** (2016) 101 [1605.03602]. 1.3, 1.3.3, 1.3.3, 1.3.4, 2, 4, 4.2, 4.3.1

- [40] T. Cohen, N. Craig, X. Lu and D. Sutherland, *Unitarity violation and the geometry of Higgs EFTs*, *JHEP* **12** (2021) 003 [2108.03240]. 1.3, 2, 2.1.1, 4, 4.3
- [41] T. Cohen, N. Craig, X. Lu and D. Sutherland, *Is SMEFT Enough?*, *JHEP* **03** (2021) 237 [2008.08597]. 1.3, 1.3.2, 1.3.4, 1.4, 1.5.3, 1.5.4, 1.5.4, 1.5.4, 2, 2.4, 4, 4.2, A
- [42] A. Helset, E.E. Jenkins and A.V. Manohar, *Geometry in scattering amplitudes*, *Phys. Rev. D* **106** (2022) 116018 [2210.08000]. 1.3, 4
- [43] R. Gómez-Ambrosio, F.J. Llanes-Estrada, A. Salas-Bernárdez and J.J. Sanz-Cillero, *Distinguishing electroweak EFTs with $WLWL \rightarrow n \times h$* , *Phys. Rev. D* **106** (2022) 053004 [2204.01763]. 1.3, 4
- [44] C. Cheung, A. Helset and J. Parra-Martinez, *Geometric soft theorems*, *JHEP* **04** (2022) 011 [2111.03045]. 1.3, 4
- [45] “David tong: Lectures on general relativity.”
<http://www.damtp.cam.ac.uk/user/tong/gr.html>. 1.3.1
- [46] A. Falkowski and R. Rattazzi, *Which EFT*, *JHEP* **10** (2019) 255 [1902.05936]. 1.3.4, 2
- [47] S.R. Coleman, J. Wess and B. Zumino, *Structure of phenomenological Lagrangians. 1.*, *Phys. Rev.* **177** (1969) 2239. 1.3.4
- [48] A. Adams, N. Arkani-Hamed, S. Dubovsky, A. Nicolis and R. Rattazzi, *Causality, analyticity and an IR obstruction to UV completion*, *JHEP* **10** (2006) 014 [hep-th/0602178]. 1.5, 2.3
- [49] G. Chew, *The Analytic S Matrix*, Benjamin, New York (1966). 1.5
- [50] C. Itzykson and J.B. Zuber, *Quantum Field Theory*, International Series In Pure and Applied Physics, McGraw-Hill, New York (1980). 1.5.1
- [51] M.D. Schwartz, *Quantum Field Theory and the Standard Model*, Cambridge University Press (2013). 1.5.2
- [52] M.E. Peskin and D.V. Schroeder, *An Introduction to quantum field theory*, Addison-Wesley, Reading, USA (1995). 1.5.2
- [53] T. Cohen, X. Lu and D. Sutherland, *On Amplitudes and Field Redefinitions*, 2312.06748. 1.5.2, 1.5.2
- [54] S. Weinberg, *The Quantum Theory of Fields*, Cambridge University Press (1995). 1.5.2
- [55] K. Fujikawa, *Path-integral measure for gauge-invariant fermion theories*, *Phys. Rev. Lett.* **42** (1979) 1195. 1.5.2
- [56] A.V. Manohar, *Introduction to Effective Field Theories*, 1804.05863. 1.5.2

- [57] C. Arzt, *Reduced effective Lagrangians*, *Phys. Lett. B* **342** (1995) 189 [hep-ph/9304230]. 1.5.2
- [58] B. Henning, X. Lu and H. Murayama, *How to use the Standard Model effective field theory*, *JHEP* **01** (2016) 023 [1412.1837]. 1.5.3
- [59] I. Brivio and M. Trott, *The Standard Model as an Effective Field Theory*, *Phys. Rept.* **793** (2019) 1 [1706.08945]. 2
- [60] F. Feruglio, *The Chiral approach to the electroweak interactions*, *Int. J. Mod. Phys. A* **8** (1993) 4937 [hep-ph/9301281]. 2
- [61] B. Grinstein and M. Trott, *A Higgs-Higgs bound state due to new physics at a TeV*, *Phys. Rev. D* **76** (2007) 073002 [0704.1505]. 2
- [62] A. Helset, A. Martin and M. Trott, *The Geometric Standard Model Effective Field Theory*, *JHEP* **03** (2020) 163 [2001.01453]. 2
- [63] A. Falkowski, S. Rychkov and A. Urbano, *What if the Higgs couplings to W and Z bosons are larger than in the Standard Model?*, *JHEP* **04** (2012) 073 [1202.1532]. 2.1, 2.3
- [64] S. Coleman, J. Wess and B. Zumino, *Structure of phenomenological lagrangians. i*, *Phys. Rev.* **177** (1969) 2239. 2.1
- [65] A. Hatzinikitas, *A Note on Riemann normal coordinates*, hep-th/0001078. 2.1.1
- [66] ATLAS collaboration, *Combined measurements of Higgs boson production and decay using up to 80 fb^{-1} of proton-proton collision data at $\sqrt{s} = 13 \text{ TeV}$ collected with the ATLAS experiment*, *Phys. Rev. D* **101** (2020) 012002 [1909.02845]. 2.1.2
- [67] CMS COLLABORATION collaboration, *Search for Higgs boson pair production via vector boson fusion with highly Lorentz-boosted Higgs bosons in the four b quark final state at $\sqrt{s} = 13 \text{ TeV}$* , Tech. Rep. 1, CERN, Geneva (2021). 2.1.2
- [68] M. Cepeda et al., *Report from Working Group 2: Higgs Physics at the HL-LHC and HE-LHC*, *CERN Yellow Rep. Monogr.* **7** (2019) 221 [1902.00134]. 2.1.2
- [69] FCC collaboration, *FCC-ee: The Lepton Collider: Future Circular Collider Conceptual Design Report Volume 2*, *Eur. Phys. J. ST* **228** (2019) 261. 2.1.2
- [70] I. Brivio, T. Corbett, O.J.P. Éboli, M.B. Gavela, J. Gonzalez-Fraile, M.C. Gonzalez-Garcia et al., *Disentangling a dynamical Higgs*, *JHEP* **03** (2014) 024 [1311.1823]. 2.2
- [71] ATLAS collaboration, *Search for heavy resonances decaying into WW in the $e\nu\mu\nu$ final state in pp collisions at $\sqrt{s} = 13 \text{ TeV}$ with the ATLAS detector*, *Eur. Phys. J. C* **78** (2018) 24 [1710.01123]. 2.3.2

- [72] G. Panico and A. Wulzer, *The Composite Nambu-Goldstone Higgs*, vol. 913, Springer (2016), 10.1007/978-3-319-22617-0, [1506.01961]. 2.4
- [73] R. Alonso, E.E. Jenkins and A.V. Manohar, *Sigma Models with Negative Curvature*, *Phys. Lett. B* **756** (2016) 358 [1602.00706]. 2.4
- [74] N.S. Manton, *Topology in the Weinberg-Salam Theory*, *Phys. Rev. D* **28** (1983) 2019. 3, 3, 3.1, 3.1, 3.1, 3.1
- [75] F.R. Klinkhamer and N.S. Manton, *A Saddle Point Solution in the Weinberg-Salam Theory*, *Phys. Rev. D* **30** (1984) 2212. 3.1, 3.1, 3.1, 3.1, 3, 3.2, 3.3
- [76] S.H.H. Tye and S.S.C. Wong, *Bloch Wave Function for the Periodic Sphaleron Potential and Unsuppressed Baryon and Lepton Number Violating Processes*, *Phys. Rev. D* **92** (2015) 045005 [1505.03690]. 3.1, 3.1, 3.2
- [77] M. van der Meulen, D. Sexty, J. Smit and A. Tranberg, *Chern-Simons and winding number in a tachyonic electroweak transition*, *JHEP* **02** (2006) 029 [hep-ph/0511080]. 3.1
- [78] S.H.H. Tye and S.S.C. Wong, *The Chern-Simons number as a dynamical variable*, *Ann. Math. Sci. Appl.* **01** (2016) 123 [1601.00418]. 2
- [79] M. Spannowsky and C. Tamarit, *Sphalerons in composite and non-standard Higgs models*, *Phys. Rev. D* **95** (2017) 015006 [1611.05466]. 3.1, 4
- [80] J.Y. Araz, J.C. Criado and M. Spannowsky, *Elvet – a neural network-based differential equation and variational problem solver*, 2103.14575. 3.2
- [81] J. Ellis, K. Sakurai and M. Spannowsky, *Search for Sphalerons: IceCube vs. LHC*, *JHEP* **05** (2016) 085 [1603.06573]. 3.2
- [82] J. Ellis and K. Sakurai, *Search for Sphalerons in Proton-Proton Collisions*, *JHEP* **04** (2016) 086 [1601.03654]. 3.2
- [83] A. Papaefstathiou, S. Plätzer and K. Sakurai, *On the phenomenology of sphaleron-induced processes at the LHC and beyond*, *JHEP* **12** (2019) 017 [1910.04761]. 3.2, 3.3
- [84] F.L. Bezrukov, D. Levkov, C. Rebbi, V.A. Rubakov and P. Tinyakov, *Semiclassical study of baryon and lepton number violation in high-energy electroweak collisions*, *Phys. Rev. D* **68** (2003) 036005 [hep-ph/0304180]. 3.2
- [85] V.V. Khoze and D.L. Milne, *Suppression of Electroweak Instanton Processes in High-energy Collisions*, *Int. J. Mod. Phys. A* **36** (2021) 2150032 [2011.07167]. 3.2
- [86] S. Kanemura and M. Tanaka, *Higgs boson coupling as a probe of the sphaleron property*, *Phys. Lett. B* **809** (2020) 135711 [2005.05250]. 3.2

- [87] R. Gómez-Ambrosio, F.J. Llanes-Estrada, A. Salas-Bernárdez and J.J. Sanz-Cillero, *SMEFT is falsifiable through multi-Higgs measurements (even in the absence of new light particles)*, *Commun. Theor. Phys.* **75** (2023) 095202 [2207.09848]. 4
- [88] K. Finn, S. Karamitsos and A. Pilaftsis, *Frame Covariance in Quantum Gravity*, *Phys. Rev. D* **102** (2020) 045014 [1910.06661]. 4
- [89] C. Cheung, A. Helset and J. Parra-Martinez, *Geometry-kinematics duality*, *Phys. Rev. D* **106** (2022) 045016 [2202.06972]. 4
- [90] A. Salas-Bernardez, J.J. Sanz-Cillero, F.J. Llanes-Estrada and R. Gomez-Ambrosio, *SMEFT as a slice of HEFT's parameter space*, *EPJ Web Conf.* **274** (2022) 08013 [2211.09605]. 4
- [91] T. Cohen, N. Craig, X. Lu and D. Sutherland, *On-Shell Covariance of Quantum Field Theory Amplitudes*, *Phys. Rev. Lett.* **130** (2023) 041603 [2202.06965]. 4
- [92] A. Helset, E.E. Jenkins and A.V. Manohar, *Renormalization of the Standard Model Effective Field Theory from geometry*, *JHEP* **02** (2023) 063 [2212.03253]. 4
- [93] B. Assi, A. Helset, A.V. Manohar, J. Pagès and C.-H. Shen, *Fermion Geometry and the Renormalization of the Standard Model Effective Field Theory*, 2307.03187. 4
- [94] M. Alminawi, I. Brivio and J. Davighi, *Jet Bundle Geometry of Scalar Field Theories*, 2308.00017. 4
- [95] L. Gráf, B. Henning, X. Lu, T. Melia and H. Murayama, *Hilbert series, the Higgs mechanism, and HEFT*, *JHEP* **02** (2023) 064 [2211.06275]. 4
- [96] H. Sun, Y.-N. Wang and J.-H. Yu, *Hilbert Series and Operator Counting on the Higgs Effective Field Theory*, 2211.11598. 4
- [97] I. Banta, *A strongly first-order electroweak phase transition from Loryons*, *JHEP* **06** (2022) 099 [2202.04608]. 4
- [98] S. Kanemura, R. Nagai and M. Tanaka, *Electroweak phase transition in the nearly aligned Higgs effective field theory*, *JHEP* **06** (2022) 027 [2202.12774]. 4
- [99] M. Chala, C. Krause and G. Nardini, *Signals of the electroweak phase transition at colliders and gravitational wave observatories*, *JHEP* **07** (2018) 062 [1802.02168]. 4
- [100] R. Alonso, M.B. Gavela, G. Isidori and L. Maiani, *Neutrino Mixing and Masses from a Minimum Principle*, *JHEP* **11** (2013) 187 [1306.5927]. 4

- [101] M. Laine and A. Vuorinen, *Basics of Thermal Field Theory*, vol. 925, Springer (2016), 10.1007/978-3-319-31933-9, [1701.01554]. 4.1, 4.1, 4.1, 4.3.3, 4.5.1
- [102] M. Quiros, *Finite temperature field theory and phase transitions*, in *ICTP Summer School in High-Energy Physics and Cosmology*, pp. 187–259, 1, 1999 [hep-ph/9901312]. 4.1, 4.3.1, 4.3.2
- [103] D. Croon, *TASI lectures on Phase Transitions, Baryogenesis, and Gravitational Waves*, 2307.00068. 4.1, 4.3
- [104] L. Dolan and R. Jackiw, *Symmetry behavior at finite temperature*, *Phys. Rev. D* **9** (1974) 3320. 4.1
- [105] I. Affleck, *Quantum-statistical metastability*, *Phys. Rev. Lett.* **46** (1981) 388. 4.1
- [106] C. Caprini et al., *Science with the space-based interferometer eLISA. II: Gravitational waves from cosmological phase transitions*, *JCAP* **04** (2016) 001 [1512.06239]. 4.1, 4.6, 7, 4.6, 4.6
- [107] D. Dunsky, L.J. Hall and K. Harigaya, *Higgs Parity, Strong CP, and Dark Matter*, *JHEP* **07** (2019) 016 [1902.07726]. 4.2
- [108] D. Croon, O. Gould, P. Schicho, T.V.I. Tenkanen and G. White, *Theoretical uncertainties for cosmological first-order phase transitions*, *JHEP* **04** (2021) 055 [2009.10080]. 4.3
- [109] A.D. Linde, *Infrared Problem in Thermodynamics of the Yang-Mills Gas*, *Phys. Lett. B* **96** (1980) 289. 4.3, 4.3.2
- [110] D. Croon, E. Hall and H. Murayama, *Non-perturbative methods for false vacuum decay*, 2104.10687. 2
- [111] J. Elias-Miro, J.R. Espinosa and T. Konstandin, *Taming Infrared Divergences in the Effective Potential*, *JHEP* **08** (2014) 034 [1406.2652]. 4.3.1
- [112] D. Curtin, P. Meade and H. Ramani, *Thermal Resummation and Phase Transitions*, *Eur. Phys. J. C* **78** (2018) 787 [1612.00466]. 4.3.2
- [113] F. Csikor, Z. Fodor and J. Heitger, *Endpoint of the hot electroweak phase transition*, *Phys. Rev. Lett.* **82** (1999) 21 [hep-ph/9809291]. 4.3.2
- [114] M. D’Onofrio and K. Rummukainen, *Standard model cross-over on the lattice*, *Phys. Rev. D* **93** (2016) 025003. 4.3.2
- [115] M. Laine and K. Rummukainen, *What’s new with the electroweak phase transition?*, *Nucl. Phys. B Proc. Suppl.* **73** (1999) 180 [hep-lat/9809045]. 4.3.2

- [116] P.B. Arnold and O. Espinosa, *The Effective potential and first order phase transitions: Beyond leading-order*, *Phys. Rev. D* **47** (1993) 3546 [hep-ph/9212235]. 4.3.2
- [117] G. Degrassi, S. Di Vita, J. Elias-Miro, J.R. Espinosa, G.F. Giudice, G. Isidori et al., *Higgs mass and vacuum stability in the Standard Model at NNLO*, *JHEP* **08** (2012) 098 [1205.6497]. 4.3.2
- [118] C. Delaunay, C. Grojean and J.D. Wells, *Dynamics of Non-renormalizable Electroweak Symmetry Breaking*, *JHEP* **04** (2008) 029 [0711.2511]. 4.3.2
- [119] E.J. Weinberg and A.-q. Wu, *UNDERSTANDING COMPLEX PERTURBATIVE EFFECTIVE POTENTIALS*, *Phys. Rev. D* **36** (1987) 2474. 4.3.2
- [120] G.B. Gelmini, M. Gleiser and E.W. Kolb, *Cosmology of Biased Discrete Symmetry Breaking*, *Phys. Rev. D* **39** (1989) 1558. 4.4, 4.4
- [121] A. Lazanu, C.J.A.P. Martins and E.P.S. Shellard, *Contribution of domain wall networks to the CMB power spectrum*, *Phys. Lett. B* **747** (2015) 426 [1505.03673]. 4.4
- [122] C.L. Wainwright, *CosmoTransitions: Computing Cosmological Phase Transition Temperatures and Bubble Profiles with Multiple Fields*, *Comput. Phys. Commun.* **183** (2012) 2006 [1109.4189]. 4.5.1, 4.5.1
- [123] A. Masoumi, K.D. Olum and B. Shlaer, *Efficient numerical solution to vacuum decay with many fields*, *JCAP* **01** (2017) 051 [1610.06594]. 4.5.1, 4.5.1
- [124] A. Linde, *On the vacuum instability and the higgs meson mass*, *Physics Letters B* **70** (1977) 306. 4.5.1
- [125] S.R. Coleman, *The Fate of the False Vacuum. 1. Semiclassical Theory*, *Phys. Rev. D* **15** (1977) 2929. 4.5.2
- [126] G.B. Gelmini, S. Pascoli, E. Vitagliano and Y.-L. Zhou, *Gravitational wave signatures from discrete flavor symmetries*, *JCAP* **02** (2021) 032 [2009.01903]. 4.6, 4.6
- [127] T. Hiramatsu, M. Kawasaki and K. Saikawa, *On the estimation of gravitational wave spectrum from cosmic domain walls*, *Journal of Cosmology and Astroparticle Physics* **2014** (2014) 031. 4.6
- [128] C. Caprini et al., *Detecting gravitational waves from cosmological phase transitions with LISA: an update*, *JCAP* **03** (2020) 024 [1910.13125]. 7, 4.6, 4.6, 4.6, 4.6, 4.6
- [129] L. Husdal, *On Effective Degrees of Freedom in the Early Universe*, *Galaxies* **4** (2016) 78 [1609.04979]. 4.6

- [130] D.J. Fixsen, *The Temperature of the Cosmic Microwave Background*, *Astrophys. J.* **707** (2009) 916 [0911.1955]. 4.6
- [131] P. Athron, C. Balázs, A. Fowlie, L. Morris and L. Wu, *Cosmological phase transitions: from perturbative particle physics to gravitational waves*, 2305.02357. 4.6, 4.6, 4.6
- [132] M. Hindmarsh, S.J. Huber, K. Rummukainen and D.J. Weir, *Shape of the acoustic gravitational wave power spectrum from a first order phase transition*, *Phys. Rev. D* **96** (2017) 103520 [1704.05871]. 4.6, 4.6, 8, 4.6
- [133] M. Hindmarsh, S.J. Huber, K. Rummukainen and D.J. Weir, *Numerical simulations of acoustically generated gravitational waves at a first order phase transition*, *Phys. Rev. D* **92** (2015) 123009 [1504.03291]. 4.6, 4.6
- [134] J.R. Espinosa, T. Konstandin, J.M. No and G. Servant, *Energy Budget of Cosmological First-order Phase Transitions*, *JCAP* **06** (2010) 028 [1004.4187]. 4.6
- [135] A. Roper Pol, S. Mandal, A. Brandenburg, T. Kahniashvili and A. Kosowsky, *Numerical simulations of gravitational waves from early-universe turbulence*, *Phys. Rev. D* **102** (2020) 083512 [1903.08585]. 4.6
- [136] A.N. Kolmogorov, *The local structure of turbulence in incompressible viscous fluid for very large Reynolds numbers*, *Proceedings of the Royal Society of London Series A* **434** (1991) 9. 4.6
- [137] C. Caprini, R. Durrer and G. Servant, *The stochastic gravitational wave background from turbulence and magnetic fields generated by a first-order phase transition*, *JCAP* **12** (2009) 024 [0909.0622]. 4.6
- [138] A. Kosowsky, A. Mack and T. Kahniashvili, *Gravitational radiation from cosmological turbulence*, *Phys. Rev. D* **66** (2002) 024030 [astro-ph/0111483]. 4.6
- [139] A. Roper Pol, A. Brandenburg, T. Kahniashvili, A. Kosowsky and S. Mandal, *The timestep constraint in solving the gravitational wave equations sourced by hydromagnetic turbulence*, *Geophys. Astrophys. Fluid Dynamics* **114** (2020) 130 [1807.05479]. 4.6
- [140] A. Brandenburg, G. Gogoberidze, T. Kahniashvili, S. Mandal, A. Roper Pol and N. Shenoy, *The scalar, vector, and tensor modes in gravitational wave turbulence simulations*, *Class. Quant. Grav.* **38** (2021) 145002 [2103.01140]. 4.6
- [141] J. Ellis, M. Lewicki, J.M. No and V. Vaskonen, *Gravitational wave energy budget in strongly supercooled phase transitions*, *JCAP* **06** (2019) 024 [1903.09642]. 4.6

- [142] T. Alanne, T. Hugle, M. Platscher and K. Schmitz, *A fresh look at the gravitational-wave signal from cosmological phase transitions*, *JHEP* **03** (2020) 004 [1909.11356]. 4.6
- [143] D.J. Weir, *Gravitational waves from a first order electroweak phase transition: a brief review*, *Phil. Trans. Roy. Soc. Lond. A* **376** (2018) 20170126 [1705.01783]. 4.6
- [144] ATLAS collaboration, *Search for nonresonant pair production of Higgs bosons in the $b\bar{b}b\bar{b}$ final state in pp collisions at $\sqrt{s} = 13$ TeV with the ATLAS detector*, 2301.03212. 4.7
- [145] ATLAS collaboration, *Combined measurements of Higgs boson production and decay using up to 139 fb^{-1} of proton-proton collision data at $\sqrt{s} = 13$ TeV collected with the ATLAS experiment*, . 4.7
- [146] ATLAS collaboration, *Combination of searches for non-resonant and resonant Higgs boson pair production in the $b\bar{b}\gamma\gamma$, $b\bar{b}\tau^+\tau^-$ and $b\bar{b}b\bar{b}$ decay channels using pp collisions at $\sqrt{s} = 13$ TeV with the ATLAS detector*, . 4.7
- [147] I. Zurbano Fernandez et al., *High-Luminosity Large Hadron Collider (HL-LHC): Technical design report*, . 5
- [148] “Capturing the ripples of spacetime: Lisa gets go-ahead.”
https://www.esa.int/Science_Exploration/Space_Science/Capturing_the_ripples_of_spacetime_LISA_gets_go-ahead. 5